A REFINED TRUE TRIAXIAL APPARATUS FOR TESTING UNSATURATED SOILS UNDER SUCTION-CONTROLLED STRESS PATHS

by

DIEGO D. PEREZ-RUIZ

Presented to the Faculty of the Graduate School of

The University of Texas at Arlington in Partial Fulfillment

of the Requirements

for the Degree of

DOCTOR OF PHILOSOPHY

THE UNIVERSITY OF TEXAS AT ARLINGTON

August 2009

This work is dedicated to my beloved mother.

ACKNOWLEDGEMENTS

I would like to thank my supervisor Dr. Laureano R. Hoyos for his guidance and assistance throughout the process of this research work. I would also like to thank all the committee members: Dr. Anand J. Puppala, Dr. Melanie Sattler, Dr. Mohammad Najafi and Dr. Chien-Pai Han for their valuable advice, helpful comments, and careful review of this dissertation. I would like to especially thank Dr. Anand J. Puppala for his friendship, continuous support, and enthusiasm. I also must acknowledge all faculty and staff in the Department of Civil Engineering for their support and collaboration.

Especial thanks are extended to my friends for their friendship and kindness, especially to Dr. Maria F. Serrano, Rosa Santoni, and Katherine Torres. Also I would like to thank all Thai and Indian friends at the University of Texas at Arlington.

I would like to express my very special thanks from the bottom of my hard to my mother, Zoraida Ruiz, for her great care, support and love. Last but not least, I would like to express my gratitude to my father, brothers, sister and nephew: Alvaro F., Alvaro A., Carlos F., Nancy, and Carlos A. for all their help, support and encouragement.

Once again, I would like to thank all of them for their help and support. I have learned too much about friendship, the way to live, and especially how to treat people. This very last is even more valuable than any degree.

July 17, 2009

ABSTRACT

REFINED TRUE TRIAXIAL APPARATUS FOR TESTING UNSATURATED SOILS UNDER SUCTION-CONTROLLED STRESS PATHS

Diego D. Pérez-Ruiz, Ph.D.

The University of Texas at Arlington, 2009

Supervising Professor: Laureano R. Hoyos

A novel, computer-driven, true triaxial (cubical) apparatus has been developed to test unsaturated soil specimens under suction-controlled multi-axial stress paths that are not achievable in a conventional cylindrical apparatus. The cubical cell implemented in this research work is a considerably refined version of those previously reported by Hoyos (1998) and Laikram (2007). The refined version is a servo-controlled, mixed boundary type of cell that allows for full control and real time measurements of matric suction, net principal stresses and soil deformations along a wide range of simple-to-complex stress paths induced on cubical specimens of unsaturated soil. The specimen seats on top of a high-air-entry ceramic disk with a 5-bar entry value.

A comprehensive series of drained (constant-suction) hydrostatic compression (HC), conventional triaxial compression (CTC), triaxial compression (TC), triaxial extension (TE), and simple shear (SS) tests were conducted on compacted, 3 in (7.62 cm) per side, cubical specimens of clayey sand (SP-SC) under constant suction states. Target suction levels are induced and kept constant during testing using the axis-translation technique. Results from suction-controlled tests under axisymmetric conditions ($\sigma_2 = \sigma_3$) were used for a thorough calibration of the elasto-plastic, critical state-based frameworks previously postulated by the Barcelona Basic Model (Alonso et al., 1990), the Modified Barcelona Basic Model (Josa et al., 1992), and the Oxford Model (Wheeler and Sivakumar, 1995).

Results from suction-controlled conventional triaxial compression (CTC) and triaxial compression (TC) tests were used for the validation of these models in predicting stress-strain response of compacted clayey sand under 50, 100, and 200 kPa suction states. Results were also used to validate the modifications proposed under the Refined Barcelona Basic Model framework developed in the present work.

Finally, results from the series of suction-controlled triaxial compression (TC), triaxial extension (TE), and simple shear (SS) tests were used to evaluate the nature of the major, minor and intermediate principal strain response of compacted clayey sand under multi-axial shearing, as well as the influence of suction on the shape and position of the failure envelope of compacted clayey sand in the octahedral plane.

TABLE OF CONTENTS

LIST OF ILLUSTRATIONS

Figure Page

LIST OF TABLES

CHAPTER 1

INTRODUCTION

1.1 Background and Importance

Unsaturated conditions predominate in all ground that lies above the water table. This may be natural level ground or slopes, fill materials and other earth structures that are constructed above the water table. The water meniscus formed between adjacent particles of unsaturated soil is subjected to tensile stress (i.e. negative pore water pressure) and thus creates a normal force between the particles, which bonds them in a temporary way. This phenomenon, known as soil suction, can improve the stability of earth structures (Kayadelen et al., 2007). Soil suction also provides an attractive force for free water, which can result in a loss of stability in loosely compacted soils or swelling in densely compacted soils. A large number of engineering problems involve the existence of partially saturated soils where the space between particles (i.e. pores) is filled with air, water, or a mixture of air and water. Conventional soil mechanics only consider soils as either fully saturated (i.e. pores fully occupied by water) or completely dry (i.e. pores fully occupied by air). Nevertheless, it has been recognized that unsaturated soil behaviour could be completely different to that of saturated or dry soils.

The development and understanding of soil mechanics for unsaturated soils has been relatively arduous due to the experimental and theoretical complexities of the subject. However, the rapid development of computers and powerful analytical methods

in recent years has changed the way to approach the solution of soil engineering problems. Less idealized geometrical and boundary conditions allow for the analysis of more realistic, necessarily non-linear and inelastic soil behaviour. The solutions obtained through these methods have to be complemented by the description of the material properties, typically formulated in terms of strength and stress-strain relationships (Sture and Desai, 1979). Several theoretical frameworks and constitutive models have been proposed to represent the mechanical behaviour of partially saturated soils. Although the constitutive models proposed are able to reproduce important features of unsaturated soil behaviour, most of them offer plenty of room for improvement and are usually restricted to a specific type of soil. Therefore, it is necessary to increase our understanding of the mechanical behaviour of unsaturated soils in order to improve the constitutive models developed in this area.

In order to obtain realistic predictions from the analytical methods an accurate assessment of the constitutive behavior of the material is required. It is well known that the intermediate principal stress σ_2 plays a fundamental role on soils' stress-strain response. However, most experimental equipments, and therefore, methods of analysis employing constitutive relations, have usually been restricted to axisymmetric stress state with major and minor principal stresses only ($\sigma_2 = \sigma_3$). Due to the complexity of specimen preparation, equipment operation, and experiment execution, multiaxial testing where the principal stresses are independently controlled ($\sigma_1 \neq \sigma_2 \neq \sigma_3$) are conducted only in research laboratories. A variety of practical problems have been found during the use of multiaxial testing techniques. The principal is the interference

of the corners and edges of the cubical sample confined by rigid or flexible membranes. The friction generated between rigid platens and the sample observed in a triaxial apparatus with rigid boundaries tends to produce a confining effect that can compromise the test results (Sture and Desai, 1979). The application of multiaxial loads through flexible membranes, on the other hand, may result in uniform and known boundary stresses on all six faces of the cubical specimen. However, the inability of measuring the deformation accurately when measured at three discrete points on each of the faces of the cubical specimen confined by flexible membranes becomes a limitation in the capability of triaxial devices with flexible boundaries.

True triaxial devices have been previously implemented with relative success to study the behaviour of partially saturated soils (Hoyos and Macari, 2001; Matsuoka et al., 2002; Park, 2005; Pyo, 2006; Laikram, 2007). The mixed-boundary type true triaxial implemented by Hoyos and Macari (2001) presented serious limitations, among them, occasional clogging of the HAE ceramic disk due to the debris generated by the cubical steel frame corrosion, low durability of the latex membranes when exposed to hydraulic fluid for a extended period of time, and delay in the equalization stage due to the impossibility of controlling pore-water temperature. Additionally, changes in pore-water and pore air-volume could not be measured in this setup.

On the other hand, the rigid type true triaxial cell implemented by Matsuoka et al. (2002) presented undesirable boundary effects experienced with the rigid loading platens. This limitation reduces the capability of the device to induce a wide range of stress paths on the octahedral plane. In addition, the method used to impose suction to

the soil specimen by using negative pore-water pressure, via the ceramic disks located in the upper and lower loading plates, reduce the capability of the device to perform tests at high values of matric suction.

Laikram (2007) utilized a mixed boundary type true triaxial device similar to the one used by Hoyos and Macari (2001). Although several limitations detected in the cell used by Hoyos and Macari (2001) were corrected, the low resolution of the pressure transducers in the pressure control panel used to apply and control the stress application restrict the load rate to a minimum value of 1 psi (6.9 kPa). In addition, load increments of 2 psi (13.8kPa) were applied equally spaced in time. The load increment is applied instantly at the beginning of the time period and not in an incremental way as it would be required during a ramped loading process. Moreover, the deformation induced on each face of the sample was obtained by averaging the readings of the three LVDTs located on each wall assembly (top and lateral) at the end of this period. Therefore, the strain data acquisition becomes manual with no data recorded between two consecutive load increments. Furthermore, corrosion of the springs in the extension rods of LVDT's occasionally clogged the core housing, thus increasing the friction with the extension rods of the LVDT’s.

The refined, mixed-boundary type true triaxial device implemented in this research work is a servo-controlled cubical device that allows for measurement and control of stress, strain, and soil suction in real time. Once the sample is mounted into the cubical cell, no manual intervention is required and the test is completely computer-driven via three servo valves. The output signal generated by the pressure sensors is

used to control the stress path when used completing a stress-controlled test. The output signal from the pressure sensors is captured by the computer, which controls the three separate servo valves to either increase or reduce the pressure applied to each sample face. On the other hand, when the cubical device is used to complete strain-controlled tests, the deformation in a specific direction (i.e X, Y, or Z) of the cubical soil specimen is used by the computer to control the test by changing the external pressure on each face in real time. In both cases, the applied pressure and the induced deformation were measured and stored in a data file in real time.

Results of shearing tests conducted on soil samples prepared using tamping compaction method show that test repeatability cannot be easily achieved using this compaction method. Therefore, in order to reduce the anisotropy of the soil specimens, all the samples were statically compacted in one lift using a triaxial frame at a monotonic displacement rate of 1.0 mm/min. This procedure permits to reproduce samples with similar soil fabric and characteristics that have been proven to offer the necessary conditions to guarantee the repeatability of the tests conducted in the true triaxial apparatus.

The experimental data obtained from a comprehensive suction-controlled test program on compacted clayey sand via the refined cubical cell have been used to validate the prediction capabilities of the Barcelona Basic Model (Alonso et al., 1990), the Modified Barcelona Basic Model (Josa et al., 1992), and the Oxford Model (Wheeler and Sivakumar, 1995). Considering the limited prediction capabilities observed in these models, a refinement of the Barcelona Basic Model framework has

been proposed. Although no perfect predictions have been obtained with the modifications proposed, the results show considerable improvement and better predictions over those obtained with the models evaluated in their original frameworks.

1.2 Objective and Scope

In this research work, an attempt has been made to achieve an accurate assessment of the constitutive behavior of statically compacted clayey sand specimens subjected to multiaxial loading under constant matric suction state in order to validate and further refine, wherever possible, the pioneering elasto-plastic constitutive frameworks previously proposed to predict the mechanical response of an unsaturated soil. To achieve this goal, the results from a series of drained (constant suction) stress-controlled true triaxial tests conducted on cubical samples of compacted clayey sand (SP-SC) were used to evaluate the prediction capabilities of these previously proposed, elasto-plastic, critical-state based constitutive models. The main objective of the present study is hence threefold, as described in the following.

First, to identify and further refine, to the largest extent that is technically possible, the features and testing capabilities of an existing true triaxial device previously used by Park (2005), Pyo (2006) and Laikram (2007). The cubical device has been used to study the stress-strain response of 3 in (7.62 cm) per side cubical specimens of unsaturated soil under different matric suction conditions and for various stress paths not achievable using conventional triaxial cells.

Second, to conduct a comprehensive review of the most widely used critical state based constitutive models for unsaturated soils. Some of the constitutive models

proposed for unsaturated soils have been thoroughly reviewed and parametrically studied.

Third, to validate and further refine, wherever possible, the investigated models. True triaxial test data from a series of drained, suction-controlled HC, CTC, and TC tests conducted on cubical SP-SC soil specimens have been used to calibrate all models parameters. In addition, true triaxial test data from a series of drained, suction-controlled TC, TE, and SS tests are used to evaluate the soil response under different matric suction conditions for a wide range of stress paths on the octahedral plane.

1.3 Thesis layout

This dissertation has been divided into eight chapters. A brief summary of each chapter is presented in the following.

Chapter 2 presents a brief review of the basic concepts of unsaturated soil mechanics. Special attention is given to the concept of soil suction, the relationship between soil suction and water content, and the relevant stress state and volumetric state variables used for unsaturated soil behaviour representation.

Chapter 3 includes a comprehensive review of the elasto-plastic, critical state based frameworks previously proposed to describe the constitutive response of unsaturated soils. A brief description of the original and modified Cam Clay models is also included in this chapter.

Chapter 4 presents a brief description of the previous work accomplished by Hoyos and Macari (2001), Matsuoka et al. (2002), and Laikram (2007), and summarizes

the main features and refinements of the computer driven, suction controlled true triaxial testing device developed in this research work.

Chapter 5 presents a detailed description of the basic laboratory tests conducted to classify the test soil used in this research work, the soil-water characteristic curve (SWCC), the selection of the compaction method and appropriate dry unit weight, as well as the procedure recommended to obtained identically prepared specimens with an adequate value of isotropic yield stress, $p_o(0)$.

Chapter 6 describes the experimental program undertaken in this work and the procedures followed to conduct drained (suction-controlled) hydrostatic compression (HC), conventional triaxial compression (CTC), triaxial compression (TC), triaxial extension (TE), and simple shear (SS) tests. The chapter includes all of the experimental results from this program, as well as results from tests performed to validate the dependability of the cubical cell in producing repeatable results and to select the adequate loading rate.

Chapter 7 describes the models' calibration process and presents the numerical predictions of compacted clayey sand behaviour from Barcelona Basic Model (BBM), Modified Barcelona Basic Model (MBBM), Oxford Model (OM), and the Refined Barcelona Basic Model (RBBM) proposed as a result of the current research work.

Chapter 8 summarizes the main conclusions of this research work and presents some recommendations for future experimental investigations in this discipline.

CHAPTER 2

BASIC UNSATURATED SOIL MECHANICS CONCEPTS

2.1 Introduction

In natural condition, soils are subjected to temporal and spatial water content variation. Water can infiltrate during precipitation providing a downward flux into the soil, eventually saturating the material. The depth at which soil become fully saturated with water is called the water table. Conversely, water can be removed by evaporation and/or evapotranspiration processes generating an upward flux of water out the soil, producing a gradual drying and cracking of the material (Fredlund and Rahardjo, 1993). Groundwater is also often withdrawn for agricultural, municipal and industrial use by constructing and operating extraction wells.

Considering that groundwater table is controlled by the climate variation, it is possible to differentiate the saturated and the unsaturated zone in natural soils (See Figure 2.1). The thickness and depth of these two zones is subjected to the influence of meteorological forces, the soil cover, and the characteristics and type of soil. According to Nan et al. (2005), the magnitude of soil water variation becomes smaller with increases in soil depth and the influence of meteorological forces is reduced gradually with distance downward.

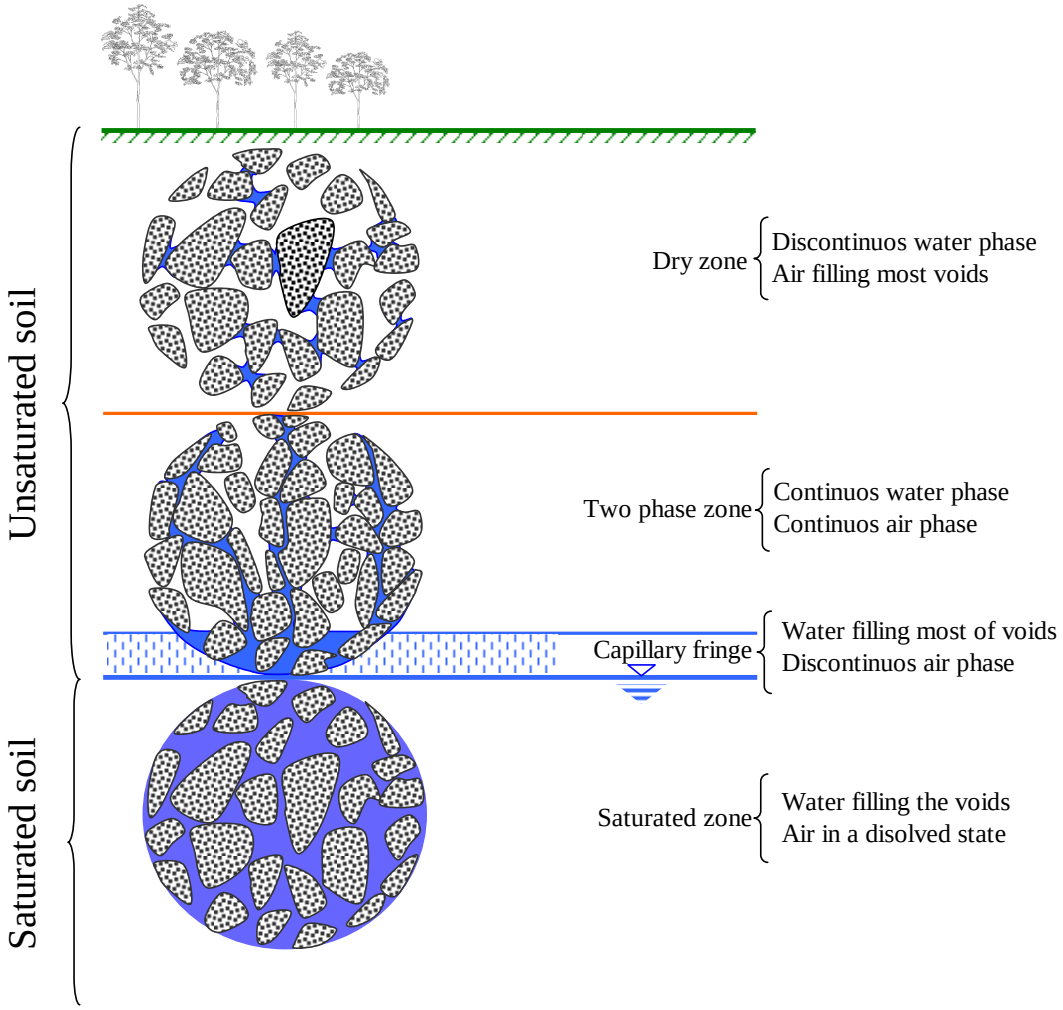

Figure 2.1 Soil classification based on the degree of saturation (modified from: Fredlund, 1996).

The unsaturated zone is the zone between the land surface and the regional water table. It includes the capillary fringe. The capillary fringe is the soil layer in which groundwater rise from a water table due to capillary force. At the base of the capillary fringe pores are completely filled with water. However, due to variation in pore size, the saturated portion of the capillary fringe is less than the total capillary rise. Consequently, soils with small and relatively uniform pore size can be completely saturated with water for several feet above the water table. On the other hand, the

saturated portion will extend only a few inches above the water table when pore size is large (Fredlund, 1996). Therefore, capillary action supports a fringe zone above the saturated zone where water content decreases with distance above the water table.

Except for the saturated portion of capillary fringe zone, pores in the unsaturated zone contain both water and air. However, the pore-water pressure is negative relative to the pore-air pressure (Fredlung and Rahardjo, 1993). According to Fredlund (2006), in the unsaturated soil zone the pore-water pressure can range from zero at the water table to a maximum tension of approximately 1,000,000 kPa under dry soil conditions. In contrast, the unsaturated zone differs from the saturated zone in that pores in the latter are almost always completely filled with water and water pressure is greater than atmospheric pressure.

2.2 Unsaturated Soils

Below the phreatic surface, the soil may be saturated and water in soil voids is normally continuous, although there may be air present in dissolved state. Pore pressures in saturated soils are derived from the weight of the water column lying above the given elevation and the drainage conditions below. Under saturated conditions pore pressure normally has a positive value and can be measured using a piezometer with a porous filter material attached at the end, making intimate contact with the water in the soil.

According to Fredlung and Rahardjo (1993), any shallow soil (i.e., near to the ground surface) in a relatively dry environment or subjected to excavation, remolding and compaction processes, could result in unsaturated conditions and consequently

subjected to negative pore-water pressure. A saturated soil is considered to have two phases mixture (i.e., solids and water). Although an unsaturated soil is considered to have three phases mixture (i.e., solids, air, and water), it is important to consider an additional fourth phase in order to adequately describe the stress satate (Fredlund, 2006). The fourth phase, called the contractile skin or the air water interface, act as a partition between the air and water phase. According to Fredlund (2006), the contractile skin can be considered as part of the water phase, however, to adequately describe the stress state and phenomenological behavior of unsaturated soil, it must be considered as an independent phase.

2.3 Soil Suction

Porous materials have a fundamental ability to attract and retain water (Bulut et al., 2001). This property is generally referred as suction, which is no other than the negative stress in the pore water. Under dry conditions, if the water contained in the voids of a soil were subjected just to gravity force, the soil lying above the water table would be completely dry (Ridley et al., 2004). However, molecular and physico-chemical forces, stronger than the gravitational force, acting at the boundary between the soil particles and the water, cause the water to be drawn up into the empty void spaces or held there without drainage. The attraction that the soil exerts on the water is termed soil suction and manifests itself as a tensile hydraulic stress in a saturated piezometer with a porous filter placed in intimate contact with the water in the soil (Fredlung and Rahardjo, 1993).

There are weak intermolecular physical attractions which result from short range dipole-dipole or induced dipole-dipole interaction. These forces, commonly referred as van der Waals' forces, are additive and may result in considerable attraction for large molecules. On the other hand, hydrogen bounding is a type of dipole-dipole interaction where hydrogen atoms serve as a bridge between two electronegative atoms. The forces of attraction are weaker than ionic but stronger than van der Waals' forces (Cresser et al, 1993). Therefore, a field of strong interaction between water and soil particles can result from the combination of hydrogen bounds and van der Waals' forces (Susuki, 2000). This field where water molecules are strongly adsorbed, forming a film covering the soil particle, is represented in Figure 2.2 by the dotted line surrounding the soil particle.

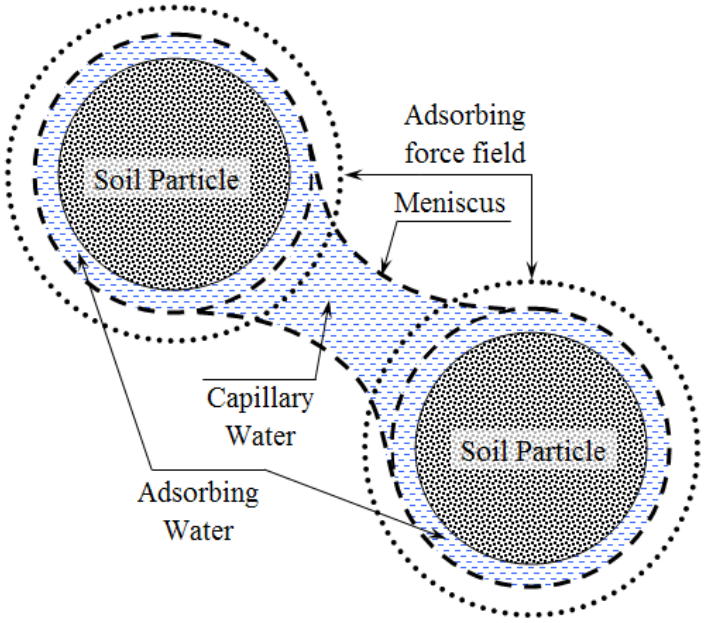

Figure 2.2 Schematic diagram of water soil interaction (modified from: Suzuki, 2000).

On the other hand, due to the capillary force produced by the surface tension occurring between water and air, water is retained near to the contact point of two particles. The contact angle between water and soil particles determines the concave surface of the meniscus. In general, water is retained either by the strong adsorbing forces at the surface of the soil particle (i.e. retaining water at surface) and by capillary forces at the contact point of the soil particles (i.e. retaining water in voids). The magnitude of the attractive force that soil above the water table exerts on water is governed by the size of the voids in manner similar to the way that the diameter of a small bore glass tube governs the height to which water will rise inside the tube when it is immersed in water. The smaller the void, the harder it is to remove the water from the void (Fredlund and Rahardjo, 1993).

Hence, soil suction is a quantity that can be used to characterize the effect of moisture on the mechanical behavior of soils, and it is a measure of the energy or stress that holds the soil water in the pores or a measure of the pulling stress exerted on the pore water by the soil mass (US Army Corps, 1983). The total soil suction, ψ, is expressed as a positive quantity and is defined as the sum of matric suction, $(u_a - u_w)$, and osmotic suction, π (US Army Corp of Engineers, 1983; Fredlund and Rahardjo, 1993).

2.3.1 Osmotic Suction

The osmotic suction, π, is caused by the concentration of soluble salts in the pore water, and it is pressure-independent (Department of the Army USA, 1983). It can be measured as the difference between the partial pressure of water vapor in equilibrium

with pure water to that in equilibrium with the groundwater. Although the osmotic effect has been associate more than unsaturated soils than with saturated soils, Salt in the pore water can be found in both saturated and unsaturated soils. Therefore, osmotic suction is equally applicable to both saturated and unsaturated soils (Fredlund and Rahardjo, 1993).

The osmotic effect may be observed if the concentration of soluble salts in the pore water differs from that of the externally available water. Therefore, if the salt content in a soil changes there will be a change in the overall volume and shear strength of the soil (Fredlund and Rahardjo, 1993). For example, swell may occur in the specimen if the external water contains less soluble salts than the pore water (Department of the Army USA, 1983). The effect of the osmotic suction is assumed small when compared with the effect of the matric suction (Fredlung and Rajardjo, 1993). Hence, the osmotic suction should not significantly affect the soil behavior if the salt concentration is not altered. Consequently, a change in total soil suction, ψ, is essentially equivalent to a change in matric suction, $(u_a - u_w)$ (Gardner, 1961; Department of the Army USA, 1983; Fredlund and Rahardjo, 1993; Öberg, 1997).

2.3.2 Matric Suction

The matric suction, $(u_a - u_w)$, is related to capillary tension in the pore water, and water sorption forces of the soil particles, both of them associated to the geometrical configuration of the soil structure (Department of the Army USA, 1983; Lu and Likos, 2004). Matric suction is defined as the difference between the pore-air pressure, u_a, and the pore-water pressures, u_w (Fredlund and Rahardjo, 1993). It may

vary with time due to weather and surrounding environmental changes. Hence, as shown in Figure 2.3, dry and wet seasons cause variation in the suction profile, particularly close to the ground surface (Fredlund and Rahardjo, 1993).

Matric suction is also influenced for the depth of water table. Hence, higher matric suction can be expected for a deeper water table. On the other hand, ground surface vegetation can apply a tension to the pore-water of up to 1 MPa to 2 MPa through the evapotranspiration process. Therefore, an increase in the matric suction can result from the evapotranspiration process (Fredlund and Rahardjo, 1993).

Water is a simpler molecular structure where one molecule of water has two hydrogen atoms covalently bonded to a single oxygen atom via a shared pair of electrons (Snoeyink and Jenkins1980). Oxygen attracts electrons much more strongly than hydrogen, resulting in a net positive charge on the hydrogen atoms, and a net negative charge on the oxygen atom. The presence of a charge on each of these atoms gives each water molecule a net dipole moment. Therefore, the electrical charge made water molecules to be attracted, pulling individual molecules closer together and making it difficult to separate (Snoeyink and Jenkins, 1980). This attractive force gives water its cohesive and also adhesive properties that made water molecules stay together aggregated in drops rather than spread out over a surface as a thin film. This property also causes water to stick to the sides of vertical structures despite gravity's downward pull. Therefore, when water is carried through small diameter tube the strong intermolecular attractions hold the water column together (Snoeyink and Jenkins1980).

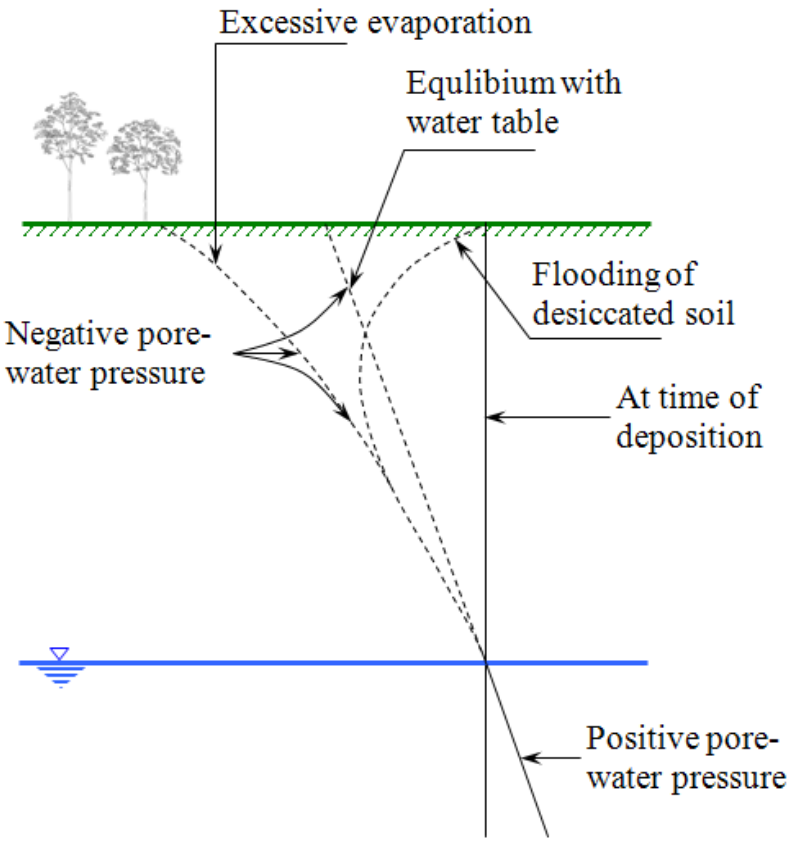

Figure 2.3 Typical pore-water pressure profile (modified from: Fredlund and Rahardjo, 1993).

2.4 Surface Tension

In a system composed of two contiguous materials (i.e. a two phases system) which have significantly uniform distribution of matter throughout their interiors (e.g. air and water) but which meet in a thin of physical inhomogeneity where the transition takes place from the distribution on one phase to that in the other (e.g. air-water interface) (Tolman, 1948). The system can be considered as precisely separated by the construction of an imaginary geometrical surface, which lies within the layer of physical inhomogeneity. Such a surface, which gives a precise separation of the system

into two parts, with the homogeneous portions of the two phases located in its opposite sites was called *"divided surface"* (Tolman, 1948). The inhomogeneous surface region is considered as a third phase, the surface phase, in equilibrium with the two bulk phases (Navascués, 1979).

The theory of surface tension given by Gibbs (1928) was developed with a minimum of hypothesis as to the detailed structure of the transition layer, this being reduced essentially to the assumption that all the properties of the layers can be regarded as determined by the area and curvature of some selected imaginary divided surface. This procedure has the advantage of providing a very general theory, which is valid for a wide range of possible kinds of transition layers (Tolman, 1948).

Therefore, applying to a system of two homogeneous fluids at pressures p' and p'', separated by a spherical membrane without rigidity (i.e. surface of tension), having a radius R_s and tension T_s. The pressure in the interphase will gradually change from one bulk value, say p' to the other, p''. Therefore, the molecules within the divided surface experiences an unbalanced force which is equilibrated by the tensile pull generated along the surface of tension called surface tension, T_s (Tolman, 1948; Kuz et al., 1987; Navascués, 1979; Schmelzer et al., 1996). Moreover, due to the inhomogeneity of the interphase, the pressure on an element of area depends on the orientation of that area in the interphase (Figure 2.4).

It is important to have an expression where the surface tension can be related to other macroscopic properties of the system. Hence, considering the hydrostatic

equilibrium of the equivalent system shown in Figure 2.5, the total force acting in the horizontal direction requires that

$$\pi R_s^2 \left(p' - p''\right) = 2\pi R_s T_s \tag{2.1}$$

The following equation, which is the well-known Laplace equation, is a relation between surface tension, T_s, the two bulk pressures, and the radius, R_s, of the surface of tension (Navascués, 1979).

$$p' - p'' = \frac{2T_s}{R_s} \tag{2.2}$$

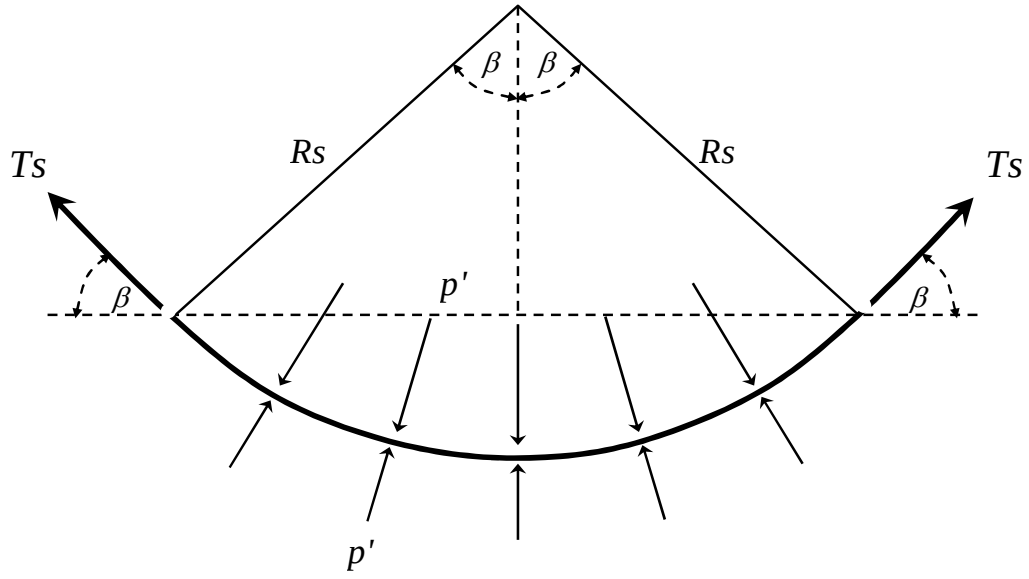

Figure 2.4 Surface tension on a spherical surface (modified from: Fredlund and Rahardjo, 1993).

Assuming than T_s is constant, it is possible to deduce from this equation that $p' > p''$ and the radius R_s decreases as $\Delta p \equiv p' - p''$ increases. On the other hand, if the interphase is not spherical, the Laplace equation can be generalized easily as (Navascués, 1979):

$$\Delta p = T_s\left(\frac{1}{R_1}+\frac{1}{R_2}\right) \tag{2.3}$$

With R_1 and R_2 been the radii of the curvature of the non spherical divided surface in two orthogonal principal planes (see Figure 2.6).

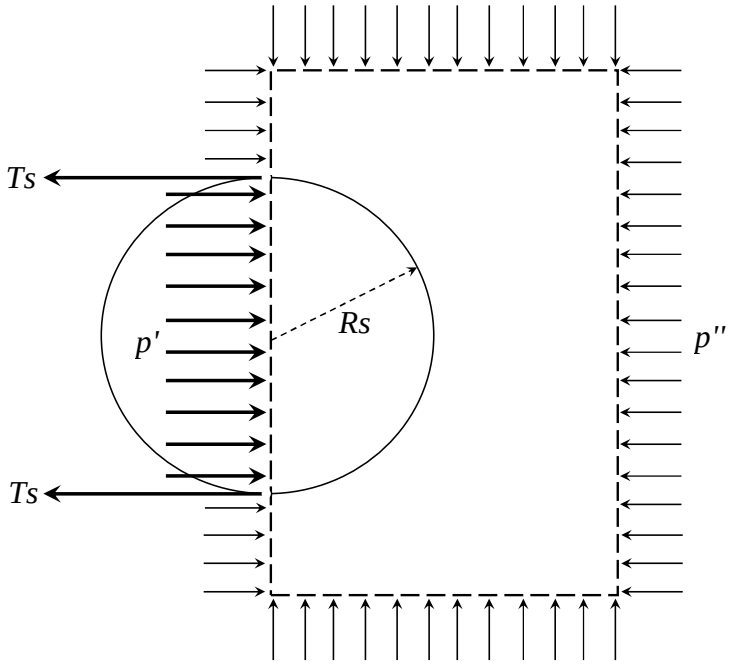

Figure 2.5 Diagram of the hydrostatic equivalent to a drop in equilibrium with its vapor (modified from: Navascués, 1979).

As mentioned before, a soil is commonly referred to as a three-phase mixture (i.e., solids, air, and water). However, more recently a fourth independent phase called the contractile skin or the air-water interface has been included for purposes of stress analysis (Fredlund and Morgenstern, 1977; Fredlund, 2006). Tolman (1948) referred to the air-water interface as *"divided surface"* in the surface tension physics literature. Hence, an element of an unsaturated soil can be analyzed considering a mixture with two phases (i.e. solid and contractile skin) coming to equilibrium under applied external

stresses, and another two phases (i.e. air and water) flowing under applied external stress. As a result, the contractile skin provides an isotropic stress to the pore-water pressure. The surface tension causes the contractile skin to behave like and elastic membrane. Therefore, Equation (2.2) can be used to calculate the pressure difference across a curved surface with the same radius of curvature, R_s, in all directions and surface tension T_s.

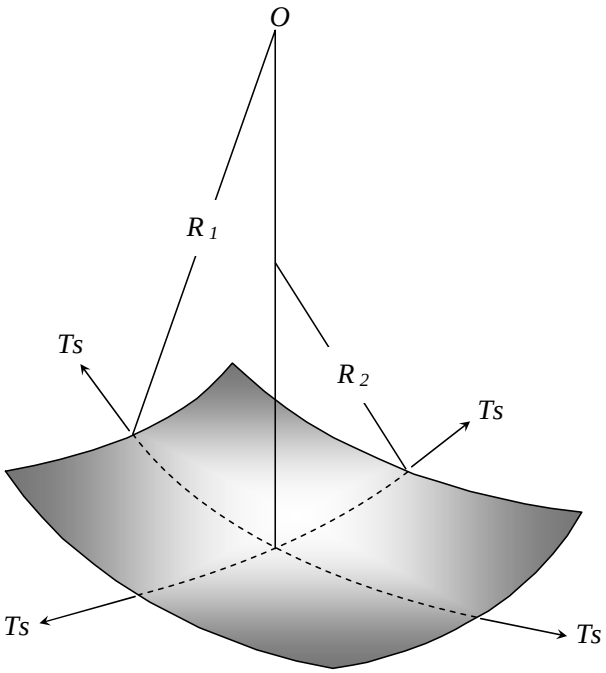

Figure 2.6 Surface tension on a non-spherical surface (modified from: Fredlund and Rahardjo, 1993).

In an unsaturated soil, the contractile skin would be subjected to an air pressure, u_a, which is greater than the water pressure, u_w (Fredlund and Rahardjo, 1993), and Equation (2.2) becomes

$$(u_a - u_w) = \frac{2T_s}{R_s} \qquad (2.4)$$

The pressure difference is referred, $(u_a - u_w)$, is referred to as matric suction.

According to Wang and Fredlund (2003), based on the assumption that the surface tension is 71.99 mN/m and the thickness of contractile skin is 5 Å at 25 °C, the equivalent tensile stress in the contractile skin can be estimated as 140,000 kPa. Therefore, the contractile skin is under a high tensile stress.

2.5 Capillary phenomena

Capillary in porous materials is defined as the movement of water within the interconnected void spaces due to the forces of adhesion, cohesion, and surface tension. According to Pakarinen et al. (2005), the capillary force in a porous material is caused by the condensation of humidity forming a meniscus or a liquid capillary neck between particles. This meniscus grows in size, until its surface curvature has decreased to a value where the rate of evaporation and condensation is in equilibrium. The surface curvature of the meniscus determines the pressure inside the meniscus. The capillary force is often said to arise from the pressure difference between the inside and the outside of the meniscus. The nature of the interaction between the particle and surface is strongly modified by the water meniscus which forms between them. This meniscus results in an additional capillary force increasing the particle's adhesion to the surface.

A simple capillary tube model can be used to describe the pressure changes across an air-water interface and explain an important component of suction in unsaturated soil. However, due to the various particles sizes and shapes, assumptions must be made about the complex pore geometry in order to extend the capillary tube model to analyze the unsaturated soil (Lu and Likos, 2004).

2.6 Soil-Water Characteristic Curve

The unsaturated soil properties can be better interpreted if the influence of matric suction is taken into account (Fredlund 2000). Hence, the soil-water characteristic curve (SWCC) describes the relationship between suction and the water storage capacity of a soil. The water content defines the amount of water contained into the soil pores. It can be expressed in various forms such as gravimetric water content, w, volumetric water content, θ, or degree of saturation, S. The suction can be either the matric suction (i.e. $u_a - u_w$), or total suction of the soil, which is defined as matric plus osmotic suction. The total suction related to zero water content appears to be basically the same for all types of soils and a value slightly below of 1,000,000 kPa has been reported for several researcher (Fredlund and Xing, 1994; Vanapalli et al., 1999).

When the suction range used for soil testing is small (i.e. 0 to 1,000 kPa), the soil-water characteristics are plotted on an arithmetic scale However, if the suction range used for testing is large, it is common to plot the soil-water characteristic curve behavior on a semi-logarithmic plot (Vanapalli et al., 1999). A typical soil-water characteristic curve, adopts an S-shape when the soil suction is plotted on logarithmic scale. Several features of the soil characteristic curve can be identified on in Figure 2.7 (Vanapalli et al., 1999).

2.6.1 Air-Entry Value of Soil

According to Fredlund and Rahardjo (1993), the air-entry value of the soil, is the matric suction value that must be exceeded before air resides into the soil pores. It represents the differential pressure between the air and water that is required to cause

desaturation of the largest pores (Vanapalli et al., 1999). Thus, the air-entry value of the soil is obtained by extending the constant slope portion of the soil-water characteristic to intersect the line on the portion of the curve for suction at 100% saturation, as shown in Figure 2.7. The corresponding value of suction for that point of intersection is taken as the air entry value of the soil.

2.6.2 SWCC Identifiable Zones

Based on the S-shape of the soil-water characteristic curve it is possible to identify three zones of desaturation (Figure 2.7): the residual zone of unsaturation, the transition zone, and the boundary effect zone (Vanapalli et al., 1994).

As shown in Figure 2.7, in the boundary effect zone, almost all of the soil pores are filled with water. In this zone, the flow of water is in the liquid phase. As the applied suction increases, water is released and the soil dries at slow rate until the air entry value is reached.

The soil desaturates at the air-entry value of suction, which is the point indicating the beginning of the so called transition zone. In this zone, the flow of water remains in liquid phase (Vanapalli et al., 1994). However, as the applied suction increases, water is released faster and the soil dries rapidly producing reduction in the connectivity of the water in the voids or soil pores. Eventually, at the end of the transition zone, large increases in suction lead to relatively small changes in soil water content. This is the so called residual zone of saturation.

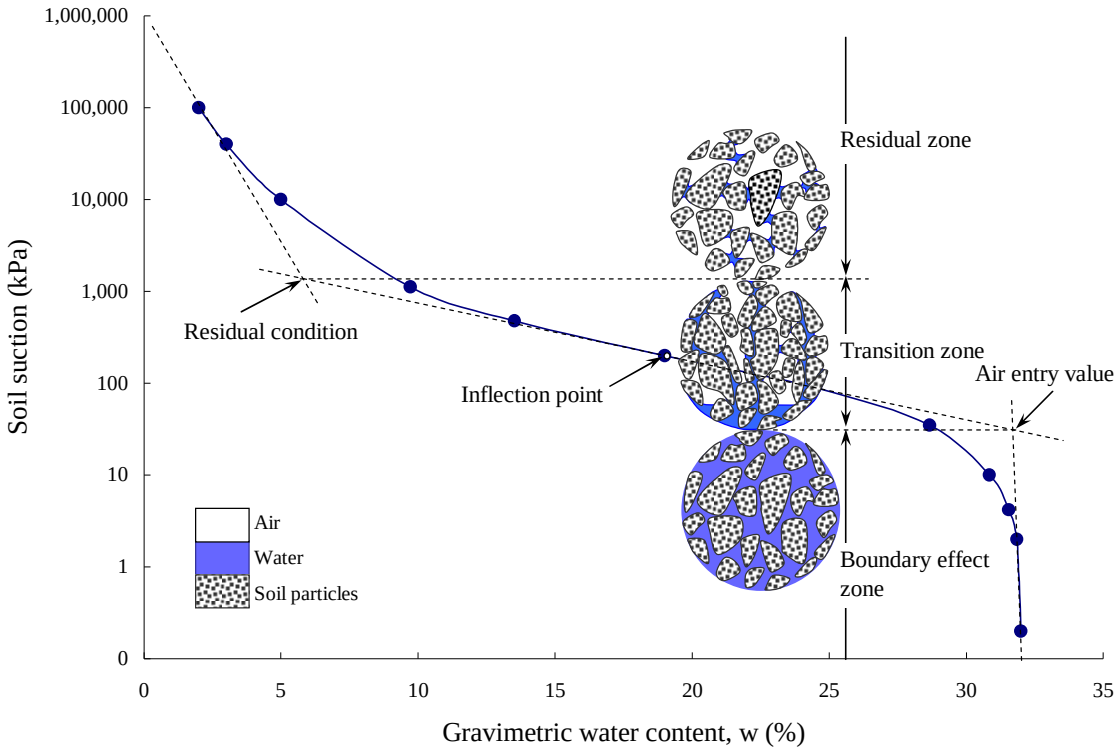

Figure 2.7 Typical soil-water characteristic curve showing different zones (modified from: Vanapalli et al., 1999).

The residual zone of saturation can be considered to be the zone where the liquid phase becomes discontinuous due to the low soil water content (Vanapalli et al., 1999). Hence, the residual zone of saturation represents humidity at which it becomes increasingly difficult to remove water from a specimen by increasing the suction. The point at which residual saturation is reached is not always clearly defined. A suction value of 1500 kPa, corresponding to the wilting point for many plants is recommended as residual suction (van Genuchten, 1980). However, a graphical procedure can be used to better define the residual condition of saturation when the entire suction range is used (Vanapalli et al., 1999). Thus, the residual point can be obtained on the intersection of

the tangent line through the inflection point, on the central straight portion of the soil-water characteristic curve, and the line extending from 1,000,000 kPa tangent to the final portion of the curve.

2.6.3 Soil-moisture Hysteresis

The complex nature of the liquid-phase in an unsaturated soil, produce a no unique relationship between water pressure and water content and presents hysteresis effects (Richards, 1941; Poulovassilis, 1962; Topp and Miller, 1966; Poulovassilis and Tzimas, 1974). The drying and wetting SWCCs are significantly different an in many cases it becomes necessary to differentiate the soil properties associates with the drying curve from those associates with the wetting curve (Fredlund et al., 1994; Fredlund, 2006). The essence of this phenomenon in soils is that water required less mechanical work to go into unsaturated soil than that required to be drained from it (Hillel, 1982). Thus, due to the hysteretic nature of the soil-water characteristic curve, the drying and wetting curves differ significantly with reference to each other.

As shown in Figure 2.8, for a specific matric suction a soil typically shows a water content that is lower on a wetting process than that found on a drying process (Maqsoud et al., 2004; Tami et al., 2004). Therefore, it becomes necessary to differentiate the soil properties associated with the drying process, such as evaporation or drainage, from these associated with the wetting process, such as infiltration. This means that it is convenient to establish under which condition the material is been tested and/or decide which process is to be modeled. It could also be appropriate in some cases

to use an average of the drying and wetting soil-water characteristic curve (Fredlund, 2006).

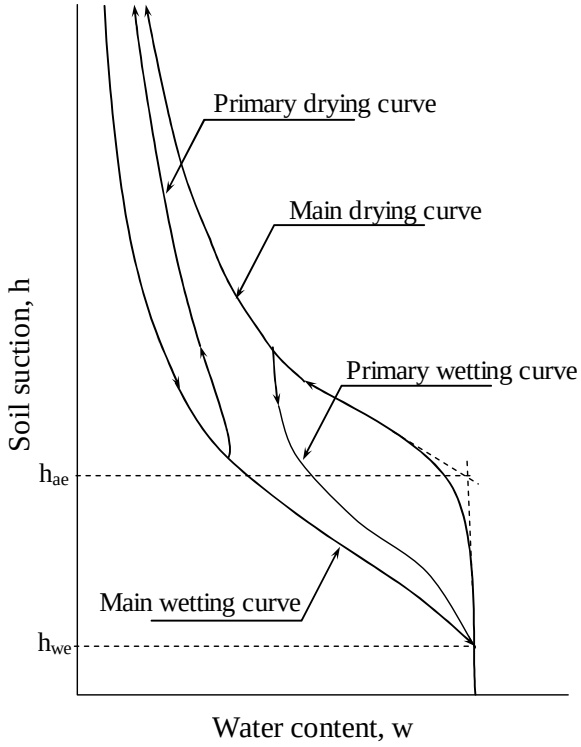

Figure 2.8 Schematic representation of the soil-water characteristic curve with hysteresis effect (modified from: Maqsoud et al., 2004).

Several factors can cause hysteresis of the soil-water characteristic curve (Bear, 1979; Hillel, 1980; Iwata et al., 1995; O'Kane et al., 2004): geometric nonuniformity of individual pores, variation in contact angle between liquid and soil particles, the entrapped air in the voids, and the aging due to wetting and drying history, and the air-water interface development during the wetting or drying process. The air-water interface or meniscus between the same soil particle and the receding air water interface during the drying process is different from that during the wetting process. It is due to

the different spatial connectivity of pores during drying or wetting process. This phenomenon is called the rain-drop effect (Bear, 1979).

During the drying process the water drainage from the pore is controlled by the "neck pore diameter" or "open pore diameter". On the other hand, the wetting process is controlled by the "body pore diameter" (Haines, 1930). Therefore, an increase in pressure is required on the water front in order to water re-enters in small pores. This condition generates an unbalanced in pore pressure that does not allow water flowing into the small pores until the surrounding pores are completely filled. This phenomenon is called the ink-bottle effect (Bear, 1979). Many researchers have used the ink-bottle effect to develop hysteresis models for predicting soil water characteristic curve hysteresis (Everett, 1955; Poulovassilis, 1962; Topp, 1971; Jaynes, 1984; Mualem, 1984; Haverkamp and Parlange, 1986; Hogarth et al., 1988; Jaynes, 1992). Important and successful mathematical descriptions of soil-moisture have been suggested by several authors (Parlange, 1980; Haverkamp and Parlange, 1986; Parlange et al., 1999; Poulovassilis and Kargas, 2000; Angulo-Jaramillo et al., 2003; O'Kane et al., 2004, Gandola et al., 2004).

2.6.4 Measurement Methods

Soil-water characteristic curve can be determined in the laboratory using either direct or indirect methods (Ridley and Wray, 1996). A number of devices have been developed to adequately measure soil suction. Tensiometers, null pressure plates, pressure membranes, or suction plates are some of the conventional equipment used in the measurement of matric suction in the laboratory (Power et al., 2008). A detailed

description of these devices and their correspondent testing procedure are provided for different authors (Fredlund and Rahardjo, 1993; Marinho, 1994; Öberg, 1997; Khanzode, 1999; Khanzode et al., 1999; Yaldo, 1999; ASTM, 2003; Fredlund, 2006).

On the other hand, indirect methods use measurements or indicators of water content or another physical property that is sensitive to a change in water content to measure either the matric or total suction of a specimen. Examples of those methods are relative humidity, electrical resistance, or heat dissipation (Power et al., 2008). Some Instruments used for the measurement of suction in the field and laboratory are Psychrometers (e. g. transistor, thermocouple, or chilled-mirror), filter paper method, thermal conductivity sensors, capacitance-based polymer sensors, and electrical conductivity sensors (Gourley and Schreiner, 1995; Albrecht et al., 2003; Leong et al., 2002; Agus and Schanz, 2007).

2.6.4.1 Pressure Plate Drying Test

A pressure plate consists of a pressure vessel with a high-air entry ceramic disk (Figure 2.9). The high-air entry ceramic disk is used as an interface between air and water pressure. As long as the applied matric suction does not exceed the air entry value of the disk, air will not be able to pass through the saturated high-air entry disk (Aung et al 2001). The axis-translation technique (Hilf, 1956) is employed in the pressure plate test to apply matric suction to soil specimens. Air pressure is supplied within the pressure vessel and the lower part of the high-air entry disk is connected to a burette of water under atmospheric pressure. Since the water pressure below the disk is atmospheric, the applied air pressure represents the applied matric suction.

2.6.4.2 Filter Paper

Filter paper can be used to measure either total or matric suction. The filter paper method is based on the premise that a filter paper will come to equilibrium with respect to moisture flow with a soil having a specific suction. When the filter paper is placed in direct contact with the soil, water will flow from the soil into the filter paper until equilibrium is achieved (Leong and Rahardjo, 2002). When the filter paper is not in contact with the soil, only water vapor flow will occur. In the contact method the filter paper measures matric suction, whereas in the noncontact method the filter paper measures total suction (Fredlund and Rahardjo, 1993).

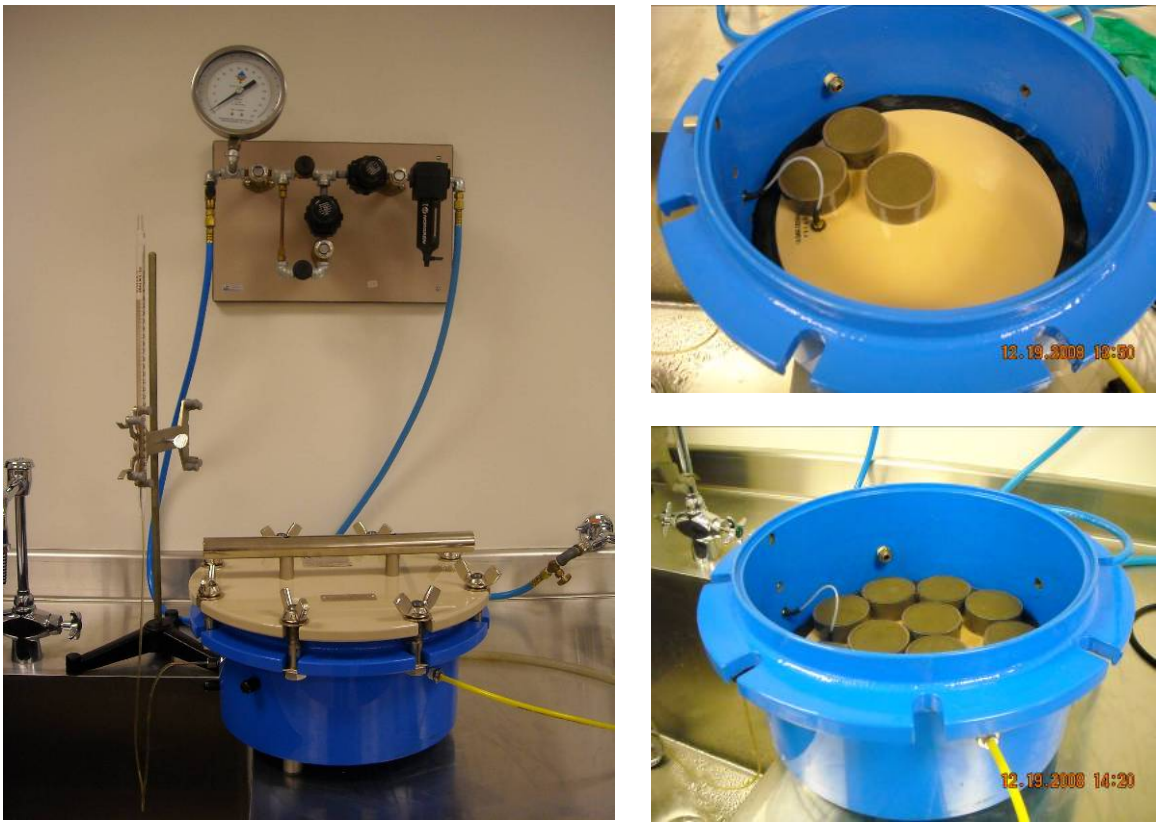

Figure 2.9 A 15 bar ceramic plate extractor.

The filter paper method measures suction indirectly, and the measurement accuracy is dependent on the moisture-suction relationship of the filter paper (Fredlund and Rahardjo, 1993). In essence, filter paper method is based on that the humidity of the filter paper will come to equilibrium with the soil having a specific suction. Equilibrium can be achieved by either liquid or vapor moisture exchange between the soil and the filter paper. Hence, the filter paper is used as a sensor which when placed in direct contact with the soil specimen, allows determining the matric suction (Figure 2.10). Theoretically, the matric suction is related to the water content of the filter paper when the paper is placed in direct contact with the water in the soil (Fredlund and Rahardjo, 1993).

On the other hand, when a dry filter paper is not in direct contact with the soil, vapor of water will flow from the soil to the filter paper until equilibrium is achieved (Figure 2.10). Due to the possible presence of dissolved salts in the soil, the water-vapor molecules have to escape from the soil not just by overcoming the matric suction in the soil but also the possible osmotic suction due to the presence of salts. Therefore, the air space left between the soil water and the filter paper provides a barrier to the salts, allowing only water vapor to flow (Marinho and Oliveira, 2006). The measure of the water content of the filter paper leads to the total suction value (Fredlund and Rahardjo, 1993).

Figure 2.11 shows the laboratory procedure followed to obtain matric suction using filter paper method.

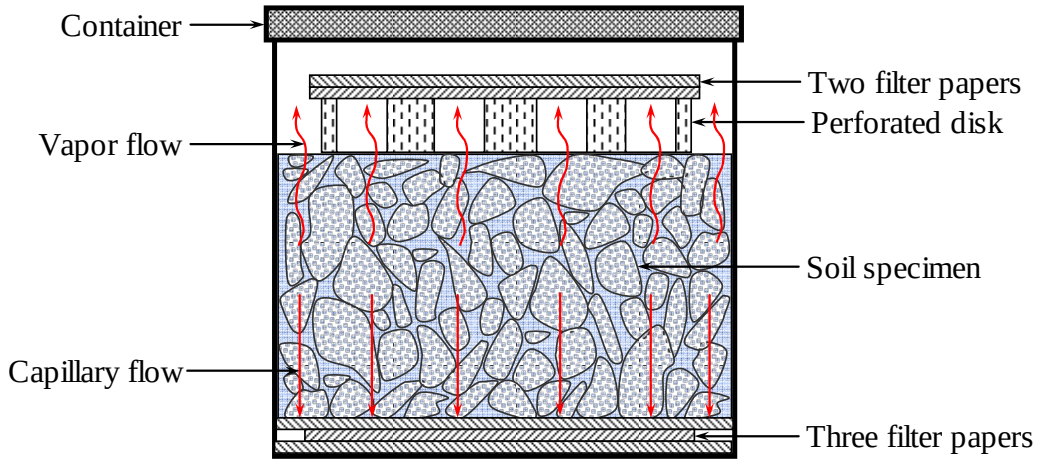

Figure 2.10 Filter paper method for measuring matric and total suction (modified from: Fredlund and Rahardjo, 1993).

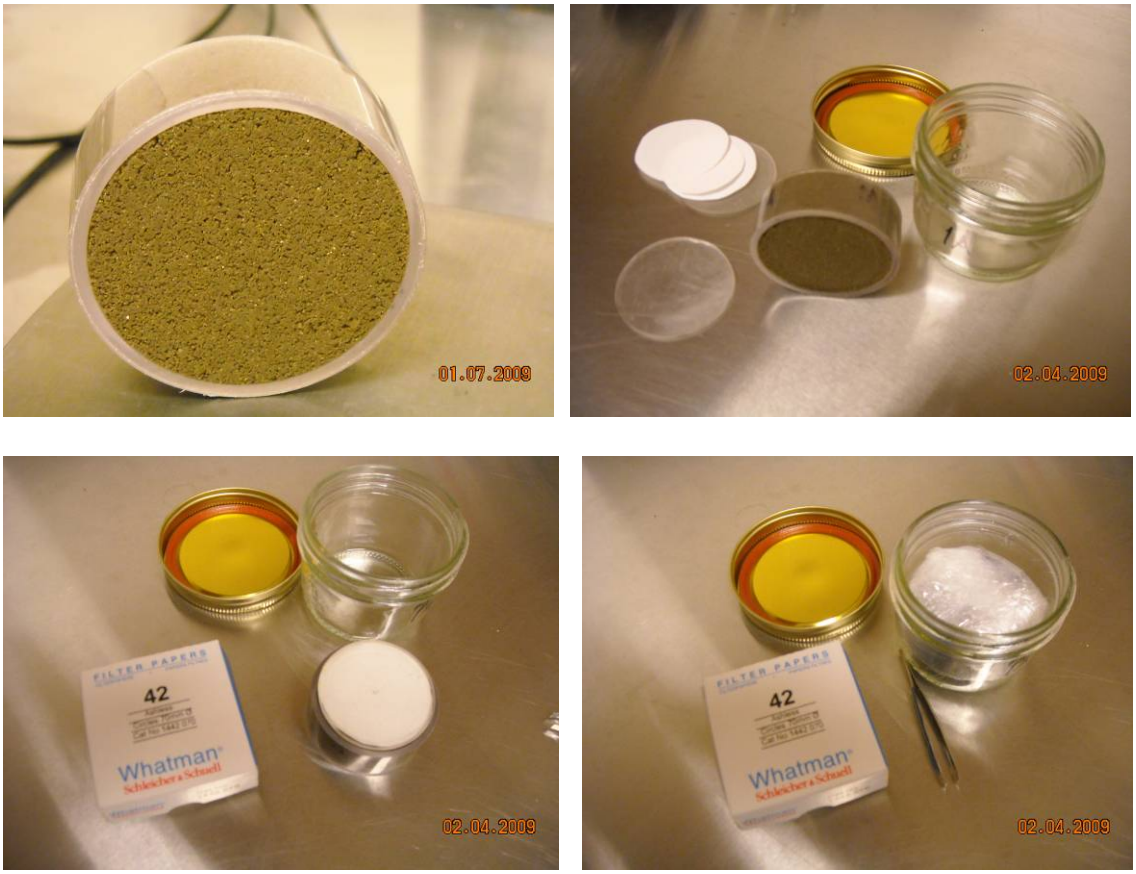

Figure 2.11 Filter paper method for measuring matric suction.

The ASTM D5298-03 standard states that “the precision of the filter paper test method is currently being evaluated”. Also, they state that “there is no accepted reference value for this test method therefore bias cannot be determined”. For that reason, the ASTM D5298-03 propose to discard filter paper results if the “difference in suction between the two filter papers exceeds 0.5 log(kPa).” Nevertheless, the filter paper method has as an advantage that it is not based on high air pressure such as the axis translation technique. This allows performing the test in environments which closely simulate in situ conditions (Ridley et al., 2003).

2.6.4.3 Calibration Equations from Filter Paper Test

The water content of the filter paper is related to a suction value though the filter paper calibration curve or equation. The calibration curve for the filter paper is the equivalent to the soil water characteristic curve for that porous material. Considering the rigorous quality control during the filter paper production, the retention curve should not change from batch to batch (Marinho and Oliveira, 2006).

The calibration curve for a specific filter paper can be obtain by measuring the water content of filter paper once it reaches equilibrium with a salt solution having a known osmotic suction (Fredlund and Rahardjo, 1993; Marinho and Oliveira, 2006; Power et al, 2008). Hence, several water contents can be plotted against their corresponding suction values to obtain the calibration curve. However, different researchers have suggested different calibration curves for the same filter paper (Fawcett and Collis-George, 1967; van Genuchten, 1980; McKeen, 1980; Hamblin, 1981; Chandler and Gutierrez, 1986; Chandler et al., 1992a; Chandler et al., 1992b;

Fredlund and Xing, 1994; Deka et al., 1995; Leong and Rahardjo, 2002; and Power et al., 2008). Furthermore, the experimental procedure of the contact filter paper method published in ASTM standard D5298-03 covers the two most commonly used filter papers, Whatman No. 42 and S&S 589. The equations for the matric suction calibration curves of Whatman No. 42 filter papers recommended by various researchers are presented Table 2.1 in plotted in Figure 2.12.

Table 2.1 Calibration equations for Whatman 42 filter paper

Author	Matric Suction Equation	Suction Rrange (kPa)
van Genuchten (1980)	$\psi = 0.051\left[\left(\frac{248}{w_{fp}}\right)^{9.651} - 1\right]^{0.473}$	N/A
Hamblin (1981)	$\log \psi = 8.022 - 3.683 \log(w_{fp})$	1 – 3000
Chandler et al. (1992b)	$\log \psi = 4.84 - 0.0622\, w_{fp}, \quad w_{fp} < 47\%$	≥ 80
	$\log \psi = 6.05 - 2.48 \log w_{fp}, \quad w_{fp} \geq 47\%$	≤ 80
Fredlund and Xing (1994)	$\psi = 0.23\left[e^{\left(\frac{268}{w_{fp}}\right)^{0.629}} - e\right]^{2.101}$	N/A
Leong and Rahardjo (2002)	$\log \psi = 4.945 - 0.0673 w_{fp}, \quad w_{fp} < 47\%$	<1000
	$\log \psi = 2.909 - 0.0229 w_{fp}, \quad w_{fp} \geq 47\%$	<1000
ASTM D5298-03 (2007)	$\log \psi = 5.327 - 0.0779 w_{fp}, \; w_{fp} < 45.3\%$	N/A
	$\log \psi = 2.412 - 0.0135 w_{fp}, \; w_{fp} \geq 45.3\%$	N/A
Power et al. (2008)	$\log \psi = 151.13 - 94.343 \log(w_{fp}), \; w_{fp} \leq 38\%$	300
	$\log \psi = 6.712 - 2.933 \log(w_{fp}), \; w_{fp} > 38\%$	20 – 300

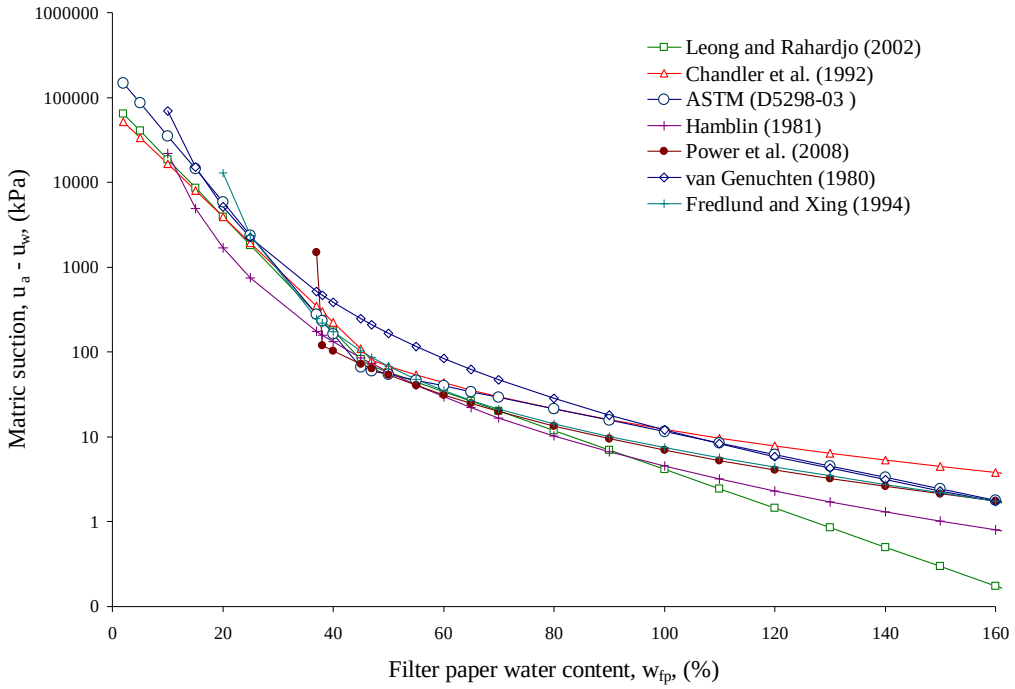

Figure 2.12 Calibration curves for Whatman No. 42 filter paper.

Several factors may affect the filter paper calibration (Leong and Rajardjo, 2002): quality of filter paper, suction source used in calibration, hysteresis and equilibration time. Since the accuracy of the filter paper method is dependent on its moisture-suction relationship, the calibration procedure for the filter papers as well as the quality control during the application of the filter paper method is very important.

2.6.5 SWCC Mathematical Models

Several empirical equations describing the soil-water characteristic curve has been established by numerous researchers (van Genuchten, 1980; Fredlund and Rahardjo, 1993; Fredlund and Xing, 1994; Fredlund and Xing, 1994; Durner, 1994; Rahardjo et al., 1995; Fredlund et al., 1996; Tzimopouos, 1996; Leong and Rajardjo, 1997; Kastanek and Nielsen, 2001; Sillers and Fredlund, 2001; Zhou and Yu, 2005;

Fredlund, 2006; Lu and Likos, 2006; Sreedeep and Singh, 2006). Many of these equations have been developed to achieve reliable estimates of the unsaturated hydraulic conductivity required for simulating fluid flow and mass transport in the unsaturated zone (van Genuchten, 1980; Lappala, et al., 1987; Tindall and Kundel, 1999; Assouline and Tartakovsky, 2001; Šimůnek and van Genuchten, 2005). Reliable estimates of the unsaturated hydraulic conductivity are particularly difficult to obtain, in part because of its extensive variability in the field, and partly because measuring this parameter is time-consuming and expensive (van Genuchten, 1980).

Although each of the proposed empirical equations can be best fit to either the dry or wetting curves (Fredlund, 2006), the most universally used model are those proposed by Brooks and Corey (1964) and van Genuchten (1980), which are discussed in this document. Due to its simplicity, the model proposed by Brutsaert (1967) is also considered as, well as the model proposed by Fredlund and Xing (1994).

The effective water content, S_e, also known as normalized water content, defined as:

$$S_e = \frac{\theta - \theta_r}{\theta_s - \theta_r} \tag{2.5}$$

where

θ = any volumetric water content

θ_s = saturated water content

θ_r = residual volumetric water content.

The effective water content can also be expressed in terms of the gravimetric water content as:

$$S_e = \frac{w - w_r}{w_s - w_r} \tag{2.6}$$

where

w = any gravimetric water content

w_s = gravimetric water content at saturation

w_r = residual gravimetric water content.

The soil-water characteristic equations suggested by Brooks and Corey (1964) is given as follows:

$$S_e = \left(\frac{\psi_b}{\psi}\right)^{\lambda}, \psi < \psi_b$$
$$S_e = 1, \psi \geq \psi_b \tag{2.7}$$

where

ψ = soil suction

S_e = effective water content as defined by Equation (2.6)

ψ_b = air-entry value of the soil

λ = pore size distribution index that is a function of soil texture

The van Genuchten (1980) equation is given as follows:

$$S_e = \left[\frac{1}{1+\left(\frac{\psi}{\alpha}\right)^n} \right]^m \qquad (2.8)$$

$$m = 1 - \frac{1}{n}$$

where

m, n, α = empirical parameters

In addition, a simple two-parameter model proposed by Brutsaert (1967) can be considered as follows:

$$S_e = \frac{1}{1+\left(\frac{\psi}{\alpha}\right)^\beta} \qquad (2.9)$$

where

α – pressure potential at which Se = 0.5

β – empirical parameter

The Fredlung and Xing (1994) equation is as follows:

$$w(\psi) = C(\psi) \frac{w_s}{\left\{ \ln\left[e + \left(\frac{\psi}{a_f}\right)^{n_f} \right] \right\}^{m_f}} \qquad (2.10)$$

$$C(\psi) = 1 - \frac{\ln\left(1+\frac{\psi}{\psi_r}\right)}{\ln\left[1+\left(\frac{1{,}000{,}000}{\psi_r}\right)\right]} \qquad (2.11)$$

a_f = soil parameter which is primarly function of the air entry value of the soil

n_f = soil parameter which is function of the rate of water extraction of the soil

m_f = soil parameter which is function of the soil water content

$C(\psi)$ = correction factor function which is function of the suction of the suction at which residual water occurs.

A list of more common equations appearing in the literature can be found in Fredlund et al. (1994), Fredlund (2006), Sillers and Fredlund (2001) and various forms of equations are evaluates for different types of soils by Leong and Rajardjo (1997).

2.7 Unsaturated Soil State Variables

To study particular aspects of soil behavior it is required to develop physical models. An example of physical model is a full-scale testing where all features of the phenomenon been studied is reproduced at full scale (Wood, 2004). However, most physical models are constructed at a reduced scale to obtain information more rapidly, reducing the cost and complexity related with full scale-testing.

Hence, the application of techniques of physical geotechnical modeling requires extrapolating the observed behavior in small physical models to the expected behavior in the full-scale prototype. Therefore, it required to understand the factors that influence the behavior of the material that are being modeled (Wood, 2004).

Considering that simple models are easier to describe and comprehend, and extra complexities can always be incorporated if necessary, the complex behavior of heterogeneous materials could be described in terms of stress-strain which has been successfully used to describe continuous materials (Beer and Watson, 1992; Wood, 2004; Smith and Griffiths, 2004; Yu, 2006). Therefore, a simplest partial description of

the structure of the soil can be made by using volumetric state variable (Fredlund and Rahardjo, 1993; Wood, 1999).

2.7.1 Volumetric Variables

Different to continuous materials, soils have a large portion of volume made up of voids. The voids may be filled with two ore more fluids, usually water and air, but also oil or gas instead or even in addition (Wood, 1999; Wood, 2004; Fredlund and Rahardjo, 1993). Hence, when a soil is deformed, it might experience significant and often irreversible changes in volume. For that reason, description of soil response must incorporate the possibility of large volumetric changes.

Considering the percentage of the void space occupied by water, which is expressed as the degree of saturation, *S*, soils can be subdivided into three groups (Fredlund and Rahardjo, 1993): (1) Dry soils where not water is present, consist of soil particles and air (i.e., $S = 0\%$) and (2) Saturated soils where all of the voids are filled with water (i.e., $S = 100\%$).

Unsaturated soils also referred as partially saturated soils can be further subdivided, depending upon whether the air phase is continuous or occluded. Thus, an unsaturated soil with a continuous air phase generally has a degree of saturation less than 80%. Occluded air bubbles commonly occur in unsaturated soils having a degree of saturation greater than 90%. The transition zone occurs when the degree of saturation is between 80% and 90%.

The water content, *w*, is defined as the ratio of the mass of water to the mass of solids in any volume of soil. On the other hand, the void ratio, *e*, is defined as the ratio

of the volume of voids to the volume of solid solids. With knowledge of the specific gravity of the soil particles, G_s, the void ratio of a saturated soil can be linked to the water content by

$$e = \frac{G_s w}{S} \tag{2.12}$$

The specific volume, v = 1 + e, which is the volume composed of a unit volume of solids with its surrounding void, defined by

$$v = 1 + e \tag{2.13}$$

In addition, the specific water volume, v_w, which is the volume composed of a unit volume of solids with its surrounding voids filled with water, is defined by

$$v_w = 1 + G_s \tag{2.14}$$

It is recommended by Wheeler and Sivakumar (1995) to be used as the parameter describing the amount of water within a soil element, rather than water content, w. Figure 2.13 shows the three phases diagram and volumetric state variables for an unsaturated soil.

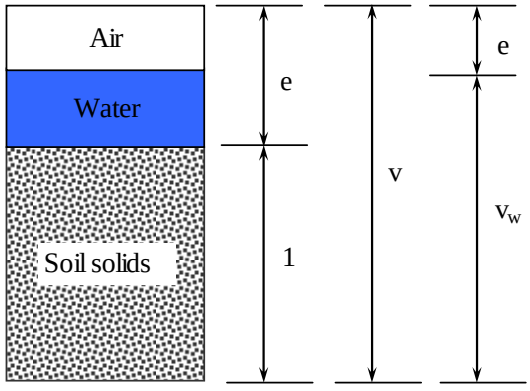

Figure 2.13 Three phases diagram and volumetric state variables for unsaturated soils (modified from: Wood, 1999).

2.7.2 Effective Stress Variables

Development of models describing the link between changes in stress and changes in strain require correct choice of strain increments and stress variables (Wood, 2004). As mention before, soils are referred as to a three-phase system (i.e. soil, water, and air phase). Therefore, volume changes are an important characteristic of the mechanical response of soils.

Effective stress, σ', has been considered a fundamental state variable for describing the state of stresses in soil (Wood, 2004; Fredlund and Rahardjo, 1993). For saturated soils, Therzaghi (1943) expressed the stress state variable controlling the soil behavior as the difference between the total stress, σ, and the pore pressure, u_w. Considering the effective stress as the stress acting on the soil skeleton of a saturated soil, the effective stress theory establishes that the effective stress controls the deformation behavior of the soil. However, two additional factors must be considered for unsaturated soils (Lu and Likos, 2004): (1) the pore air pressure, u_a, which is the stress acting through the air phase and (2) the matric suction, ψ, which is the difference between the pore air pressure, u_a, and the pore water pressure, u_w. In order to consider these factors, Bishop (1959) expanded Therzaghi's classic effective stress theory as follow (Fredlund and Rahardjo, 1993; Wood, 2004)

$$\sigma' = (\sigma - u_a) + \chi(\sigma - u_w) \qquad (2.15)$$

where

σ' = effective normal stress

σ = total normal stress

u_a = pore-air pressure

u_w = pore-water pressure

χ = a parameter related to the degree of saturation of the soil, known as effective stress parameter

The magnitude of the effective stress parameter varies between zero and unity, where χ parameter is unity for a saturated soil and zero for a dry soil (Fredlund and Rahardjo, 1993). Hence, for fully saturated soils equation 2.11 reduces to classical Terzaghi's effective stress equation ($\sigma' = \sigma - u_w$).

The first term on the right-hand side of equation 2.11 (i.e. the difference $\sigma - u_a$) is referred as the net normal stress applicable to bulk soils. On the other hand, the second term $\chi(\sigma_a - u_w)$ represents the stress due to suction linking soil particle referred as to as suction stress.

Several other equations to calculate the effective stress have been proposed (Fredlund and Rahardjo, 1993), all of them trying to incorporate a soil parameter in order to form a single-valued effective stress variable. However, experimental results have shown that there is dependence on the stress path followed (Fredlund and Rahardjo, 1993). It is possible to evaluate the magnitude of the effective stress parameter by considering the microscale forces acting between and among idealized assemblies of spherical particles under unsaturated conditions (Lu and Likos, 2004).

According to Lu and Likos (2004), the water meniscus formed between spherical particles might be described by the particle radius, R, the two radii describing

the curvature of the water phase, r_1 and r_2, and the filling angle. The two particles system also known as contacting sphere model is shown in Figure 2.14. The relationship between matric suction, $u_a - u_w$, surface tension, T_s, and the variables describing the geometry of the water meniscus between two spherical particles of identical radius R can be written as (Lu and Likos, 2004).

$$u_a - u_w = T_s\left(\frac{1}{r_1} - \frac{1}{r_2}\right) \tag{2.16}$$

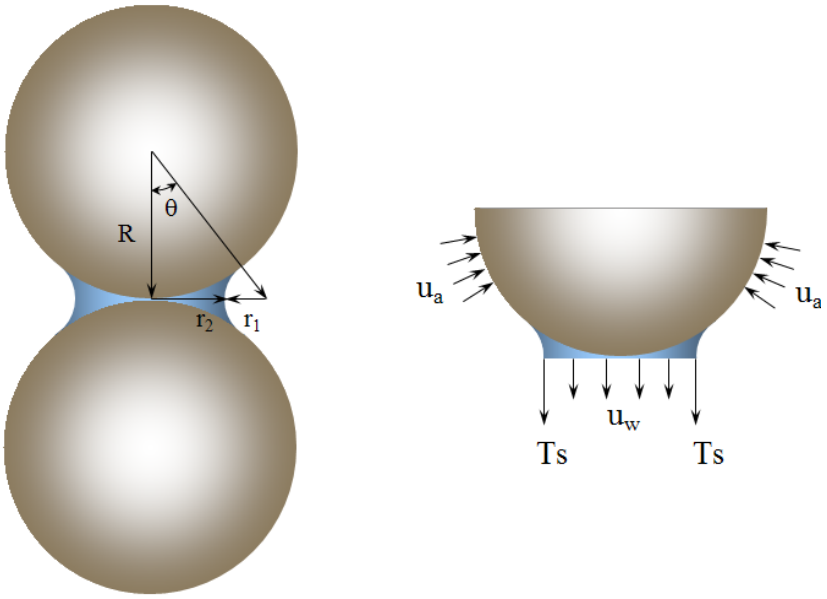

Figure 2.14 Air-water-solid interaction for two spherical particles and water meniscus (modified from: Lu and Likos, 2004).

The relationships between r_1, r_2, R, θ, and contact angle α is given by (Lu and Likos, 2004)

$$r_1 = R\frac{1-\cos\theta}{\cos(\theta+\alpha)} \tag{2.17}$$

$$r_2 = R\tan\theta - r_1\left(1 - \frac{\sin\alpha}{\cos\theta}\right) \quad (2.18)$$

As shown in Figure 2.15 two different packing orders for uniform spherical particles can be considered as two limit cases. The losses possible packing of a soil can be represented by considering an idealized material comprised of uniform spherical particles organized in a simple cubic (SC) packing. On the other hand, the densest possible packing can be represented by considering an idealized material comprised of uniform spherical particles organized in a simple tetrahedral (TH) packing (Lu and Likos, 2004).

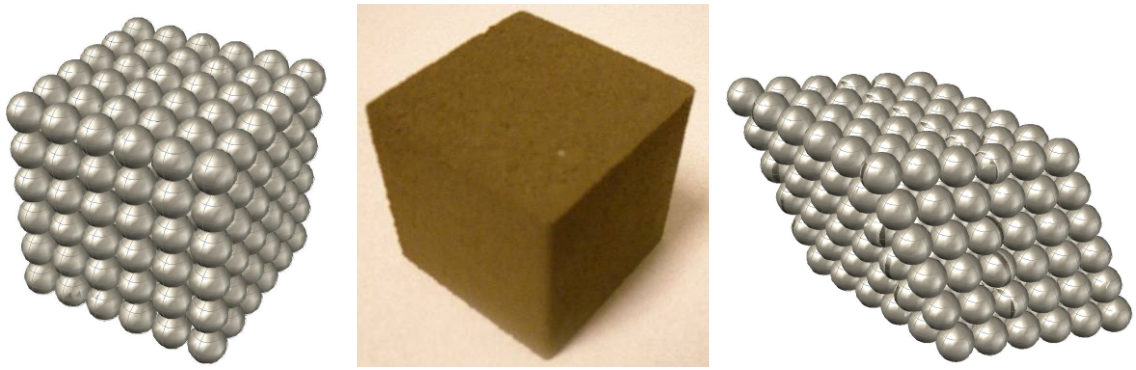

(a) (b)

Figure 2.15 Packing order for uniform spherical particles: (a) simple cubic packing representing the loosest packing order, and (b) tetrahedral packing representation densest packing order (modified from: Lu and Likos, 2004).

The water content of an idealized soil of uniform spherical particles organized in a simple cubic (SC) packing can be written in terms of the filling angle, θ, and contact angle, α, as (Lu and Likos, 2004)

$$w_{SC} = \frac{9}{2G_s}\left[\sin^2\theta - \sin^2\theta\cos\theta - \frac{1}{3}(1-\cos\theta)^2(2+\cos\theta) - \frac{V_r}{2\pi R^3}\right] \quad (2.19)$$

where

$$V_r = \pi r_1^2 \left[r_2 + r_1 - \frac{2r_1 \cos^3(\theta+\alpha)}{\frac{3\pi}{2} - (\theta+\alpha) - \sin(\theta+\alpha)\cos(\theta+\alpha)} \right] \left[\pi - 2(\theta+\alpha) - \sin 2(\theta+\alpha) \right] \tag{2.20}$$

G_s = specific gravity

The gravimetric water content in a TH packing is twice that of SC packing (i.e. $w_{TH} = 2W_{SC}$)

As shown in Figure 2.16, Equation 2.15 can be used to evaluate the effect of the contact angle, a, on the water content on an idealized soil. For both SC and TH packing, larger contact angles result in larger values for water content.

The effective stress parameter, χ, as a function of filling angle, θ, and contact angle, α, can be calculated by (Lu and Likos, 2004)

$$\chi = \left[\tan\theta - \frac{1-\cos\theta}{\cos(\theta+\alpha)} \frac{\cos\theta - \sin\alpha}{\cos\theta} \right]^2 \frac{\tan\theta + \left(\frac{\sin\alpha}{\cos\theta} \right) \frac{1-\cos\theta}{\cos(\theta+\alpha)}}{\tan\theta - \left[2 - \frac{\sin\alpha}{\cos\theta} \right] \frac{1-\cos\theta}{\cos(\theta+\alpha)}} \tag{2.21}$$

According to equation (2.17), large contact angles, a, result in large values of χ. Figure 2.17 and Figure 2.18 shown that χ exceeds unity which is contrary to previous experimental results (Lu and Likos, 2004).

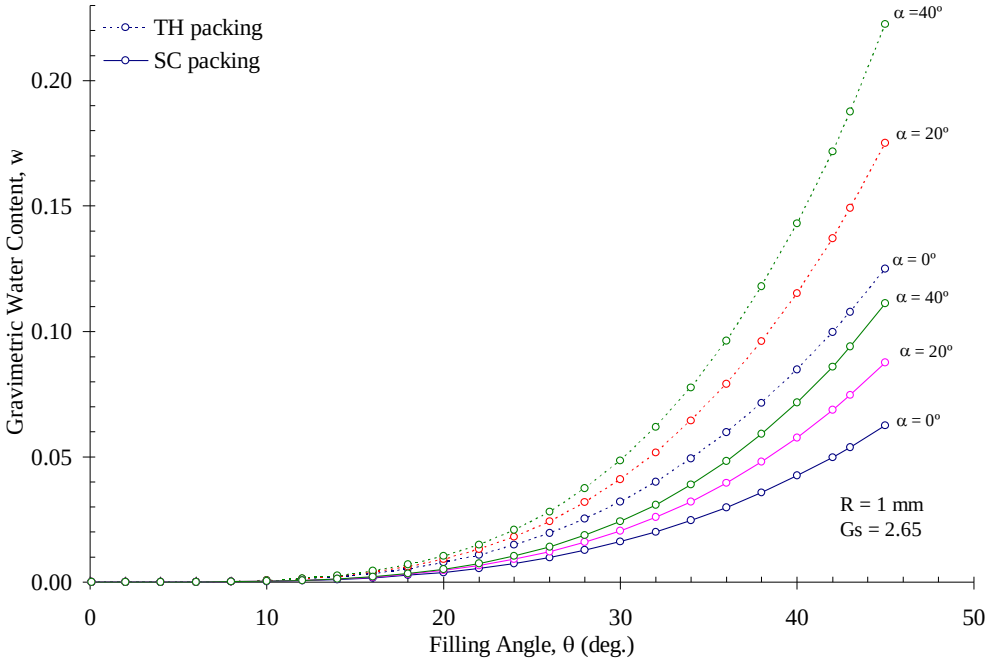

Figure 2.16 Effect of the contact angle, α, on the gravimetric water content for simple cubic (SC) and tetrahedral (TH) packing (modified from: Lu and Likos, 2004).

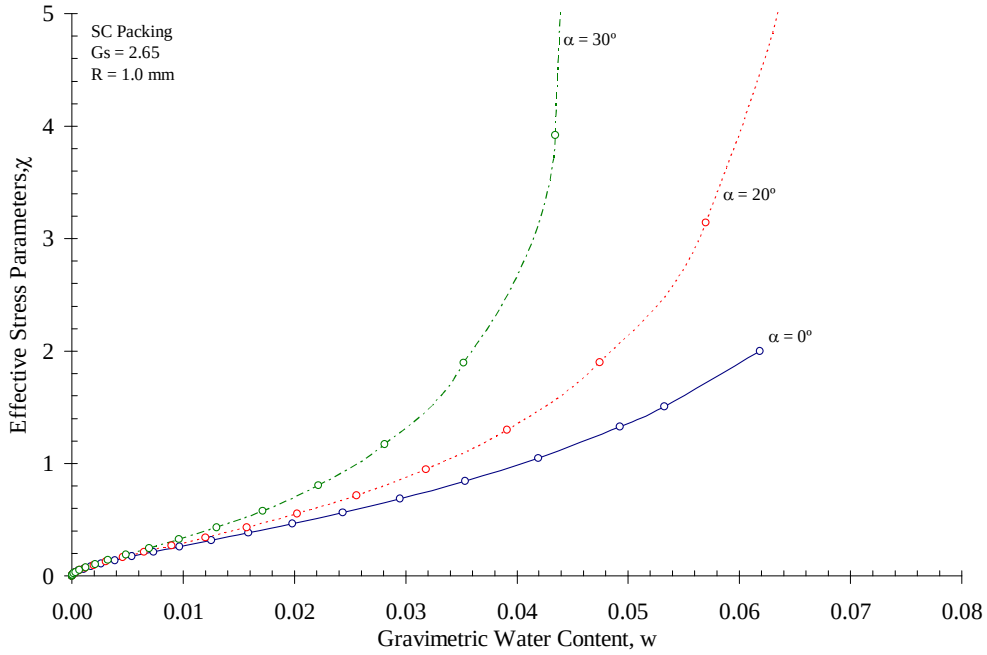

Figure 2.17 Theoretical relationship between water content, *w*, and effective stress parameter, χ, for particles in SC packing (modified from: Lu and Likos, 2004).

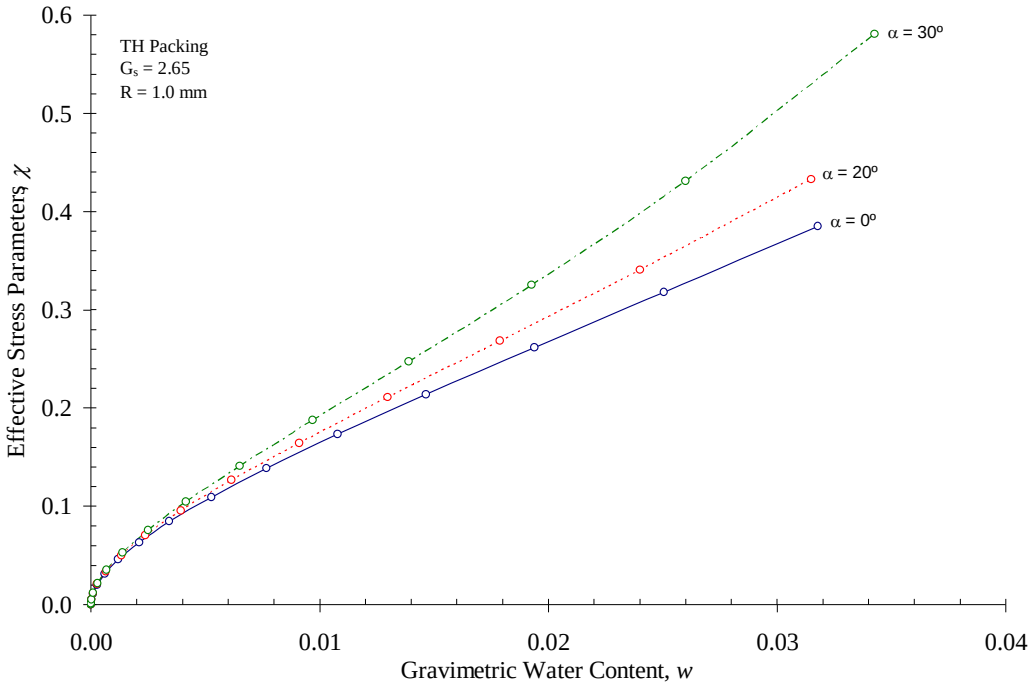

Figure 2.18 Theoretical relationship between water content, *w*, and effective stress parameter, χ, for particles in TH packing (modified from: Lu and Likos, 2004).

2.8 Stress Tensor Representation

Generally, unsaturated soils are modeled within the framework of continuum solid mechanics, which is concerned with the mechanical behavior of solids on the macroscopic scale (Yu, 2006). Continuum solid mechanics ignores the discrete nature of matter and treats materials as uniformly distributed and generally isotropic. Stresses are forces per unit area inside the solid. They can be visualized by cutting the solid in a particular plane (i.e. x-y, x-z, y-z). Figure 2.19 shows the stresses acting on an infinitesimally small cube. There are three normal stress components, one in each coordinate direction (σ_x, σ_y, σ_z), and three shear stress components (τ_{xy}, τ_{xz}, τ_{yz}).

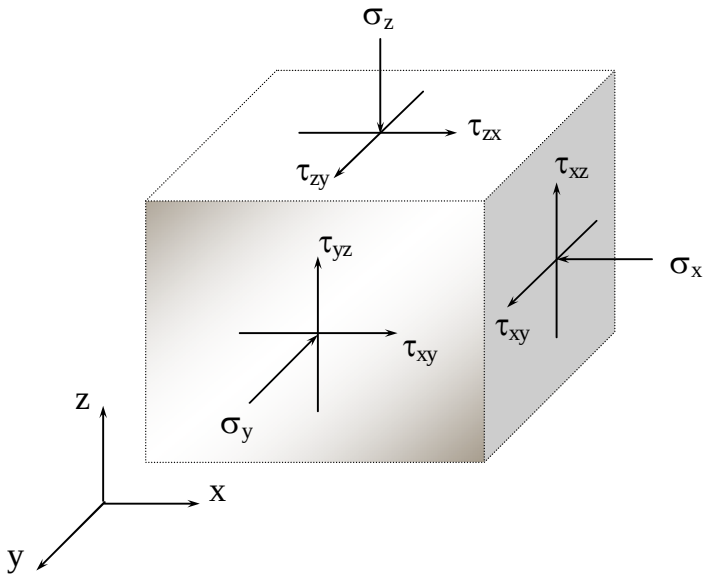

Figure 2.19 Stresses acting on an infinitesimal cube.

The state of stress on a soil can be described by three stress variables namely, the total stress, σ, the pore-air pressure u_a, and the pore-water pressure u_w (Fredlund and Morgenstern, 1977; Fredlund and Rahardjo, 1993; Li, 2003; Wood, 2004; Tarantino and Mongiovi, 2005). Usually these three stress variables can be reduced to two stress state variables by assuming that the soil particles and water are incompressible and thus eliminating the stress state variable u_a (Fredlund and Morgenstern, 1977; Lu and Likos, 2004).

In dry soils the stress variables are the principal stress in each coordinate direction and the pore-air pressure (Lu and Likos, 2004). Hence, as shown in Figure 2.20, the stress state variable in dry soil is the net normal stress, which is the difference between the total normal stress and the pore-air pressure ($\sigma - u_a$). On the other hand, in saturated soils the stress state variables are the principal stress in each coordinate

direction and the pore water pressure (Lu and Likos, 2004). Thus, the stress state variable in this case is the Terzaghi's classic stress, which is the difference between the total normal stress and the pore-air pressure ($\sigma' = \sigma - u_w$). Figure 2.21 shows the stress state variables for a cubic element of fully saturated.

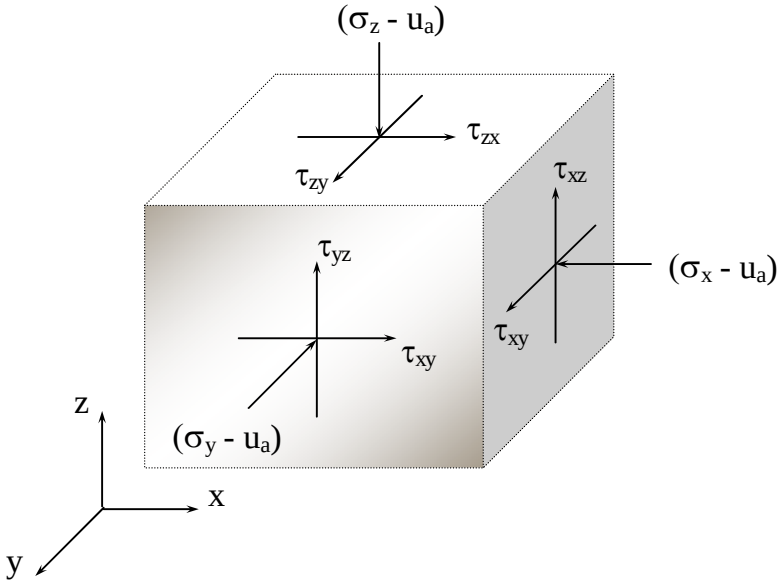

Figure 2.20 Normal and shear stress on a cubical element of dry soil.

Unsaturated soil behavior is more complicated than saturated soil behavior. However, unsaturated soil mechanics may be effectively approached as an extension of saturated soil mechanics assuming that the state of stress can be described by two independent stress state variables namely, net normal stress, $\sigma - u_a$, and matric suction, $u_a - u_w$ (Figure 2.22). These two variables are commonly referred to as state stress variables for an unsaturated soil (Fredlund and Morgenstern, 1977; Fredlund and Rahardjo, 1993).

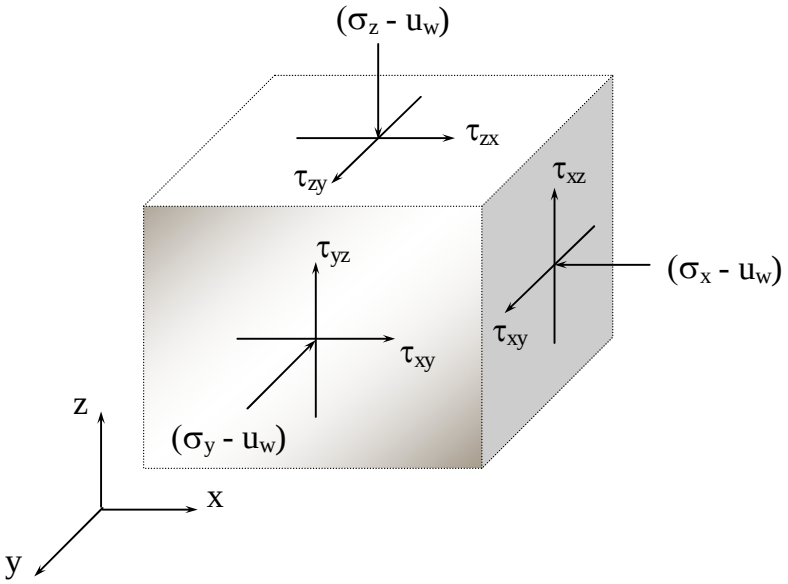

Figure 2.21 Normal and shear stress on a cubical element of fully saturated soil.

Therefore, in accordance with the continuum solid mechanics methodology, the stress state variables can be represented in three-dimensional space as two independent tensors. The normal stress tensor, $\sigma_{ij} - u_a\delta_{ij}$, with δ_{ij} being the Kronecker delta

$$\sigma_{ij} - u_a\delta_{ij} = \begin{bmatrix} \sigma_x - u_a & \tau_{yx} & \tau_{zx} \\ \tau_{xy} & \sigma_y - u_a & \tau_{zy} \\ \tau_{xz} & \tau_{yz} & \sigma_z - u_a \end{bmatrix} \tag{2.22}$$

and the matric suction tensor, $(u_a - u_w)\delta_{ij}$

$$(u_a - u_w)\delta_{ij} = \begin{bmatrix} u_a - u_w & 0 & 0 \\ 0 & u_a - u_w & 0 \\ 0 & 0 & u_a - u_w \end{bmatrix} \tag{2.23}$$

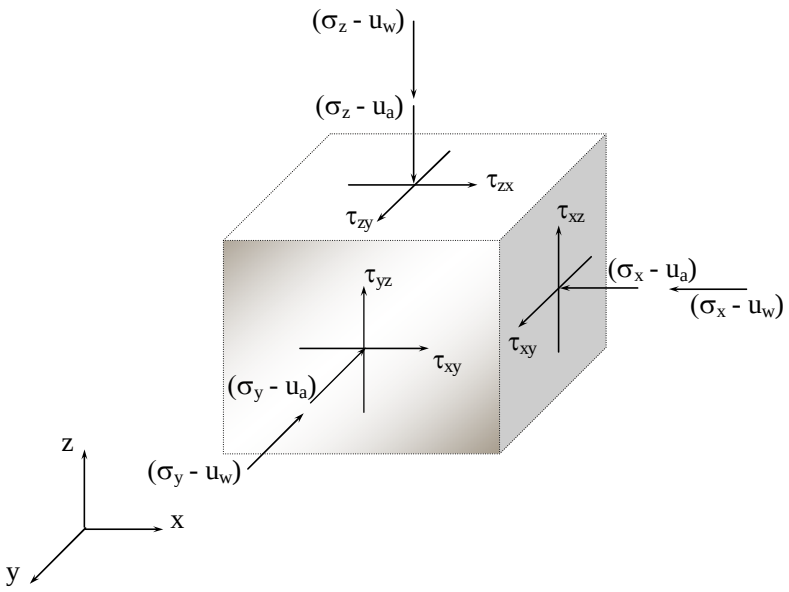

Figure 2.22 Normal and shear stress on a cubical element of unsaturated soil.

2.9 Axis Translation Technique

As mentioned before, soil suction is one of the two variables that control the behavior of unsaturated soils (Fredlund and Morgenstern, 1977; Fredlund et al, 1994; Lu and Likos, 2004). The volume of water in an unsaturated soil is determined by the suction present in the soil. Therefore, matric suction is an important variable in describing the state of stress in an unsaturated soil. Consequently, measurement or control of matric suction is essential when the behavior of an unsaturated soil is been evaluated for different conditions of stress. However, the measurement and control of negative pore-water pressure has practical limitations (Lu and Likos, 2004).

Cavitation is a phenomenon which occurs when water pressure goes below -1 amt. As cavitation take place, the water phase in both soil and measurement systems become discontinuous, forcing the water to move from the measurement systems into

the soil making the measurements unreliable (Fredlund and Rahardjo, 1993). For that reason, alternatives to measure or control of negative water pressures less than -1 atm are desirable.

In general, the axis translation technique consists on elevating pore air pressure in the unsaturated soil while the pore-water pressure maintain at atmospheric pressure. Hence, the matric suction, $u_a - u_w$, may be controlled over a range greater than the cavitation limit for water under negative pressure (Lu and Likos, 2004). The procedure involves the translation of the origin of reference (i.e. axis) for the matric suction (Hilf, 1956; Fredlund, 1989; Lu and Likos, 2004). Therefore, the pore-water pressure can be referenced to a positive air pressure rather than negative pressure. In this manner, matric suction can be easily controlled by applying and measuring positive air pressure.

The axis translation technique requires the control of the pore-air pressure and the control or measurement of the pore-water pressure. This process is accomplished by separating the air and water phase of the soil using a saturated high-air-entry (HAE) material, usually a ceramic disk. The high air entry material is a porous material which when saturated allows free advection of water but prevent the advection of free air.

In order to establish the matric suction adequately it is essential to guaranty continuity between the water in the soil and the water in the ceramic disk. Therefore, by placing a soil specimen in good contact with a HAE material, positive air pressure can be applied to the sample on one side of the HAE material, increasing the pore-air pressure, while allowing the pore water to drain freely through the pores of the HAE material to the other side, which is maintained under atmospheric pressure. Drainage

continues until the water content of the specimen reaches equilibrium with the applied matric suction. The pressure in the soil specimen, which is the induced matric suction, must not exceed the air entry value of the HAE material. The entry value for a HAE material range between 0.5 bars (50.5 kPa) up to 15 bars (1515 kPa) for ceramic disks (Fredlund and Rahardjo, 1993) and can be as high as 10,000 kPa for special cellulose membranes (Lu and Likos, 2004).

2.10 Shear Strength and Extended Mohr-Coulomb Failure Envelope

Strength can be defined as the ability of a material to carry stresses (Wood, 2004). The shear strength of soils may be defined as "the maximum internal resistance per unit area that the soil is capable of sustaining along the failure plane under external or internal stress loading" (Lu and Likos, 2004). For saturated soils, shear strength is described using the Mohr-Coulomb failure criterion, which defines shear strength in terms of the material variables and effective stress as (Terzaghi, 1936)

$$\tau_f = c' + (\sigma_f - u_w)_f \tan\phi' \qquad (2.24)$$

where

τ_f = shear stress on the failure plane at failure

c' = effective cohesion

$(\sigma_f - u_w)_f$ = effective normal stress on the failure plane at failure

σ_f = total normal stress on the failure plane at failure

u_w = pore-water pressure at failure

ϕ' = effective angel of internal friction.

Mohr's circles can be used to represent the state of normal and shear stress acting on any plane in a soil element. As shown in Figure 2.23, Equation (2.24) defines a line with a slope equal to tanϕ'. This line is commonly referred as the failure envelope, which represents all the possible combinations of shear stress and normal stress on the failure plane at failure. For some state of stress, the tangent point on the Mohr's circle at failure represent the stress state on the failure plane at failure. Hence, the failure envelope is obtained by plotting a line tangent to a series of Mohr's circles representing failure condition. Therefore, if the Mohr's circle for a specific state of stress falls entirely below the failure envelope, the shear strength is not exceeded and the soil mass remains stable.

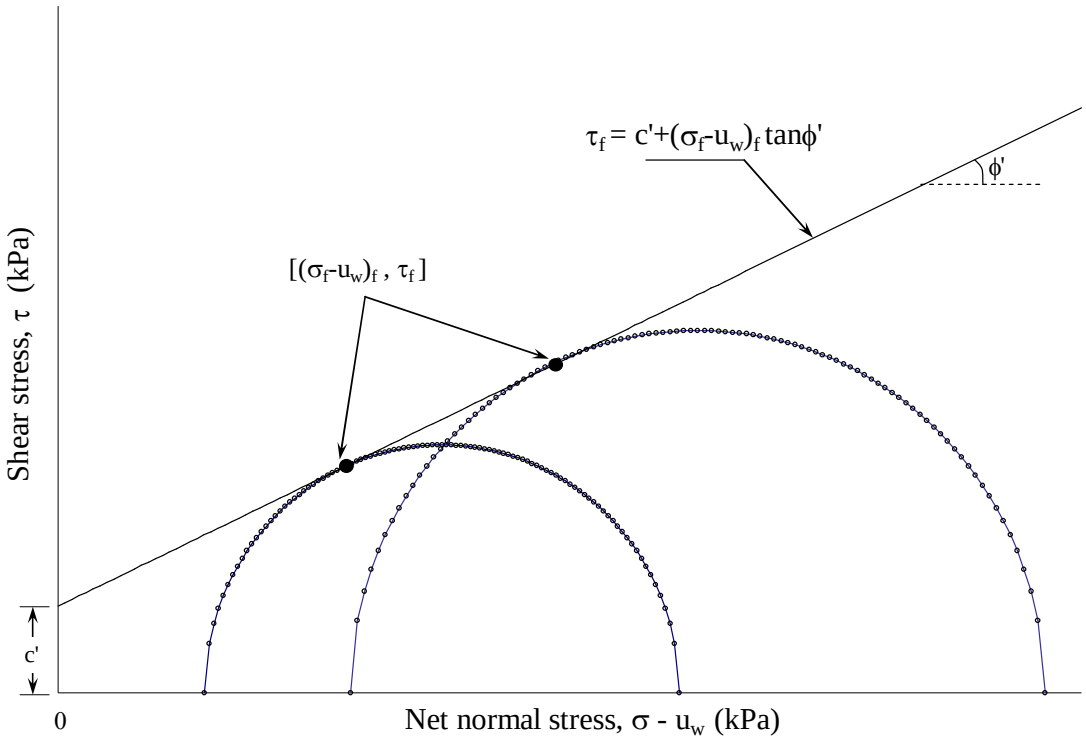

Figure 2.23 Mohr-Coulomb failure envelope for a saturated soils.

Fredlund et al. (1978) proposed the so called extended Mohr-Coulomb criterion to determine the shear strength of unsaturated soils in terms of two stress state variables (i.e. net normal stress, $\sigma - u_a$, and matric suction, $u_a - u_w$). Hence, the shear stress may be calculated by

$$\tau_f = c' + (\sigma_f - u_a)_f \tan\phi' + (u_a - u_w)_f \tan\phi^b \qquad (2.25)$$

where

c' = effective cohesion, which is the shear strength intercept when the net normal stress and the matric suction are equal to zero

$(\sigma_f - u_a)_f$ = net normal stress state on the failure plane at failure

u_a = pore-air pressure on the failure plane at failure

ϕ' = effective angel of internal friction associated with the net normal stress state variable, $(\sigma_f - u_a)_f$

$(u_a - u_w)_f$.=matric suction on the failure plane at failure

ϕ^b = angle describing the rate of increase in shear strength associate with matric suction, $(u_a - u_w)_f$.

As shown in Figure 2.24, the first two terms on the right hand side of above equation describes the Mohr's Coulomb failure envelope for unsaturated soils on the shear stress, τ, and normal stress, $\sigma - u_a$, plane. The third term incorporates the increase in shear strength with increasing matric suction.

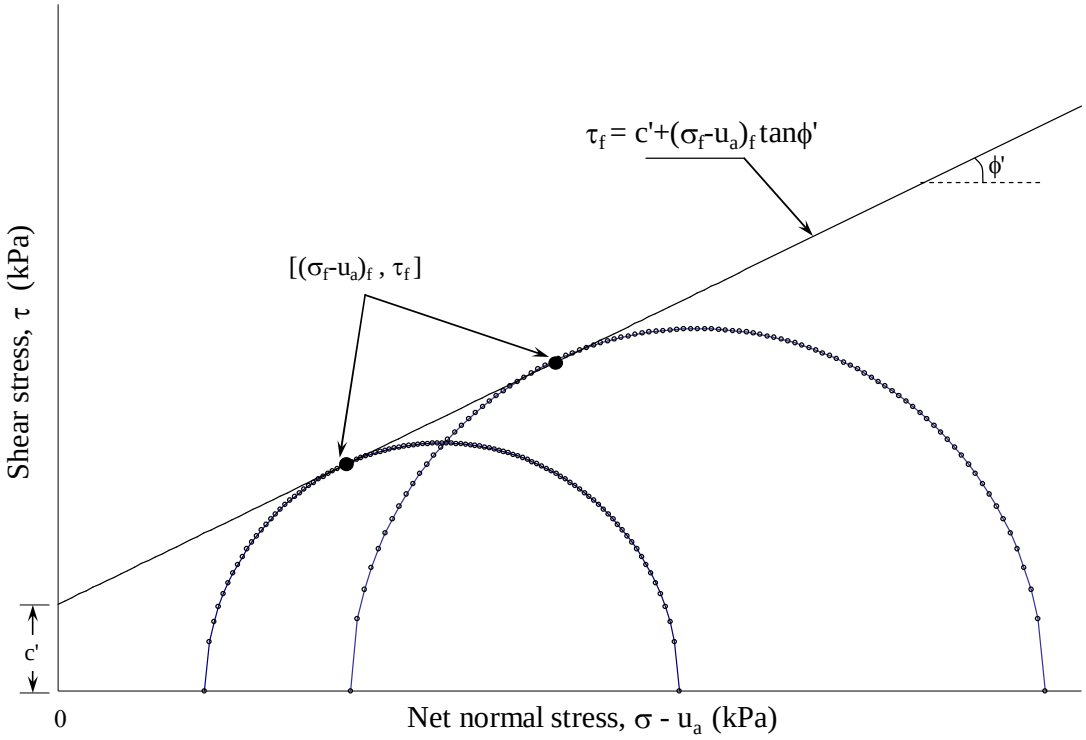

Figure 2.24 Mohr-Coulomb failure envelope for a unsaturated soils.

The failure envelope for an unsaturated soil is obtained by plotting a series of Mohr' circles corresponding to a failure condition in a three dimensional space (Figure 2.25). Different to saturated soils where the Mohr's circles are plotted with respect to effective stress axis, $\sigma - u_w$, the Mohr's circles for unsaturated soils are plotted with respect to the net normal stress axis, $\sigma - u_a$ (Figure 2.24). However, the location of the Mohr; circle plotted in the third dimension is a function of the matric suction. The matric suction axis extends orthogonally from the shear stress versus net normal stress plane. The surface tangent to the whole Mohr's circles at failure is referred to as the extended Mohr Coulomb failure envelope for unsaturated soils (Figure 2.26). This plane defines the shear strength for an unsaturated soil. The frontal plane represents a

saturated soil (i.e. matric suction is zero) and the intersection line between the extended Mohr Coulomb failure envelope and the frontal plane is the failure envelope for the saturated condition.

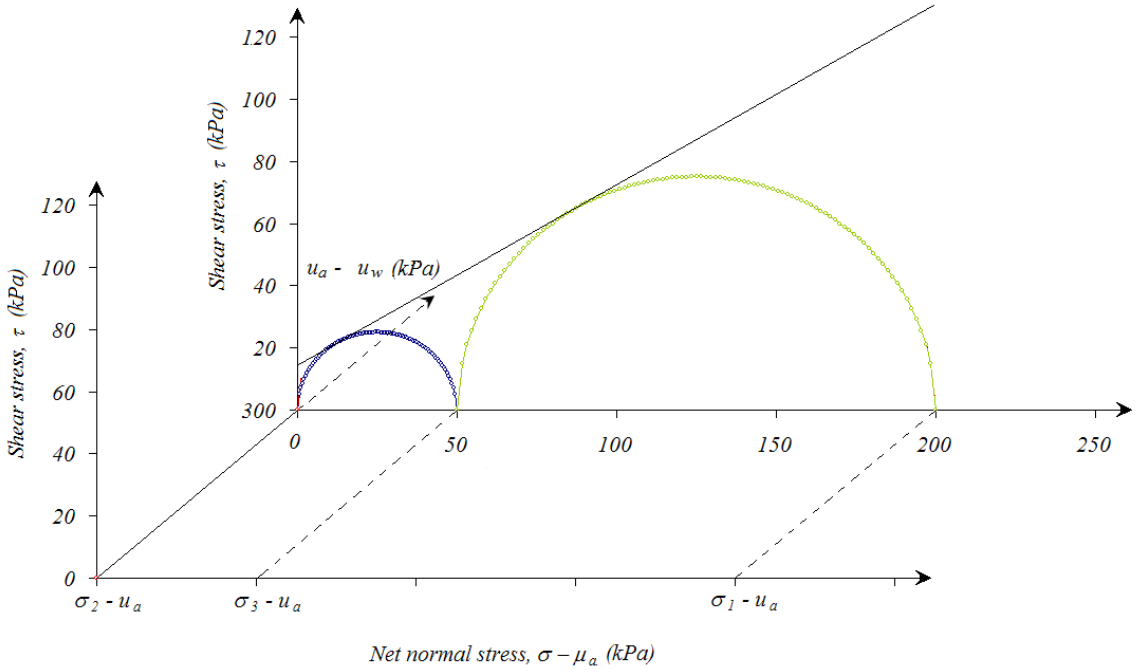

Figure 2.25 Mohr'circle failure envelope for unsaturated soils.

As shown in Figure 2.27, the horizontal projection of the failure surface for a constant matric suction results in a series of contours in the space of net normal stress, $\sigma - u_a$, and shear stress, τ,. Each line has different cohesion intercept, c_i, which is a function of the corresponding matric suction. Hence, for a matric suction equal to zero the intercept (i.e. c_o in Figure 2.27) becomes the effective cohesion, c'. I addition, all contours have the same slope angle, ϕ', as long as the failure plane is planar (Fredlund and Rahardjo, 1993). Thus the shear strength for a specific matric suction at failure can be calculated as

$$\tau_f = c_i + (\sigma_f - u_a)_f \tan\phi' \qquad 2.26$$

where

c_i = total cohesion also called the apparent or total cohesion for each matric suction

$$c_i = c' + (u_a - u_w)_f \tan\phi^b \qquad 2.27$$

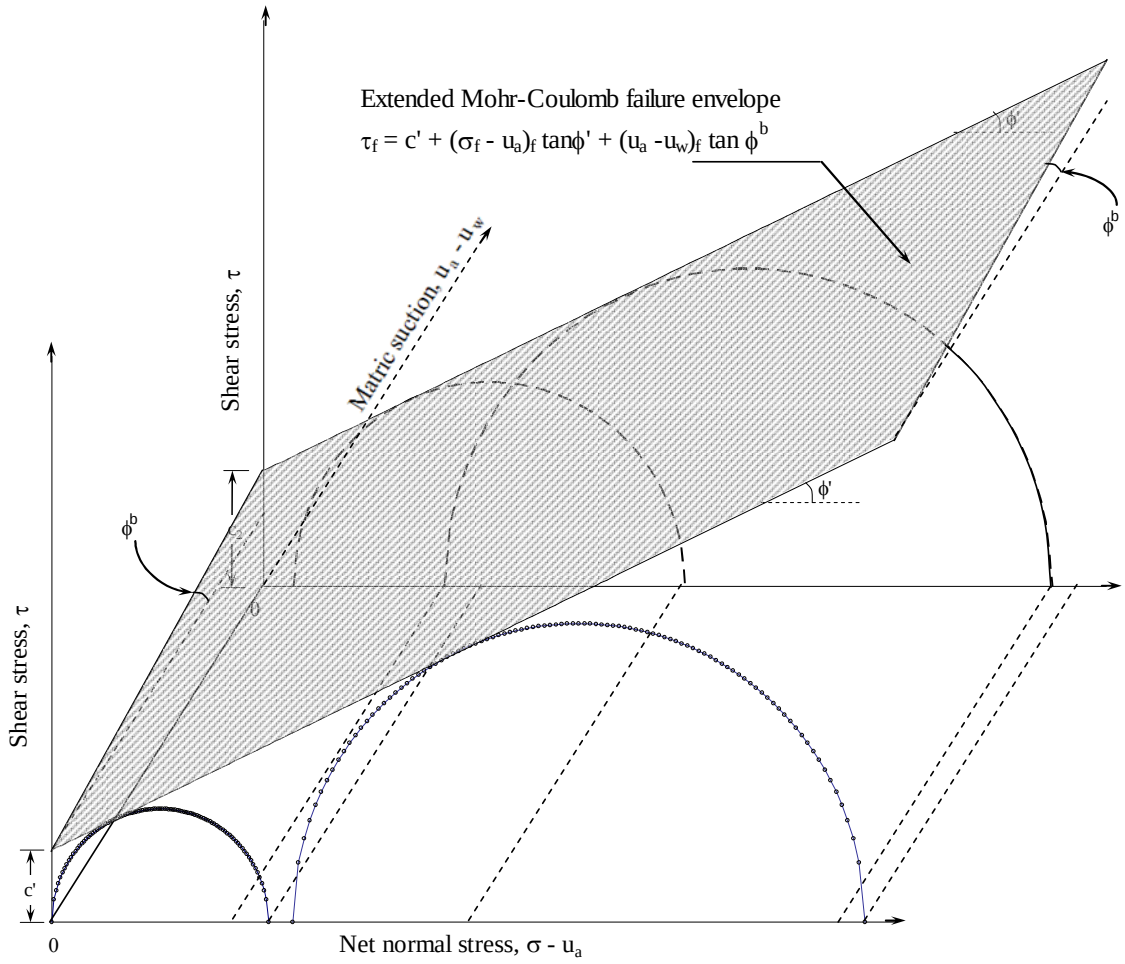

Figure 2.26 Extended Mohr-Coulomb failure envelope for unsaturated soils (modified from: Fredlund and Rahardjo, 1993).

On the other hand, the projection of the failure surface for constant net normal stress, $\sigma - u_a$, results in a series of contours in the space of matric suction, $\sigma - u_w$, and shear stress, τ, as illustrated in Figure 2.28. The line intercepts can be calculated by

$$c = c' + (\sigma_f - u_a)_f \tan \phi' \qquad 2.28$$

Although the extended Mohr-Coulomb criterion can adequately describe the behavior of unsaturated soils, it has some limitations. According to Vanapalli et al. (1996) the shear strength can be adequately described using the extended Mohr-Coulomb criterion for values of matric suction below the air entry value of the soil. However, The increase in shear strength becomes no linear between the air entry value and the suction corresponding to residual water content condition (Gan et al., 1988; Escario et al., 1989; Vanapalli et al., 1996; Fredlund et al. 1996).

To describe a physical process, it is necessary to observe and understand its characteristics and the conditions under which it occurs. Hence, it is convenient to determine qualitatively the variables influencing the process and what relations exist between them. Furthermore, it is appropriate to establish the connections and mutually operative conditions affecting the variables which, under given circumstances, are reproducible (Muller, 1978). Therefore, measurements are necessary to allow a comparison of these observations. This is achieved with the aid of suitable physical processes using units or comparative standard (Greca and Moreira, 2001). The physical quantities observed are mapped to facilitate the comparison between different observed quantities or with a defined variable of the same kind.

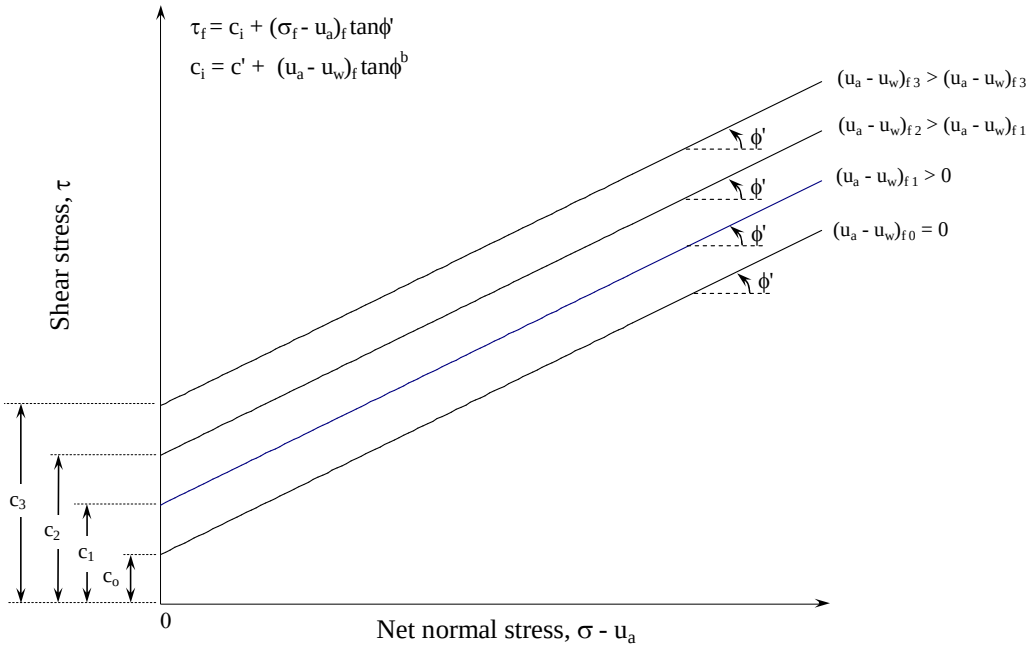

Figure 2.27 Contour lines of failure envelope on the t versus $\sigma - u_a$ plane (modified from: Fredlund and Rahardjo, 1993).

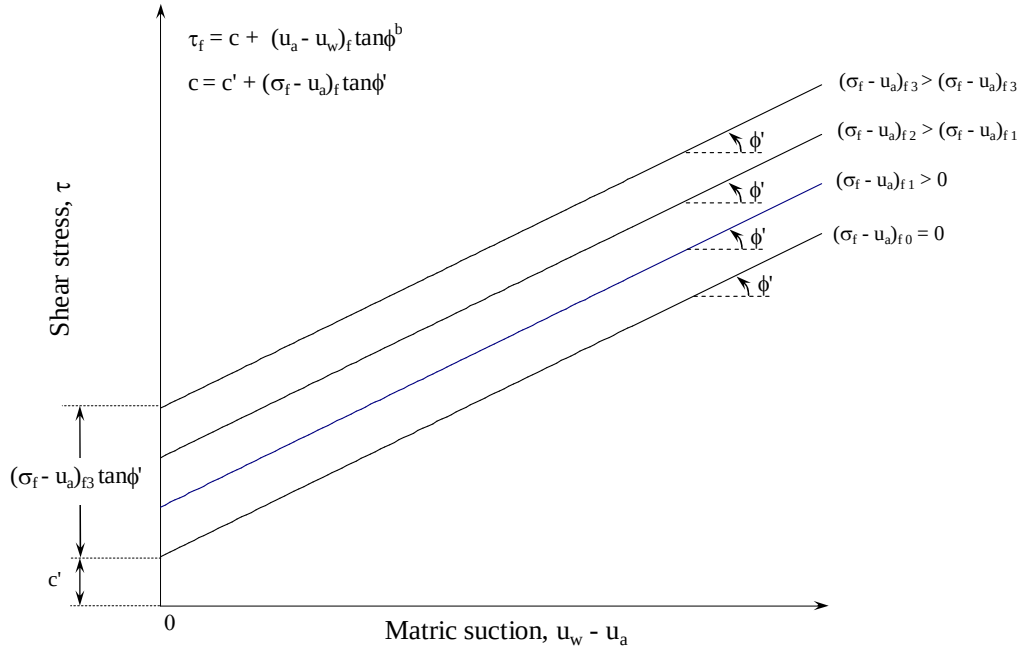

Figure 2.28 Contour lines of failure envelope on the t versus $u_w - u_a$ plane (modified from: Fredlund and Rahardjo, 1993).

To study particular physical processes some times it is required to use models. Minshull (1975) states that a model can be a theory, law, hypothesis, structured idea, equation, reasoning or synthesis of data. According to Wood (2004), “a model is an appropriate simplification of reality.” Therefore, a model may also be a physical representation or abstraction of the reality.

Next chapter briefly describes the original Cam clay model (Roscoe and Schofield, 1963), and the modified Cam clay model (Roscoe and Burland, 1968) both of which have been used as the basis fro describing the constitutive behavior of saturated soils. In addition, a brief description of the Barcelona Basic Model –BBM (Alonso et al., 1990), the Modified Barcelona Basic Model –MBBM (Josa et al., 1992), and the Oxford Model –OM (Wheeler and Sivakumar, 1995) is included in next chapter. These three models have been proposed to describe the constitutive behaviour of partially saturated soils.

CHAPTER 3

CONSTITUTIVE MODELING OF UNSATURATED SOIL BEHAVIOUR

3.1 Introduction

To describe a physical process, it is necessary to observe and understand its characteristics and the conditions under which it occurs. Therefore, it is convenient to determine qualitatively the variables influencing the process and what relations exist between them. Furthermore, it is appropriate to establish the connections and mutually operative conditions affecting the variables which, under given circumstances, are reproducible (Muller, 1978). Measurements are necessary to allow a comparison of these observations. This is achieved with the aid of suitable physical processes using units or comparative standard (Greca and Moreira, 2001). The physical quantities observed are mapped to facilitate the comparison between different observed quantities or with a defined variable of the same kind.

To study particular physical processes some times it is required to use models. Minshull (1975) states that a model can be a theory, law, hypothesis, structured idea, equation, reasoning or synthesis of data. According to Wood (2004), “a model is an appropriate simplification of reality.” Therefore, a model may also be a physical representation or abstraction of the reality.

Generally, to study particular aspects of soil behavior it is required to perform physical modeling. An example of physical modeling is a full-scale testing where all

features of the phenomenon been studied are reproduced at full scale (Wood, 2004). This kind of representation is usually referred as field testing. However, in representations with models, nonessential elements, or variables which do not have a particular influence on the nature of the process are disregarded or neglected (Muller, 1978). Consequently, a process under consideration can be represented by a simplified physical process or physical model. In this manner, it is possible to even go so far as "to represent one process onto another physical process which has nothing more in common with the original than a formally identical mathematical description" (Muller, 1978). This simplification of the reality let us to create a system where is easier to measure the so called essential variables and consider just the necessary elements abstracted from the process in consideration. Hence, most physical models are constructed at a reduced scale to obtain information more rapidly, reducing the cost and complexity related with full scale-testing.

Once the model has been conceived and measures have been taken, it is necessary to establish the mathematical relationship between the variables. To do this, it is convenient to create a mental model of the process and then represent it analytically. The analytical function or functions describing the process permit to represent the physical event by a numerical analogous procedure (Muller, 1978). In other words, it is possible to use a mathematical model to describe the physical process. Mathematical models are extremely powerful because they usually allow making prediction about a process. The predictions may provide information for further experimentation or model improvements.

The application of techniques of physical geotechnical modeling requires extrapolating the observed behavior in small physical models (i.e. reduced scale prototype) to the expected behavior in the full-scale prototype. Therefore, it required to understand the factors that influence the behavior of the material that are being modeled. Considering that natural soils are heterogeneous and some of their properties are likely to vary from place to place. It could seem unlikely that the behavior of heterogeneous materials could be described in terms of stress-strain which has been successfully used to describe continuous materials (Beer and Watson, 1992; Wood, 2004; Smith and Griffiths, 2004; Yu, 2006). However, different authors have proposed several models to represent the soil behaviour relating stress state variables (Roscoe and Schofield, 1963; Roscoe and Burland, 1968; Fredlund and Morgenstern, 1977; Lloret et al., 1987; Lade and Nelson, 1987; Alonso et al., 1990; Gens and Alonso 1992; Alonso et al., 1994; Shuai and Fredlund, 1998; Alonso et al., 1999; Matsuoka et al., 2002; Matsuoka and Hajime, 2006; Sun et al., 2006; Yao et al., 2008)

3.2 Critical State Theory

"The critical state theory assumes that soils under stress ultimately reach a state of plastic behaviour characterized by continuous deformation without further increase in stress" (Adams, 1996.).

According to Yu (2006), it is possible to say that the critical state soil mechanics theory may be regarded as the ultimate state anticipated by Drucker et al. (1957). However, the concept of critical state emerged from the observed behaviour of saturated clay based on limited triaxial data obtained on reconstituted clay (Roscoe et al., 1958;

Roscoe and Schofield 1963; Roscoe and Burland, 1968). The approach initially proposed as a framework for representing shear and volume changes behaviour of unsaturated soils under external loading, involves only the deviatoric stress, spherical stress and volumetric strain.

The earliest critical state model was the Cam Clay model proposed by Roscoe et al. (1958) which was previously modified by Roscoe and Burland (1968). Some assumptions must be made to simplify the complex nature of soils. Kurtay and Reece (1970) outline some assumptions required for formulating constitutive relations of soils based on the critical state theory:

- Soil material is homogeneous and isotropic.
- Soil is not viscous material.
- Soil behaviour can be described using the appropriate stress state variables.
- Soil behavior representation is not subjected to interaction between individual particles and can be described using macroscopic continuum mechanics theory.
- Soil behaviour is not time dependent.

3.3 Constitutive Models

The constitutive model for a material is a set of equations relating stress to strain and possibly strain history of the soil and the future stress changes that the soil is likely to experience (Wood, 1990). Constitutive models combines laws of equilibrium and continuity through so called constitutive relations which relates the changes in loads applied on the soil material to the deformation or gradients of displacement developed on the soil (Wood, 2004).

The constitutive models presented in this research work can be groped in two categories; elastic models and elastoplastic models. Elastic or recoverable materials are those for which the deformation produced by applying a load is fully recovered when the load is removed. However, most materials experience irrecoverable deformations when the applied load exceeds the elastic deformations. The irrecoverable or permanent deformation that remains under zero load are plastic deformations.

The classical elastic model has been derived from the properties of elastic solids such as metals. Hence, the behavior of an isotropic elastic material can be described by relating strain increments to increments of net stress and suction (Fredlund and Morgenstern, 1977; Lloret et al., 1987; Lade and Nelson, 1987). Although the measurement of the relevant parameters of this kind of models is relatively easy and the numerical implementation is moderately simple, there are major disadvantages. The most important is that elastic models do not differentiate between reversible and irreversible strains (Wheeler and Karube, 1996). However, modeling a complex process lead to a complex model which requires more soil parameters and consequently more complex laboratory testing to determine those parameters, a balance should be found between the cost of testing large number of samples to evaluate a large number of parameters for heterogeneous soil and the possible benefit of using a complex rather than a simple model (Wood, 1990).

Different to metal materials which do not experience volume changes, frictional materials (i.e. soil, rock, concrete, among others) experience both plastic compaction and dilation (Lade, 1988). Therefore, once certain stress level has been reached on

frictional materials irrecoverable or permanent deformation will appear. Nonetheless, if the loading is subsequently removed the strains do not revert to zero as they do for elastic materials. The strains remaining after the loading has been removed are called plastic strains and the stress level at which plastic strains start to occur is the yield stress (Beer and Watson, 1992).

Elasto-plastic models can be divided into two main categories; expansive and non-expansive models. Some models for expansive soils have been proposed by Gens and Alonso (1992), Alonso et al. (1994), Shuai and Fredlund (1998), and Alonso et al. (2000). However, expansive soil modelling is not discussed in this document.

Low plasticity soil behaviour can be described using Non-expansive models. Non-expansive models can be separated into two categories. Models relating net mean stress and suction as stress variables which are called total stress models (Alonso et al., 1990; Wheeler, 1991; Josa et al., 1992; Wheeler and Sivakumar, 1995; Georgiadis et al., 2005) and those using effective stress and suction as stress variables called effective stress models (Bolzon and Schrefler, 1995; Bolzon et al., 1996).

The Cam clay model is an ideal elastoplastic constitutive model that adopt the metal plasticity theory to describe the behaviour of normally consolidated clay (Matsuoka and Sun, 2006). This model, is considered a classical model in the field of the constitutive studies of geomaterials. Large number of models has been developed basis on the Cam clay model (Alonso et al., 1990; Wheeler, 1991; Josa et al., 1992; Wheeler and Sivakumar, 1995; Bolzon et al., 1996; Kohgo et al., 1993; Kohgo et al.,

1993b, Kim and Lade, 1988a; Kim and Lade, 1988a; Cui et al., 1995, Kato et al. (1995), Georgiadis et al., 2005)

3.3.1 Original Cam Clay Model

Cam clay is a critical state-based, strain hardening plasticity model that can represent the mechanical behaviour of normally consolidated clays (Roscoe and Schofield, 1963).

In the elastoplastic constitutive model, the total strain increments ca by expressed by

$$d\varepsilon = d\varepsilon^{e} + d\varepsilon^{p} \tag{3.1}$$

where

$d\varepsilon^{e}$ = elastic strain increment calculated by Hooke's law

$d\varepsilon^{p}$ = plastic strain increments determined based on the plasticity theory

3.3.1.1 Principal Direction of Plastic Strain Increments

As shown in Figure 3.1, similar to most of elastoplastic models, the Cam-Clay model assumes that the principal direction of stresses, σ_{ij}, and plastic strain ε_{ij} increment are coaxial.

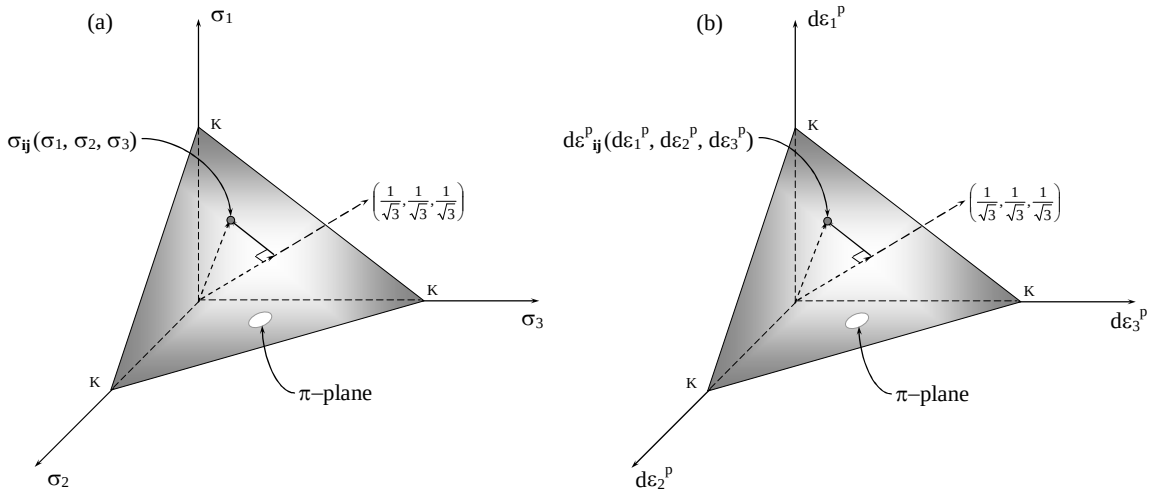

Figure 3.1 (a) principal stress space, and (b) principal plastic strain increment space (modified from: Matsuoka and Sun, 2006).

The stress sate variables adopted in the Cam Clay model are the net mean stress, p, also known as octahedral normal stress σ_{oct}, and the deviatoric stress, q. The plastic strain increments are $d\varepsilon_v^p$ and $d\varepsilon_q^p$. The mean stress and deviatoric stress are defined as follows:

$$p = \frac{\sigma_1 + \sigma_2 + \sigma_3}{3} \tag{3.2}$$

$$q = \sqrt{\frac{(\sigma_1 - \sigma_2)^2 + (\sigma_2 - \sigma_3)^2 + (\sigma_3 - \sigma_1)^2}{2}} \tag{3.3}$$

where

σ_1 = vertical principal stress

σ_2 = horizontal principal stress (y axis direction)

σ_3 = horizontal principal stress (x axis direction)

$$d\varepsilon_v^p = d\varepsilon_1^p + d\varepsilon_2^p + d\varepsilon_3^p \tag{3.4}$$

$$d\varepsilon_q^p = \frac{\sqrt{2}}{3}\sqrt{(d\varepsilon_1^p - d\varepsilon_2^p)^2 + (d\varepsilon_2^p - d\varepsilon_3^p)^2 + (d\varepsilon_3^p - d\varepsilon_1^p)^2} \quad (3.5)$$

where

$d\varepsilon_v^p$ = plastic volumetric strain increment

$d\varepsilon_q^p$ = plastic deviatoric strain, also known as shear plastic strain.

3.3.1.2 Plastic Potential and Yield Function

The energy dissipation equation was used in the Cam clay model to determine the plastic potential surface. The plastic work per unit volume of a true triaxial sample with the externally applied principal stresses can be expressed by (Matsuoka and Sun, 2006)

$$dW = \sigma_1 d\varepsilon_1^p + \sigma_2 d\varepsilon_2^p + \sigma_3 d\varepsilon_3^p = pd\varepsilon_v^p + qd\varepsilon_q^p \quad (3.6)$$

To determine how the plastic energy is dissipated it is assumed that all the plastic work is dissipated entirely in friction. Therefore, at failure q = Mp and $d\varepsilon_v^p = 0$ and the energy dissipation equation becomes (Yu, 2006)

$$dW = pd\varepsilon_v^p + qd\varepsilon_q^p = Mpd\varepsilon_q^p \quad (3.7)$$

where

M = the ratio q/p at critical state

In addition, Cam clay model assume that there is a family of surfaces normal to the plastic strain increment in the stress space (i.e. the normality condition). This surface is the plastic potential, g, which can be derived from the energy dissipation equation and written as (Yu, 2006)

$$g = g(p,q) = \frac{q}{pM} + \ln\left(\frac{p}{p_o}\right) = 0 \qquad (3.8)$$

where

p_o = constant which indicates the size of the plastic potential.

Figure 3.2 shows the plastic potential function in the p – q plane which have been obtained combining the direction of plastic strain increments vector and stress ratio with the normality condition. It can be observed on the intersection of the plastic potential function and the Critical State Line (CSL), that the volumetric strain increment is equal to zero when q/p = M. It is also true for any stress ratio falling on the plastic potential surface.

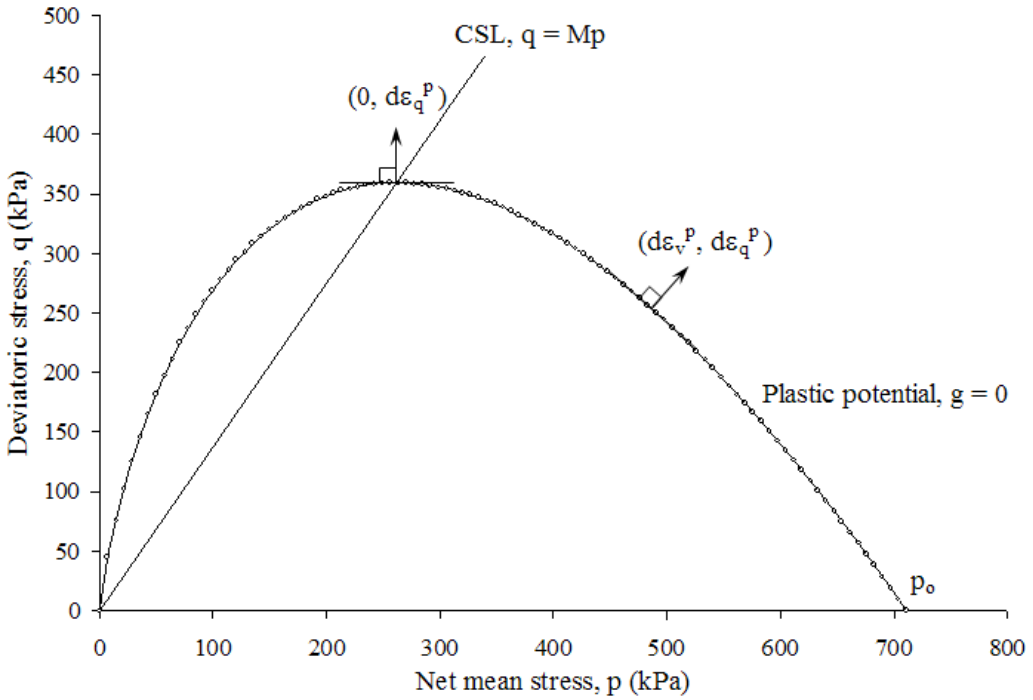

Figure 3.2 Plastic potential and plastic strain increment vectors in Cam Clay model.

Additionally, in the Cam clay model, it is assumed that the soil obeys and associative flow rule, i.e. the yield function, *f*, is identical to the plastic potential function, *g*, (Wood, 1990; Wood 2004; Yu, 2006; Matsuoka and Sun, 2006). Thus the yield function, *f*, may be expressed as

$$f = f(p, q, p_o) = \frac{q}{pM} + \ln\left(\frac{p}{p_o}\right) = 0 \tag{3.9}$$

Figure 3.3 shows the shape of the yield surface expressed by the yield function. The yield surface, also known as yield locus, contains all stress ratio combinations producing only elastic strain. Therefore, elastoplastic strain occurs when the stress state is outside the current yield locus.

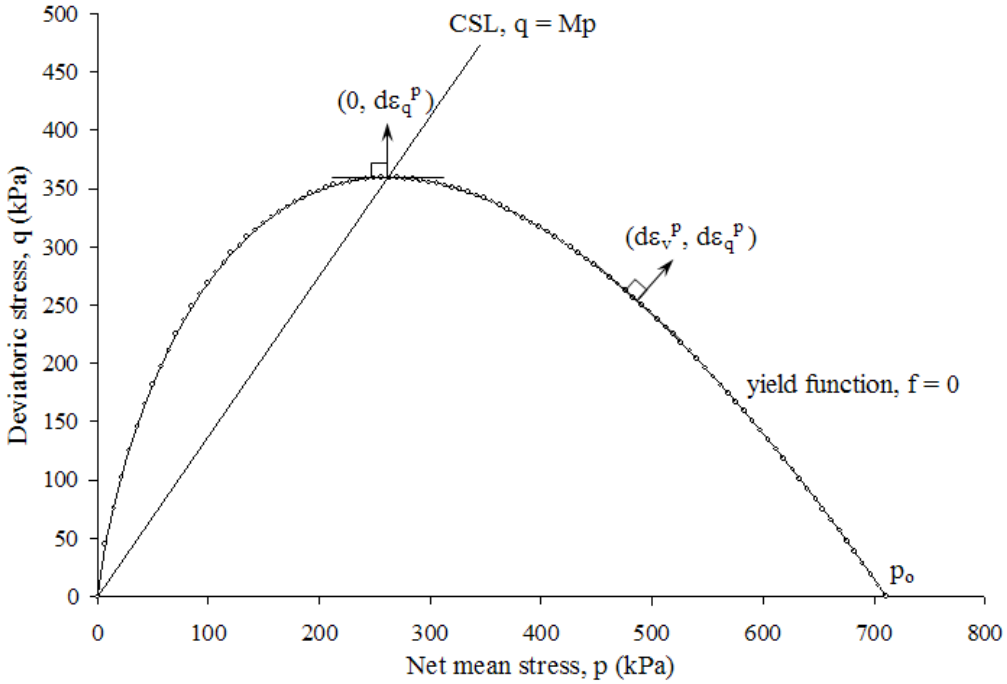

Figure 3.3 Yield surface and critical state line (CSL) in Cam Clay model.

In Figure 3.3, p_o is the preconsolidation pressure which acts as the hardening parameter that changes with the plastic strain (Figure 3.4).

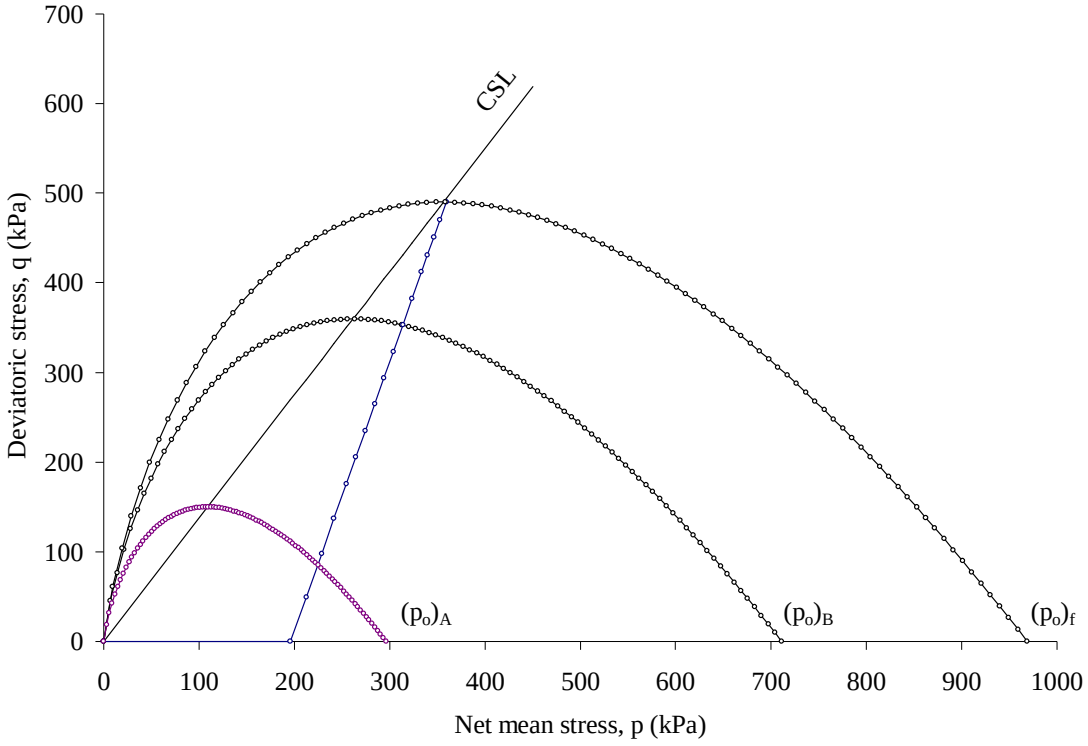

Figure 3.4 Yield loci progress in Cam clay model.

3.3.1.3 Strain-hardening Rule

When plastic strain is reached in a soil sample, knowing the strain increment ratio is not sufficient to calculate the magnitude of plastic strain. To do so, it is necessary to introduce the so called strain-hardening rule. As mentioned before, in Cam clay the preconsolidation pressure, p_o, is assumed to change with the plastic volumetric strain. It can be observed from Figure 3.4 and equation (3.9) that the size of the yield surface is represented by, p_o. The change in p_o may be calculated by

$$dp_0 = \frac{vp_o}{\lambda - \kappa} d\varepsilon_v^p \qquad (3.10)$$

where

v = specific volume = 1 + e

κ = elastic stiffness parameter

λ = stiffness parameter.

In Cam Clay model, these parameters can be determinate from the results of an isotropic compression test. In other word, an isotropic test can be used to derive the strain-hardening rule. As is well known, an isotropic test is a simple test that measures the stress–strain relation of a soil sample under isotropic stress state. As shown in Figure 3.5 the results are usually plotted in the v – ln p plane and the virgin loading curve, also known as normal consolidation line (ncl), and the unloading-reloading curve (url) are assumed to be straight lines. The slopes of the two lines are generally denoted by λ and κ respectively. In the v – log p plane the slopes of the slopes of the two lines are the compression index, C_c, and the swelling index, C_s, respectively (Matsuoka and Sun, 2006). The compression index, C_c, and λ are related by $\lambda = 0.434C_c$. In a similar way $\kappa = 0.434C_s$ (Wood, 1990).

3.3.2 Modified Cam Clay Model

Cam clay model was modified by Roscoe and Burland (1968) by deriving a new plastic potential and yield equation which leads to a different relation between the stress ratio and the strain increment ratio. To do that the authors adopted the following work equation.

$$dW = pd\varepsilon_v^p + qd\varepsilon_q^p = p\sqrt{(d\varepsilon_v^p)^2 + (Md\varepsilon_q^p)^2} \quad (3.11)$$

Under the same assumptions the resulting plastic potential, g, and therefore the yield function, f, can be written as

$$f = f(p, q, p_o) = q^2 + M^2 p^2 - M^2 p p_0 = 0 \quad (3.12)$$

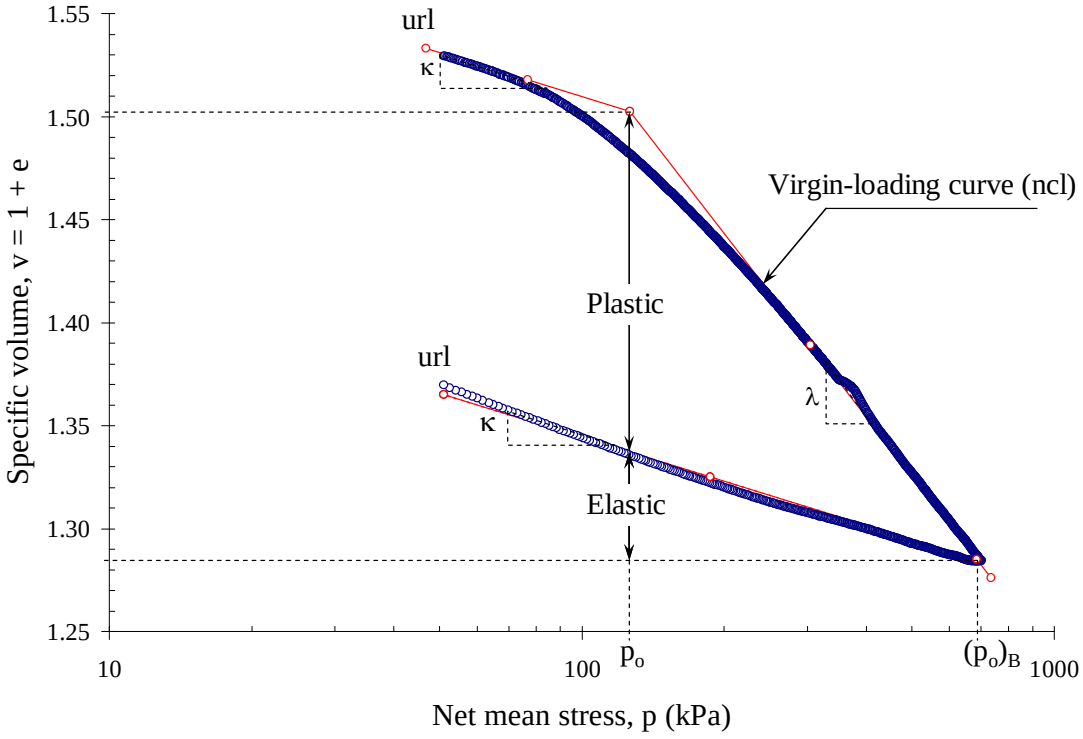

Figure 3.5 Results of isotropic compression test.

As shown in Figure 3.6, in the modified Cam clay model, the plastic potential curve as well as the yield surface is normal to the p-axis. The modification proposed overcome with the limitation of the original Cam clay model which predicts plastic strain during isotropic compression loading which contradicting experimental results. Figure 3.7 shows the yield surface for both original and modified Cam clay model.

The strain-hardening rule used in the modified Cam clay model is the same as that used in the original Cam clay model. As shown in Figure 3.8, the yield loci of the modified Cam clay model are ellipses in the q – p plane. It also can be observed that the volumetric plastic strain gradually increment as the yield surface expands.

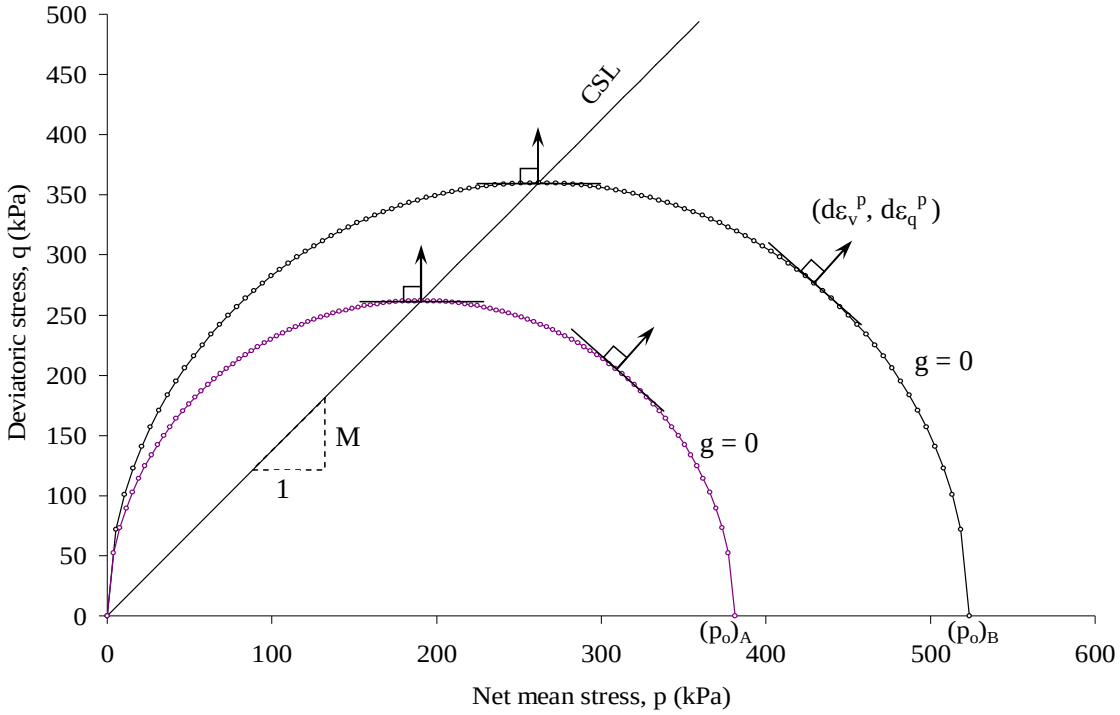

Figure 3.6 Plastic potential and plastic strain increments vectors in the modified Cam Clay model.

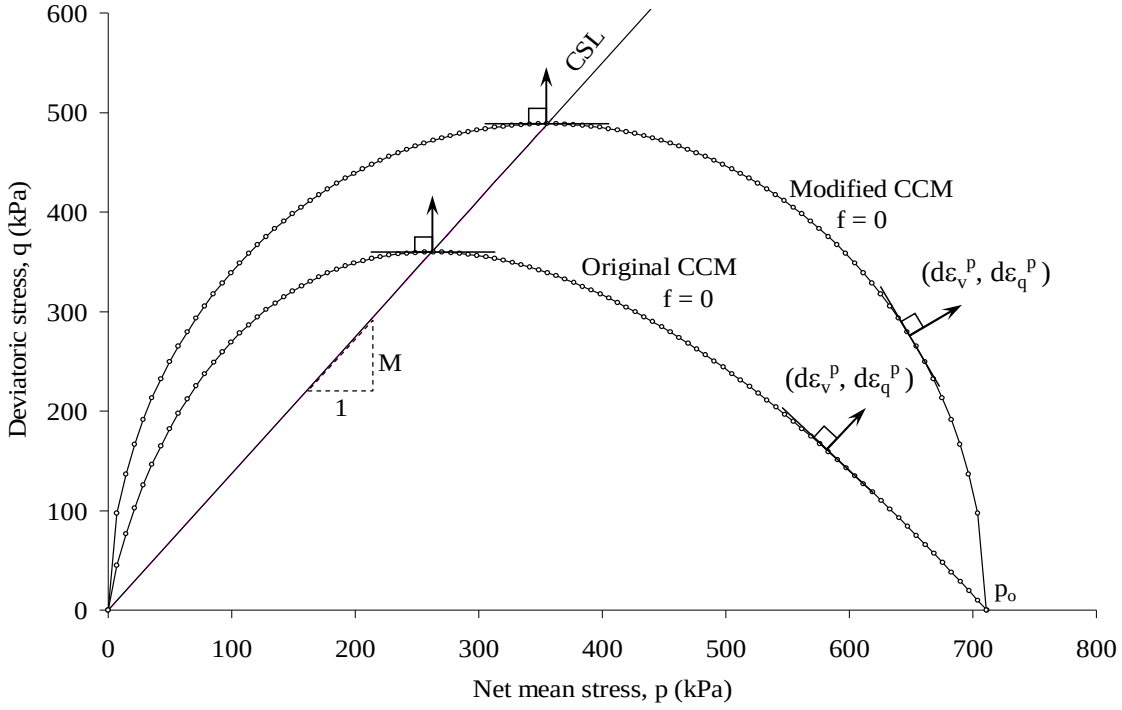

Figure 3.7 Yield surface of original and modified Cam Clay model.

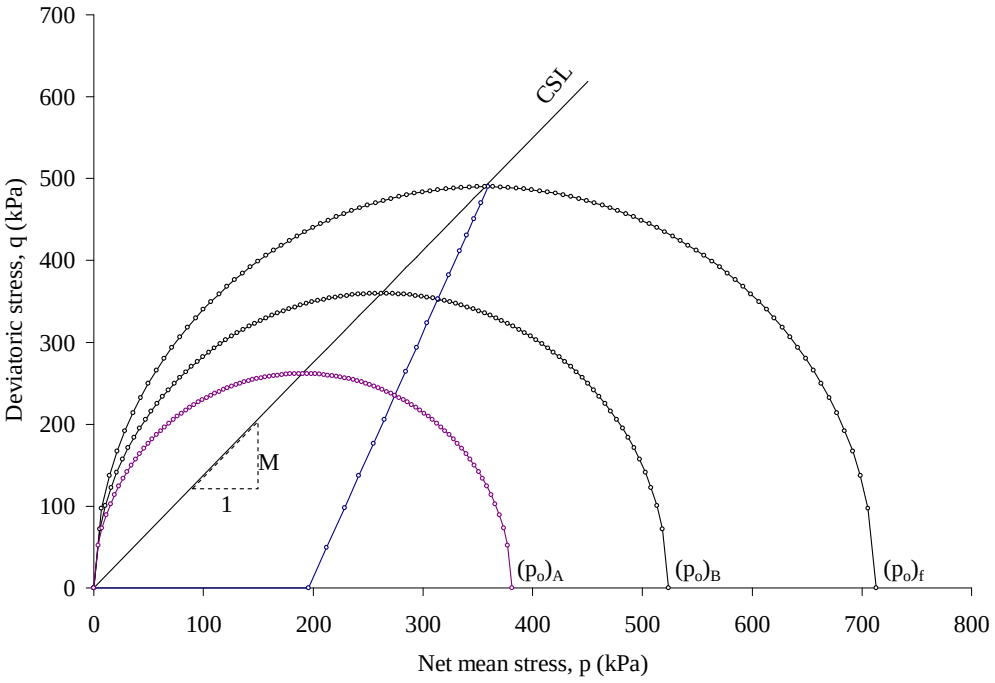

Figure 3.8 Yield surface progress in Cam Clay model.

3.3.3 Barcelona Basic Model

The Barcelona Basic model (BBM) proposed by Alonso et al. (1990) is a critical state model for describing the most important features of partially saturated soils behaviour. The model has been formulated within the framework of the strain-hardening plasticity, and can be used to represent the behaviour of unsaturated soils. The model is intended for partially saturated soils such as sand, silts, clayey sands, sandy clays and low plasticity clays which are slightly or moderately expansive.

The Barcelona basic model is an extension of the modified Cam clay model proposed by Roscoe and Burland (1968). Therefore, it is also defined in terms o the net mean stress, p, and the deviatoric stress, q, as stress state variables. In addition, the matric suction, $s = u_a - u_w$, has been included as a third stress state variable in order to incorporate the suction effect, particularly important in unsaturated soils. Hence, the Barcelona basic model rigorously continues working under the well established framework of the modified Cam clay model and been consistent with this framework, the model can predict saturated behaviour of the soil when the value of suction reduces to zero. Consequently, the modified Cam clay model becomes a particular case of the Barcelona basic model when the soil suction is equal to zero.

3.3.3.1 Principal Direction of Plastic Strain Increments

Similar to the Cam-Clay model, the Barcelona basic model assumes that the principal direction of stresses, σ_{ij}, and plastic strain ε_{ij} increment are coaxial (Figure 3.1). The plastic strain increments are $d\varepsilon_v^p$ and $d\varepsilon_q^p$ as well.

3.3.3.2 Model Formulation for Isotropic Stress State

Alonso et al. (1990) derives the loading-collapsing (LC) yield curve in the (p, s) space considering the boundary imposed by the behaviour of the saturated condition and the isotropic and oedometer compression testing under controlled suction. Hence, on an isotropic test under controlled suction (i. e. at constant s), the variation of the specific volume, v = 1 + e, with the net mean total stress, p, and suction, s, along the virgin-loading curve is given by

$$v = N(s) - \lambda(s) \ln \frac{p}{p^c} \tag{3.13}$$

where

$\lambda(s)$ = soil stiffness parameter which depend on matric suction, s

p^c = reference stress state for which v = N(s)

The soil stiffness parameter can be obtained from the following equation:

$$\lambda(s) = \lambda(0)[(1-r)e^{-\beta s} + r] \tag{3.14}$$

where

r = constant related to the maximum stiffness of the soil, $r = \lambda(s \rightarrow \infty)/\lambda(0)$

β = parameter which control the rate of soil stiffness with matric suction.

The variation of the soil stiffness parameter, $\lambda(s)$, for several values of r, when the soil stiffness parameter for the saturated condition, $\lambda(0) = 0.23$, and $\beta = 17.33$ MPa^{-1} is presented in Figure 3.9. Additionally, the variation of the soil stiffness parameter, $\lambda(s)$, for different values of β and r = 0.268 is shown in Figure 3.10.

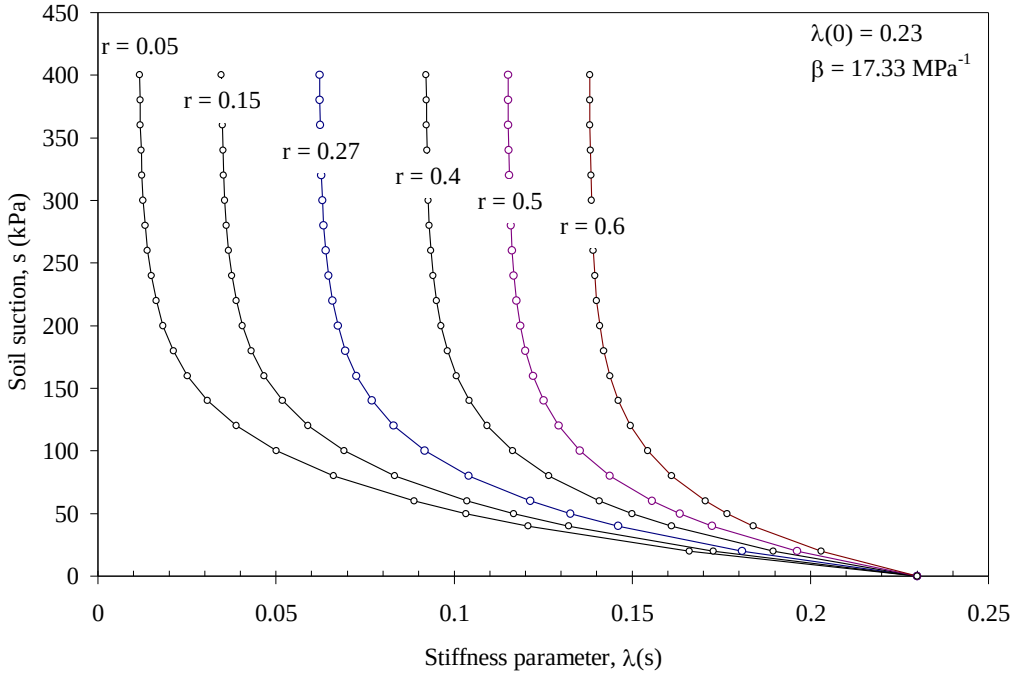

Figure 3.9 Stiffness parameter variation for different values of r.

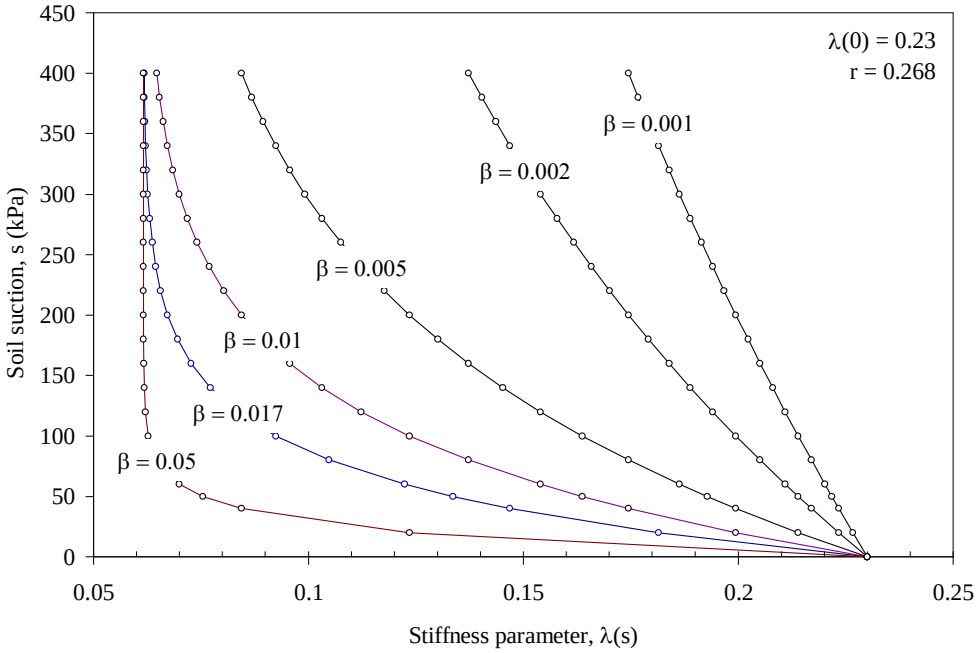

Figure 3.10 Stiffness parameter variation for different values of β.

Similar to the modified Cam clay model, the Barcelona basic model assume that on the unloading reloading line, url, the soil behave elastically. Hence, changes in specific volume can be calculated by

$$dv = -\kappa \frac{dp}{p} \tag{3.15}$$

where

k = elastic swelling index

Although changes in κ could be expected with variations in matric suction, s, the model adopt a constant value to ensure that the elastic part of the model is conservative (Alonso et al., 1990).

The proposed variation of the specific volume on an isotropic test of a saturated sample (i.e. suction s = 0) and a partially saturated sample is shown in Figure 3.11.

The saturated sample yields at a stress $p_o(0)$ (i.e. $p_o(0)$ = saturated preconsolidation stress), whereas the partially saturated sample yield at a larger isotropic stress $p_o(s)$. Assuming that both point $p_o(0)$ and $p_o(s)$ belong to the same loading-collapse yield curve, a relationship between the generic yield stress, $p_o(s)$, and the saturated preconsolidation stress, $p_o(0)$, can be writhen as (Alonso et al., 1990).

$$\frac{p_o(s)}{p^c} = \left[\frac{p_o(0)}{p^c} \right]^{\frac{\lambda(0)-\kappa}{\lambda(s)-\kappa}} \tag{3.16}$$

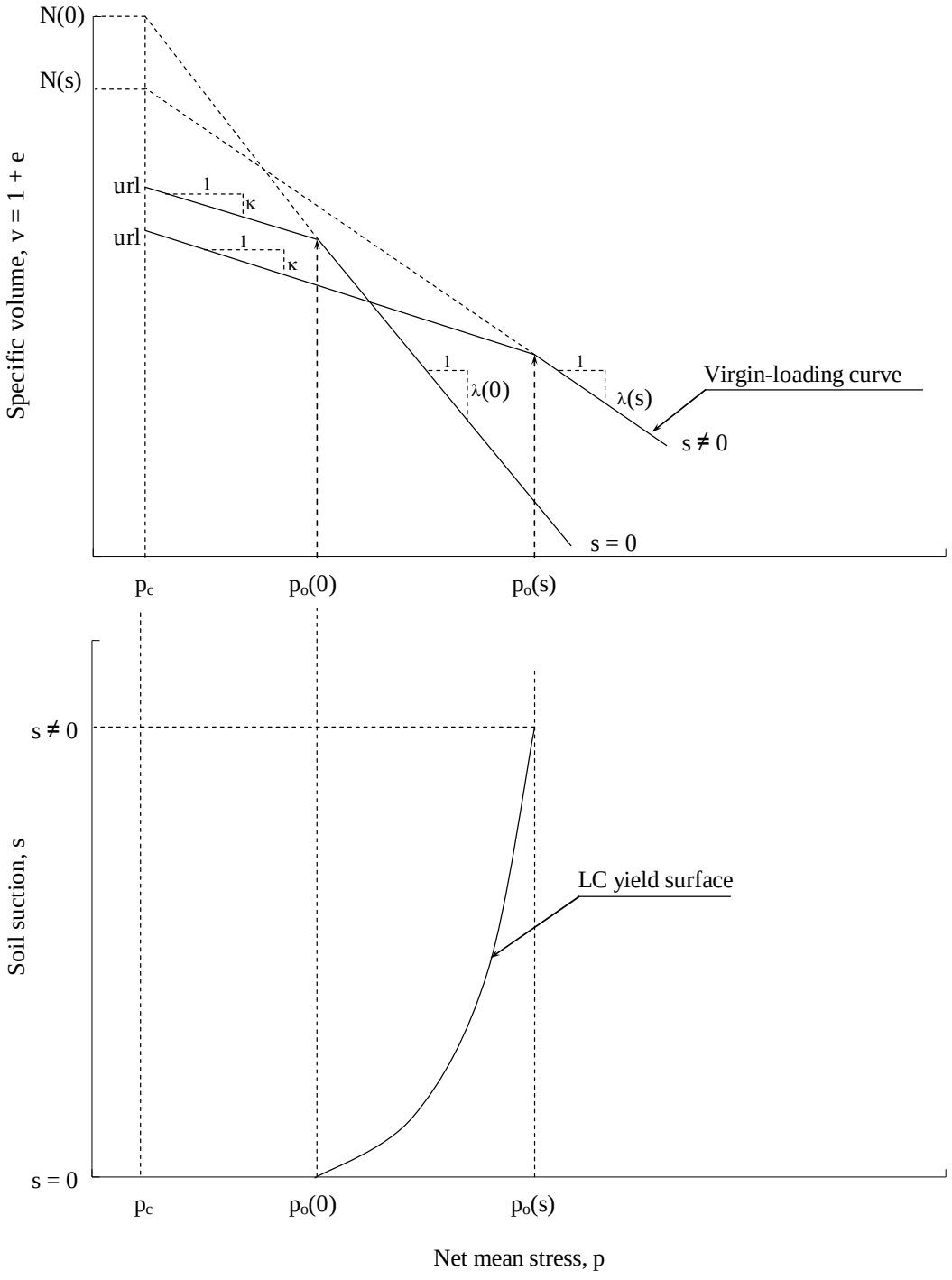

Figure 3.11 Expected specific volume variation for saturated and unsaturated soils (modified from: Alonso et al., 1990).

This equation plays a central role in the Barcelona basic model to account the apparent increase in preconsolidation stress associate with increasing suction. The variation of the shape of the loading collapse yield curves for different values of $p_o(0)$ and parameter values of β = 8.9 MPa^{-1} and r = 0.649 is shown in Figure 3.12. It is important to notice that the LC yield curve becomes a straight line when $p_o = p_c$. In this case, changes in suction do not result in plastic deformations. In order to isolate a single LC yield curve, it is necessary to specify the preconsolidation net mean pressure for saturated condition $p_o(0)$ which may be viewed as a hardening parameter in Equation (3.17) (Alonso et al., 1990).

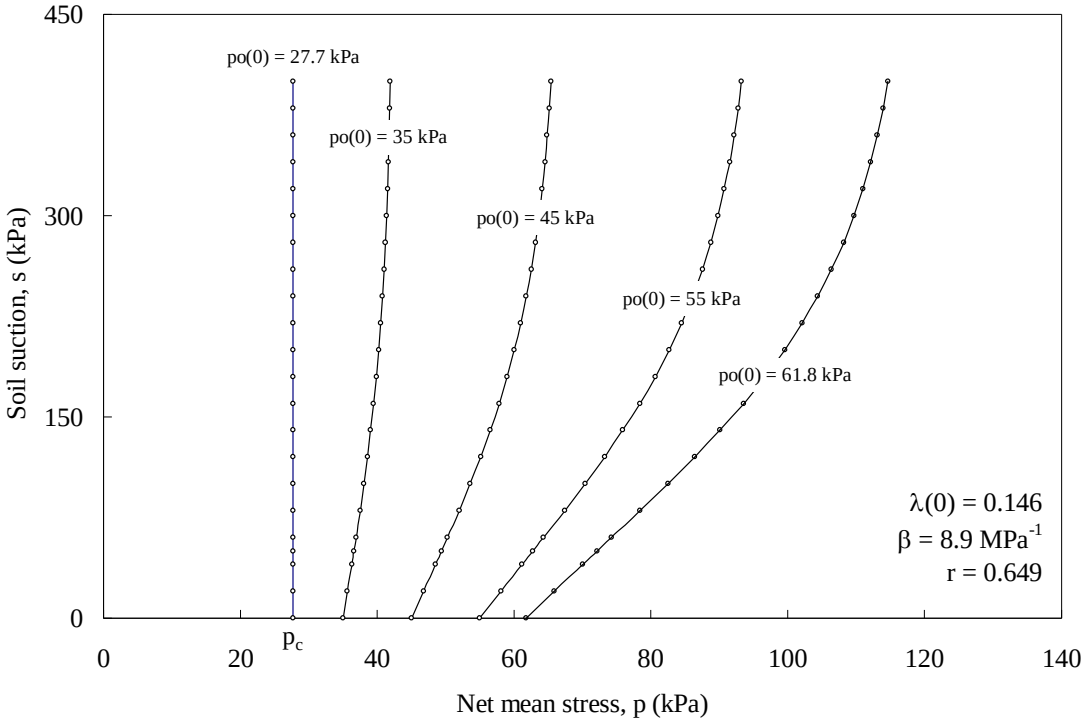

Figure 3.12 Shape of the Loading collapse yield curve for different values of $p_o(0)$.

In the same way, the soil experiences deformation when the suction increases, and at a certain value of suction, the soil could also experience irrecoverable strains. Therefore, it is possible that whenever the soil attains the maximum past suction ever experienced and bounds the transition from the elastic state to the plastic state, irreversible strains will begin to develop (Figure 3.13). Due to the lack of experimental evidence, Alonso et al. (2009) assume that the yield condition associate with the maximum previously attained value of suction, s_o, is described by $s = s_o$ = constant. This yield locus is named suction increase (SI) yield locus. Consequently, the elastic region in the (p, s) plane is enclosed by both, LC and SI yield loci as shown in Figure 3.14.

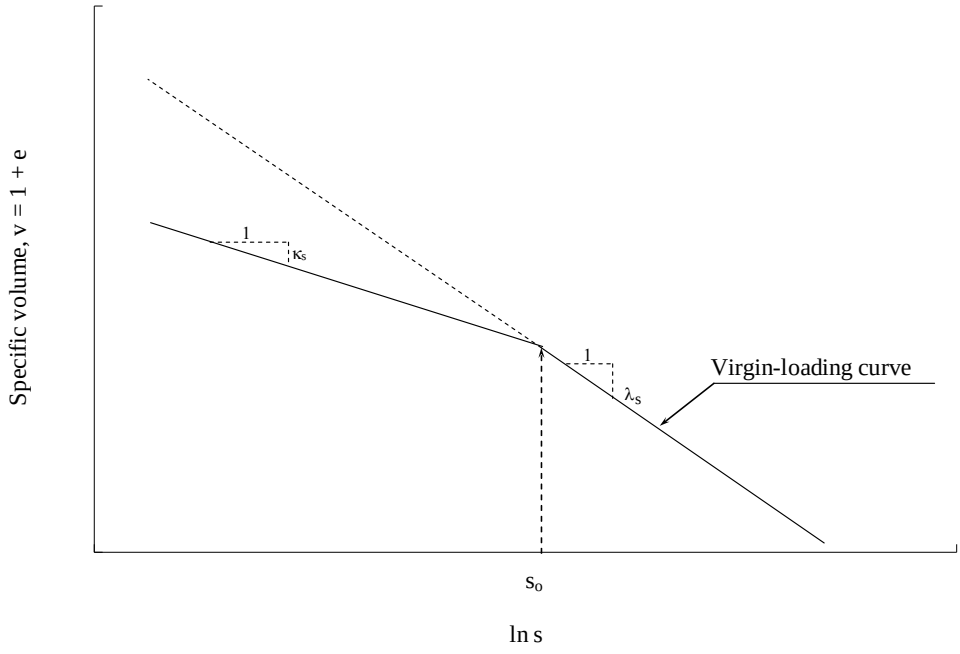

Figure 3.13 Definition of suction increase (SI) yield surface.

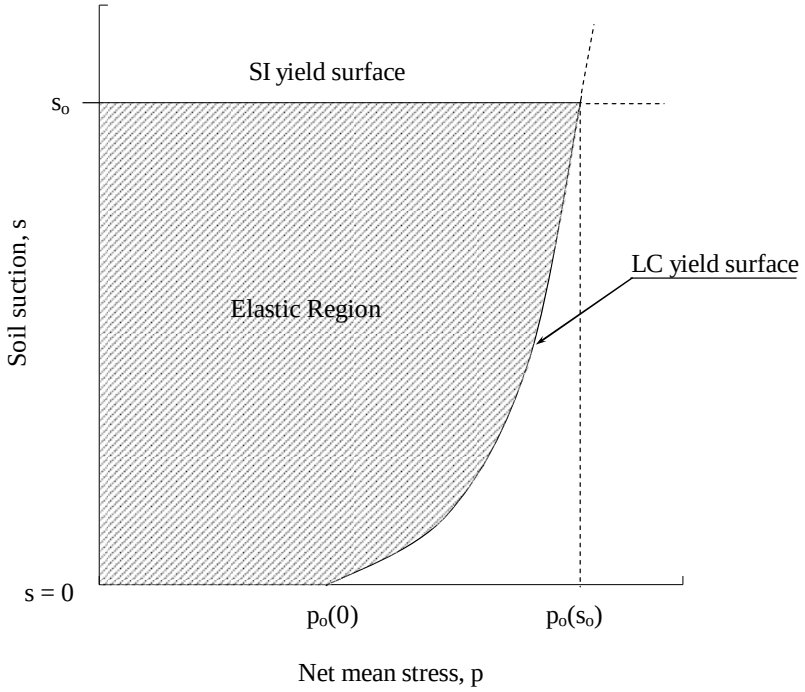

Figure 3.14 Loading collapse (LC) and suction increase (SI) yield loci (modified from: Alonso et al., 1990).

3.3.3.3 Model Formulation for General Stress State

Alonso et al. (1990) adopts the modified Cam clay model as a limit condition to represent the saturated condition of the soil sample. Consequently, the authors assume that the yield curve for a soil sample at constant suction, s, can be adequately described by a ellipse. In addition, similar to the modified Cam clay model, it is also assumed that the size of the ellipse will be determined by the value of the preconsolidation stress, p_o. However, in order to incorporate the effect of suction the Barcelona basic model assume that the increase in suction induce a increase in cohesion while maintaining the slope M of the critical state line (CSL) for saturated condition. Hence, the model also assumes that the increase in cohesion follows a linear relationship with suction. Thus, the ellipse

will intersect the p axis at a point for which $p = - p_s = -ks$ where k is the parameter controlling increase in cohesion with suction, s. Therefore, the major axes of the ellipse, which coincide with the p axis, will extent from $-p_s(s)$ to $p_o(s)$. Consequently, for a particular value of matric suction, s, the yield surface, f, in the (p, q) plane could be represented by

$$f = f(p,q,s) = q^2 - M^2(p + p_s)\left[p_o(s) - p\right] = 0 \qquad (3.17)$$

where

$p_s = ks$

k = constant

s = soil suction

The physical meaning of all parameters in Equation (3.13) as well as the representation of the yield surface for saturated condition (i.e. $s = 0$) and unsaturated condition (i.e. $s \neq 0$) are depicted in Figure 3.15. In addition, the evolution of the yield surface for lightly overconsolidated and normally consolidated soils in the (p, q, s) space is shown in Figure 3.16 and Figure 3.17, respectively. In these figures, the yield surface extends into the region $q \geq 0$ and the intersection of the yield surface with the (p, s) plane corresponds to the loading-collapse (LC) yield curve.

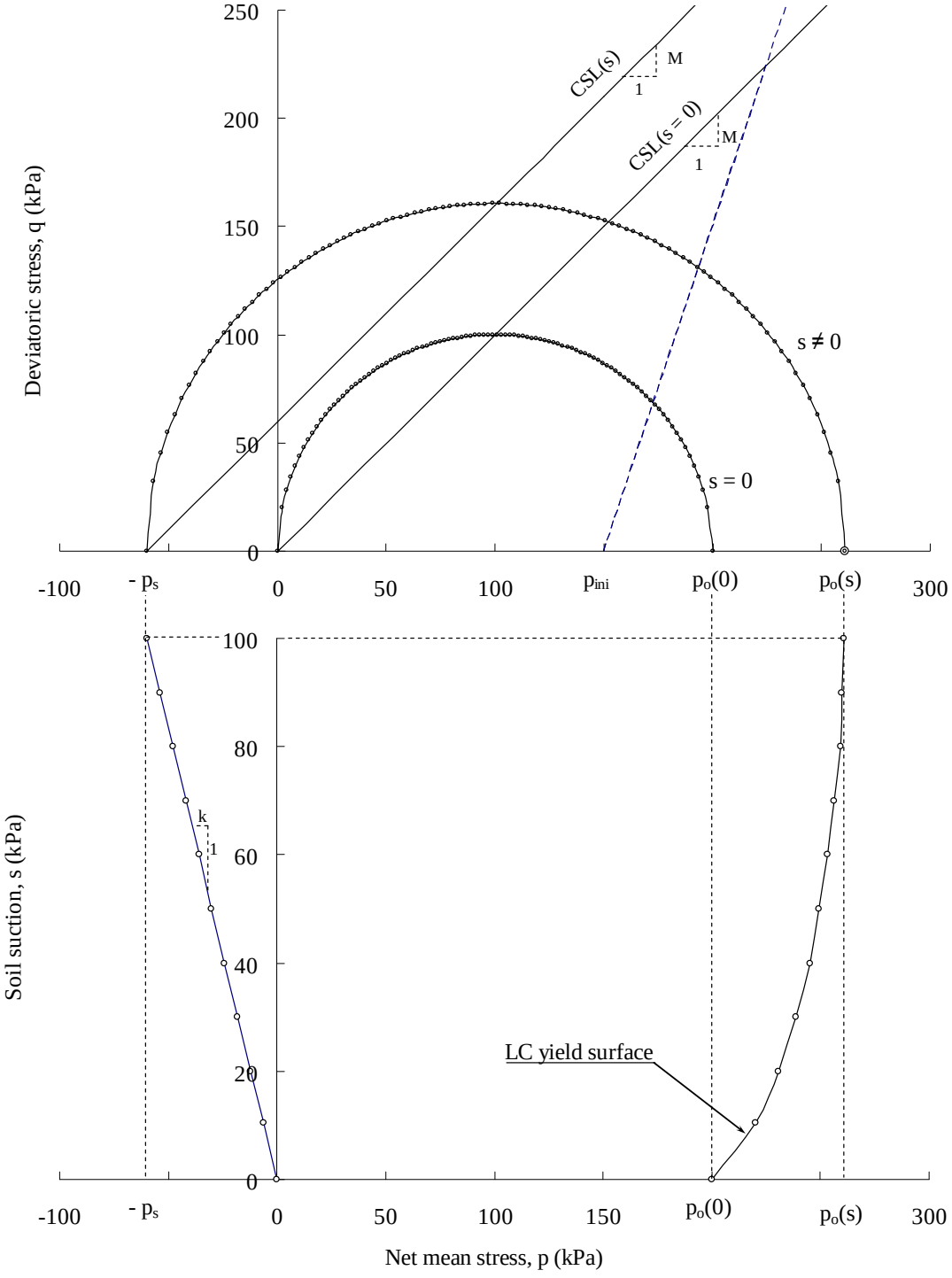

Figure 3.15 Yield surface of Barcelona basic model for s = 0 and s ≠ 0.

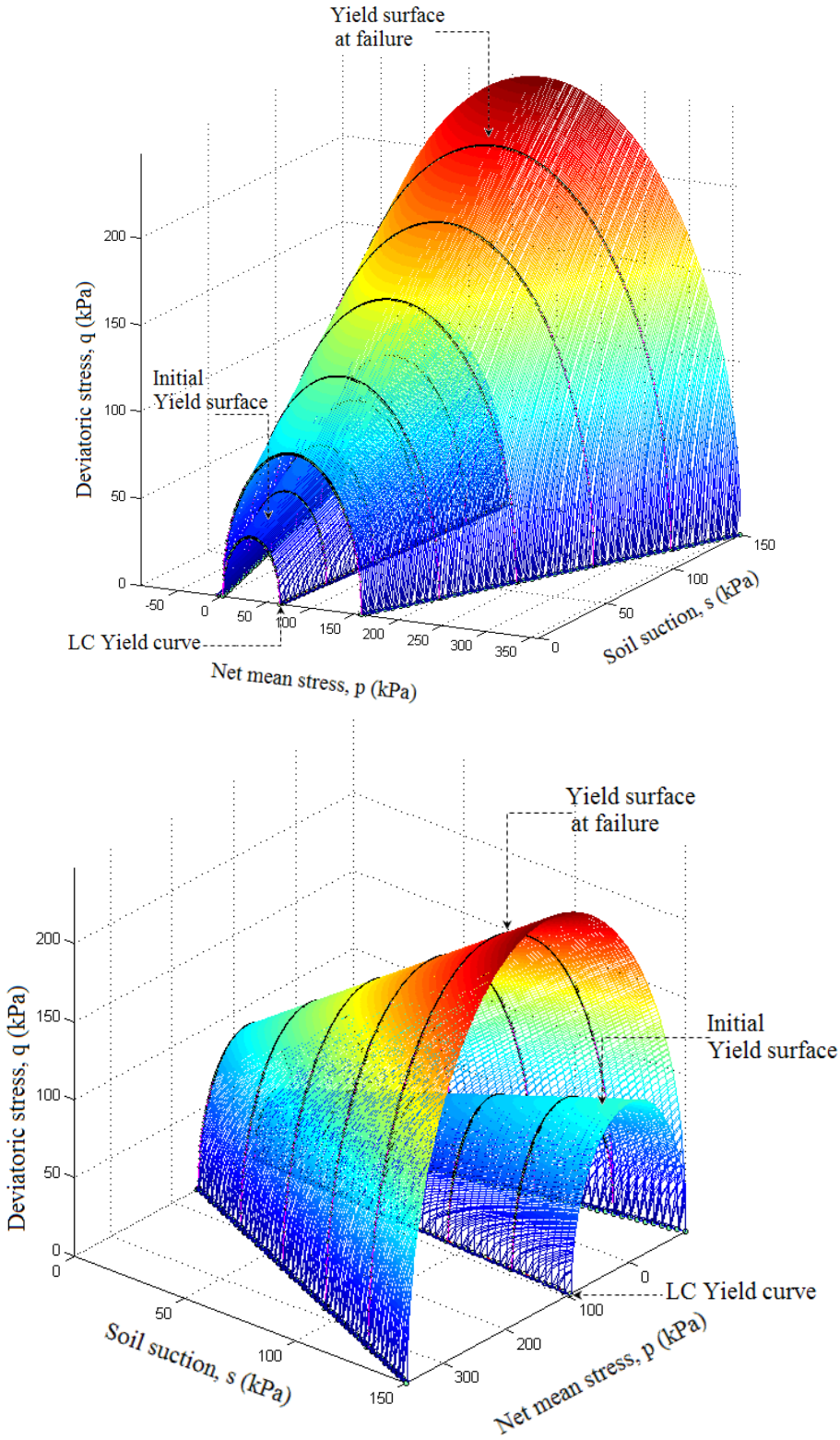

Figure 3.16 Yield surface in (p, q, s) stress space – Lightly overconsolidated soil.

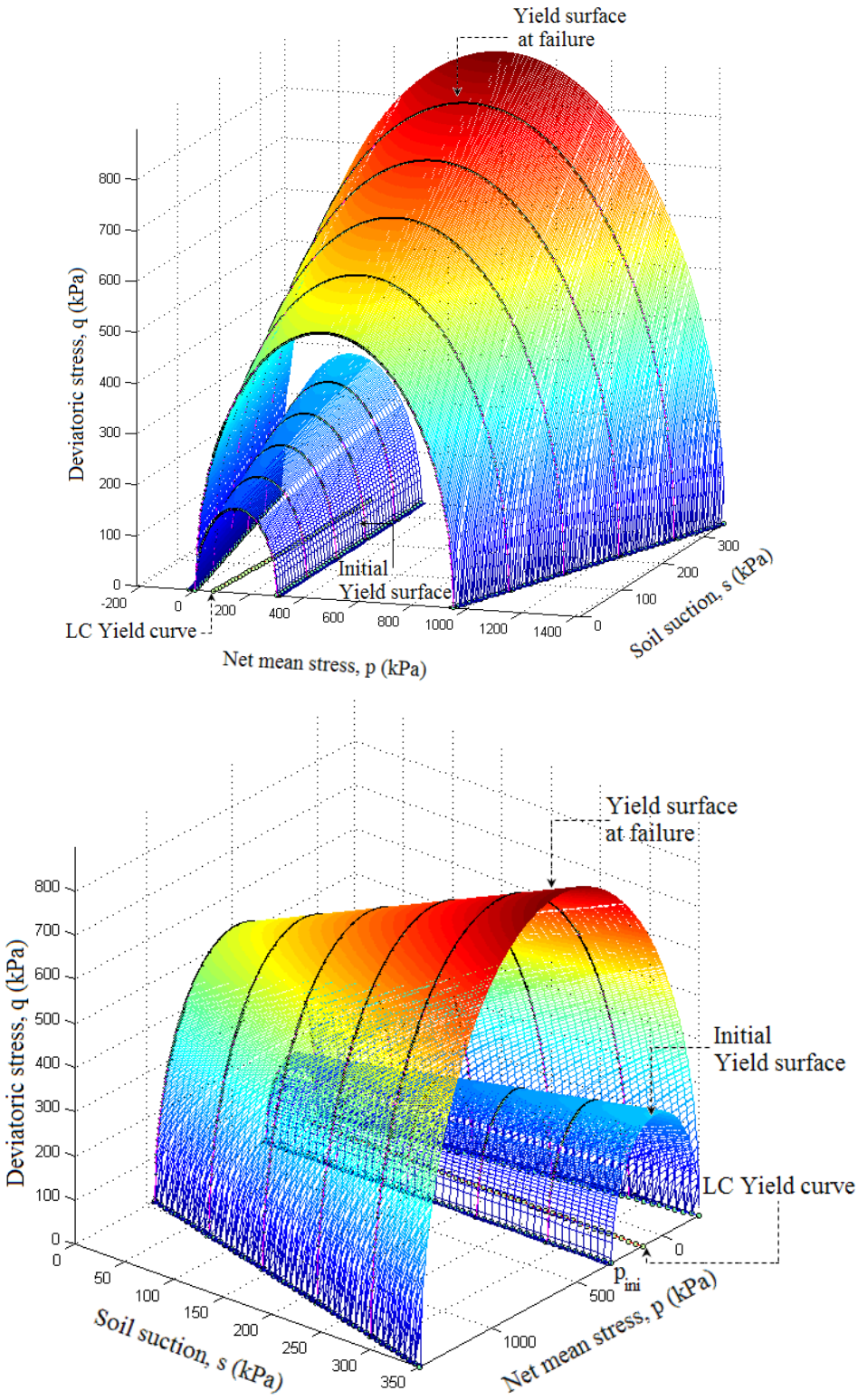

Figure 3.17 Yield surface in (p, q, s) stress space – Normally consolidated soil.

3.3.3.4 Strain-hardening Rule

When plastic strain is reached in a soil sample, knowing the strain increment ratio is not sufficient to calculate the magnitude of plastic strain. To do so, it is necessary to introduce the so called strain-hardening rule. As mentioned before, the BBM assumes that the evolution of the yield surface on unsaturated soil is controlled by the hardening parameters $p_o(0)$ and s_o. In addition the model assumes that both hardening parameters can be described as a function of the soil deformation.

Generally speaking, in elasto-plastic modelling the total volumetric strain increments can be calculated as $d\varepsilon_v = d\varepsilon_v^e + d\varepsilon_v^p$. Nevertheless, for unsaturated soil modelling purposes the elastic, $d\varepsilon_v^e$, as well as plastic, $d\varepsilon_v^p$, volumetric strain increments must be calculated considering the effect of increase in net mean stress as well as increase in suction. Then, elastic and plastic strain increments may be computed by

$$d\varepsilon_v^e = d\varepsilon_{vp}^e + d\varepsilon_{vs}^e \tag{3.18}$$

$$d\varepsilon_v^p = d\varepsilon_{vp}^p + d\varepsilon_{vs}^p \tag{3.19}$$

where

$d\varepsilon^e_{vp}$ = elastic volumetric strain increment due to changes in p

$d\varepsilon^e_{vs}$ = elastic volumetric strain increment due to changes in s

$d\varepsilon^p_{vp}$ = plastic volumetric strain increment due to changes in p

$d\varepsilon^p_{vs}$ = plastic volumetric strain increment due to changes in s.

The total volumetric strain increments due to change in net mean stress, p, can be calculated by

$$d\varepsilon_{vp} = d\varepsilon_{vp}^{e} + d\varepsilon_{vp}^{p} \tag{3.20}$$

The total volumetric strain increments due to change in matric suction, s, can be expressed as

$$d\varepsilon_{vp} = d\varepsilon_{vs}^{e} + d\varepsilon_{vs}^{p} \tag{3.21}$$

The elastic modulus is related to the swelling index, κ, from the assumption that soil behaves elastically during the isotropic unloading and reloading. Therefore, an increase of p in the elastic region will induce a volumetric deformation given by

$$d\varepsilon_{vp}^{e} = \frac{\kappa}{v}\frac{dp}{p} \tag{3.22}$$

Similarly, an increase in suction within the elastic region will result in the volumetric strain given by

$$d\varepsilon_{vs}^{e} = \frac{\kappa_s}{v}\frac{ds}{(s + p_{atm})} \tag{3.23}$$

Once the net mean stress, p, reaches the LC yield value $p_o(s)$ the total volumetric strain for any further increase in p for a specific value of matric suction, s, may be calculated as

$$d\varepsilon_{vp} = \frac{\lambda(s)}{v}\frac{dp_o(s)}{p_o(s)} \tag{3.24}$$

Therefore, the plastic component of the total volumetric strain increment can be obtained by subtracting the plastic volumetric strain increment from the total volumetric strain increment. The difference among these two values can be expressed as

$$d\varepsilon_{vp} = \frac{\lambda(s) - \kappa}{v} \frac{dp_o(s)}{p_o(s)} \tag{3.25}$$

On the other hand, if the matric suction, s, reaches the suction SI yield value s_o, any further increase in suction along a specific value of mean stress, p, will induce a total volumetric strain increment given by

$$d\varepsilon_{vs} = \frac{\lambda_s}{v} \frac{ds_o}{(s_o + p_{atm})} \tag{3.26}$$

Likewise, the plastic component of the total volumetric strain increment due to the increase in suction can be obtain by subtracting the plastic volumetric strain increment from the total volumetric strain increment. The difference among these two values can be expressed by

$$d\varepsilon_{vp}^{p} = \frac{\lambda_s - \kappa_s}{v} \frac{ds_o}{(s_o + p_{atm})} \tag{3.27}$$

Alonso et al. (1990) argue that both sets of plastic deformations have similar effect on the control of the position of the LC and SI yield surfaces. Hence, a simple manner to couple both yield curves results if their positions is controlled by the total plastic volumetric strain, $d\varepsilon_v^p$, Therefore, the change in $p_o(0)$ and s_o may be calculated by

$$dp_0(0) = \frac{vp_o(0)}{\lambda(o) - \kappa} d\varepsilon_v^p \tag{3.28}$$

$$ds_o = \frac{v(s_o + p_{atm})}{\lambda_s - \kappa_s} d\varepsilon_v^p \tag{3.29}$$

3.3.3.5 Flow Rule

According to Alonso et al. (1990), the plastic strain increments associated with the yield surface f (Equation 3.17) are the plastic volumetric strain increment, $d\varepsilon^p_{vp}$, and the plastic deviatoric strain increments, $d\varepsilon^p_q$. A non-associated flow rule has been suggested to determine the direction of plastic strain increments. Hence, considering that conventional critical state models often overestimate K_o values (Gens and Potts, 1982) the expression for the associated flow rule is modified by introducing a parameter α proposed by Ohmaki (1982), resulting in the following equation

$$\frac{d\varepsilon_q^p}{d\varepsilon_{vp}^p} = \frac{2q\alpha}{M^2[2p + p_s - p_0(s)]} \tag{3.30}$$

The value of α derived by considering $K_o = 1 - \sin(\phi') = (6 - 2M)/(6 + M)$ and ignoring the deviatoric strain increments (i.e. $d\varepsilon^p_q = 0$), can be computed by

$$\alpha = \frac{M(M-9)(M-3)}{9(6-M)\left(1-\frac{\kappa}{\lambda(0)}\right)} \tag{3.31}$$

The vector of plastic strain increment associated with the suction increase (SI) yield surface will be the plastic volumetric strain increment due to changes in s, $d\varepsilon^p_{vs}$, which is given by Equation (3.26).

The elastic strain increments induced by changes in deviatoric stress, q, can be calculated as function of shear modulus, G, by

$$d\varepsilon_d^e = \frac{\sqrt{2}}{3}\sqrt{(d\varepsilon_1^e - d\varepsilon_2^e)^2 + (d\varepsilon_2^e - d\varepsilon_3^e)^2 + (d\varepsilon_3^e - d\varepsilon_1^e)^2} = \frac{1}{3G}dq \tag{3.32}$$

3.3.4 Modified BBM (Josa et al., 1992)

Alonso et al. (1987) stated that during wetting a partially saturated soil may either expand if the confining stress is sufficiently low, or collapse if the confining stress is sufficiently high. It is also possible that a soil might experience an initial expansion followed by collapse (Escario and Saez, 1973; Josa et al., 1987; and Burland and Ridley, 1996). Therefore, when the stress state is such that collapse occurs upon wetting, the soil deformations depend on the confining stress at which wetting takes place. In general, if the stress state is not high enough to cause collapse during wetting, low plasticity non-expansive soil will be experience small and reversible swelling. On the other hand, high plasticity expansive clays can experience large and irreversible deformations (Georgiadis, 2003).

Considering that the potential collapse due to wetting initially increases with confining stress reaches a maximum value and then decreases, the potential collapse in the v –ln p space is the difference between the partially and fully saturated isotropic compression lines. Therefore, the value of $\lambda(s)$ may depend not just on the soil suction but also on the range of mean net stress at which the tests were conducted (Wheeler and Karube, 1996).

The Barcelona basic model assumes linear isotropic compression lines for partially saturated conditions. These lines diverge from the fully saturated compression line (see Figure 3.11) which implies that the potential collapse due to wetting increases indefinitely with the confining stress. However, for most partially saturated soils the amount of potential collapse initially increases with confining stress reaches a

maximum value and then decreases tending to zero at very high stresses (Josa et al., 1992). To overcome this problem, Josa et al. (1992) presented a modified elasto-plastic model for unsaturated soils which incorporates curved normal compression lines that initially diverge and then converge. The formulated model is similar to the Barcelona Basic Model and will not be discussed here in its whole extension.

The propose modification allows the prediction of the maximum collapse at some value of confining stress through the introduction of a new expression to calculate the loading collapse (LC) yield curve in the p – s space. This expression which replaces Equation (3.16) of the Barcelona Basic model is given by

$$p_o(s) = \left(p_o(0) - p^c\right) + p^c[(1-m)e^{-\alpha s} + m] \qquad (3.33)$$

where,

a = parameter controlling the shape of yield surface

m = parameter related to the difference between $p_o(s)$ for high suction values (i.e. $s = \infty$) and $p_o(0)$.

The parameter m, which is always higher that one, can be calculated by

$$m = 1 + \frac{\zeta_y - 1}{\zeta_x - p^c}\left(p_0(0) - p^c\right)e^{\frac{\zeta_x - p_o(0)}{\zeta_x - p^c}} \qquad (3.34)$$

Josa et al. (1992) suggest that ζ_x can be replaced by the value of $p_o(0)$ corresponding to maximum collapse and ζ_y by the maximum plastic volumetric strain, $e_v^{p}{}_{max}$. Although no specific limits are provided, they also establish that the expression is valid in the range where adjacent yield surfaces do not intersect one to each other. Figure 3.18 shows the variation of m with $p_o(0)$. In this figure it is possible to see that m

reaches a peak value equal to ζ_y when $\zeta_x = p_o(0)$ and m tend to one for large values of $p_o(0)$. Additionally, from Equation (3.34) it can be established that m is equal to one when $p_o(0) = p^c$.

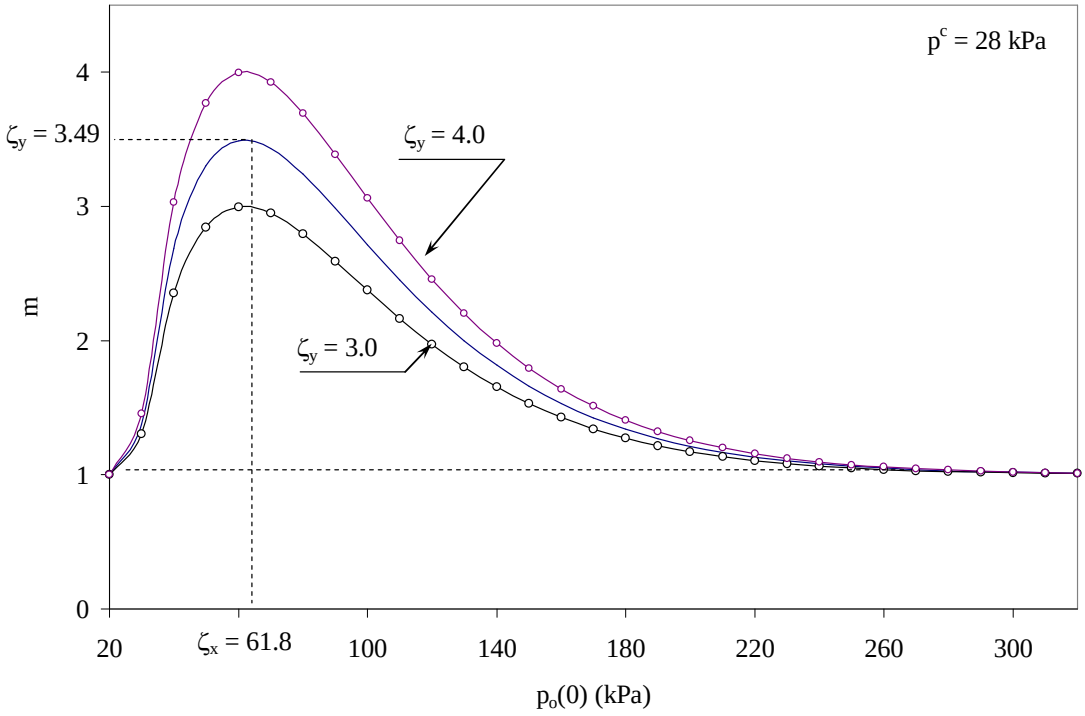

Figure 3.18 Variation of m with $p_o(0)$ for $\zeta_x = 61.8$ and $\zeta_y = 3.0$, 3.49, and 4.0.

The variation of the shape of the loading collapse yield curves for different values of α, $p_o(0) = 61.35$ kPa, $p^c = 28$ kPa and m = 3.494 is shown in Figure 3.19. In addition, the variation of the shape of the LC yield curve for different values of $p_o(0)$ and $\alpha = 0.00382$, $p^c = 28$ kPa and m = 3.494 is shown Figure 3.20.

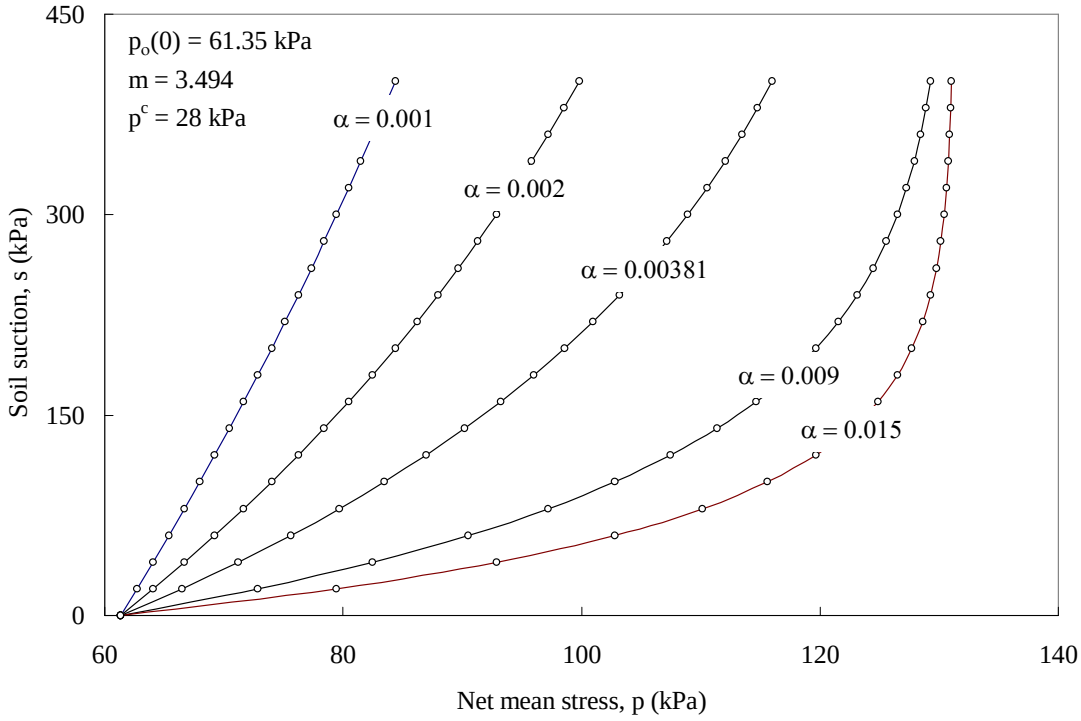

Figure 3.19 Shape of the Loading collapse yield curve for different values of $p_o(0)$.

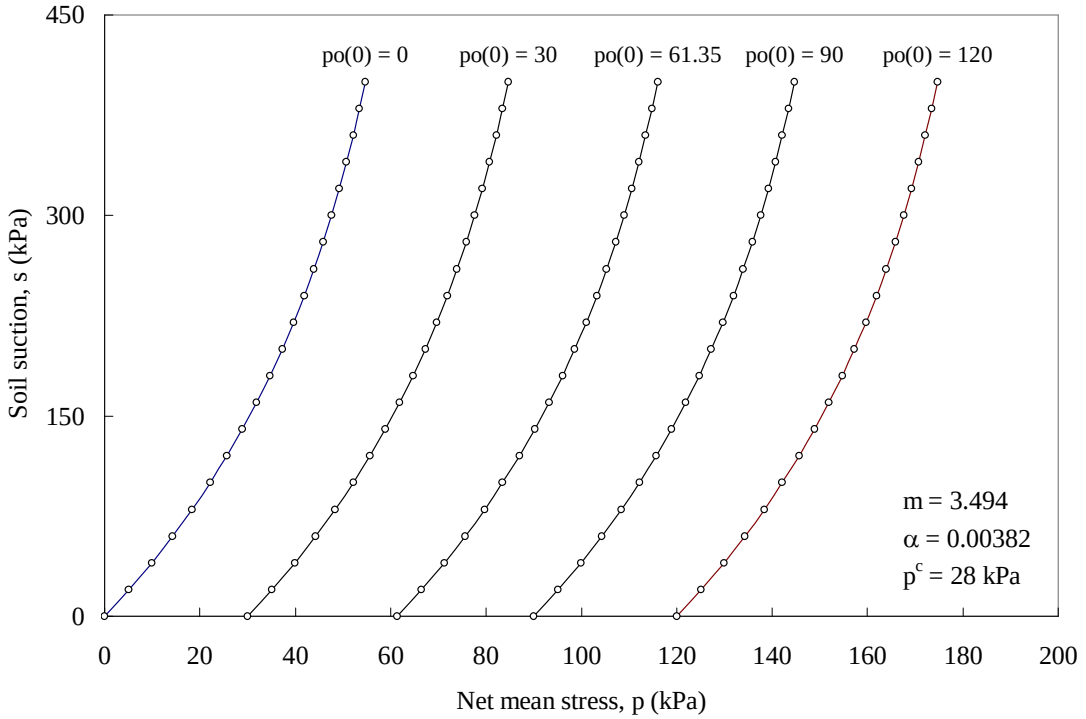

Figure 3.20 Shape of the Loading collapse yield curve for different values of $p_o(0)$.

Furthermore, Josa et al. (1992) suggest a modification on the hardening laws. Similarly to the Barcelona basic model, they assume that the evolution of the LC and SI yield curves is controlled by the hardening parameters $p_o(0)$ and S_o. However, they propose to replace Equations (3.28) and (3.29) and calculate the change in $p_o(0)$ and s_o using the following equations

$$dp_0(0) = \frac{p_o(0)}{\lambda(o) - \kappa} d\varepsilon_v^p \tag{3.35}$$

$$ds_o = \frac{(s_o + p_{atm})}{\lambda_s - \kappa_s} d\varepsilon_v^p \tag{3.36}$$

In order, to avoid negative values of void ratio, e, for high stresses or suction, it is established a hyperbolic relationship between specific volume, v, and both mean net stress, p, and soil suction, s. This contrast with the logarithmic relationship establish by the Barcelona basic model.

Similarly, hyperbolic relationship is also suggested to calculate elastic deformations as follow

$$d\varepsilon_v^e = \kappa \frac{dp}{p} + \kappa_s \frac{ds}{(s + p_{atm})} \tag{3.37}$$

3.3.5 Oxford Model (Wheeler and Sivakumar, 1995)

Wheeler and Sivakumar (1995) use the results o a series of suction-controlled triaxial tests performed on unsaturated samples of compacted speswhite kaolin, to develop an elastoplastic critical state constitutive framework for partially saturated soils. Although the proposed framework is very similar to that proposed by Alonso et al. (1990), the new framework assumes that all the model parameters are suction-

dependent. In addition, instead of use the reference stress, p^c, proposed by Alonso et al. (1990), the authors use the atmospheric pressure, p_{atm}, as reference stress. The fundamentals of the framework proposed by Wheeler and Sivakumar (1995) are presented in this section.

3.3.5.1 Model Formulation for Isotropic Stress State

Basis on results of suction-controlled hydrostatic compression tests conducted at preselected values of confinement, p, Wheeler and Sivakumar (1995) identified the existence of the LC yield curve produced by the initial compaction process. Hence, inside the LC yield curve the soil behaviour would be elastic. Therefore, increase in p would cause elastic compression and a decrease in s would cause elastic swelling. Furthermore, once the initial LC yield curve Increase is reached additional increase in p or reduction in s would cause the expansion of the LC yield surface and large component of plastic compression or collapse.

Thus, when the yield stress at a particular value of suction is exceeded, the soil fall on an isotropic normal compression that can be describe by

$$v = N(s) - \lambda(s) \ln \frac{p}{p_{atm}} \tag{3.38}$$

where

$\lambda(s)$ = soil stiffness parameter which depend on matric suction, s

p_{atm} = atmospheric pressure = 100 kPa

N(s) = specific volume at $p = p_{atm}$ which vary with matric suction, s

As mention before, Atmospheric pressure, p_{atm}, is included as a reference pressure to guarantee dimensional consistency and obtain a value of N(s) corresponding to a value of p that falls within the expected range of experimental data.

The expression to compute the LC yield curve is given by

$$\left[\lambda(s)-\kappa\right]\ln\frac{p_o(s)}{p_{atm}}=\left[\lambda(0)-\kappa\right]\ln\frac{p_o(0)}{p_{atm}}+N(s)-N(0)+\kappa_s\ln\frac{s+p_{atm}}{p_{atm}} \quad (3.39)$$

where

$\lambda(0)$ = soil stiffness parameter for saturated conditions (i.e. s = 0)

$p_o(0)$ = Isotropic yield stress for s = 0

N(0) = specific volume at $p = p_{atm}$ for s = 0

κ = elastic stiffness parameter for changes in net mean stress, p

κ_s = elastic stiffness parameter for changes in suction, s.

Some dependence of the elastic stiffness parameters κ and κ_s, on the net mean stress may be expected (Alonso et al., 1990). However, in absence of information they can be assumed to be independent p, and s (Wheeler and Sivakumar, 1995).

3.3.5.2 Model Formulation for General Stress State

The critical state corresponds to a condition where the soil structure is been continuously destroyed. Therefore, for constant soil suction, s, a soil sample subjected to continuous shearing will eventually arrive at a critical state condition, which corresponds to a certain values of net mean stress, p, and deviatoric stress, q. Hence, according to Wheeler and Sivakumar (1995) the critical state line in the p – q and p – v plane can be described respectively by

$$q = M(s)\,p + \mu(s) \tag{3.40}$$

$$v = \Gamma(s) - \psi(s)\ln\frac{p}{p_{atm}} \tag{3.41}$$

The parameters M(s), μ(s), Γ(s), and ψ(s) are function of suction. The variation of M with suction would be equivalent to a variable value of ϕ' in the conventional shear equation for unsaturated soils proposed by Fredlund et al. (1978)

$$\tau = c' + (\sigma - u_a)\tan\phi' + (u_a - u_w)\tan\phi^b \tag{3.42}$$

On the other hand, the non-linear variation of intercept μ(s) is equivalent to the non-linear variation of ϕ^b with suction reported in the literature (Wheeler and Sivakumar, 1995).

In addition, an elliptical shape has been selected to describe the yield curve on the p – q plane. Hence, the yield surface for a particular value of suction, with the apex located at the intersection of the yield curve with the critical state line (i.e. at $p = p_x$, $q = M(s)p_x + \mu(s)$), and crossing the isotropic normal compression line at $p = p_o(s)$ can be computed by

$$q^2 = M_*^2[p_o(s) - p][p + p_o(s) - 2p_x] \tag{3.43}$$

where

M_* = aspect ratio of the ellipse

$p_o(s)$ = Yield net stress at matric suction, s

p_x = net mean stress at the intersection of the yields surface with the CSL.

The yield net stress at matric suction, $p_o(s)$, which is the value of the net mean stress at the intersection of the yield surface with the isotropic normal compression line cam be calculated by

$$\frac{p_o(s)}{p} = \exp\left[\frac{N(s) - \lambda(s)\ln\left(\frac{p}{p_{atm}}\right) - v}{\lambda(s) - \kappa}\right] \tag{3.44}$$

Similarly, the net mean stress, p_x, at the intersection of the yield surface with the critical state line can be calculated by

$$\frac{p_x}{p} = \exp\left[\frac{\Gamma(s) - \psi(s)\ln\left(\frac{p}{p_{atm}}\right) - v}{\psi(s) - \kappa}\right] \tag{3.45}$$

$\psi(s)$ = slope of the critical state line.

The aspect ration of the ellipse, M_*, is the minor axis (i.e. $b = M(s)p_x + \mu(s)$) to major axis (i.e. $a = po - px$) given by

$$M_* = \frac{M(s)p_x + \mu(s)}{Po - P_x} \tag{3.46}$$

$\mu(s)$ = intersection of the critical state line with the deviatoric stress axis.

The physical meaning of all parameters in Wheeler and Sivakumar model are depicted schematically in Figure 3.21.

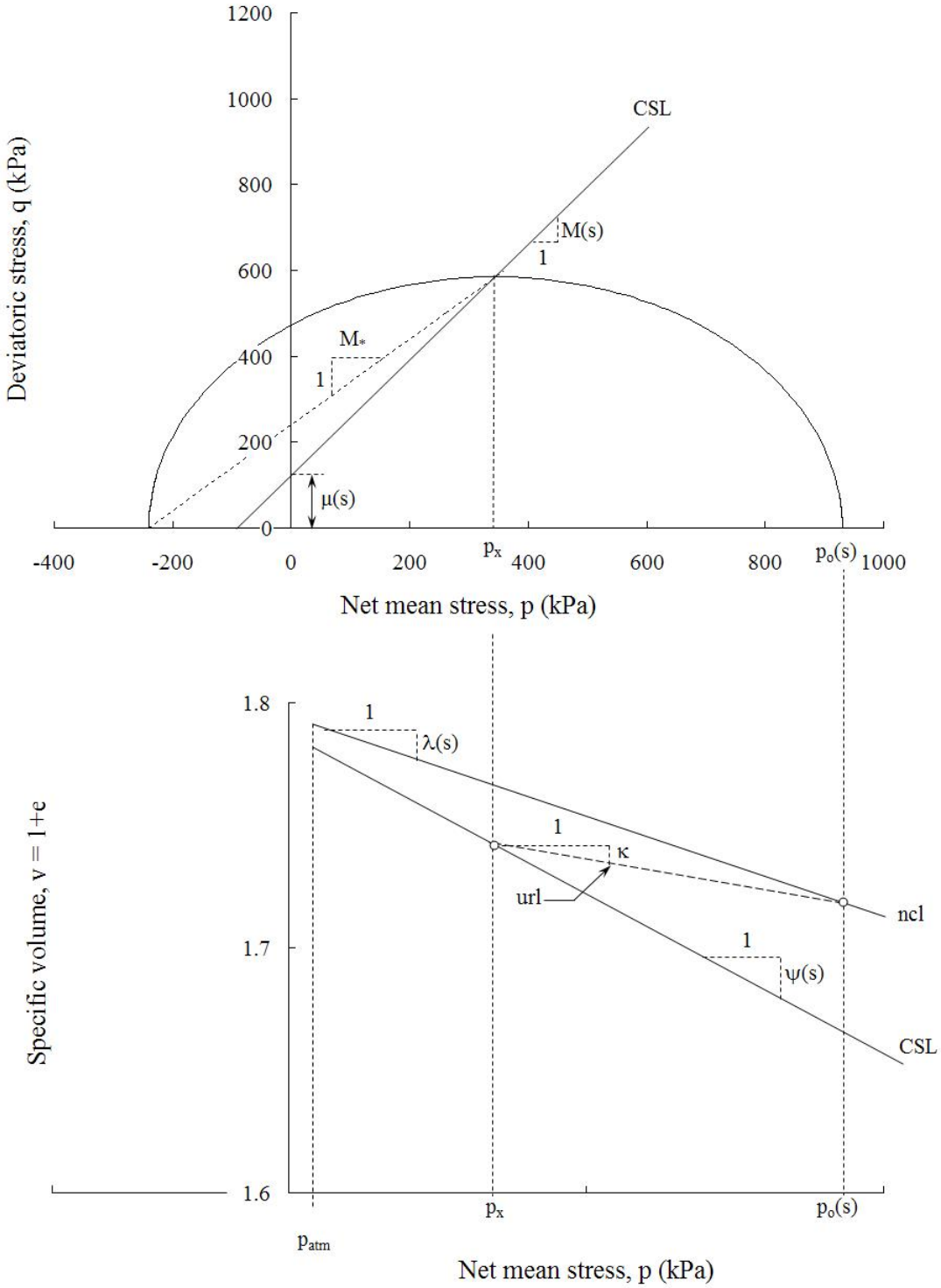

Figure 3.21 Schematic of constant suction yield surface and specific volume variation proposed by Wheeler and Sivakumar (1995) for unsaturated soils.

3.3.5.3 Flow Rule

An associated flow rule is adopted to predict the development of plastic shear strain during suction-controlled shear tests. Hence, the development plastic shear strain increments, $d\varepsilon_q$, can be predicted by

$$\frac{d\varepsilon_q^p}{d\varepsilon_{vp}^p} = \frac{q}{M_*^2(p - p_x)}$$

Elastic components of shear strain are predicted by assuming a constant value for shear modulus, G. The shear modulus is obtained as the average of the initial slope of the experimental stress-strain curve.

Next chapter presents a brief summary of the previous work considered relevant for the development of this current research work. In addition, the chapter includes a detailed description of the novel servo-controlled cubical apparatus implemented in this dissertation work.

CHAPTER 4

A REFINED SUCTION-CONTROLLED TRUE TRIAXIAL APPARATUS

4.1 Introduction

The development of true triaxial devices dates back to the 1930s. The idea of testing a cubical soil sample by applying three different normal stresses was first employed by Kjellman (1936). However, this device became popular until the 1960s, due to their capability of measuring and/or controlling deformation and stress under known stress pathS (Bell, 1965; Ko and Scott, 1967).

On the other hand, in the past four decades the description of elastoplastic deformation behaviour of soils has found significant interest in the research literature and the development and validation of constitutive models has become an important research area. Soil modeling involves interaction and feedback between analytical and experimental work. Therefore, experimental results obtained from multiaxial tests conducted in true triaxial devices have become essential to evaluate the capability of these analytical models (Reedy et al, 1992).

Several true triaxial devices have been developed by different researchers. All of them can be classified according to their boundary surfaces into three main categories (Airey and Wood, 1988; Arthur, 1988): flexible (i.e. stress-controlled) boundaries (Bell, 1965; Ko and Scott, 1967; Sture and Desai, 1979; Reedy et al., 1992; Callisto and Calabresi, 1998), rigid (i.e. deformation-controlled) boundaries (Hambly, 1969; Airey

and Wood, 1988, Lanier, 1988; Matsuoka et al., 2002), and a combination of rigid and flexible boundaries (Lade and Duncan, 1973; Hoyos, 1998; Park, 2005). Strain distribution produced by a strain-controlled rigid boundary type device could be less sensitive to intrinsic sample heterogeneity than that produced by a stress-controlled, flexible type. Unrealistic behavior and premature failure due to the strain heterogeneity introduced in soil samples by using mixed rigid and flexible boundary conditions have frequently reported (Sture and Desai, 1979).

The core system of the device implemented in this work is a mixed boundary type of device designed and manufactured at the University of Colorado-Boulder (Park, 2005). It features a rigid surface at the bottom and five flexible membranes (one top and four laterals) that are used to transmit the applied pressure uniformly to the soil specimen faces. The core system was further modified at UT-Arlinton (Laikram, 2007) to accommodate a high-air entry (HAE) ceramic disk and four pore stones located at the bottom face to allow for the application of matric suction via axis translation technique. In addition, a pressure control panel (PCP-5000) from Geotechnical Consulting and Testing Systems (GCTS) is used to control and/or measure stress and strain during suction-controlled test.

4.2 Previous Work

True triaxial devices have the capability of applying three independent principal stresses or strains to a cubical soil specimen. Therefore, as an advantage, the true triaxial device offers one or more degree of freedom than the conventional triaxial apparatus. However, the principal axes remain fixed in the true triaxial apparatus, so

they can not be used to apply the continuous rotation of principal stresses that are possible in other apparatus, such as the hollow cylinder apparatus or the directional shear cell (Airey and Wood, 1988). Nevertheless, the flexibility of the cubical cell allows applying shear loading by following any specified stress or strain path.

To take advantage of the capability offered by the true triaxial devices to test soil specimens along multi-axial stress paths, the design of true triaxial devices have been modified to conduct suction-controlled test on partially saturated soil specimens. It is in this context that the true triaxial apparatus have become a fundamental tool in the complete stress-strain characterization of the soil. As mentioned above, true triaxial apparatus have been fabricated with rigid boundaries (i.e. strain-controlled boundaries), flexible boundaries (i.e. stress-controlled boundaries), and combination of rigid and flexible boundaries. Three previous works, considered relevant for the development of this research will be discussed briefly in this section.

4.2.1 True Triaxial With Mixed Boundaries by Hoyos and Macari (2001)

Hoyos and Macari (2001) implemented a mixed boundary type true triaxial apparatus. As shown Figure 4.1, the setup consists basically of a frame that supports the bottom wall assembly and five wall assemblies (i.e. one top and four laterals). As shows in Figure 4.2, the bottom wall assembly, which imposes a rigid boundary at the bottom face of the cubical specimen, accommodates the cubical base piece housing a HAE ceramic disk. The ceramic disk is mounted in a 1.05 cm height and 8 cm diameter cavity machined on the top surface of the cubical base piece, which allows applying pore-water pressure, u_w, at the bottom of the cubical specimen. HAE ceramic disk was

saturated in place using the triaxial cell (Hoyos, 1998). A flushing mechanism at the bottom wall assembly allows eliminating air bubbles that may be trapped or have been accumulated as a result of diffusion. Pore-air pressure, u_a, is applied to the top and four lateral faces of the specimen via small cooper block attached to the flexible membranes with a threaded stem. Water pressure and external air pressure is applied via nylon tubing.

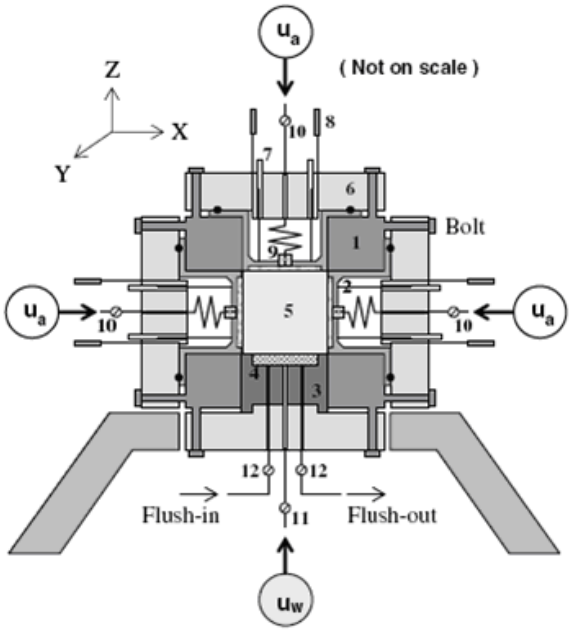

1. Cubical frame	5. Soil specimen	9. Cooper block/steam
2. LATEX/POREX	6. Wall assembly	10. Air pressure valve
3. Cubical base piece	7. LVDT	11. Water pressure valve
4. Ceramic disk	8. Pressure inlet/outlet	12. Flushing valve

Figure 4.1 Cross-sectional view of complete wall assemblies (Hoyos and Macari, 2001).

On the other hand, each lateral and top wall assembly accommodates a flexible membrane and three LVDTs. When the membranes are mounted on the frame each assembly provides an effective seal against the leaking of the pressurized fluid. The

flexible membranes transmit the applied pressure uniformly to the top and lateral faces of the cubical unsaturated soil specimen. The hydraulic pressure applied through flexible membranes to the top and bottom sides of the cubical unsaturated soil specimen is generated and controlled by a computer-driven electrohydraulic pressure system.

The deformation of the cubical soil specimen is measured at three points on the top face, and on each of the four lateral faces, using the three LVDTs located on each wall assembly. Deformations on each side of the cubical soil specimen, along a particular direction are estimated by averaging the three LVDTs' outputs.

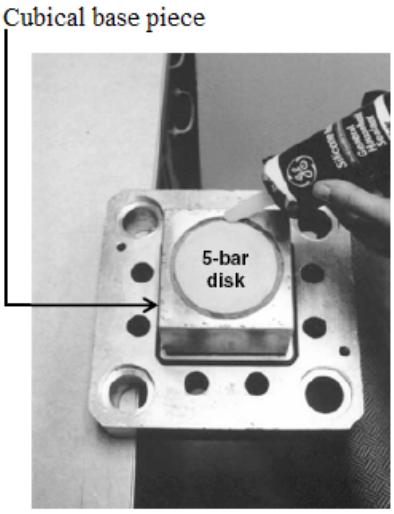

Figure 4.2 Bottom wall with HAE ceramic disk (Hoyos and Macari, 2001).

The 10 cm per side cubical soil specimen were tested following a multi-stage testing procedure by controlling the major, intermediate, and minor principal stresses. Matric suction states in the specimens were induced and maintained constant during the testing via the axis translation technique (Hoyos, 1998). The soil material used in the study is a low-plasticity silty sand (SM). All 10 cm per side cubical specimens were

prepared using tamping compaction method. A series of 8 drained controlled-suction isotropic loading tests were conducted at constant matric suction, s = 50, 100, 200, and 350 kPa. In addition a series of 12 drained, suction-controlled CTC and TC test were conducted on 6 identically prepared specimens of compacted silty sand. Figure 4.3 Figure 4.4 show the experimental and predicted stress-strain relationship for the drained stress/suction controlled CTC and TC tests conducted on cubical recompacted silty sand specimens at different values of matric suction. Numerical predictions were calculated using both explicit and implicit integration technique. Good agreement is observed.

Furthermore, soil specimens were monotonically sheared by following constant-suction triaxial extension (TE) and simple shear (SS) stress path, until apparent deviatoric stress had reached a peak value. Figure 4.5 shows the predicted strength loci in the deviatoric plane for all TC, TE, and SS tests conducted under σ_{oct} = 50 and 200 kPa. In general, good agreement is observed between the predicted and experimental soil response.

The apparatus described above presented some limitations (Hoyos et al. 2008). Among them, occasional clogging of the HAE ceramic disk due to the debris generated by the cubical steel frame corrosion, low durability of the latex membranes when exposed to hydraulic fluid for a extended period of time, and delay in the equalization stage due to the impossibility of controlling pore-water temperature. Additionally, changes in pore-water and pore air-volume cannot be measured. As an advantage over rigid boundary type triaxial devices, the application of loads through flexible membranes that contain fluid under pressure, generated by three independent channels,

results in uniform and known boundary stresses on all six faces of the specimen. Therefore, a principal stress state is assured at the boundaries (Sture and Desai, 1979).

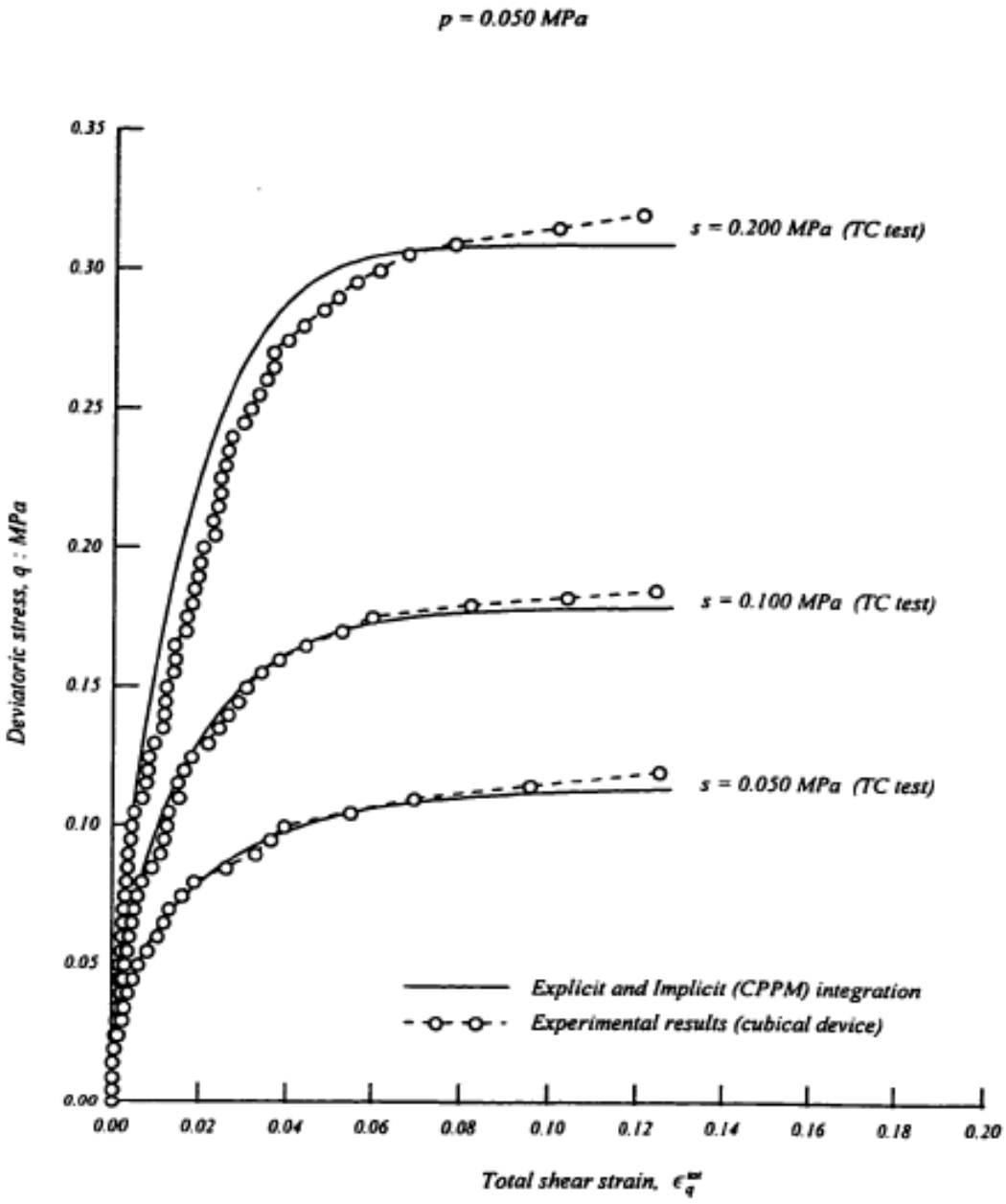

Figure 4.3 Experimental and predicted stress-strain relationship for the drained stress/suction controlled TC tests conducted on cubical recompacted silty sand specimens at different values of matric suction (Hoyos, 1998).

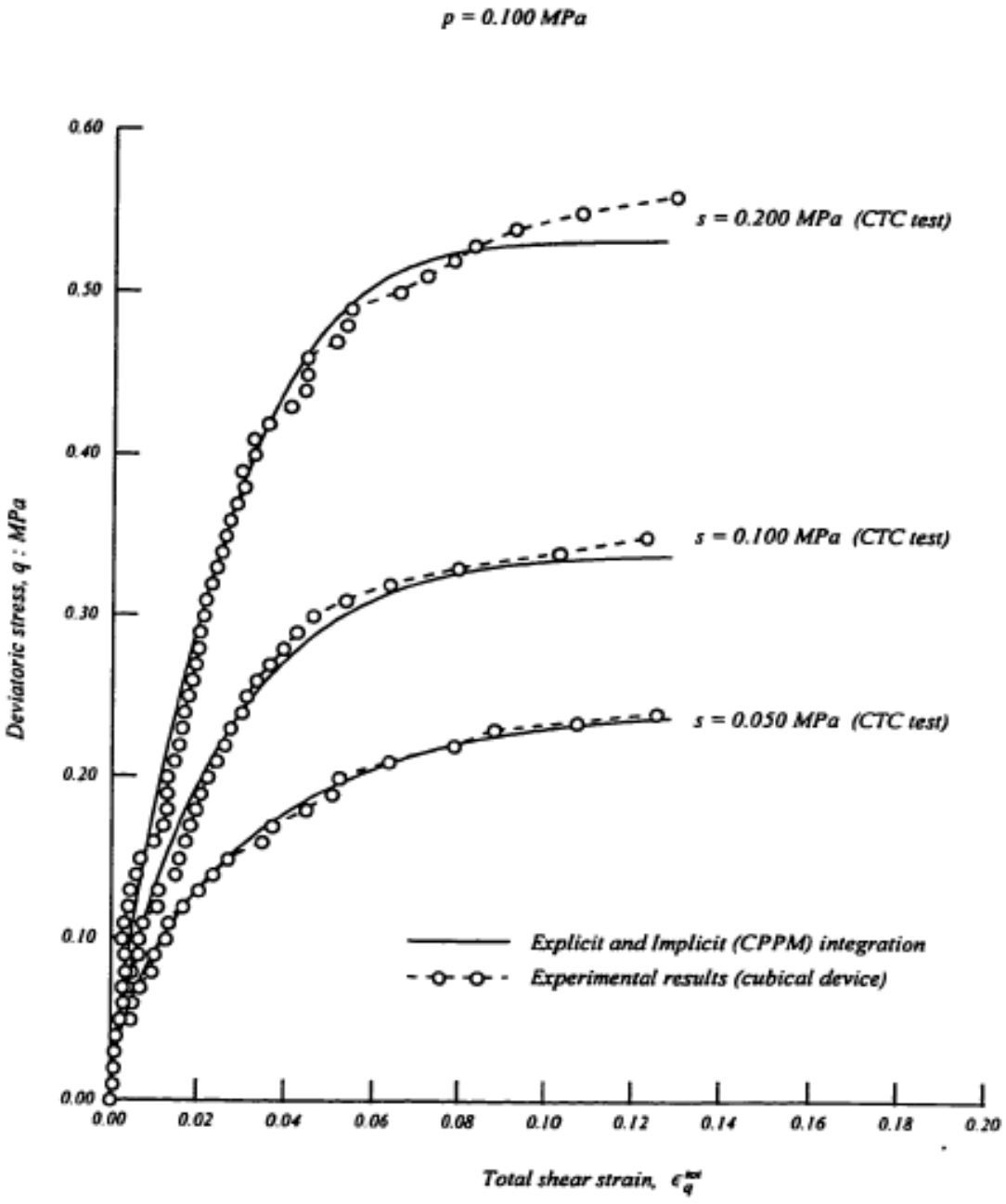

Figure 4.4 Experimental and predicted stress-strain relationship for the drained stress/suction controlled CTC tests conducted on cubical recompacted silty sand specimens at different values of matric suction (Hoyos, 1998).

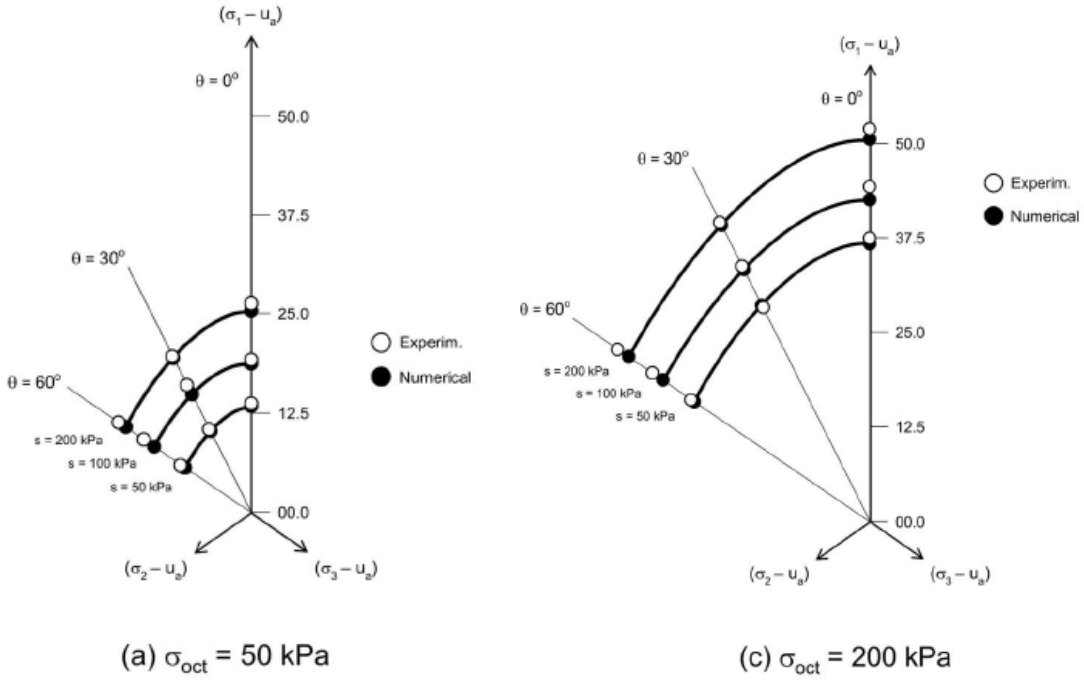

Figure 4.5 Experimental and predicted strength loci in deviatoric plane (Hoyos and Arduino, 2008).

4.2.2 True Triaxial With Rigid Boundaries by Matsuoka et al. (2002)

Matsuoka et al. (2002) described the use of a true triaxial apparatus with three pair of rigid loading plates in three orthogonal directions. As shown in Figure 4.6, one ceramic disk 70 mm diameters and two porous stones disks 5 mm diameter were mounted in both the upper and lower loading plates. With an air entry value of 300 kPa, the ceramic disks allow only water to move through by applying negative pore-water pressure to the specimen. A costume made cylindrical cell that allows saturation of the ceramic disk while mounted in the loading plate, was used to saturate the ceramic disk in the upper and lower plates before testing. The negative pressured water is connected to the pore water of the specimen trough the upper and lower loading plates through the

ceramic disks. On the other hand, the porous stones with polyfluorotetraethilene filter, allow only air to pass through.

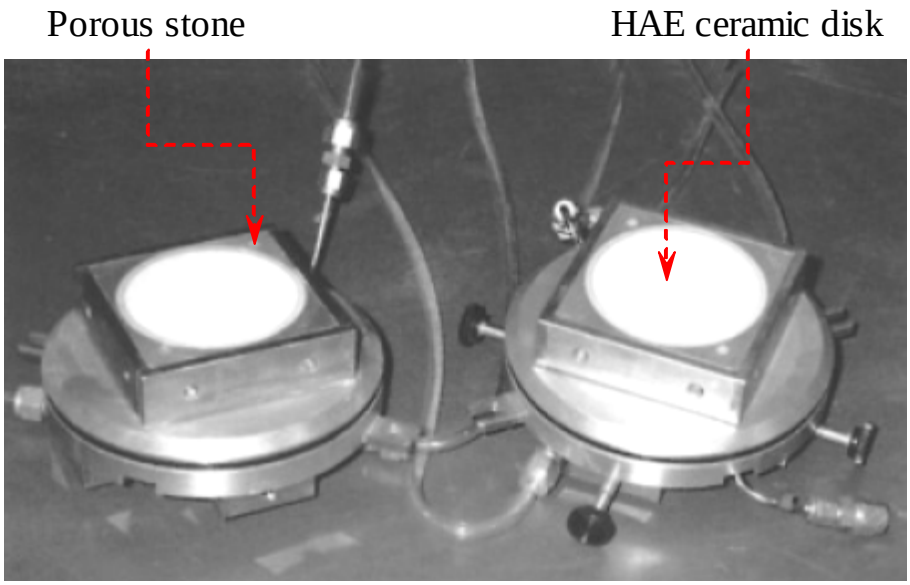

Figure 4.6 Upper and lower rigid loading plates (Matsuoka et al., 2002).

As shown in Figure 4.7, a cubical unsaturated silty soil specimens of 10 cm side, was sited between the two rigid loading plates housing the ceramic disks and the porous stones. A membrane is placed between the soil specimen and the other four rigid loading plates. Once the true triaxial device was assembled, the specimen was isotropically consolidated up to a consolidation pressure of 98 kPa under a matric suction, s = 59 kPa. After consolidation, a shear loading was applied to the cubical soil sample. The full shearing process was divided into about ten steps until peak failure. All plain-strain shear test were conducted at constant net mean stress, p_{ini} = 98 kPa, constant matric suction, s = 59 kPa, and under drained conditions.

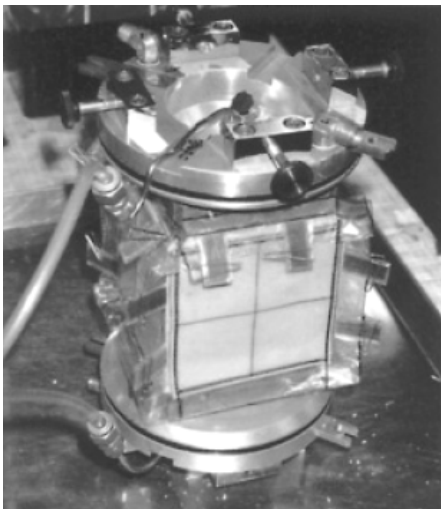

Figure 4.7 Cubical silty soil specimen with the upper and lower loading plate (Matsuoka et al., 2002).

The true triaxial tests in this study were conducted along the radial stress path in the π-plane. Since the normal stresses on the specimen are applied by three pairs of rigid plates, the interference between the loading plate in the σ_1 and σ_2 direction become notable when θ is large. For this reason, only stress paths with $0 \leq \theta \leq 30^o$ were performed (Figure 4.8).

To calibrate the developed true triaxial device for unsaturated soils, Matsuaka et al. (2002) compared the test results obtained from drained suction-controlled triaxial compression (TC) tests conducted in the cubical cell with those conducted on a conventional triaxial. In both cases the TC tests were conducted on the same soil under identical conditions. Although the pore-water pressure in the conventional triaxial was applied at the pedestal, using a HAE ceramic disk with an entry value of 275 kPa, and the air pressure was applied at the top through a filter, the stress-strain relationship measured by the two methods shows good agreement (Figure 4.9).

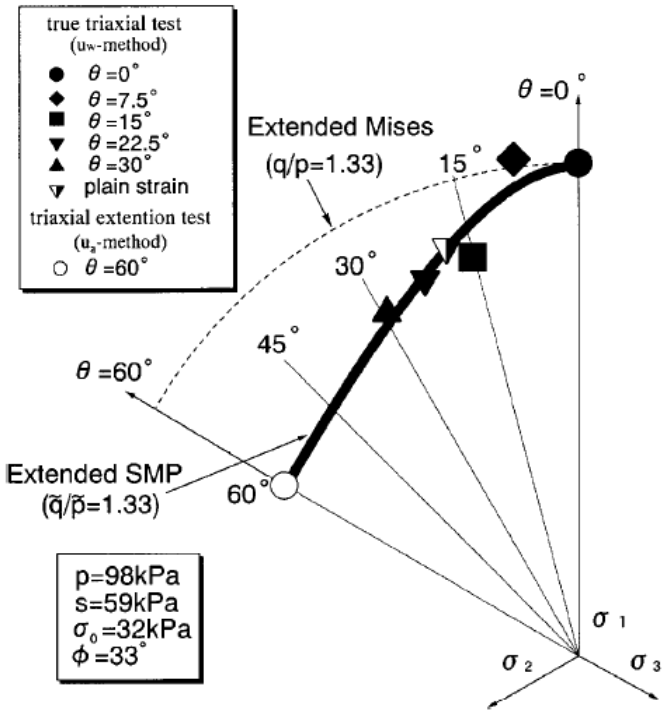

Figure 4.8 Strength of unsaturated soil in the π-plane (Matsuoka et al., 2002).

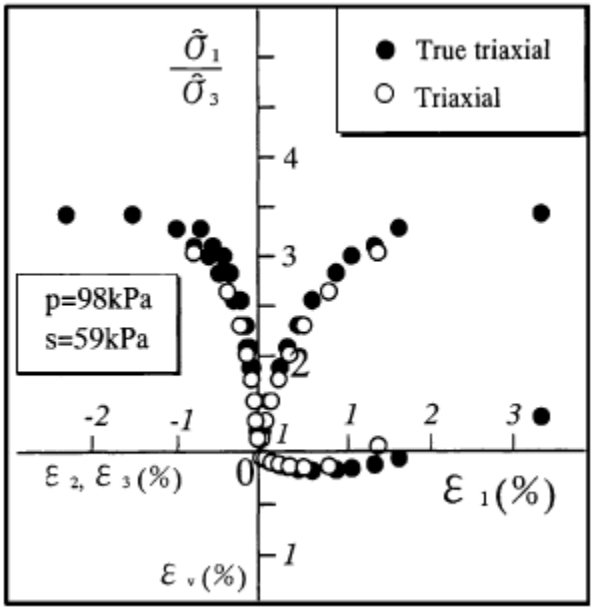

Figure 4.9 Comparison of results of suction-controlled TC tests using conventional triaxial and true triaxial apparatus (Matsuoka et al., 2002).

Although Matsuaka et al. (2002) report the use of floating suspension system counterweights to reduce the friction between the upper and lower loading plates and the surfaces of the specimen, undesirable boundary effects still experienced with the rigid loading platens are also reported. This limitation, which reduces the capability of the device to only stress paths with θ between 0^o and 30^o on the octahedral plane, could be attributed to the friction between platens and sample, normally observed in triaxial apparatus with rigid boundaries. The friction tends to produce a confining effect that can compromise the test results (Sture and Desai, 1979). Moreover, the method used to impose suction to the soil specimen through negative pressured water connected to the ceramic disks located in the upper and lower loading plates, reduce the ability of the device to perform tests at high values of matric suction.

4.2.3 True Triaxial With Mixed Boundaries by Laikram (2007)

Laikram (2007) implemented a mixed boundary type of true triaxial apparatus, similar to that implemented by Hoyos and Macari (2001). Some limitations on the cubical cell implemented by Hoyos (1998) were addressed and corrected in this research work.

An aluminum frame supports the bottom wall assembly and five (one top and four lateral) wall assemblies. The bottom wall assembly, machined from a solid aluminum plate, match into the lateral cavities of the frame. A HAE ceramic disk and four coarse porous stones accommodated on the rectangular prism machined on top of the bottom wall assembly, allows keeping constant matric suction into the soil specimen, via axis translation technique. Pore-air and pore water pressure are applied at

the bottom of the cubical soil specimen through four coarse porous stones and one HAE ceramic disk, respectively. Air and water pressure are supplied via nylon tubing from a pressure control panel (PCP-5000) developed by GCTS. The PCP-5000 unit features pore-water volume, v_w, with 0.01 cc resolution. HAE ceramic disks was saturated before testing in a custom made cylindrical cell that allows saturation of three ceramic disk at the time. Once saturated, the ceramic disk was mounted in the bottom wall assembly.

The top and later wall assemblies, also machined from solid aluminum plate, have three holes machined into each cover plate to receive the stainless steel housing of three linear variable differential transformers (LVDTs), and two additional holes for the pressure inlet/outlet connection (Figure 4.10). When the membranes are mounted onto the frame, each assembly provides an effective seal against the leaking of the pressurized water. Latex membranes transmit the applied pressure uniformly to the top and four lateral faces of the cubical soil specimen. The membranes were prepared in the laboratory using a Silastic J-RTV Dow Corning silicone rubber.

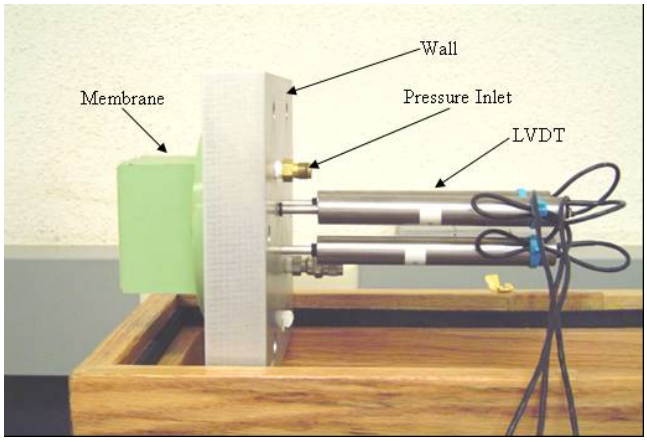

Figure 4.10 Photograph of wall assembly (Laikram, 2007).

Distilled water is used to apply pressure to the top and four lateral faces of the unsaturated cubical specimen; throughout the cubical latex membranes. A 50-gallon air compressor manufactured by Husky, with variable output pressure up to 125 psi, is used to supply pressurized air to the pressure panel shown in Figure 4.11. Three independent compressed-air pressure regulators are used to manually apply the three independent principal stresses to the cubical unsaturated soil specimen. The applied pressure is measured using three DPG 500 OM series pressure transducers, manufactured by Omega Engineering, Pressure regulators can be operated independently and almost simultaneously, allowing applying any stress path (Laikram, 2007).

Figure 4.11 Pressure panel (Laikram, 2007).

Although the test is manually conducted, an automated data acquisition system was used to monitor and store the resulting deformation measured by the LVDT's. The analog input signals (Voltage) delivered by the LVDT are converted into digital signals by an analog-to-digital converter, SCB-100 from National Instruments, connected to the direct interface card, PCI-6603E from National Instruments. A DC Power Supply

6303D from Topward was used to supply excitation power the LVDTs. A photo of the setup is presented in Figure 4.12.

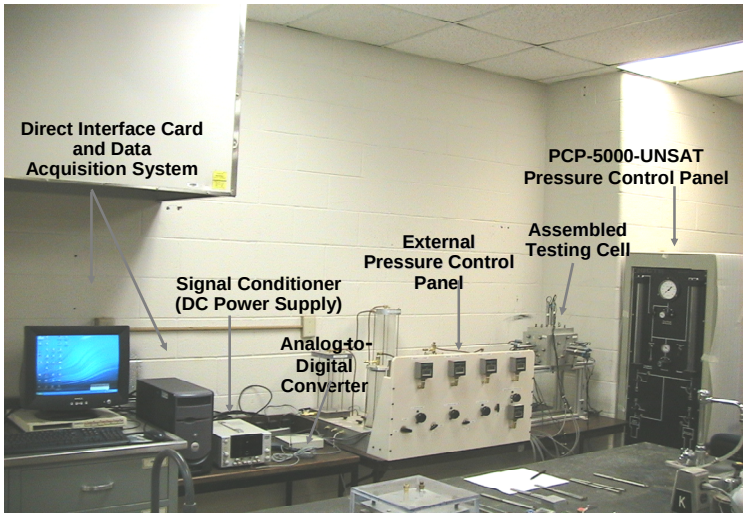

Figure 4.12 True triaxial device setup (Laikram, 2007).

After full saturation of the 5 bar HAE ceramic disk, housed by the bottom assembly of the test cell, poorly graded silty sand was used to prepare 10 cm per side cubical specimens by using tamping compaction on place. Each specimen was subjected to a multistage testing scheme in which the desired suction state was kept constant. Once the sample reached equilibrium under an initial net mean stress, p_{ini}, a monotonic shearing was imposed by following a suction-controlled CTC, TC, or TE stress path, until the deviatoric stress had reached a peak value. A detailed description of the test procedure is presented by Laikram (2007). Figure 4.13 and Figure 4.14, show the projection of the failure surface (incipient critical state condition at ε_q^{tot} = 10%), identified during TC and TE tests, on the deviatoric stress plane (or π-plane) for different values of matric suction, s = 50 kPa (7 psi), 100 kPa (14 psi), 200 kPa (29 psi), 300 kPa (44 psi), and 400 kPa (58 psi), as a function of the initial net mean stress.

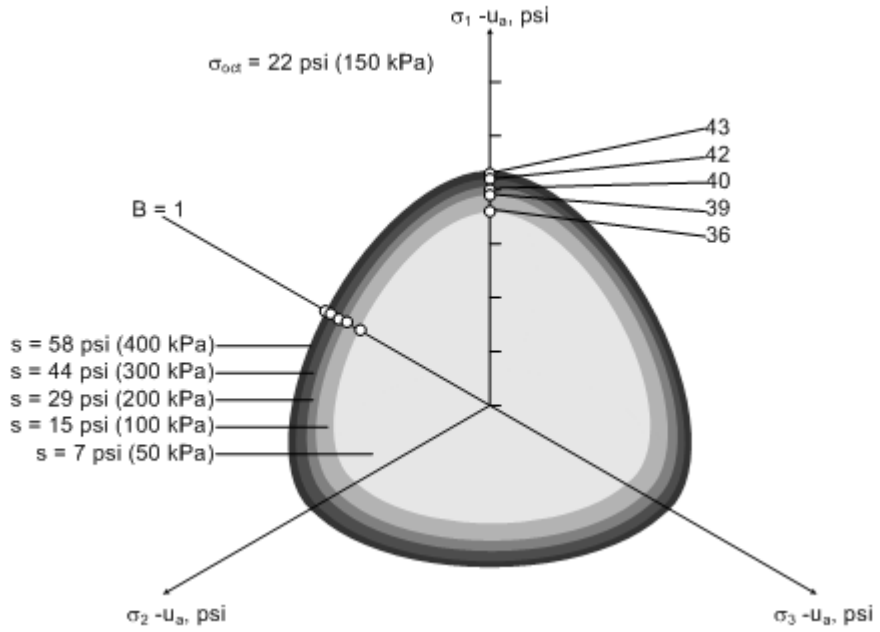

Figure 4.13 Projections of failure envelopes on octahedral plane at σ_{oct} = 150 kPa (Laikram, 2007).

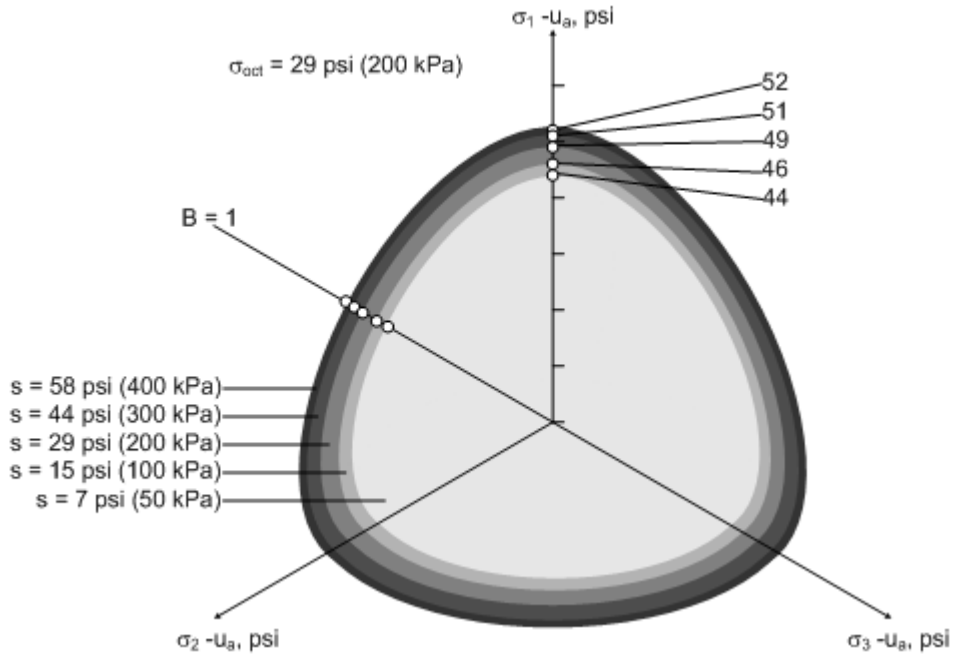

Figure 4.14 Projections of failure envelopes on octahedral plane at σ_{oct} = 200 kPa (Laikram, 2007).

Although several limitations of the cell used by Hoyos and Macari (2001) have been corrected, the pressure control panel used to apply and control the stress application and the low resolution of the DPG 500 OM series pressure transducers restrict the load rate to a minimum value of 1 psi (6.9 kPa). Load increments of 2 psi (13.8kPa) are applied equally spaced in time. The increment is applied instantly at the beginning of the time period. At the end of the period, the deformation experienced on each face of the sample is obtained by averaging the readings of the three LVDTs located on the wall assemblies (top and lateral). Therefore, the strain data acquisition becomes manual and no data is acquired between any two consecutive load increments.

4.3 A Refined True Triaxial Apparatus

The suction-controlled cubical test cell used in this research work is similar to that reported by Reedy et al. (1992), Hoyos and Macari (2001), and Laikram (2007). The true triaxial device consists of the following main components: a cubical frame, five wall assemblies, a bottom wall assembly, a deformation measuring system, a stress-control system, five cubical latex membranes, a pore-air pressure control/monitoring system, a data acquisition and process control system, and a suction-controlled control/monitoring system. A detail, illustrated description of these components is provided in this section.

4.3.1 Core Frame

The true triaxial cubical frame shown in Figure 4.15 was machined from solid aluminum. A square cavity was machined into each of the six faces to accommodate the membranes and to form the pressure cavities. The frame supports the top and lateral

wall assemblies, and the bottom wall assembly with the high-air entry disk and four coarse porous stones. The six walls are securely attached onto the cubical frame through the six connection bolts provided on each face of the frame. The outside of the fame was machined to a dimension of 19 cm (7.5 in), while the inner cubic cavity has dimension of 8.15 cm (3.2 in).

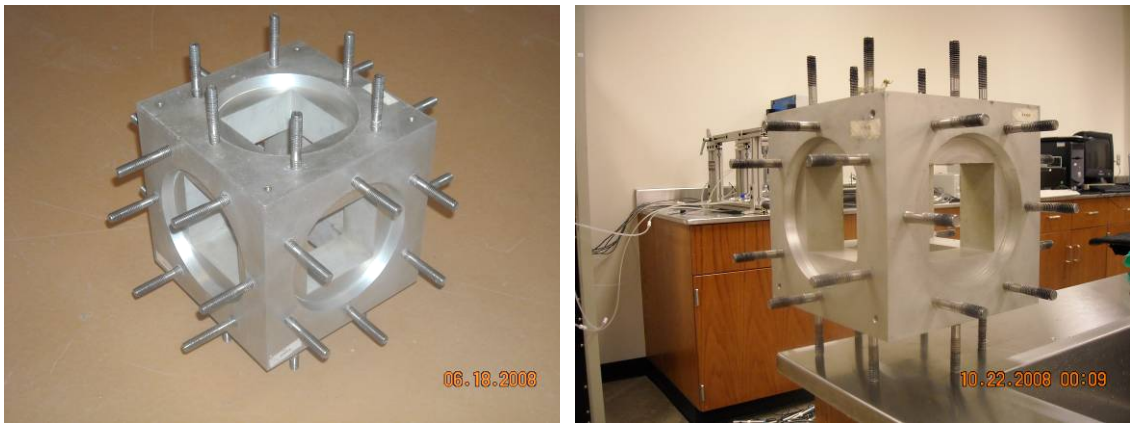

Figure 4.15 Core cubical frame.

4.3.2 Bottom Wall Assembly

The bottom wall assembly was machined from solid aluminum by Geotechnical Consulting and Testing Systems (GCTS). This assembly, which holds the high-air entry ceramic disk and four coarse porous stones, imposes a rigid boundary at the bottom face of the cubical unsaturated soil specimen. The 8.65 cm (3.4 in) height, 19 cm (7.5 in) side aluminum piece shown in Figure 4.16 was designed to conform the bottom wall assembly of the cubical frame. Therefore, a rectangular prism with 8.145 cm (3.2 in) side dimension and 5.46 mm (2.15 in) in height was machined on top of the bottom wall to match the bottom square cavity of the cubical frame.

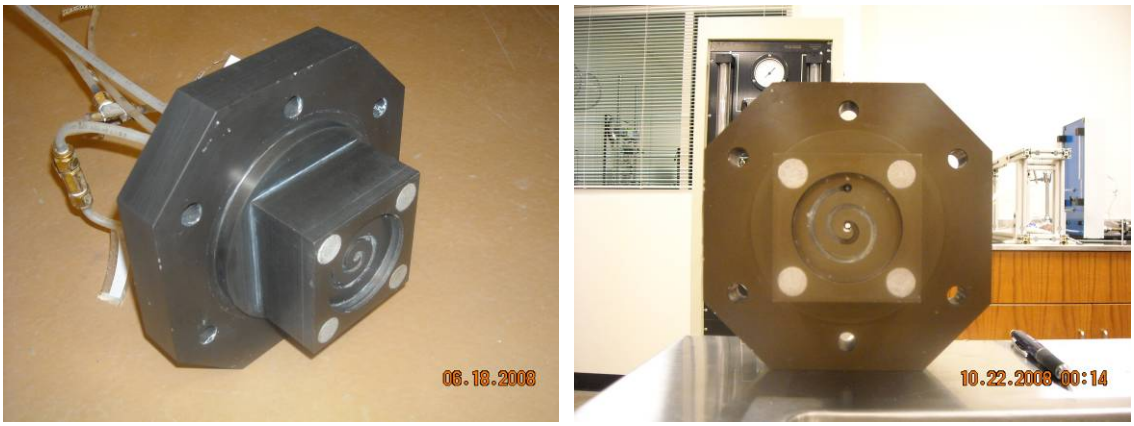

Figure 4.16 Bottom wall assembly.

A 0.76 cm (0.30 in) depth, 6.05 cm (2.38 in) diameter cavity was machined at the center of the top surface of the rectangular prism on the bottom wall to accommodate the HAE ceramic disk. This cavity has a grooved water compartment underneath the ceramic disk that serves as water channels for flushing air bubbles that may be trapped or have accumulated as a result of diffusion. In addition, the cavity allows uniform distribution of the pressure applied to the pore-water via the HAE disk. The ends of the water channel have been connected to the exterior face of the bottom wall assembly through two small 0.3 cm (1/8 in) diameter holes. As shown Figure 4.17, a 0.6 mm (1/4 in) fitting fastened on the outside face allows connecting 1/4 in OD tubing to each hole to control pore-water pressure, u_w, and serve as flushing mechanism.

In addition, four small 1.9 cm (0.75 in) diameter 0.6.5 mm (1/4 in) depth cavities were machined on each corner of the rectangular prism base, to accommodate equal number of coarse porous stones used to diffuse the pore-air pressure supplied to the cubical soil specimen. Each pore stone cavity is connected with the outside face of the wall assembly through a 0.3 cm (1/8 in) diameter hole. Air-pressure is supplied to

the bottom of the soil specimen using nylon tubing connected to the fittings fastened to the outside of the bottom wall assembly (Figure 4.17). The pore stones have been bound and sealed into the bottom wall assembly using slight amount of water-proof silicon resin along its perimeters.

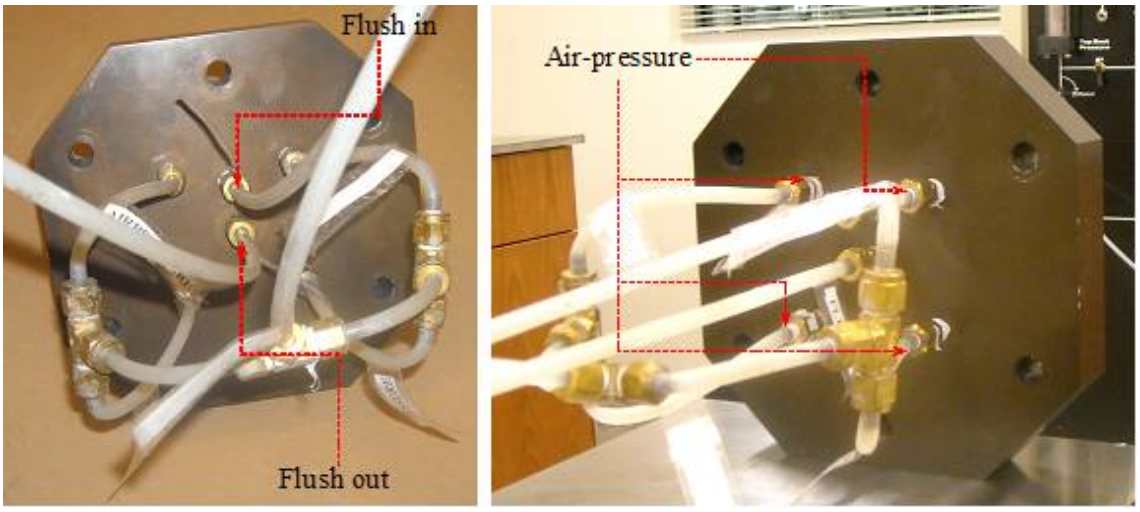

(a) (b)

Figure 4.17 Outside face bottom wall assembly: (a) Tubing fittings for pore-water control and flushing; (b) Tubing fittings for air-pressure control and supply.

The HAE ceramic disk shown in Figure 4.18 has been secured and sealed into the stainless steel ring using water-proof silicon resin along its perimeter. The 70 mm (2.8 in) diameter o-ring used to attach the stainless steel ring to the cubical aluminum base cavity ensures that air will not leak into the water compartment located beneath the HAE ceramic disk. Once all the components of the bottom assembly are in place, the bottom assembly is fastened to the bottom face of the cubical frame by six steel studs mounted in threaded holes on the exterior of the frame as shown in Figure 4.19. The

cubical frame with the bottom assembly is secured to the supporting frame as shown in Figure 4.20.

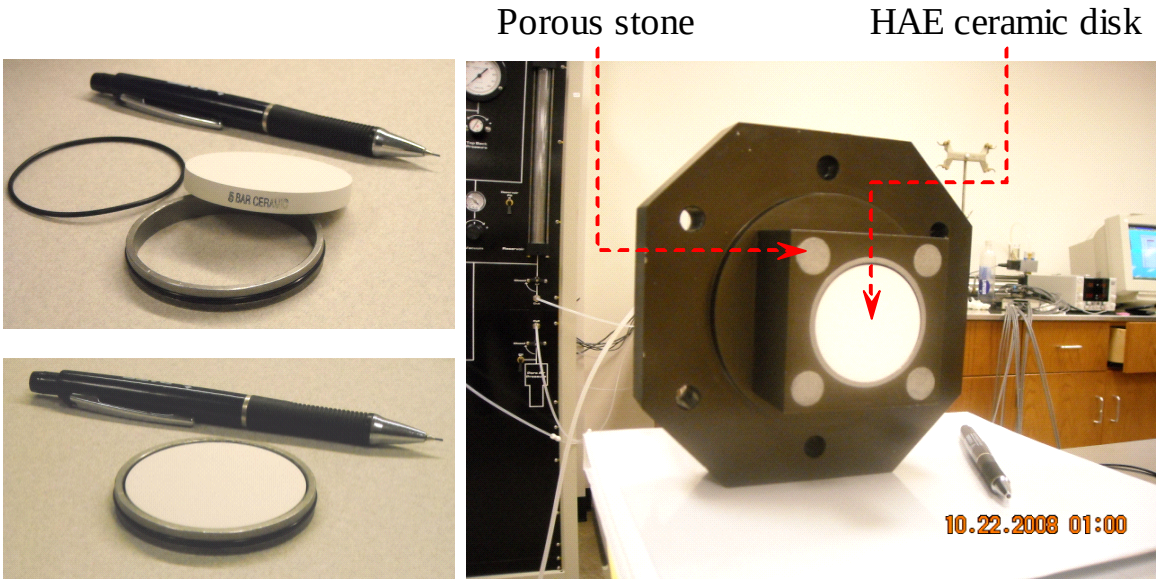

Figure 4.18 Bottom wall assembly with HAE ceramic disk and four coarse stones.

Figure 4.19 Cubical frame with the bottom assembly (shown upside down).

Figure 4.20 Cubical frame with the bottom assembly secured to the supporting frame.

4.3.3 Top and Lateral Wall Assemblies

The wall assemblies were machined from solid aluminum plates. As shown in Figure 4.21 the main plate, which provides the wall seal for the interior pressure cavity, has two threaded holes to connect the fluid pressure inlet and outlet respectively, and three holes to receive the stainless steel housing of the linear variable differential transformers (LVDT's). Once the membranes are mounted on each wall assembly (Figure 4.22) and the cubical soil sample is in place (Figure 4.23), the lateral wall assemblies are fastened to the frame by steel bolts mounted in tapped holes on the exterior of the frame (Figure 4.24). Each membrane forms a pressure seal between the wall assembly and the reaction frame and also provides an effective seal against the leaking of the pressurized fluid.

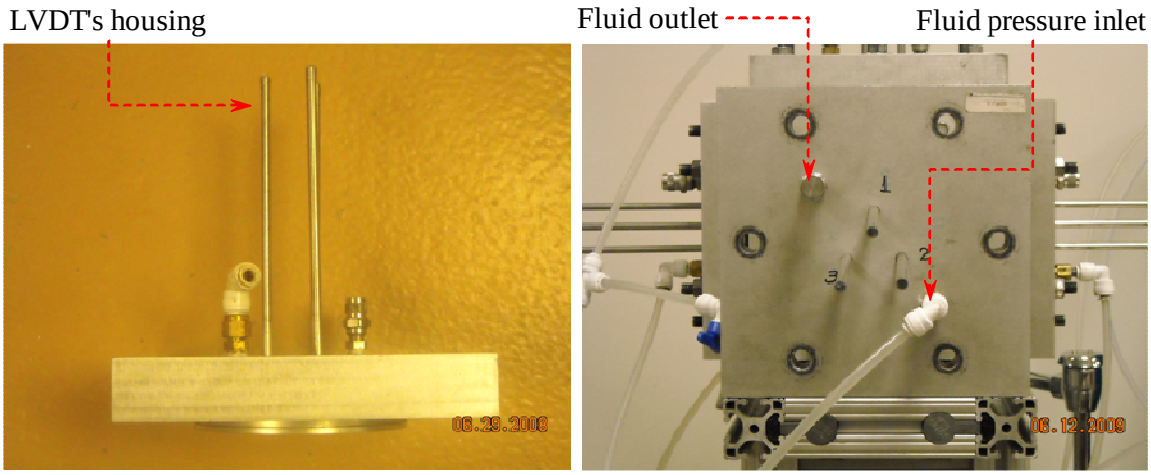

Figure 4.21 Top and lateral wall assembly.

Figure 4.22 Top/lateral wall assembly with rubber membrane.

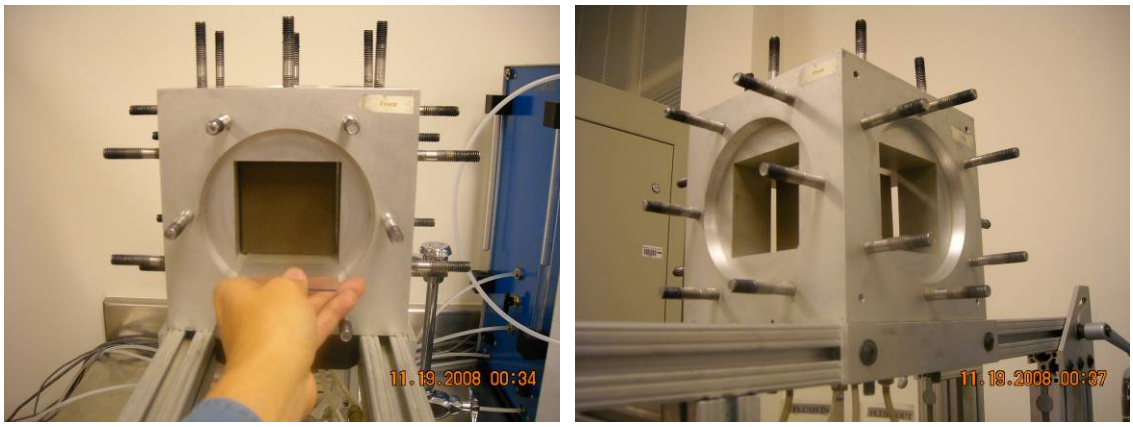

Figure 4.23 Sample into the cubical core frame.

Figure 4.24 Lateral and top wall assemblage.

4.3.4 Flexible Membranes

An assembly consisting of top and bottom molds machined from aluminum was used in this research work to prepare custom-made membranes (Figure 4.25). The membranes were prepared in the laboratory using Dow Corning silicone rubber, a Silastic J-RTV type that allows obtaining high tear strength and low stiffness rubber membranes.

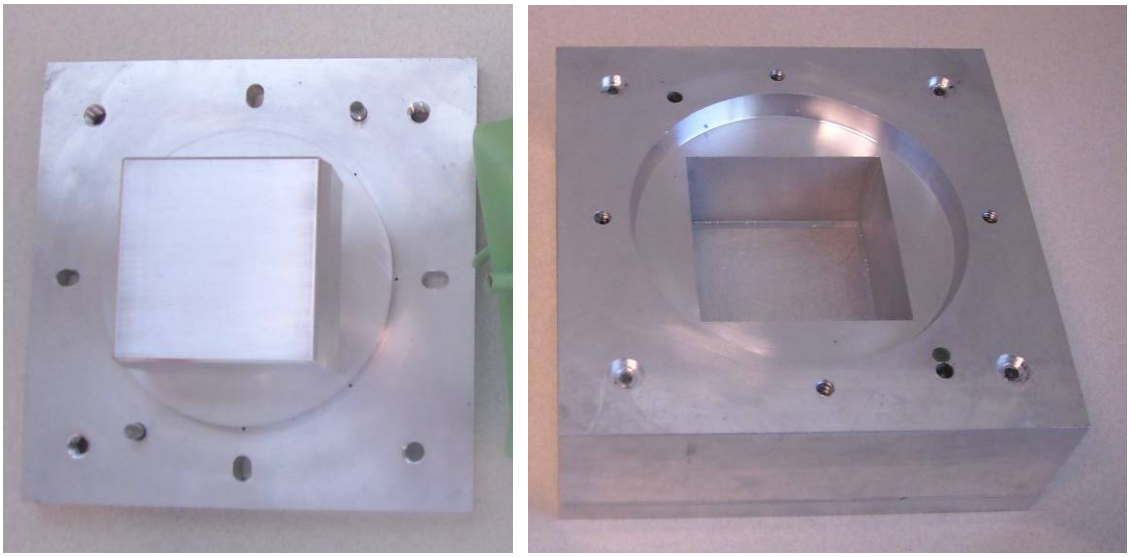

Figure 4.25 Top and bottom molds used to make the membranes.

The J RTV Silicone Rubber curing agent was mixed into the base material in the amounts of 10 parts base to one part curing agent by weight. As shown in Figure 4.26, the mixture was then poured into the bottom mold and inclusion of air was removed by applying a vacuum of 28 to 30 psi during 1 hour. Next, the top plate of the mold was carefully bolted in place and the mixture was allowed to cure for two days. The membrane was removed from the mold and stored for future use. As show in Figure 4.27, the weight of the finished membrane is approximately 85 g.

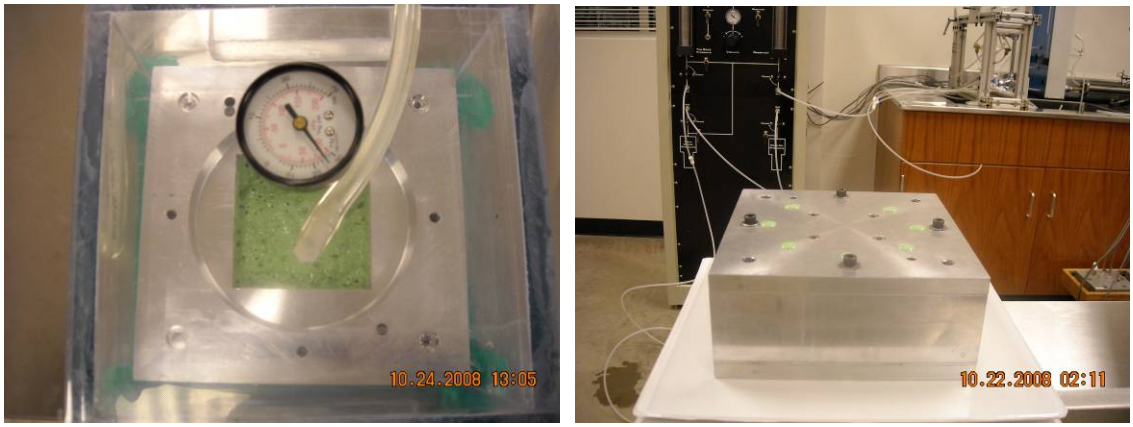

Figure 4.26 Custom-made mold and fabrication precces of cubical latex membranes.

Figure 4.27 Rubber membrane.

The flexible membranes transmit the applied hydraulic pressure to the top and lateral faces of the cubical soil specimen. In addition, the membranes act as a fluid barrier between water inside the pressure cavity and the cubical unsaturated soil specimen. Figure 4.28 shows photographs illustrating the suitable flexibility of the rubber membrane for experimental stress-strain analyses of soil materials. The shape adopted by the membranes shows that the use of LVTD's is not adequate to measure total principal strain increment experienced by the cubical soil sample along a particular direction. Measurements of change in volume could be more reliable.

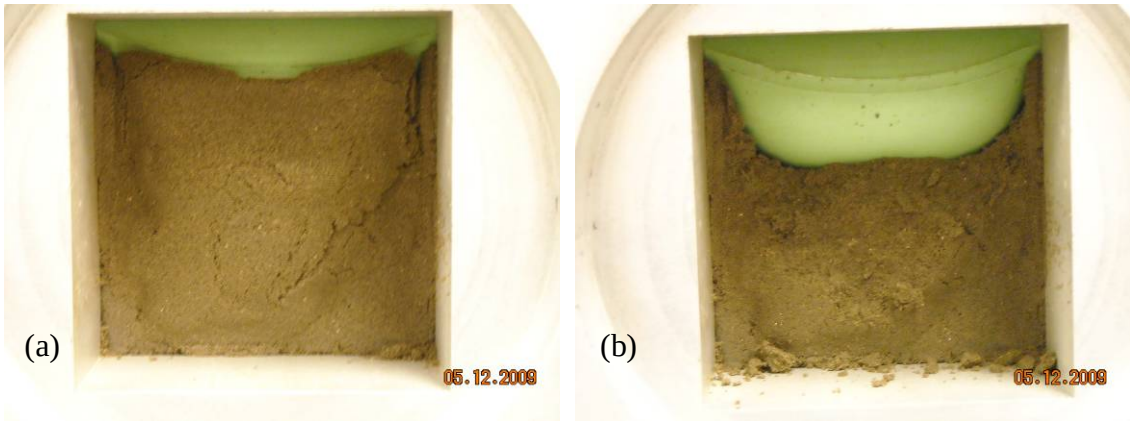

Figure 4.28 Stretched membrane at the end of a triaxial compression (TC) test: (a) failed sample, (b) exposed membrane by partial removal of soil

4.3.5 Stress Application and Control System

The hydraulic pressure applied trough flexible rubber membranes to the top and lateral faces of the cubical unsaturated soil specimen, is generated and controlled by a computer-driven Pressure Control Panel (PCP-5000) and a computer-driven pressure volume control system (PVC-100), both developed by GCTS, Tempe, AZ. Both units use hydraulic digital servo control that allows maintaining the necessary test conditions.

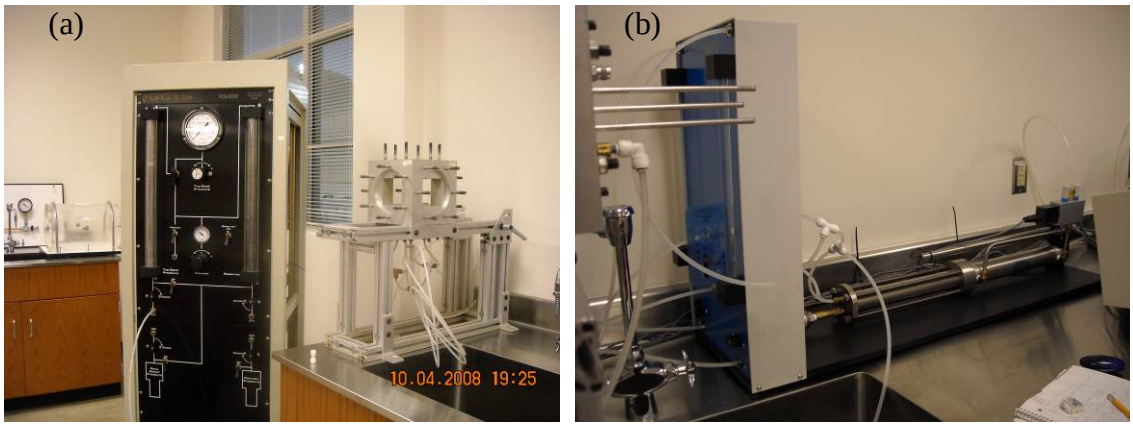

Figure 4.29 Computer-driven Pressure Control Panel:(a) PCP-5000, and (b) PVC-100.

The PCP-500 has been used in this research work to apply pressure to the soil sample in Z and X axes direction (i.e. σ_1 and σ_3). On the other hand, the PVC-100 has been used to apply pressure in the Y axis direction (i.e. σ_2). Three servo valves control the displacement of equal number of hydraulic pistons. A pressure transducer or external LVDT provides a direct feedback response used in the control process. The system operation is integrated with the GCTS software, which has the flexibility to follow simple or complex test conditions. Any principal stress combination path can be achieved by simultaneous control over the three computer driven servo valves. In addition, the flexibility provided by the control system allows running strain or stress controlled tests.

The output lines from the three pistons split into two lines to supply the pressure to the positive and negative faces of the cubical soil specimen. These positive and negative faces correspond to the X(+), X(-), Y(+), and Y(-), accounting for the four lateral sides, and Z(+), accounting for the top side. The output lines from PCP-5000 and PVC-100 valves are connected to the cubical cell via ¼" nylon hose having burst

strength of 2000 kPa (290 psi). Quick connect fittings at the output connection and at the pressure fluid inlet connections of the wall assemblies make easy to assembly the system.

4.3.6 Deformation Control/Measuring System

Two methods are implemented on the true triaxial device to measure deformations of the cubical soil specimen. Deformation can be measured by using a set of 15 LVDTs (i.e. 3 LVDTs on each flexible boundary) and also can be measured by using the three LVDTs attached to each of the hydraulic pistons in the stress application and control system.

The three DC-EC-500 Schaevitz series, high pressure sealed LVDTs, located on the top face, and on each lateral faces allow measuring the deformation on three different points of each side of the cubical soil specimen. Hence, the deformation along a particular direction, is estimated by averaging the three LVDTs' outputs corresponding to the soil face perpendicular to that particular direction (i.e face X(+), X(-), Y(+), Y(-), or Z(+)). No deformations are measured at the bottom side, Z(-), since this side is directly in contact with the rigid boundary where the HAE ceramic disk and the four coarse porous stones are located. Therefore, total principal strain increments in the Z direction are only measured at the top side of the unsaturated soil specimen. Specific details of the calibration, operation and use of this deformation measuring system can be found in Park (2005), Pyo (2006) and Laikram (2007).

As shown in Figure 4.15, the total principal strain increment experience by the cubical soil sample during a shearing test could not be adequately measured by

averaging the three LVDTs' outputs. Therefore, in this research work the deformation of each side of the cubical soil specimen has been determined by measuring the change in volume in each flexible membrane. Change in volume of ach membrane can be obtained by measuring the volume of water displaced by the hydraulic pistons in the stress application and control system.

Macro Sensors' DC 750-5000 Series of 1.9 cm (3/4 in) attached to each hydraulic piston has been calibrated to measure the volume of water displaced by the piston. With the 45.5 cm (17.9 in) stainless steel housing the, the DC 750 LVDT has been calibrated to have a full scale range of 300 cc total volume that allows to measure positive (i.e. compression) and negative (i.e. extension) deformations in the cubical soil specimen. The output signal generated by the displacement of the DC 750 series LVDT and the pressure sensors is interpreted by the GCTS software which uses this information to measure the change in pressure and volume in a specific direction (i.e X, Y, or Z) of the cubical soil specimen. When the cubical device is used to complete a stress-controlled test the output signal from the pressure sensors is processed by the GCTS software which controls three separate servo valves to either increase or reduce the pressure applied to each sample face. On the other hand, when the cubical device is used to complete strain-controlled tests, the deformation readings, on each axis of the cubical soil specimen, are used to control the test by changing the pressure up to the value required to impose the deformation expected on each face of the cubical soil specimen.

4.3.7 Pore-air Pressure Control/Monitoring System

Air-pressure is supplied to the bottom of the soil specimen using the air pressure outlet provided in the PCP-5000 unit. Nylon tubing connected to the quick connect fitting on the PCP-500 unit carries the pressurized air to the fittings fastened to the outside of the bottom wall assembly (Figure 4.17). The pore-air is introduced to the unsaturated soil specimen via four 1.9 cm (0.75 in) diameter 0.6.5 mm (1/4 in) thickness coarse pore stones. As shown in Figure 4.18, the pores stones are completely embedded in the bottom assembly corners, surrounding the HAE ceramic disk.

4.3.8 Pore-water Monitoring System

A ceramic disk and four coarse pore stones were used to impose matric suction in the cubical unsaturated soil specimen using the axis translation technique. The selection of the HAE ceramic disk for testing unsaturated soils should be primarily based upon the maximum possible matric suction that can occur during the test. In this research work, a maximum value of matric suction of 350 kPa was imposed to the cubical saturated specimen. The 5.4 cm (2.125 in) diameter, 0.72 cm (0.3 in) height, 5 bars (505 kPa) manufactured by Soilmoisture Equipment Corp. has an approximate pore diameter of $0.5x10^{-3}$ mm, a coefficient of permeability with respect to water, k_d, of $1.21x10^{-9}$, and an air entry vale greater that 550 kPa.

The tubing fittings for the pore water pressure, u_w, control and flushing mechanism installed on the outside face of the bottom wall assembly are shown in Figure 4.17. One tubing fitting (i.e. flush-in) is directly connected to the water supply on the PVC-100 front panel using ¼” nylon hose. The other tubing fitting (i.e. flush-

out) allows the water flow when its valve is opened. The main function of this system is to release the air bubbles entrapped into the water compartment underneath the HAE ceramic disk, during saturation of the HAE ceramic disk or suction controlled system. It is important that all tubing, as well as the water compartment underneath the ceramic disk are saturated by creating a continuous flow from the water-supply and the flush out tubing. The flushing procedure is done each 12 hours during the suction-controlled test. The HAE ceramic disk was saturated in place using the cubical cell. A detailed description of the HAE ceramic disk saturation procedure is presented by Hoyos (1998).

4.3.9 Data Acquisition System

The digital servo controller software developed by GCTS (2000) is capable of controlling up to three servo channels. To control one or more servo channels the GCTS software uses a Keithley Metrabyte DAS-16 board that serve as an interface with the hardware, and a servo amplifier to drive the servo valves. Control is always specified in terms of direct measurement inputs, like deformation and pressure. It is not possible to specify control in term of indirect parameters, like strain calculated from deformations.

The GCTS software and therefore, the deformation control/measuring system can be used to follow any specified stress or strain path. In addition, the software allows storing the output data from the sensors measuring the stress and strain on each face of the cubical soil specimen on real time. The data stored in a file can be analyzed using any data processing tool. A detailed description of the software and its capabilities are given by GCTS (2004a) and GCTS (2004b).

4.4 Calibration

Numerous factors contribute to errors in sensor measurements. Before use a sensor, the device must be calibrated to adjust its accuracy against the expected measurement scale. The calibration in the laboratory has been achieved by comparing the sensor readings with an accurate hand-held instrument reading taken near the sensor being checked or calibrated. The calibration has been performed by measuring the resistance or forward voltage of the sensor under test and the hand-held reading.

Although two point calibration method works for any linear sensor, the accuracy of this procedure depends on the accuracy of the known value read on the hand-held instrument. Therefore, several readings have been done on both, the hand-held instrument and the sensor. These values have been used to determine the zero offset of the device and the gain offset (slope). The adjustments on the sensor are made by applying the offset. Figure 4.30, Figure 4.31, and Figure 4.32, show the zero offset and the gain offset (slope) of the pressure sensors measuring the principal stresses, σ_1, σ_2, σ_3, respectively. The zero offset and the gain offset (slope) of the LVDTs measuring deformation on the face of the cubical soil specimen, perpendicular to axes X, Y, and Z, are presented in Figure 4.33, Figure 4.34, and Figure 4.35, respectively.

Next chapter presents the classification of the soil according to their engineering properties, the relationship of water content and suction for the soil (i.e. soil-water characteristic curve), the selection of the compaction method and dry unit weight, as well as the procedure recommended to obtained “identically” prepared soil samples with and adequate value of isotropic yield stress, $p_o(0)$.

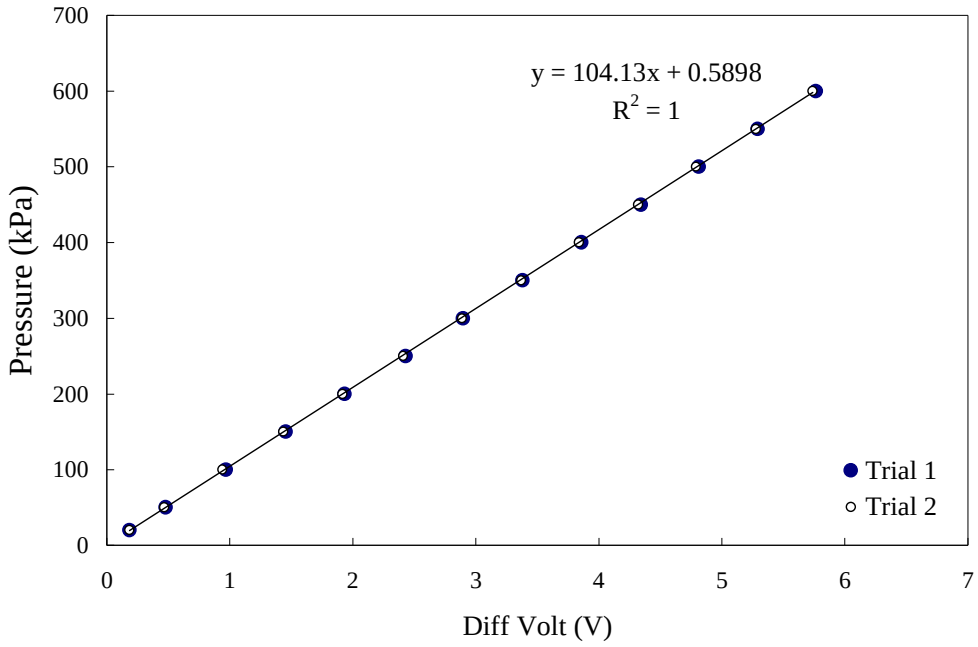

Figure 4.30 Calibration data for the pressure sensors measuring σ_1.

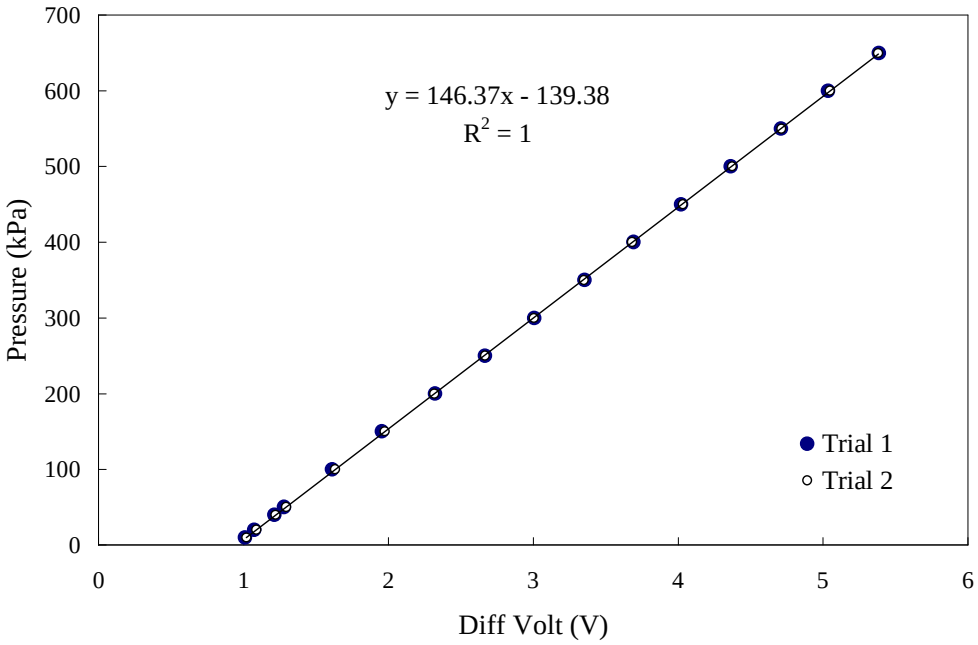

Figure 4.31 Calibration data for the pressure sensors measuring σ_2.

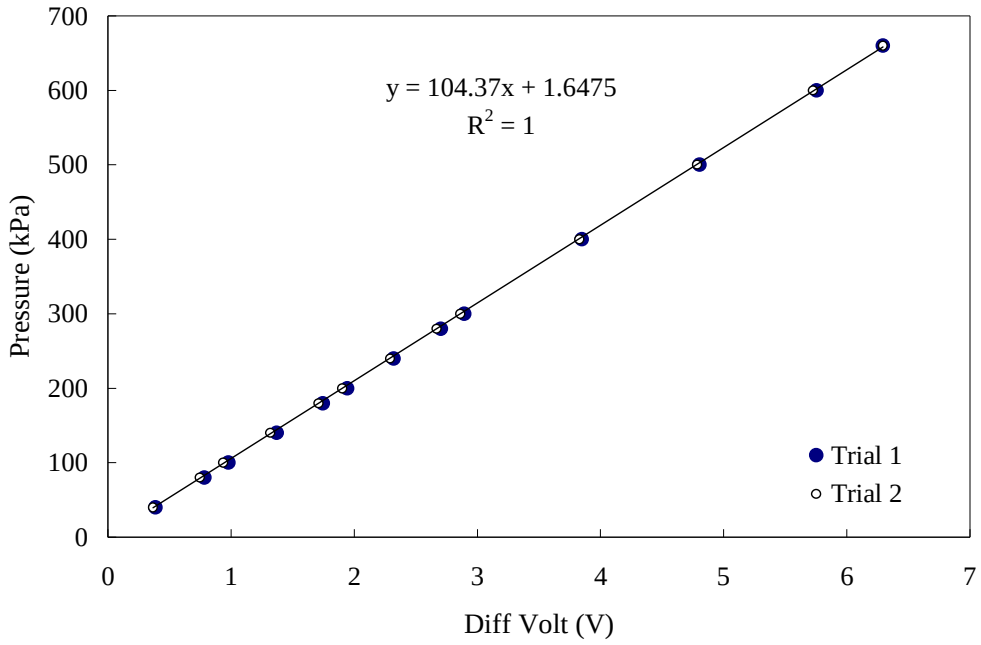

Figure 4.32 Calibration data for the pressure sensors measuring σ_3.

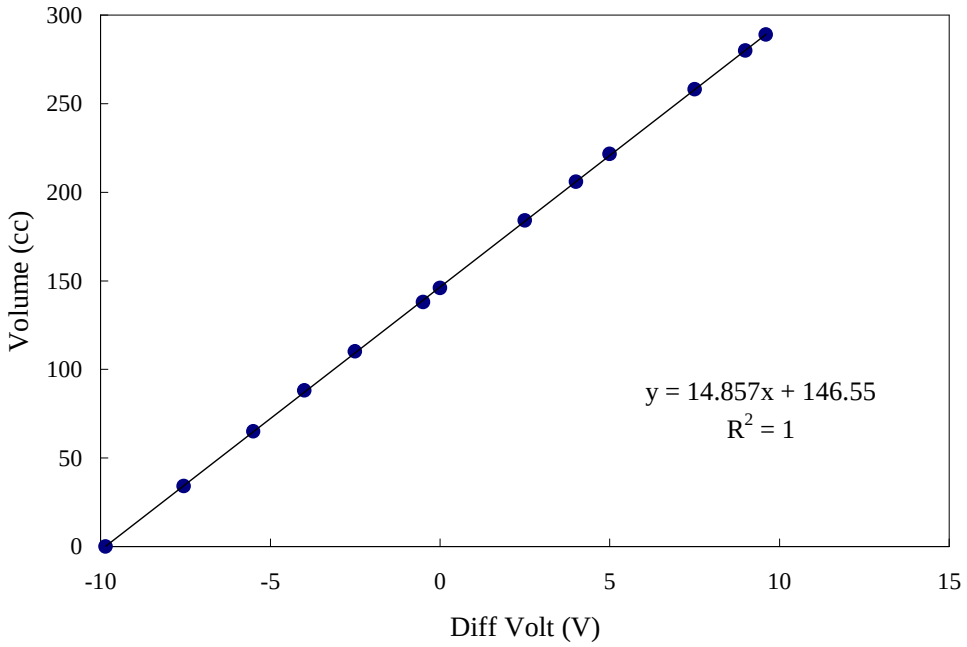

Figure 4.33 Calibration data for the LVDT measuring deformations on the cubical soil specimen faces, perpendicular to axis X.

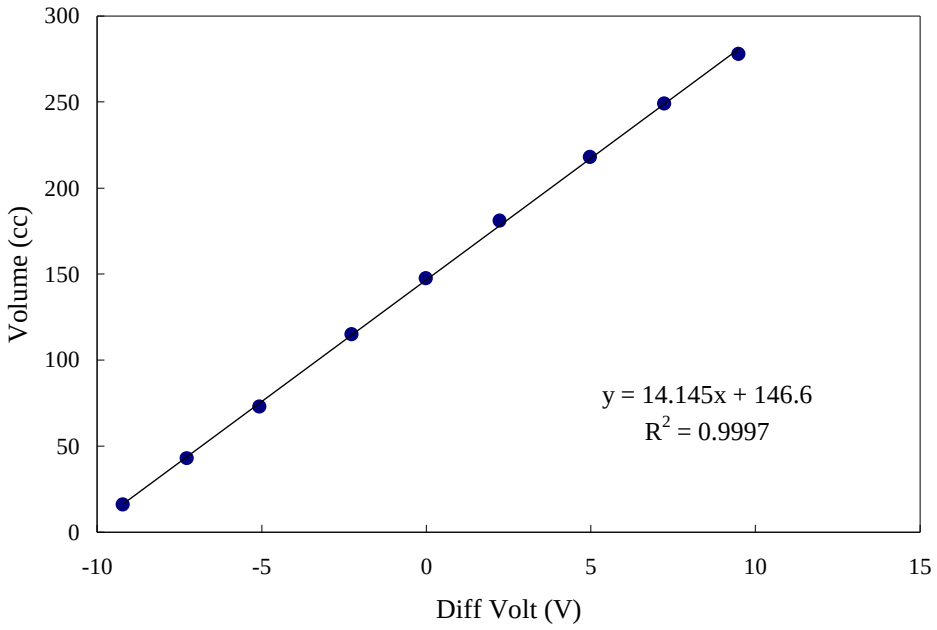

Figure 4.34 Calibration data for the LVDT measuring deformations on the cubical soil specimen faces, perpendicular to axis Y.

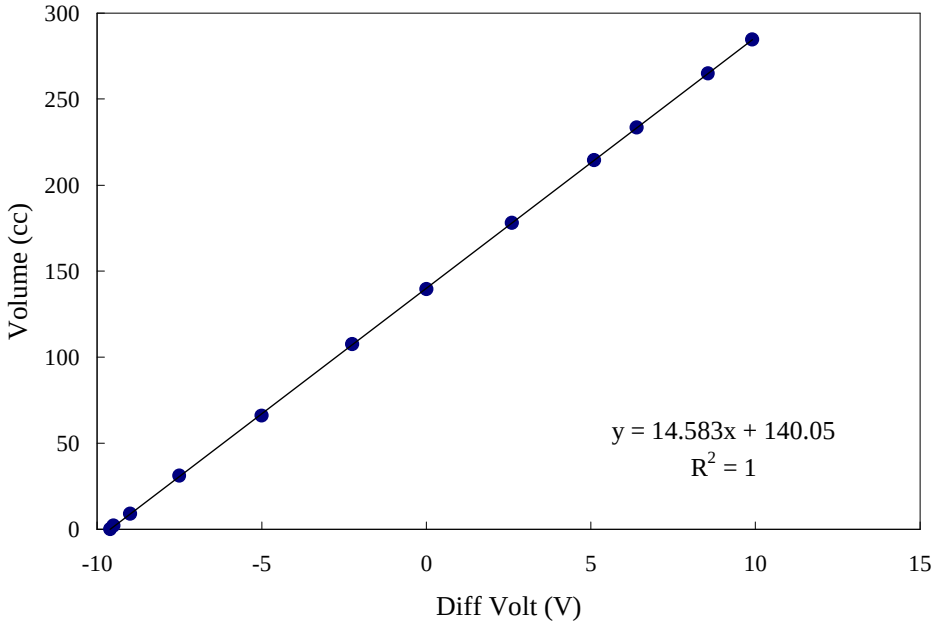

Figure 4.35 Calibration data for the LVDT measuring deformations on the cubical soil specimen faces, perpendicular to axis Z.

CHAPTER 5

SOIL PROPERTIES AND SPECIMEN PREPARATION

5.1 Introduction

A soil may be visualized as a discontinued assemblage of solid mineral particles mixed together with open spaces or pores. Solid particles in soils vary widely in size, shape, mineralogical composition, and chemical characteristics. The arrangement of the individual particles or aggregation and combination of particles is called the soil structure. Pores are created by the contacts made between irregular shaped soil particles. (Spangler and Handy, 1982).

Soils are generally classified into four groups: gravel, sands, silt, and clays. Soil texture, refers to the relative proportion of sand, silt and clay size particles in a sample of soil. Hence, fine textured soil has more pore space than coarse textured. As a result, fine textured clay soils hold more water than coarse textured sandy soils. Coarse textured soils tend to have large, well-connected pore spaces and hence it is expected that sandy soils dry out rapidly. Therefore, the distribution of the size throughout the soil mass as well as the soil texture is an important factor which influences many other soil properties and engineering behaviour.

The soil tested in this work was artificially prepared by mixing 30% of fine material obtained from North Arlington, Texas, and 70% of clean sand commercially available. The soil was classified and its basic properties determined to adequately design the suction controlled experimental program, and to better understand the

mechanical response observed from multiaxial stress states. Several tests were performed on the artificially prepared soil in order classify the material, based on the textural characteristics of its fine portion and grain size distribution of the mixture. In addition, other laboratory tests were conducted to determine some engineering properties of the soil, such as density, unit weight, and specific gravity.

5.2 Soil Classification

Similar environments that share comparable soil forming factors produce similar types of soils. This phenomenon makes classification possible. Soil Classification Systems such as ASTM D422, AASHTO, and Unified Soil Classification System (USCS) have been developed to provide generalized information about the nature of a soil. Engineer soil classification systems can be used to classify the soil and identify the expected engineering behaviour. These classifications are based upon purely subjective considerations.

Several laboratory tests are required to identify a soil using the engineering soil classification system. Among them are the grain size analysis, Attemberg limits which includes liquid limit test, and plastic limit tests. The results of these tests as well as a brief description of the physical meaning are given above.

5.2.1 Grain Size Analysis

A soil consists of particles of different shapes, size and number. The grain size analysis divides these particles into size groups and determines their relative proportion by weight. The grain size curve is plotted as the percentage finer than a given size

versus the particle size on log arithmetic scale. Figure 5.1 shows the particle size distribution for the material used during the experimental phase of this work.

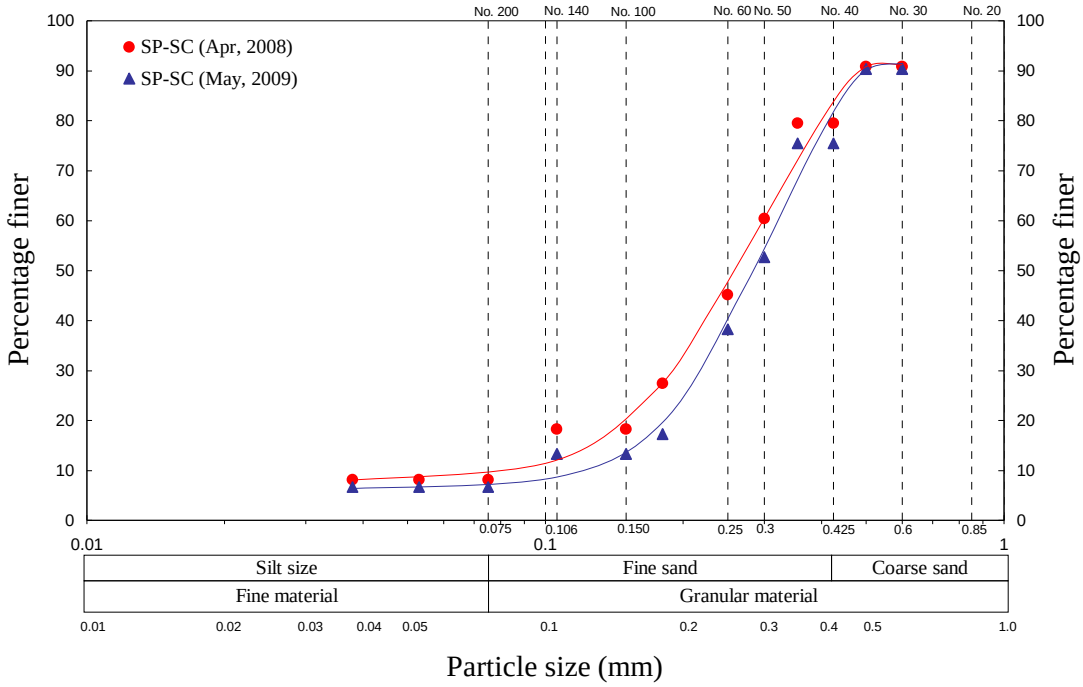

Figure 5.1 Grain size distribution of test soil.

5.2.2 Liquid Limit Test

Soil when mixed with water may exist in any one of several states of matter, depending on the amount of water in relation to the amount of soil. As the moisture content decreases a cohesive soil may goes from a true liquid at very high moisture content, through viscous, liquid, plastic solid, and semisolid, to that of a solid state. Hence, the moisture content above which a soil become upon stirring is called the liquid limit (Spangler and Handy, 1982). The liquid limit (LL) test of the fine fraction of the soil used in this work was perform using the liquid limit device (ASTM D423-66, 2004)

The flow curve and the moisture content at which it intersects the 25 blows abscissa are shown in Figure 5.2. Hence, the soil material has LL = 64.2 and the flow index FI = 9.31. The flow index is the slope of the best fit line fitted to the liquid limit laboratory data.

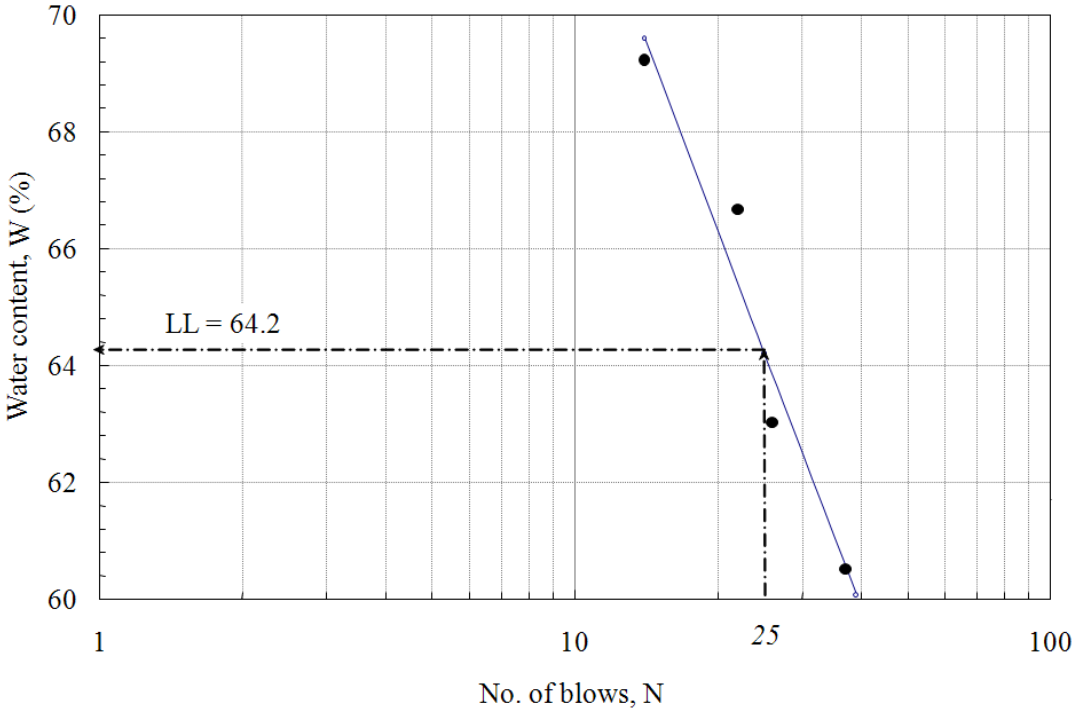

Figure 5.2 Liquid limit determination using Casagrande's device.

5.2.3 Plastic Limit Test

When the moisture content of the soil is reduced below the liquid limit the material moves to a plastic state. In this state, the material become stronger and its bearing capacity begins to increase considerably. It loses its stickiness and can be molded into almost any shape using the hands (Spangler and Handy, 1982). The minimum moisture content at which the soil behaves as a plastic solid is called the

plastic limit (PL). Three different plastic limit tests were performed on the fine portion of the soil used in this work. The average value of moisture contents obtained was PL = 22.24%

5.2.4 Plasticity Index

The range of moisture content within which the soil exhibits the properties of a plastic material is defined as the plasticity index (PI). It is a measure of the cohesive properties and indicates the degree of surface chemical activity and the bounding properties of the fine clay and colloidal fraction of the material. This property is defined by the numerical difference between the liquid limit and the plastic limit (Spangler and Handy, 1982). The plastic index for the fine portion of the material used in this work is PI = LL – PL = 41.97%.

5.2.5 Unified Soil Classification System

According to USCS clay particles are particles less than 0.002 mm in size; Silt particles are bigger than clay particles, falling between 0.002 and 0.074 mm in size; sand may be considered as medium particles with diameters between 0.074 and 2.0 mm. Soils that are dominated by clay are called fine textured soils while those dominated by larger particles are referred to as coarse textured soils. Therefore, with a 10% of the total material passing the No 200 sieve (i.e. particles size less than 0.074) the soil can be described as sand (S).

However, although the curve in Figure 5.1 can be used to describe the soil, it is convenient to use statistical measures such as uniformity coefficient, C_u, and the

coefficient of gradation, C_z. Both coefficients can be calculated basis on the grain size distribution curve as.

$$C_u = \frac{D_{60}}{D_{10}} = 3.2 \tag{5.1}$$

$$C_z = \frac{D_{30}^2}{D_{60} D_{10}} = 1.52 \tag{5.2}$$

Although both coefficients indicate that the soil is fairly uniform in size which allows classifying the coarse portion as poorly graded sand (SP).

A better description can be obtained by plotting the Atterberg limits on the so called plastic chart (Figure 5.3). Attemberg limits, which were performed on the fine portion of the soil, reveal properties related to consistency of the material. These include liquid limit (LL), plastic limit (PL) and shrinkage limit (SL) which are essential to correlate the shrink-swell potential of the soils to their respective plasticity indices (PI).

The Attemberg limits plotted in Figure 5.3 shown that the fine portion of the material is inorganic clay of high plasticity (CH). In addition, an approximate value of the shrinkage limit, which is the water content at which further loss in moisture content will not cause a decrease in its volume, is also obtained from the plastic limits chart. The resulting value of shrinkage limit is SL = 14%.

Finally, using the USCS and basis on the Attemberg limits and the grain size distribution curve, the soil is classified as poorly graded sand with clay (SP-SC). Furthermore, the soil can be also classified using the ASTM D2487-00, the soil can be classified as sandy fat clay.

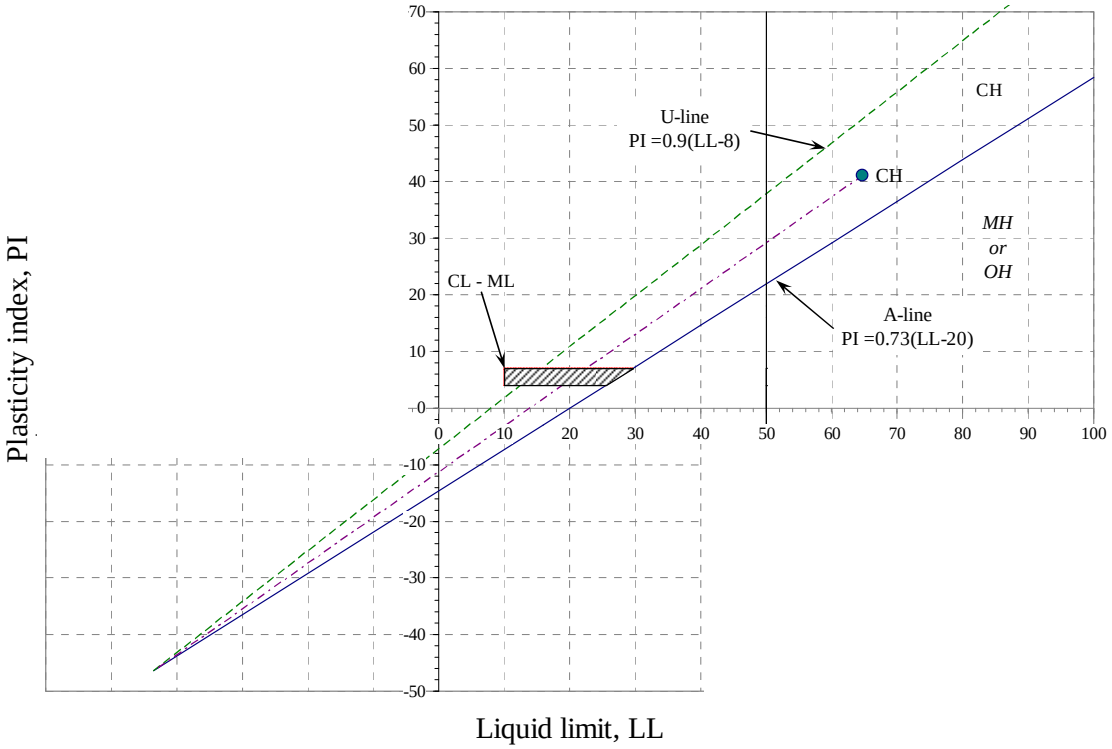

Figure 5.3 Plastic chart.

5.2.6 Specific Gravity

Specific gravity, G_s, of a soil is the ratio of density or specific weight of the soil particles to the density or unit weight of water. The specific gravity for the SP-SC was determined in the laboratory through the procedure depicted by ASTM Standard D 854-06. Three different tests were conducted on three different samples and the resulting values were G_s = 2.71, 2.70, and 2.70. An average value of G_s = 2.70 has been adopted for the SP-SC.

5.3 Soil-water Characteristic Curve

As mentioned in chapter 2 the soil-water characteristic curve of a soil relates the moisture content to the applied matric suction in the soil (Fredlund and Rahardjo,

1993). In a partially saturated soil, the pore-air pressure, u_a, is generally atmospheric and the pore -water pressure, u_w is negative. Hence, the soil matric suction of a soil is the difference between the pore-air pressure and pore-water pressure (u_a - u_w).

In the laboratory, matric suction can be measured either in a direct or indirect manner. In this work the matric suction has been measured with a pressure plate, using axis translation technique for direct measurements. In addition, filter paper has been used as a sensor to indirectly measure the matric suction at pressures that can not be reached using axis translation technique.

5.3.1 Pressure Plate Drying Test

A pressure plate extractor manufactured by Soilmoisture Equipments Corporation (see Figure 5.4) was used in the laboratory to develop a soil water characteristic curve, using the axis translation technique. The pressure plate extractor was used to apply various matric suctions to compacted SP-SC samples.

Speaking in terms of gauge pressure (i.e. the pressure relative to the local atmospheric or ambient pressure), matric suction can be applied to a soil specimen into the closed pressure chamber by applying a positive pore-air pressure while a zero pore-water pressure is sustained. Before start the test, the high air entry disk is saturated, and during the test it is always in contact with the water contained in the membrane below the disk. The water compartment is maintained at zero pressure.

The matric suction data obtained using the pressure plate is plotted against the water content on Figure 5.5. Although a 15 Bars high air entry value ceramic disk has been used, due to the maximum air pressure available in the laboratory, the data

obtained is limited to 850 kPa. However, considering that a 5 Bars high air entry value ceramic disk is installed in the base of the true triaxial cubical cell, detailed data was obtained between 50 and 500 kPa.

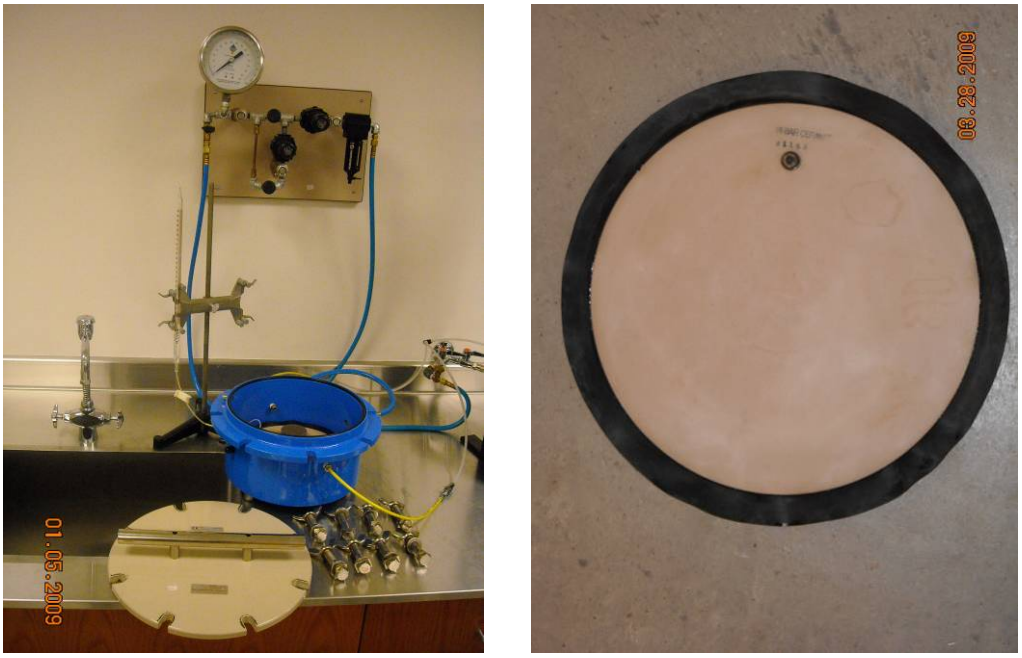

Figure 5.4 Pressure plate extractor and high-entry-value ceramic disk.

5.3.2 Filter Paper

The filter paper method to measure matric suction is based on the assumption that a filter paper will come to equilibrium with a soil having a specific suction. Therefore, when a dry filter paper is placed in direct contact with a soil specimen, it is assumed that water flows from the soil to the filter paper until equilibrium is achieved. Once equilibrium conditions are achieved, the water content of the filter paper is measured (Fredlund and Rahardjo, 1993).

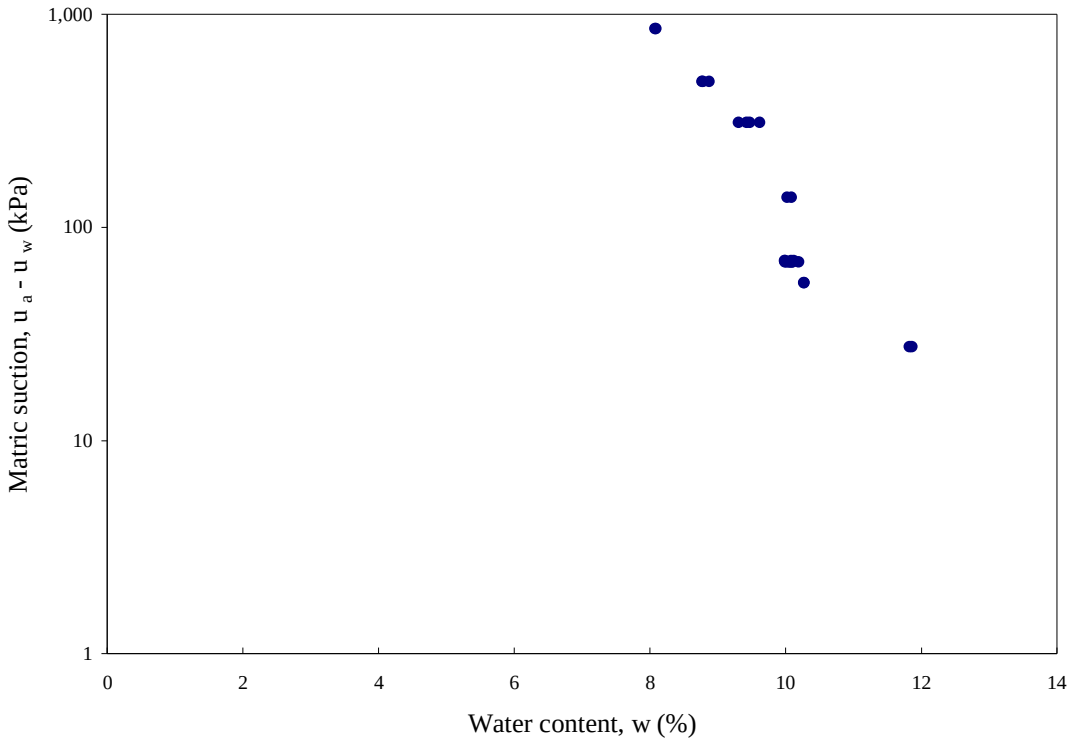

Figure 5.5 Matric suction versus water content for SP-SC soil using pressure plate.

As illustrated by Figure 5.6 the water content of the filter paper corresponds to a specific matric suction value. The equations used to calculate the calibration curves for filter paper Whatman No. 42 shown in Figure 5.6 are included in chapter 2. These equations were developed basis on the theory that equilibrium water content of the filter paper corresponds to the matric suction of the soil when the paper is placed in direct contact with the soil. The filter paper sensor used to measure the matric suction was Whatman No. 42 which is a ash-free, quantitative Type II recommended by ASTM D 5298-03. Acrylic disks where placed on the top and bottom of the sample to guaranty intimate contact between the soil sample and the filter paper. Figure 5.7 shows the filter

paper location, sample preparation and storage of the glass container. The samples were storage in the constant humidity room during the equilibration period (i.e. seven days).

In addition to the moisture content of the filter paper, the soil water content was also measure to correlate the matric suction obtained from the filter paper with the moisture content of the soil. The resulting matric suction values from Figure 5.6 are plotted against the water content as shown in Figure 5.8. Values shown in Figure 5.8 correspond to those calculated using the equation proposed by ASTM D 5298-03. Figure 5.9 presents the matric suction data obtained using the pressure plate among the values obtained using filter paper method.

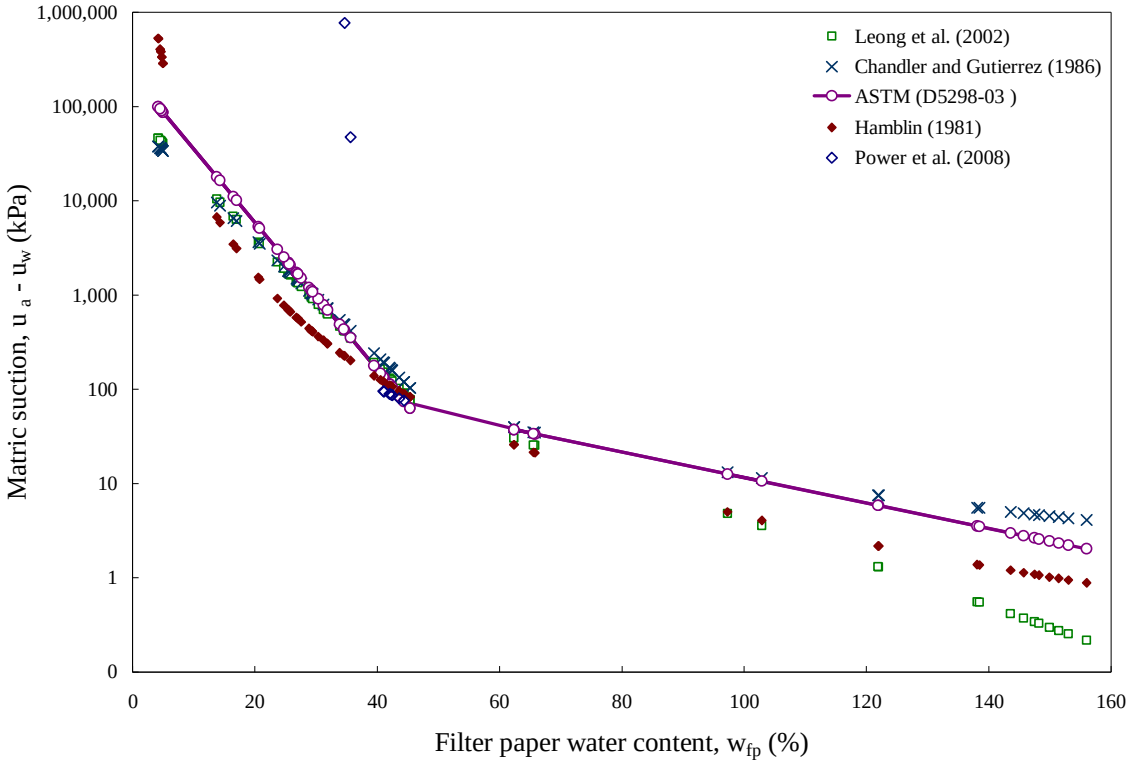

Figure 5.6 Calibration curves for filter paper Whatman No. 42.

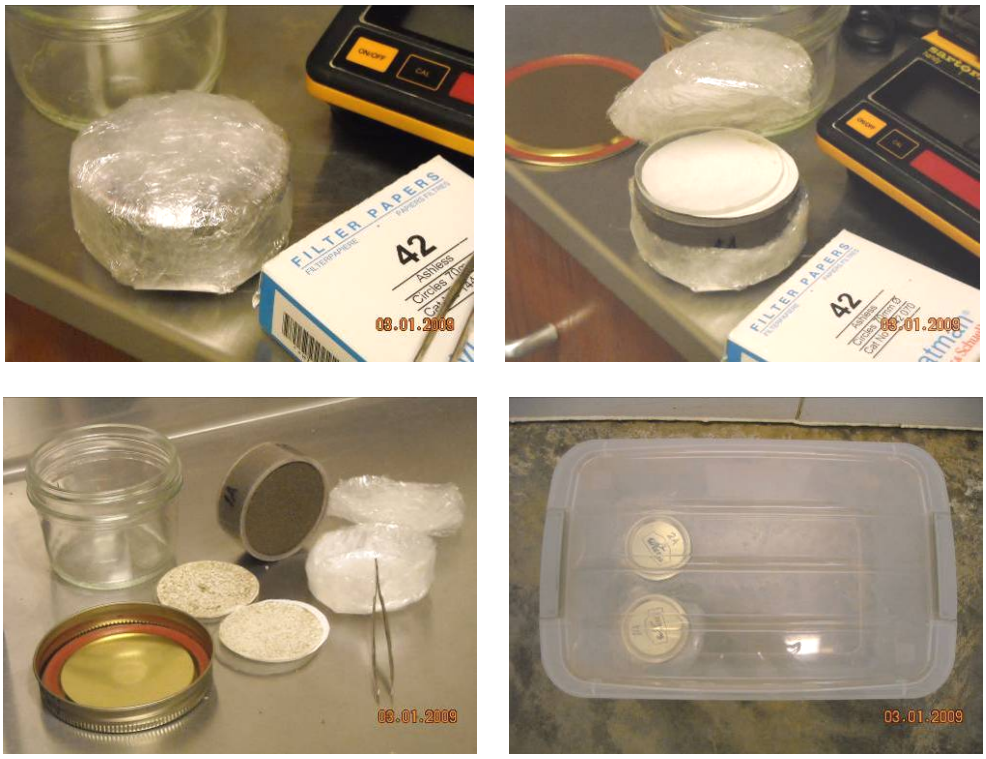

Figure 5.7 Filter paper location and sample preparation and storage.

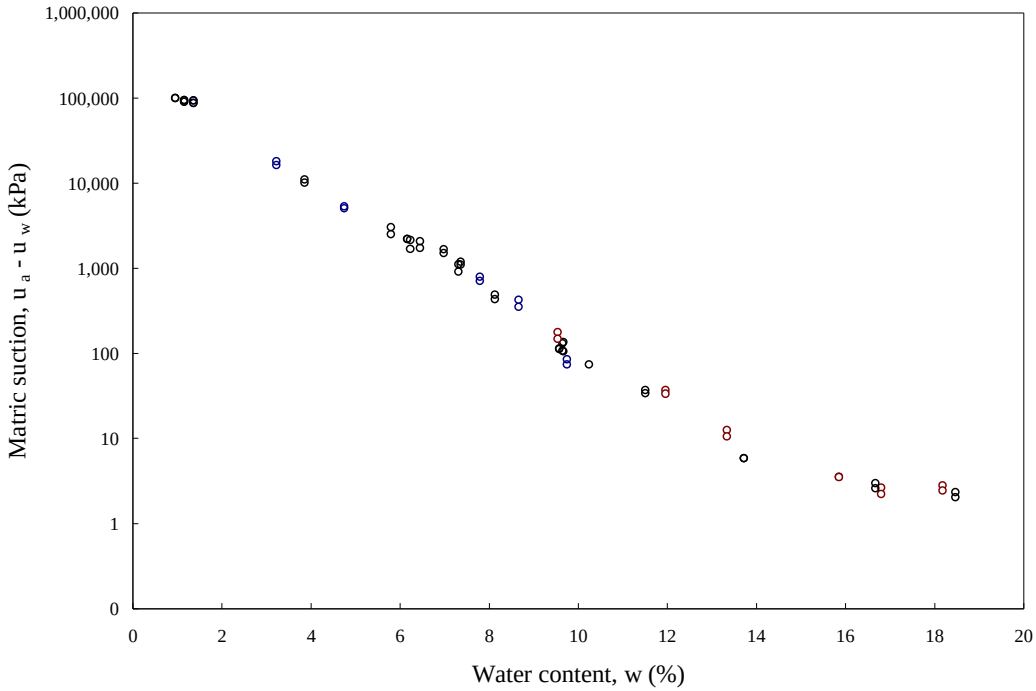

Figure 5.8 Matric suction versus water content for SP-SC soil using filter paper method.

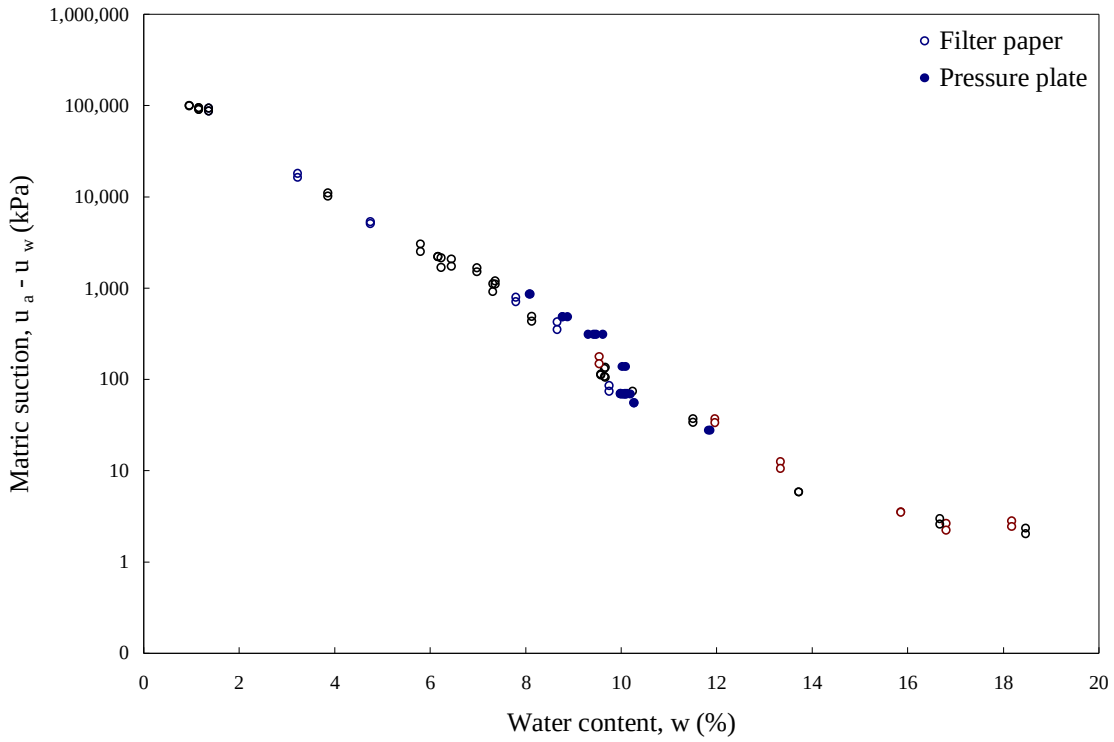

Figure 5.9 Matric suction versus water content for SP-SC soil using pressure plate and filter paper methods.

5.3.3 SWCC Modeling

As mentioned in chapter 2, several empirical equations have been proposed to best-fit soil water characteristic curve (SWCC) data. The most universally used model are those proposed by Brooks and Corey (1964), van Genuchten (1980) and Fredlund and Xing (1994). In addition to these three equations, the equation proposed by Brutsaert (1967) has been also included in this work due to its simplicity.

The parameters involved in the four selected equations have been determined using a least squares regression and its values are presented in Table 5.1. The fitted curves are plotted among the laboratory data in Figure 5.10.

Table 5.1 Fitted parameters for selected SWCC functions

Brooks and Corey, 1964 Equation (2.7)	van Genuchten, 1980 Equation (2.8)	Brutsaert, 1967 Equation (2.9)	Fredlund and Xing, 1994 Equation (2.10)
$\psi_b = 0.155$	$\alpha = 0.210$	$\alpha = 13.278$	$a_f = 0.350$
$\lambda = 0.158$	$n = 2.941$	$\beta = 0.341$	$m_f = 2.100$
	$m = 0.056$		$n_f = 0.270$
$w_r = 0.150$	$w_r = 0.150$	$w_r = 1.6648$	$w_r = 1.790$
$w_s = 26.91$	$w_s = 26.94$	$w_s = 26.94$	$w_s = 26.94$
$R^2 = 0.975$	$R^2 = 0.975$	$R^2 = 0.954$	$R^2 = 0.987$

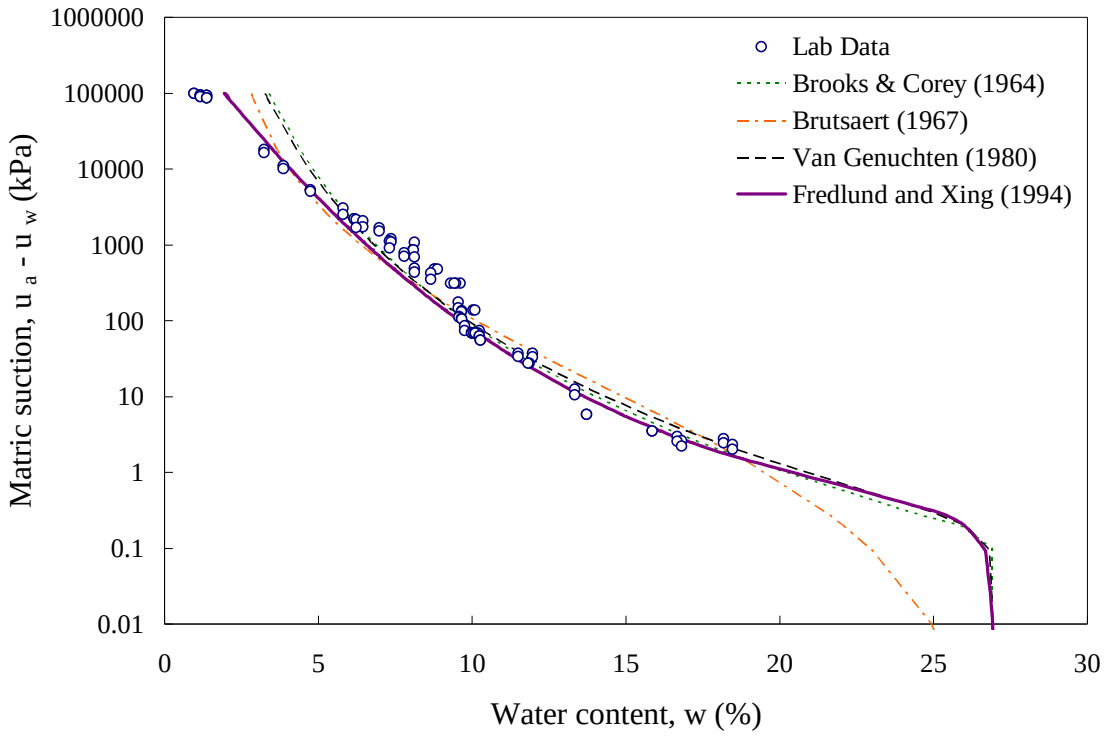

Figure 5.10 Soil water characteristic curves fitted to laboratory data.

From Table 5.1 and Table 5.1 Fitted parameters for selected SWCC functionsFigure 5.10 it can be observed that the three more universally used equations perform much better than the equation proposed by Brutsaert (1967). Among the more used equations, Fredlund and Xing (1994) perform slightly better that Brooks and Corey (1964) and

van Genuchten, 1980. However, Fredlund and Xing (1994) seems better predict the matric suction at low values of moisture content. It is worthy mentioning that regardless the simplicity of the equation proposed by Brooks and Corey (1964) it predict adequately the matric suction basis just in three parameters.

5.4 Specimen Preparation and Compaction Method

The shear strength parameter of a soil can be defined in the laboratory using soil specimens taken from the field as well as compacted samples. These samples can be tested under stress conditions that are likely to be encountered in the field. However, in order to obtain unique stress parameters the soil conditions of the specimens must be essentially identical. Therefore, only specimens with the same geological conditions and stress history should be used to define a specific set of shear stress parameters (Fredlund and Rahardjo, 1993).

In some cases, unsaturated soils testing is conducted on compacted specimens, which are usually prepared by compaction. According to Fredlund and Rahardjo (1993), in order to be considered as “identical”, specimens prepared in the laboratory must be compacted at the same initial water content to produce the same dry density. However, the compaction method has an important effect on the soil sample properties.

Soil samples are compacted by reducing the air voids present in the soil and hence increase the dry density of the sample. Dynamic compaction achieves this by permitting a moving mass to strike the surface of the soil sample and delivering energy into the sample that causes densification. On the other hand, soil samples can also be compacted by subjecting it to a static load which is built up slowly to some

predetermined value and then released. This process is referred as to static compaction. In other methods the soil is compacted by repeatedly applying a predetermined pressure to small areas of the soil, maintaining the pressure for short time, and then gradually reducing the pressure. This process is named kneading compaction.

The level of densification that can be achieved relates to a number of different parameters. The most important are the moisture content and the compacting energy transferred to the soil sample. Other factors that affect the densification are the number of blows applied to the soil, the momentum of each blow delivered by the falling mass, and the period of time during which the pressure is maintained.

5.4.1 Proctor Standard Test

To achieve the required soil density it is necessary to determine the moisture content and dry density of the specific soil material. There are a number of methods used to determine that moisture content, but the most used is the Proctor standard test. The modified Proctor test is used when the soil load is expected to be high.

The Proctor standard test has been conducted on the SP-SC soil following the ASTM standard D698-07e1, the resulting density curve is shown in Figure 5.11. The moisture content corresponding to the maximum unit weight is called the standard Optimum Moisture Content (OMC). In Figure 5.11 a dry unit weight of 19.18 kN/m^3 (122 lb/ft^3) correspond to an optimum moisture content of 11.55%.

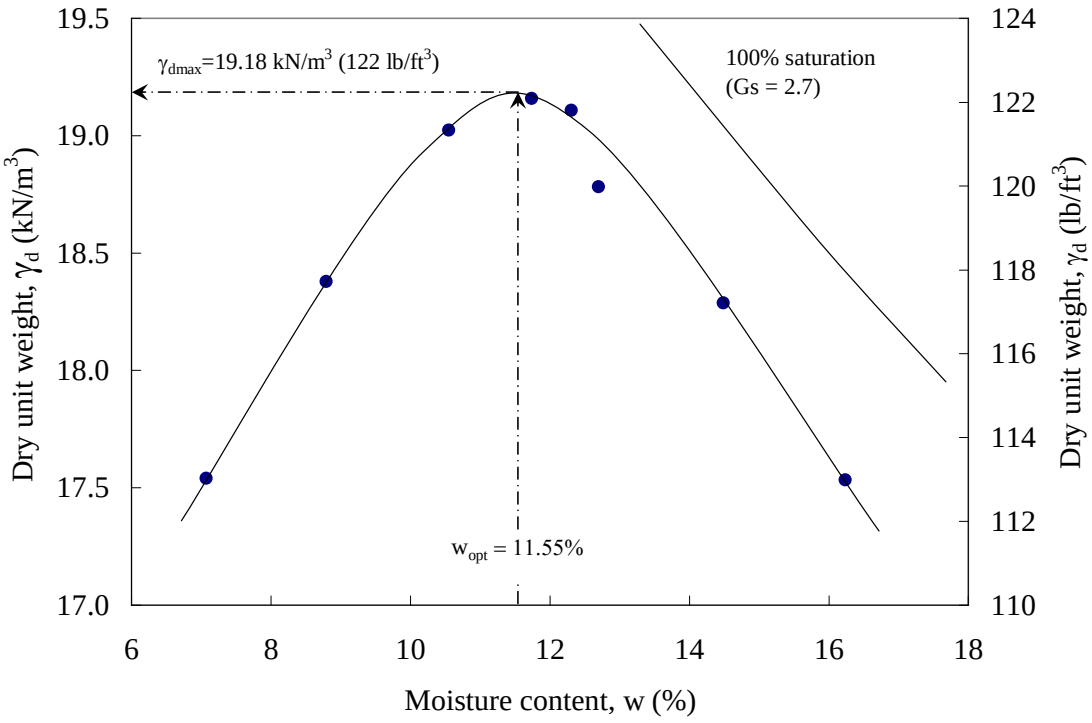

Figure 5.11 Proctor density curve for SP-SC soil.

In order to consider all the soil specimens compacted in the laboratory as "identical" all of them were compacted at the same initial water content to produce the same dry density. Therefore, considering the Proctor standard test results, a dry unit weight equal to 80% of the optimum value has been selected as a target for all the samples. As shown Figure 5.11, soil samples with a dry unit weight, γ_d = 15.344 kN/m^3 (97.6 lb/ft^3) which correspond to the 80% of the optimum, can be obtained using a moisture content higher than or lower than the optimum moisture content, w_{opt} = 11.55%. On the other hand, it can be observed in Figure 5.10 that moisture content in the order of 10% corresponds to a matric suction of 50 kPa. Therefore, to reduce the time required to equalize the matric suction in the samples, water content, w = 10% has

been selected as the initial water content. Although the samples were compacted at the same initial water content (i.e. w = 10%) to produce the same dry density (i.e. γ_d = 15.344 kN/m^3), it has been proven that the compaction method plays an important role in the isotropy of the soil characteristics.

5.4.2 Tamping Compaction

As previously mentioned, a soil material classified as poorly graded sand with clay (SP-SC) was used for suction-controlled testing. To define the compaction method to be used, a series of drained, stress/suction-controlled CTC tests were conducted on several cubical compacted, specimens 7.62 cm (3 in) per side. Initial water content, w = 10%, was used to achieve a cubical sample with unit weight, γ_d = 15.344 kN/m^3 approximately. The specimens were compacted in-place using tamping compaction process. A 1.5 mm (0.06 in) thick stainless steel shaft is introduced into the cubical cavity of the true triaxial cell to facilitate the tamping compaction process (See Figure 5.12).

As shown in Figure 5.13, specimens were prepared in approximately eight lifts, with each lift compacted at initial moisture content, w = 10%. The amount of material in each lift was controlled by weight with a 61.5 g first lift and seven other 100g lifts. Each layer was tamped using a compactive effort considerably less than that used in the Proctor standard.

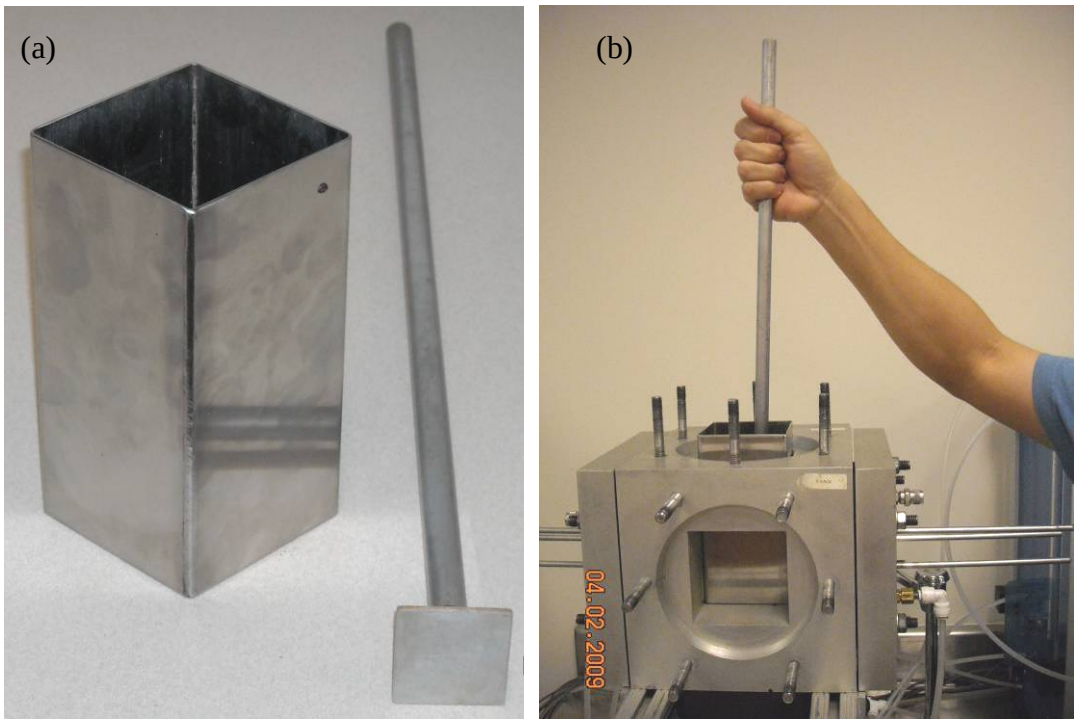

Figure 5.12 In-place tamping compaction: (a) mold and tamper, (b) compaction process.

Figure 5.13 shows that soil specimen compacted using tamping method can not be considered as “identical” samples. Although the same number of blows has been applied to each layer the resulting height is different. In addition, layers show different structure which is a clear symptom of a sample with anisotropic characteristics.

Figure 5.13 Typical layered SP-SC samples compacted using in-place tamping method.

In addition, two fully-drained CTC tests at constant matric suction, s = 50 kPa, and two fully-drained CTC tests at constant matric suction, s = 100 kPa, were conducted on four different SP-SC specimens. Tamping method were used to prepare the four samples, with initial water content, w = 10%, and the effort required to achieve a cubical sample with unit weight, γ_d = 15.344 kN/m3.

The principal strain response during the CTC tests conducted at matric suctions, s = 50kPa and s = 100 kPa, is presented in Figure 5.14 and Figure 5.15, respectively. The tests results shown that not consistent behavior can be obtained using samples compacted by taping method.

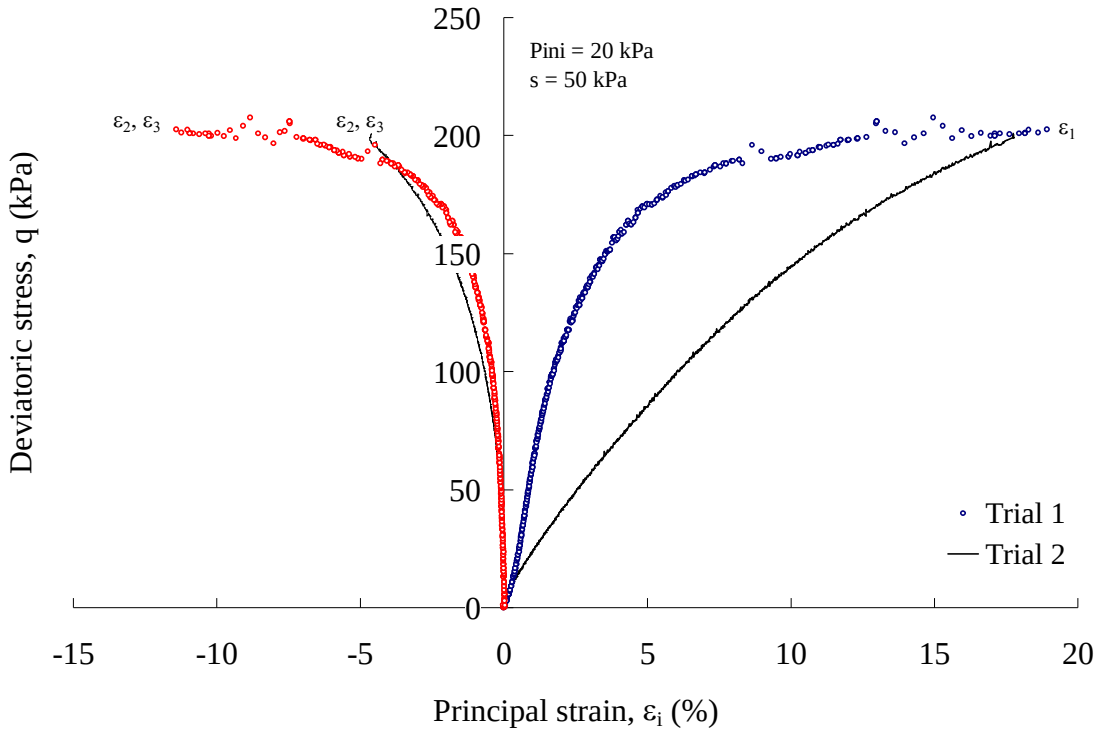

Figure 5.14 Response from two CTC trial tests at s = 50 kPa on SP-SC specimens prepared by tamping.

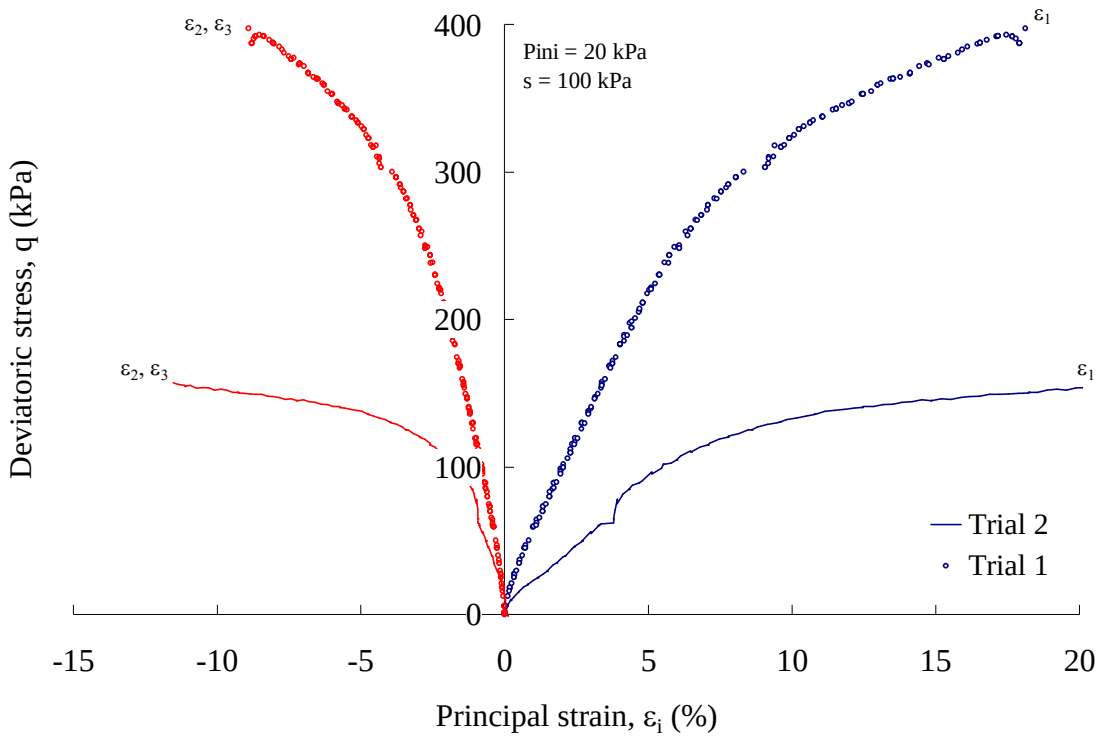

Figure 5.15 Response from two CTC trial tests at s = 100 kPa on SP-SC specimens prepared by tamping.

5.4.3 Static Compaction

Several cubical, compacted specimens of dimensions of 7.62 cm (3 in) per side were prepared using static compaction. Same as the samples prepared using tamping method, initial water content, w = 10%, was used to achieve a cubical sample with unit weight, γ_d = 15.344 kN/m^3 approximately. As shown in Figure 5.16 the triaxial load frame was use to apply a quasi static axial load to reduce the void of the soil and achieve the volume required.

The sample was prepared by using a custom-made stainless steel mold shown in Figure 5.17. The mold was filled with 761.5 g of poorly graded sand with high plasticity clay (SP-SC). Then, the loose material in the mold was sited on the triaxial load frame

and the axial load was applied at a monotonic rate of 1 mm per minute. Once the sample was compacted, it was extruded from the stainless steel mold and delivered into the cubical cell to be tested. In Figure 5.18, the texture of the sample prepared using static compaction can be compared to that texture obtained by tamping method.

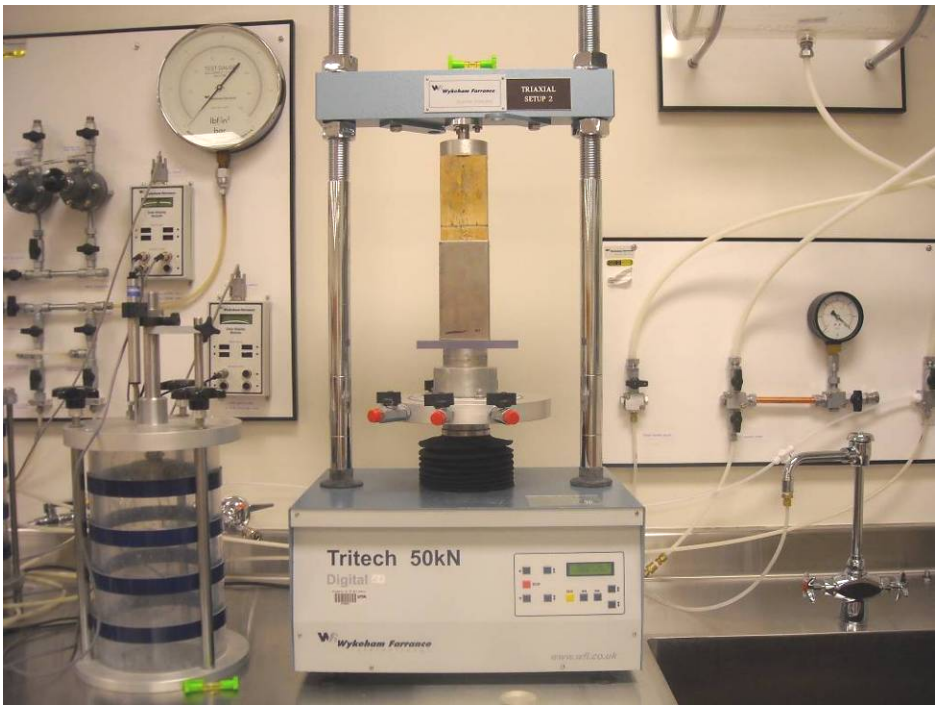

Figure 5.16 Static compaction using triaxial load frame.

Figure 5.17 Homogeneous SP-SC sample compacted using static approach.

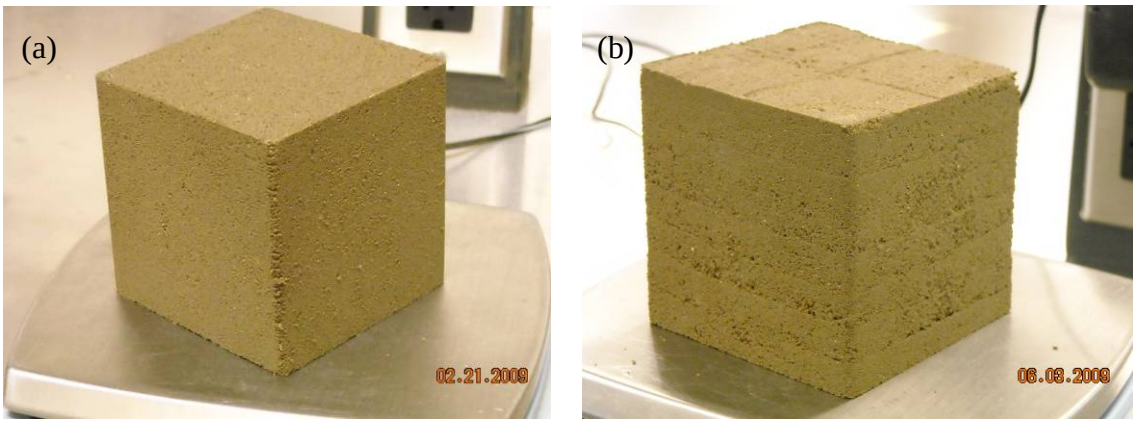

Figure 5.18 Compacted SP-SC samples using: (a) static compaction method, and (b) tamping compaction method.

A homogeneous specimen obtained by static compaction contrasts with a layered sample compacted using the tamping method. Four SP-SC samples were prepared using static compaction. Two of them were tested following a drained CTC path at constant matric suction, s = 50 kPa, and two were tested following a fully-drained CTC path at constant matric suction, s = 100 kPa. The principal strain response during the CTC tests conducted at matric suction, s = 50 and 100 kPa, is presented in Figure 5.19 and Figure 5.20 respectively. The tests results show that consistent behavior can be obtained using samples prepared using static compaction method.

5.4.4 Selection of Dry Unit Weight for SP-SC soil

A series of four fully drained isotropic loading tests were conducted at constant matric suction, s = 100 kPa in the cubical testing device, to experimentally determine the adequate density of the soil sample to be tested during the experimental program. The intent was to reproduce specimens with a relatively small preconsolidation pressure so that it was feasible to bring the soil to a virgin state and, hence, induce elasto-plastic deformations.

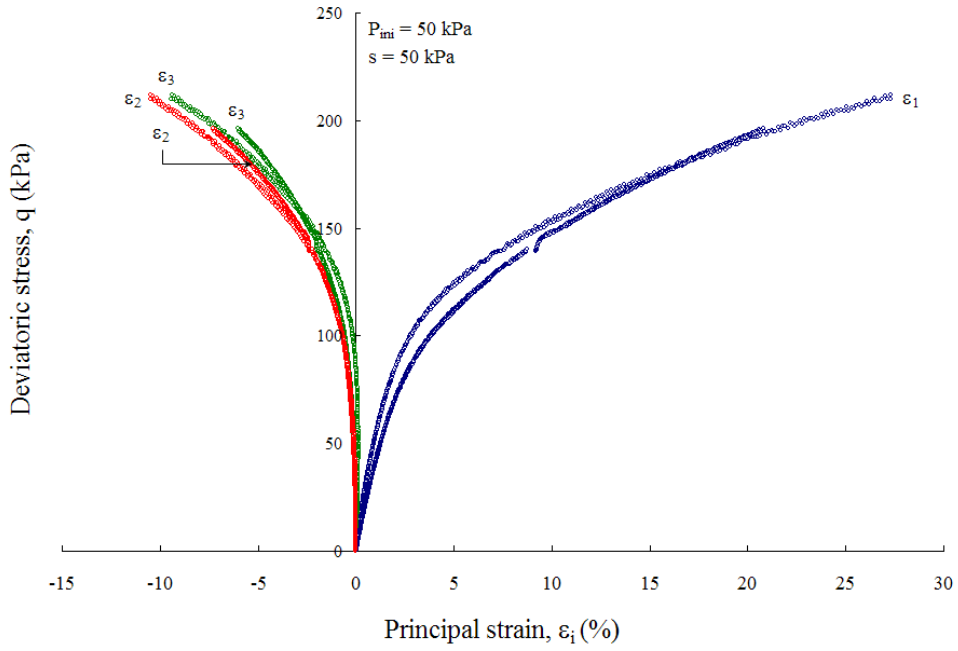

Figure 5.19 Response from two CTC trial tests at s = 50 kPa on statically compacted SP-SC specimens.

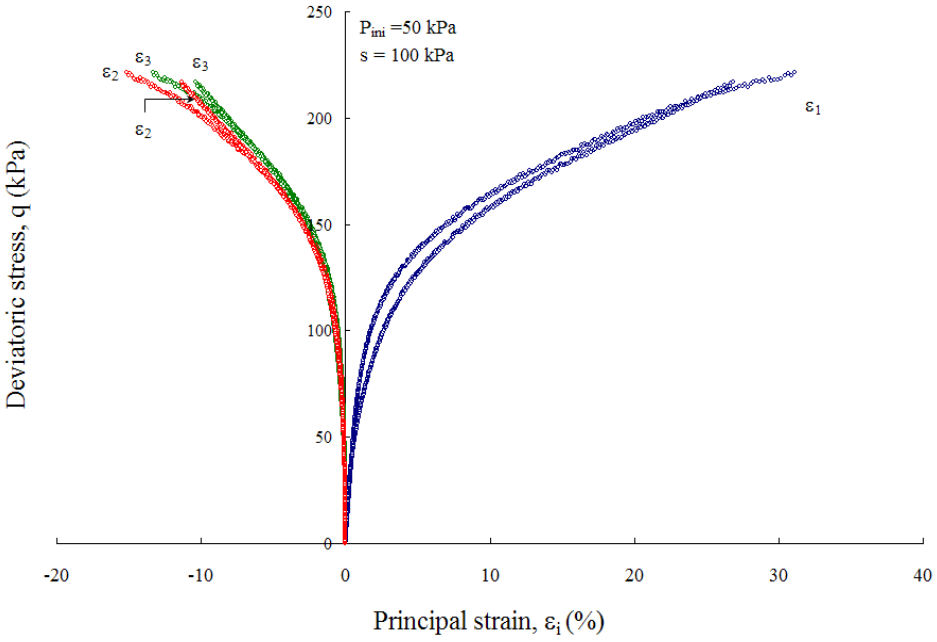

Figure 5.20 Response from two CTC trial tests at s = 100 kPa on statically compacted SP-SC specimens.

Four cubical compacted sand specimens SP-SC were prepared using static compaction method. Although the four samples were compacted at the same initial water content (i.e. w = 10%) each of them had enough solid mass to attain different dry unit weight at the same total volume. The selected dry unit weights were γ_d = 19.18, 17.26, 16.30, and 15.34 kN/m^3 which correspond, respectively, to 100%, 90%, 85%, and 80% of the maximum dry unit weight, $\gamma_{d,\ max}$. In order to obtain similar soil fabric and texture for every soil specimen, all of them were compacted following the same procedure. The reason for choosing this lower average value of dry unit weights were, γ_d, was to try to ensure "identical" soil specimens with adequate value of isotropic yield stress, $p_o(0)$. Thus, it was possible to reconsolidate the soil samples to a virgin state for calibration of the elasto-plastic models parameters (Alonso et al, 1990; Josa et al., 1992; Wheeler and Sivakumar, 1995).

Figure 5.21 shows the variation of the specific volume, v = 1 + e, with the neat mean pressure, p, during isotropic loading tests conducted at constant matric suction, s = 100 kPa and initial confinement, p_{ini} = 20 kPa. Based on the results, a dry unit weight, γ_d = 15.34 kN/m^3, was selected to produce "identical" samples hard enough to be easily reconsolidated to the virgin state and determine the value of isotropic yield stress, $p_o(0)$. All the subsequent cubical sand SP-SC samples were prepared with initial average moisture content, w = 10%, following the procedure previously described for static compaction. The resulting samples had and average dry unit weight, γ_d = 15.34 kN/m^3, with an initial average specific volume, v = 1+ e = 1.72, and an average degree of saturation, S = 37.5%.

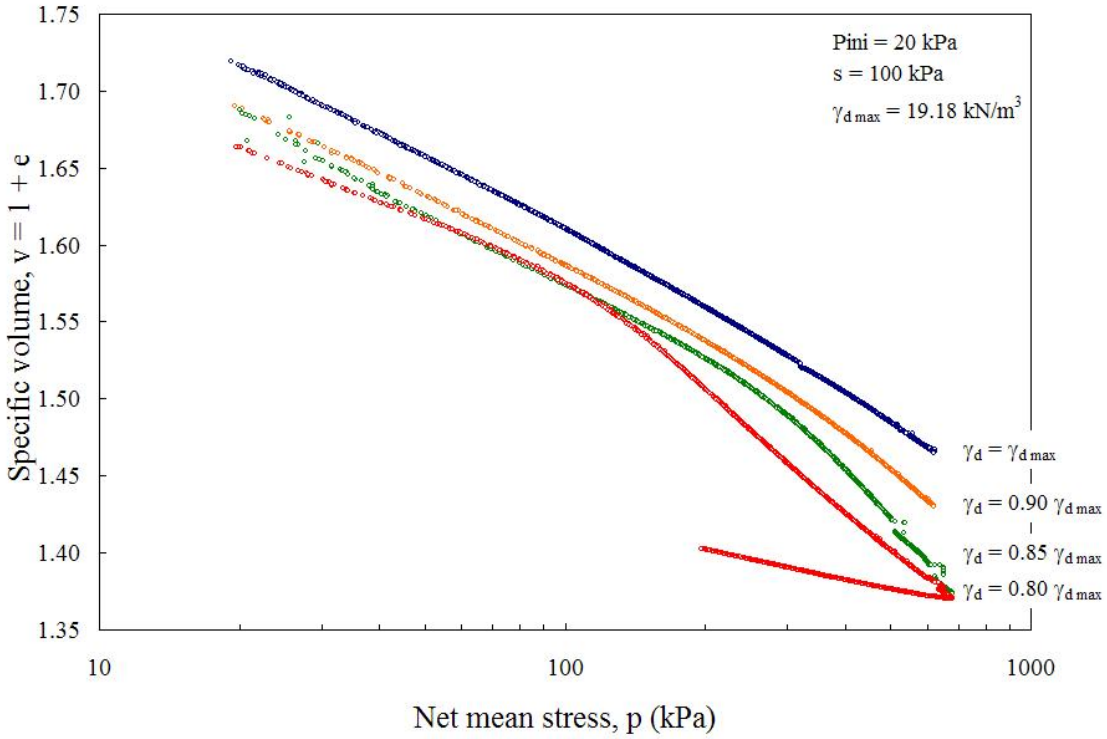

Figure 5.21 Response from HC tests at s = 100 kPa on four statically compacted SP-SC specimens prepared at different dry densities.

Next chapter describes the experimental procedure to conduct drained suction-controlled hydrostatic compaction (HC), conventional triaxial compression (CTC), triaxial compression (TC), triaxial extension (TE), and simple shear (SS) tests. In addition, the chapter includes some experimental results verifying repeatability of suction controlled testing in the refined cell, as well as tests conducted to select the appropriate loading rate.

CHAPTER 6

SUCTION-CONTROLLED EXPERIMENTAL PROGRAM AND RESULTS

6.1 Introduction

The fully computer-driven, suction-controlled cubical test cell described in chapter 5 was used to validate three of the most widely used elasto-plastic constitutive models for unsaturated soils: BBM (Alonso et al., 1990), MBBM (Josa et al., 1992), and Oxford Model (Wheeler and Sivakumar, 1995). In addition, further refinement of the Barcelona Basic Model, proposed as part of this research work, has also been validated with the experimental data. For this purpose, a series of suction-controlled hydrostatic compression (HC) tests and suction-controlled shear loading (CTC, TC, TE, and SS) tests were conducted on identically prepared cubical specimens 3 in (7.62 cm) per side of SP-SC soil.

This chapter presents a comprehensive analysis of all these test results, focusing on the effect of matric suction and net confinement on the general stress-strain response of SP-SC soil in q-p plane, principal stress plane and octahedral plane.

6.2 Experimental Procedures

A series of 26 suction-controlled triaxial tests was performed on an equal number of samples of poorly graded sand with high plasticity clay (SP-SC). Cubical samples, 76.2 mm (3 in) per side, were identically prepared by using static compaction in a cubical stainless steel mold at water content of 10%, as explained in Chapter 5. All

samples were compacted in one lift using a triaxial compression frame at a monotonic fixed displacement rate of 1.0 mm/min. This procedure yields a compactive effort considerable less than that of standard proctor test, which permits to reproduce samples with an average dry unit weight, γ_d = 15.34 kN/m^3, initial average specific volume, v = 1+ e = 1.72, and an average degree of saturation, S = 37.5%. All the samples were prepared following the same procedure in order to produce samples with similar soil fabric prior to suction controlled testing.

Soil volume changes as well as the applied external load, can be controlled and/or measured in real time by a computerized system developed by GCTS. Pore water pressure, u_w, was controlled through a high air entry value ceramic disk of 5 bar (505 kPa), located beneath the cubical soil sample. Matric suction, $(u_a - u_w)$, was controlled by using the axis translation technique proposed by Hilf (1956). Pore-air pressure, u_a, was applied at the bottom of the sample through a set of four pore stones with a low air entry value. Although the system allows controlling pore-water pressure, u_w, was kept at atmospheric pressure.

A typical fully-drained suction-controlled axisymmetrical loading test performed as part of this research started with the sample preparation process described in Chapter 5. Once the sample was prepared, the cubical specimen was gently slid in through one of the lateral cavities of the cubical frame as shown in Figure 6.1. The specimen ultimate sits on top of the already saturated HAE ceramic disk, as shown in Figure 6.1.

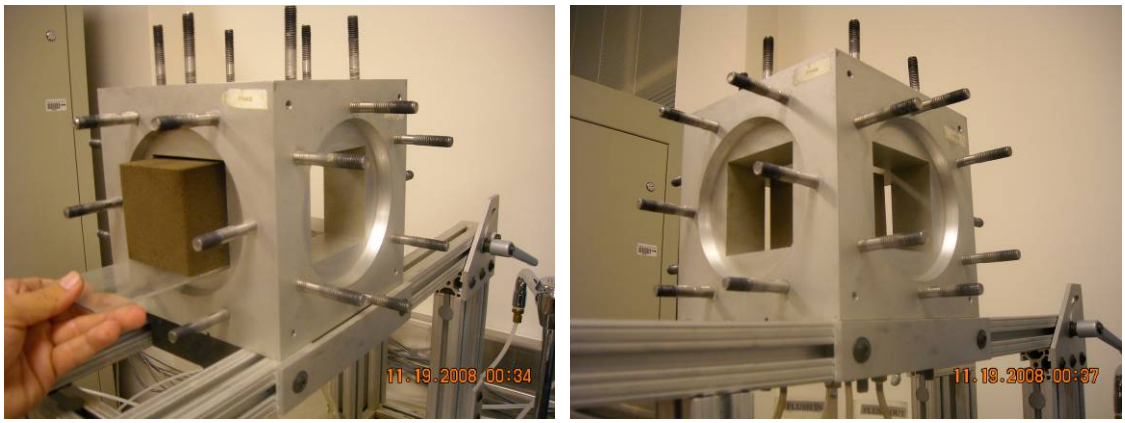

Figure 6.1 Sample placement in the cubical cell.

Once the soil sample was adequately placed into the cubical cell cavity, the remaining five walls were securely attached onto the cubical frame, as shown in Figure 6.2. After the true triaxial testing device was fully assembled (Chapter 4), the cubical specimen inside the cubical cell was subjected to an initial hydrostatic confinement, ($\sigma - u_a$), and a constant matric suction, ($u_a - u_w$). Then, equalization was allowed until no water change was detected. Finally, the sample was subjected to either isotropic consolidation or shearing loading in accordance with the programmed test.

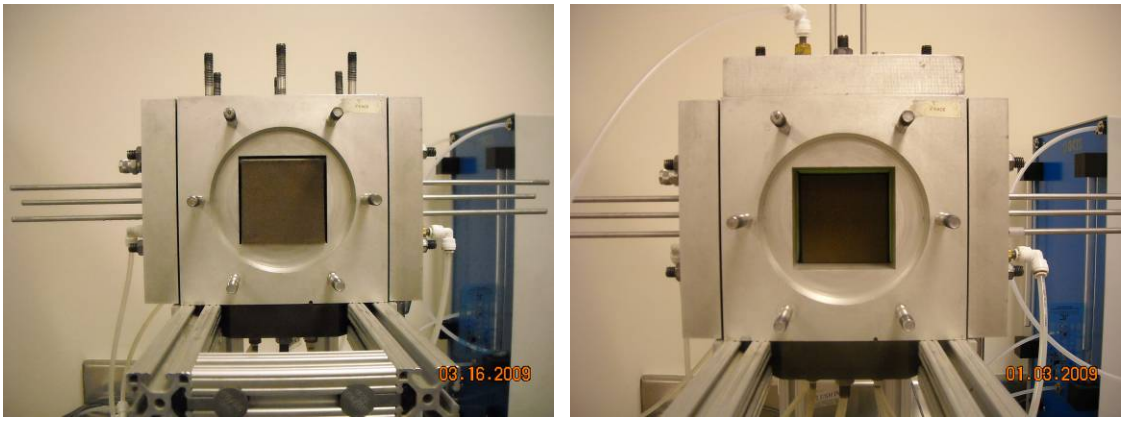

Figure 6.2 Cubical cell assemblage

6.2.1 Equalization Stage

After sitting up the soil sample and completely assembling the true triaxial device, the equipment is ready to perform the programmed test. The first stage of each test requires to bring the sample to a pre-selected initial net mean stress, p_{ini}, of 50, 100, or 200 kPa, and a corresponding matric suction, s, of 50, 100, 200, or 350 kPa. To accomplish this, the cell pressure was increased isotropically on each face of the cubic sample, starting at p = 0. When the cell pressure reached the desired initial net mean stress, $p = p_{ini}$, the air pressure was increased while being supplied to the soil pores at the bottom of the specimen until the selected value of matric suction, $s = (u_a - u_w)$, was reached. To ensure that the initial net mean stress induced on the test specimen remains constant, both matric suction and the principal stresses were incremented in the same magnitude at the same rate throughout the entire equalization stage.

The equalization stage in every test specimen was considered accomplished when the rate of change of specific water volume was less than 0.035 ml per day. Considering that each soil specimen was prepared with the same moisture content (i.e. w = 10%), which corresponds to a matric suction below 50 kPa, all the suction-controlled tests were readied by achieving suction along the drying path of the SWCC of the soil; therefore, not hysteresis was induced in the soil specimens. The time required for the equalization ranged between 5 to 10 days, depending on the selected value of suction.

Figure 6.3 presents the change in specific volume, Δv, with time that occurred during typical equalization stage from suction values of 50, 100, 200, and 350 kPa. All

tests started with an immediate reduction in specific volume due to the rapid increase of mean net stress, p, from zero to the selected p_{ini} = 50, 100, or 200 kPa. In all tests, the initial compression was followed by small changes in specific volume. In addition, due to the initial moisture content of the samples (i.e. w=10%), corresponding to a matric suction close to 40 kPa, no swelling was expected.

Special care was taken at the beginning of the hydrostatic loading, to avoid premature failure of the sample due to the unequal application of confinement pressure on each face. Premature failure can occur when not all of the membranes are in full contact with the sample and the initial pressure is applied fully on one of the axis, with no adequate support on the other axis, as shown in Figure 6.4.

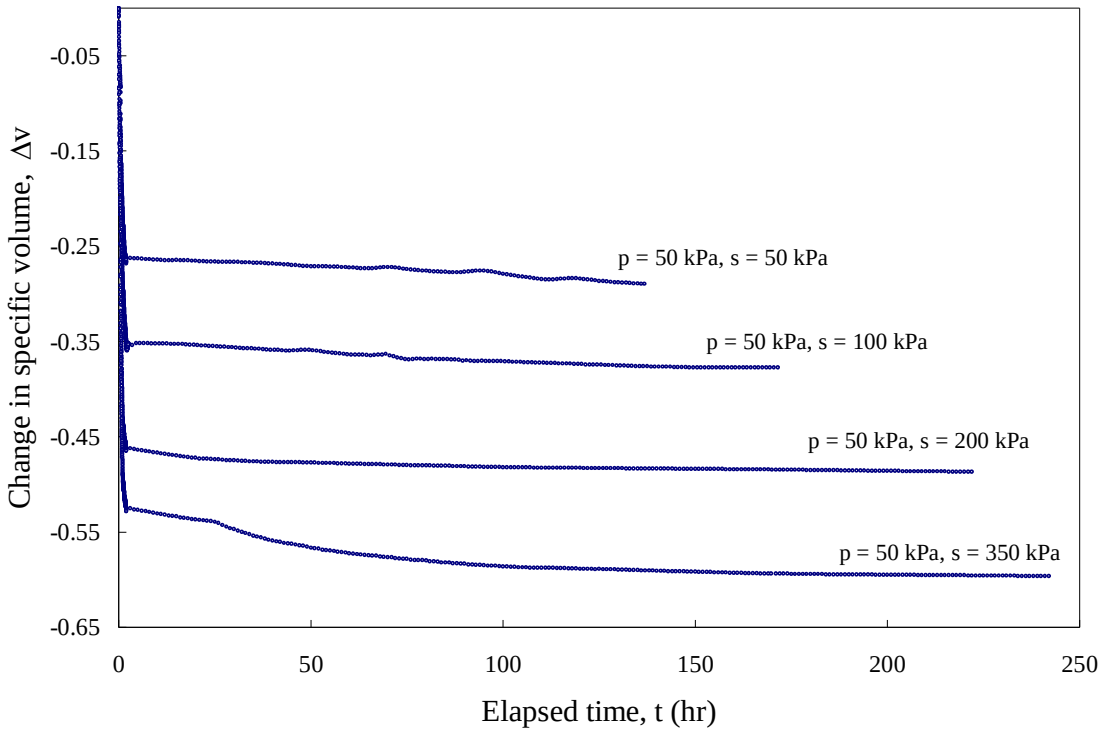

Figure 6.3 Typical change in specific volume with time during equalization stage.

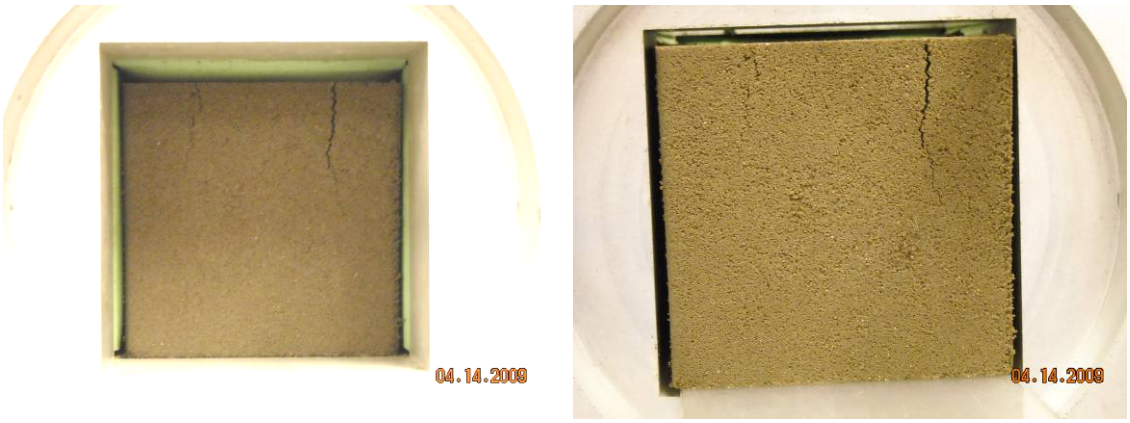

Figure 6.4 Premature failure of soil specimen under initial isotropic confinement due to inadequate contact between soil and membrane.

6.2.2 Isotropic Consolidation Stage

After completion of the equalization stage, each sample was isotropically consolidated by increasing the cell pressure at a rate of 8 kPa/h while holding constant the air pressure (i.e. maintaining constant suction). The rate of increase of the cell pressure was selected to ensure repeatability of test results. The loading conditions and stress path followed during the equalization and consolidation stages are presented in Figure 6.6 and Figure 6.7.

At the beginning of the test (i.e. point O in Figure 6.6), the cell pressure and pore-air pressure were both zero, and each compacted specimen was at a suction state close to 50 kPa. With the isotropic increment of the principal stresses, $\sigma_i = \sigma_1 = \sigma_2 = \sigma_3$, the sample goes to point C where the pressure cell reaches the preselected initial net mean stress, $p = p_{ini}$. At this point the air pressure was increased at the same rate of the principal stresses increment, $\Delta\sigma_i = \Delta\sigma_1 = \Delta\sigma_2 = \Delta\sigma_3$, until the selected matric suction, $s = (u_a - u_w)$, was reached on point H_{50}, H_{100}, H_{200}, or H_{350}, accordingly with the

conditions established for the test. Finally in the isotropic consolidation stage, the net mean pressure, p, was isotropically incremented up to 800 kPa approximately while the matric suction, s, remained constant.

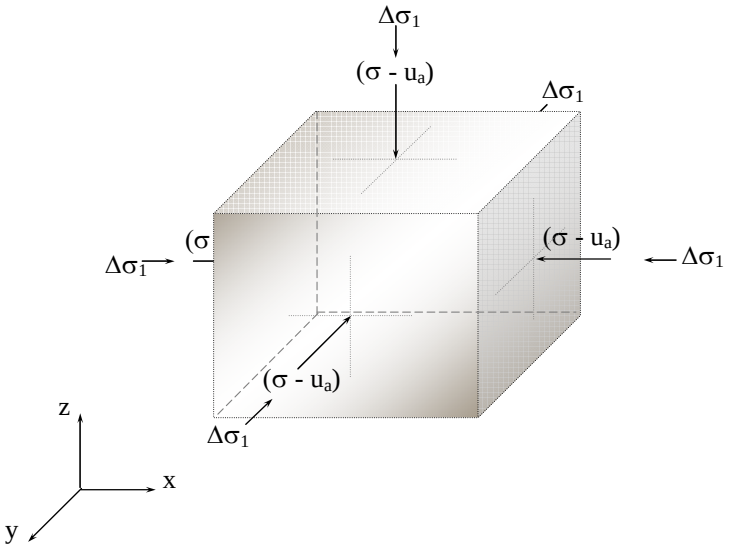

Figure 6.5 Hydrostatic compression (HC) loading condition.

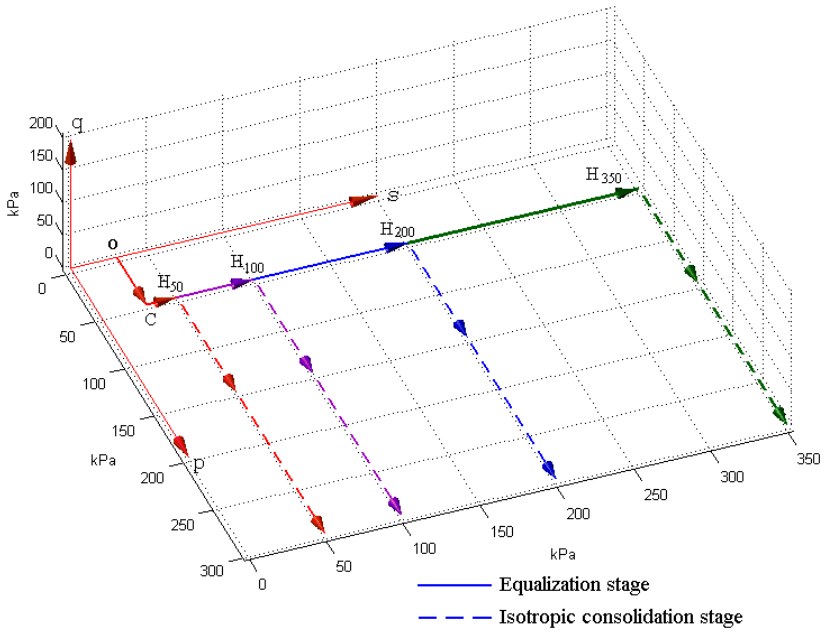

Figure 6.6 Typical stress paths during equalization and isotropic consolidation stage.

6.2.3 Shear Loading Stage

At the end of the equalization stage, once no further water volume change is detected from the sample, the sample is considered to be in equilibrium (i.e. equalized). When the equilibrium is reached the soil specimen has a net confining pressure, p_{ini} = $(\sigma_1 - u_a) = (\sigma_2 - u_a) = (\sigma_3 - u_a)$, and a matric suction of $(u_a - u_w)$. For further shear loading, the sample was loaded at a constant stress rate, following one of four different stress paths (i.e. CTC, TC, TE, or SS) until failure was attained. Any excess in the pore-air and pore-water pressure, caused by the applied load, was dissipated by allowing the pore fluid (air and water) to flow in or out of the soil specimen.

6.2.3.1 Conventional Triaxial Compression (CTC)

As shown in Figure 6.7, during drained constant-suction conventional triaxial compression (CTC) test, after completion of the equalization stage (i.e. point D_{50}, D_{100}, or D_{200} in Figure 6.8), principal stress, $\Delta\sigma_1$, was increased while maintaining the minor, $(\sigma_3 - u_a)$, the intermediate stresses, $(\sigma_2 - u_a)$, and the matric suction, $(u_a - u_w)$, constants. As the vertical net normal stress is increased, the yield surface expands moving the stress point accordingly with the size of the new yield surface. The stress path established by joining the stress points for this loading condition is shown in Figure 6.8.

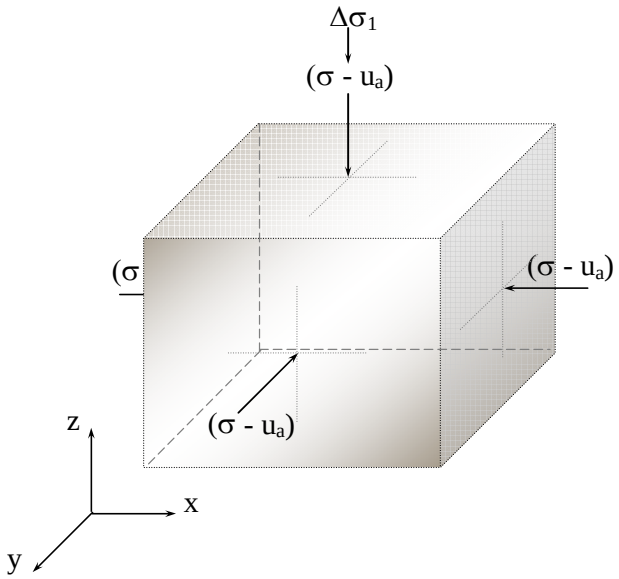

Figure 6.7 Conventional triaxial compression (CTC) loading condition

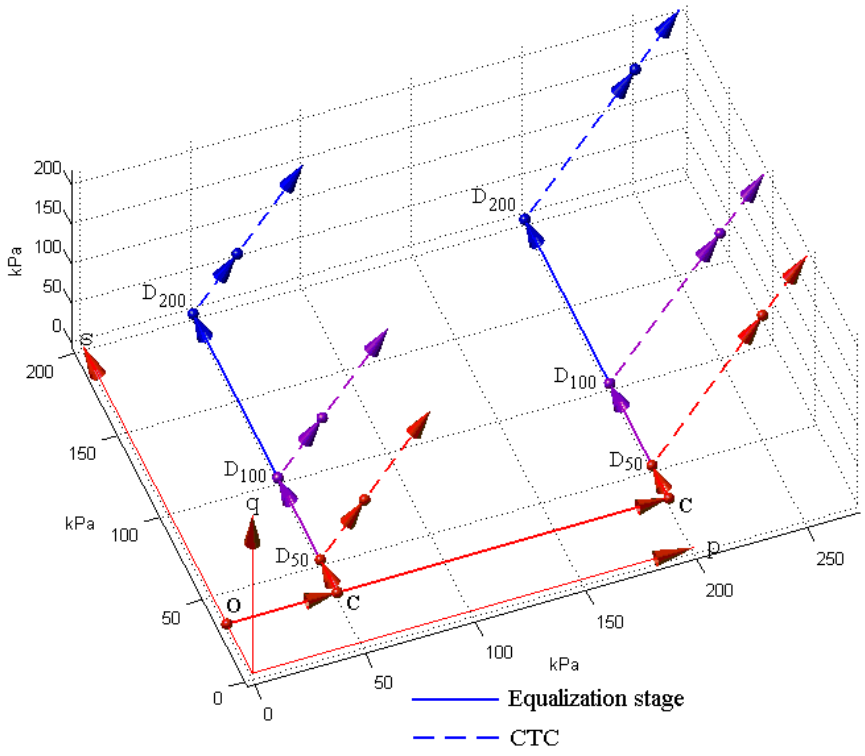

Figure 6.8 Typical stress path during equalization and conventional triaxial compression (CTC) stage.

6.2.3.2 Triaxial Compression (TC)

As shown in Figure 6.9, during drained constant-suction triaxial compression (TC) tests, starting at the end of the equalization stage (i.e. point TC_{50}, TC_{100}, or TC_{200} in Figure 6.10), the principal stress, σ_1, was increased while the intermediate and minor normal stress, σ_3 and σ_2, were reduced. As the minor and intermediate principal stresses were equally decrease (i.e. $\Delta\sigma_3 = \Delta\sigma_2 = -\frac{1}{2}\Delta\sigma_1$), the matric suction was kept constant. The stress path for this loading condition is shown in Figure 6.10.

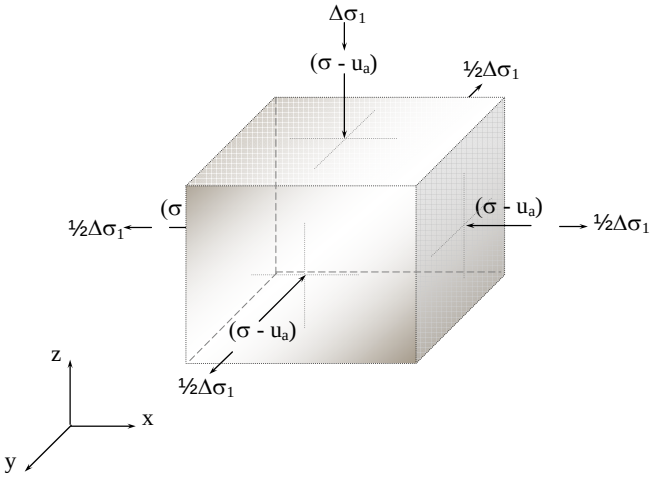

Figure 6.9 Triaxial compression (TC) loading condition

6.2.3.3 Triaxial Extension (TE)

As shown in Figure 6.10, during drained suction-controlled triaxial extension (TE) tests, after completion of the equalization stage (i.e. point TE_{50}, TE_{100}, or TE_{200} in Figure 6.12), the principal stress, σ_1, and intermediate stress, σ_2, were equally increased while minor normal stress, σ_3 was reduced (i.e. $\Delta\sigma_3 = -2\Delta\sigma_2 = -2\Delta\sigma_1$), and the matric suction was kept constant. The stress path for this loading condition is shown in Figure 6.12.

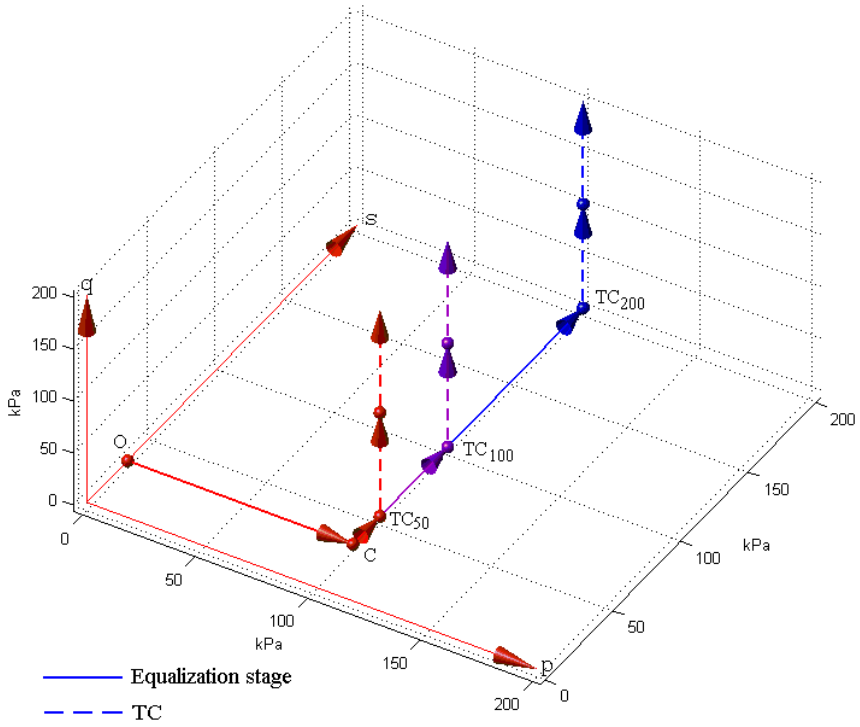

Figure 6.10 Typical stress path during equalization and triaxial compression (TC) stage.

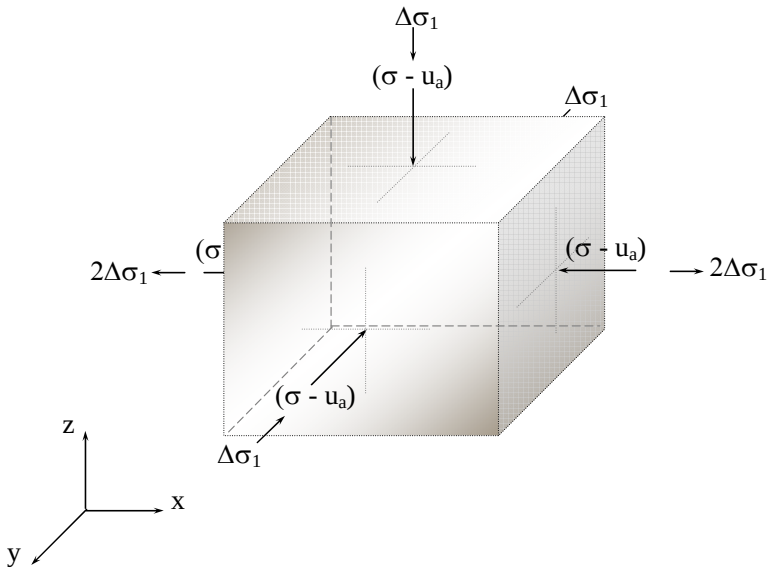

Figure 6.11 Triaxial extension (TE) loading condition

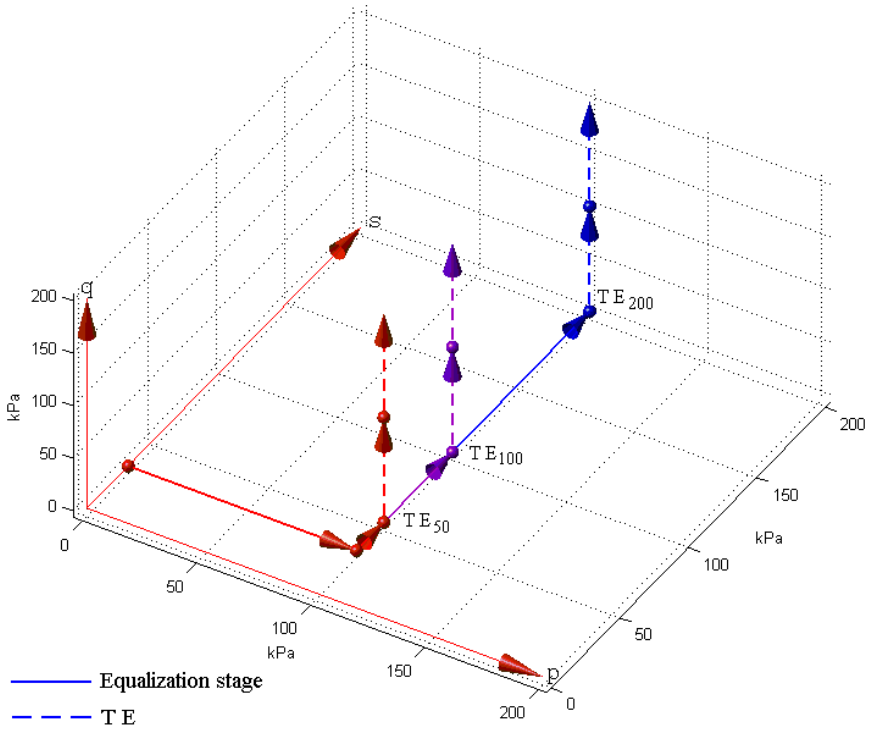

Figure 6.12 Typical stress path during equalization and triaxial extension (TE) stage.

6.2.3.4 Simple Shear (SS)

As shown in Figure 6.13, during drained suction-controlled simple shear (SS) tests, after completion of the equalization stage (i.e. point SS_{50}, SS_{100}, or SS_{200} in Figure 6.14), the principal stress, σ_1, was increase whereas the minor stress, σ_3, was decreased and the intermediate stress, σ_2, was held constant (i.e. $\Delta\sigma_3 = -2\Delta\sigma_1$ and $\Delta\sigma_2 = 0$). In these tests, the matric suction was also kept constant. The stress path for this loading condition is shown in Figure 6.14.

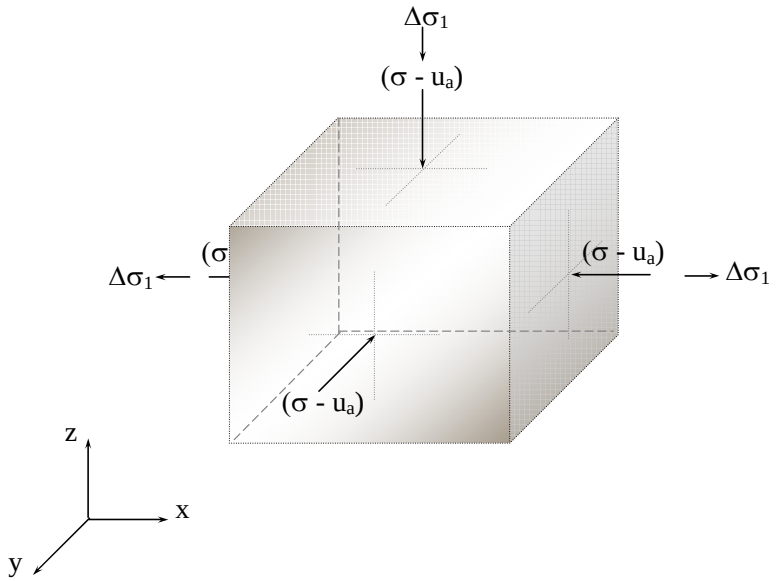

Figure 6.13 Simple shear (SS) loading condition

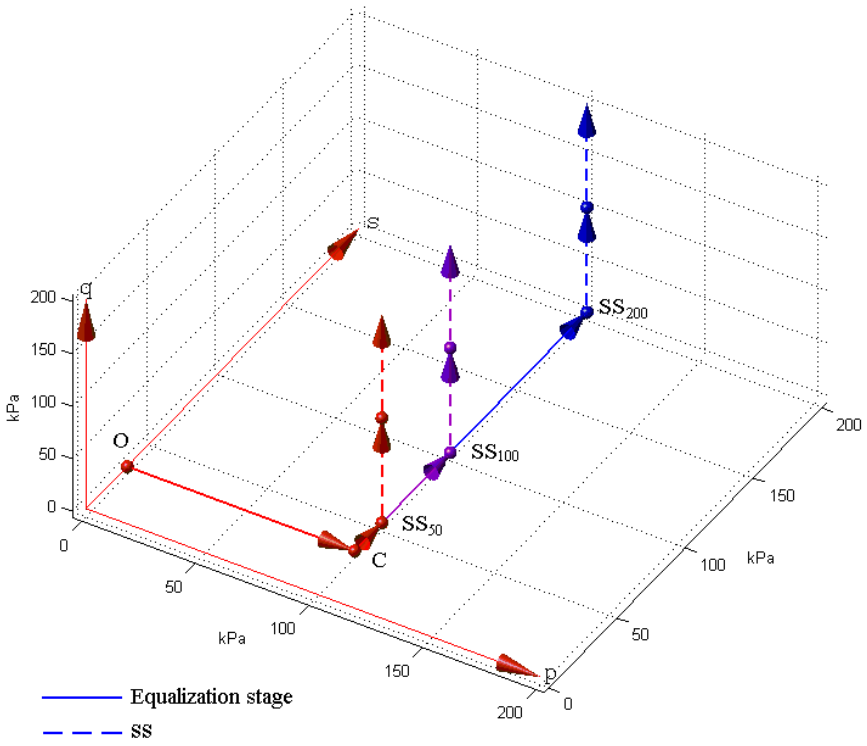

Figure 6.14 Typical stress path during equalization and simple shear (SS) stage.

6.3 Strain-controlled Versus Stress-controlled Testing Schemes

The strength testing of unsaturated soils is usually performed at a constant rate strain. Therefore an appropriate rate of strain must be selected before start the testing. However, the true triaxial apparatus used in this experimental work has the capability of perform not just constant strain rate strength tests (i.e. strain-controlled tests) but also constant load rate strength tests (i.e. stress-control tests).

When a drain triaxial test is performed very slowly (i.e. at a low strain rate or low loading rate) on a sample of soil it is likely that no pore pressure will build up in the soil and it could be observed a fully drained response of the soil. On the other hand, if the test is perform extremely fast, even if the drain connections are open, there will be no possibility for the pore-water to move into or out of the sample and it will observed a more or less fully drained response of the soil (Wood, 2004). The rate effect can be explained in terms of pore-water flow, which will obviously be more significant in a impermeable soil such as a clay that in a relative permeable soil such as a sand. However, the strain rate or load rate selection is related not just to the permeability but also to the flow path which is established by the dimension of the specimen been tested.

To determine the effect of the stress and strain rate at which the tests should be performed on the SP-SC soil, four identically prepared cubical SP-SC soil specimens were compacted to complete equal number of CTC tests under different conditions of matric suction and control. A drained stress-controlled CTC tests was conducted at strain rate of 0.1 mm/min (i.e. 125 kPa approximately), constant matric suction, s = 50 kPa, and initial net mean stress p_{ini} = 50 kPa. In addition, a drained strain-controlled

CTC test was conducted at stress rate of 10 kPa (i.e. 0.0078 mm/min approximately), maintaining the conditions of suction, s = 50 kPa, and net mean stress, p_{ini}= 50 kPa. The principal strain and total shear strain response of the soil samples tested, for both strain-controlled and tress-controlled tests, are shown in Figure 6.15 and Figure 6.16, respectively. Furthermore, Figure 6.17 shows the variation of specific volume, v = 1 + e with the net mean stress, p. Although the trend observed during the strain-controlled test is similar to that in stress-controlled test, the dispersion of the data suggest that better results can be obtained performing stress-controlled tests rather than strain-controlled test. The results also reveal the capability of the cubical cell to obtain similar results in repeated tests when the initial conditions were kept constant.

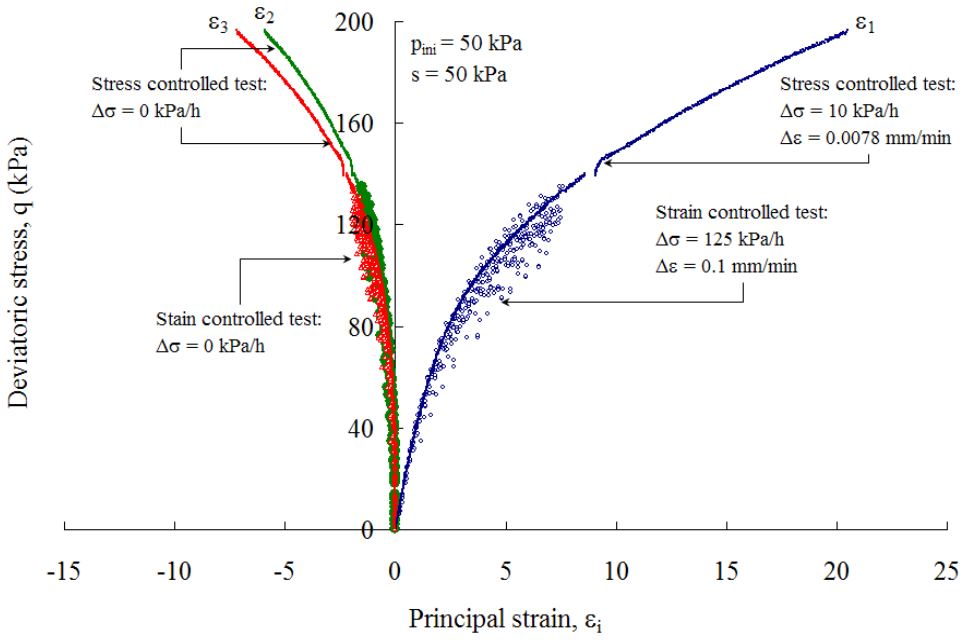

Figure 6.15 Response from strain-controlled and stress-controlled CTC tests at s = 50 kPa on compacted SP-SC soil.

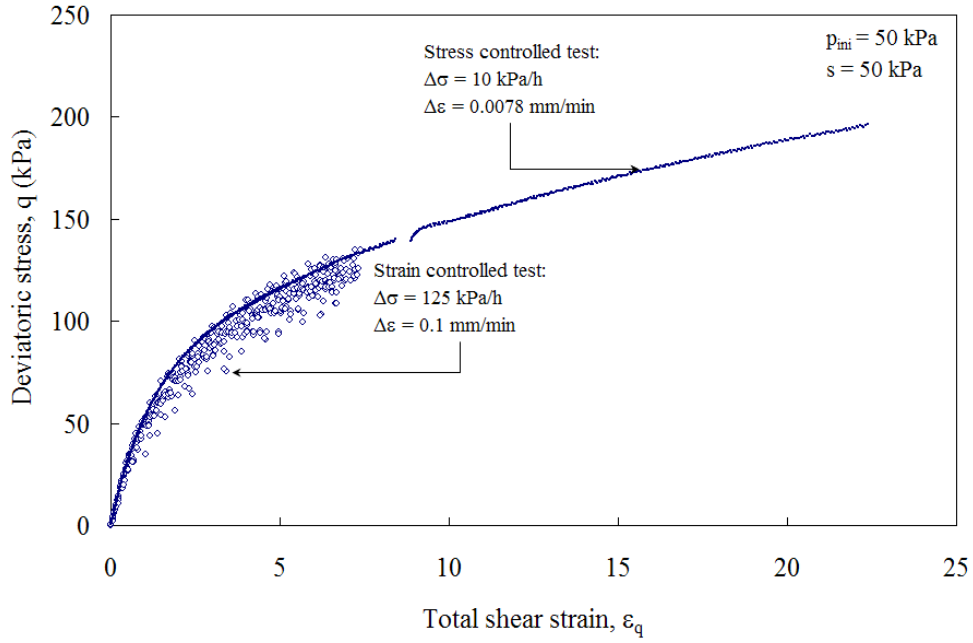

Figure 6.16 Total shear strain response from strain-controlled and stress-controlled CTC tests at s = 50 kPa on compacted SP-SC soil.

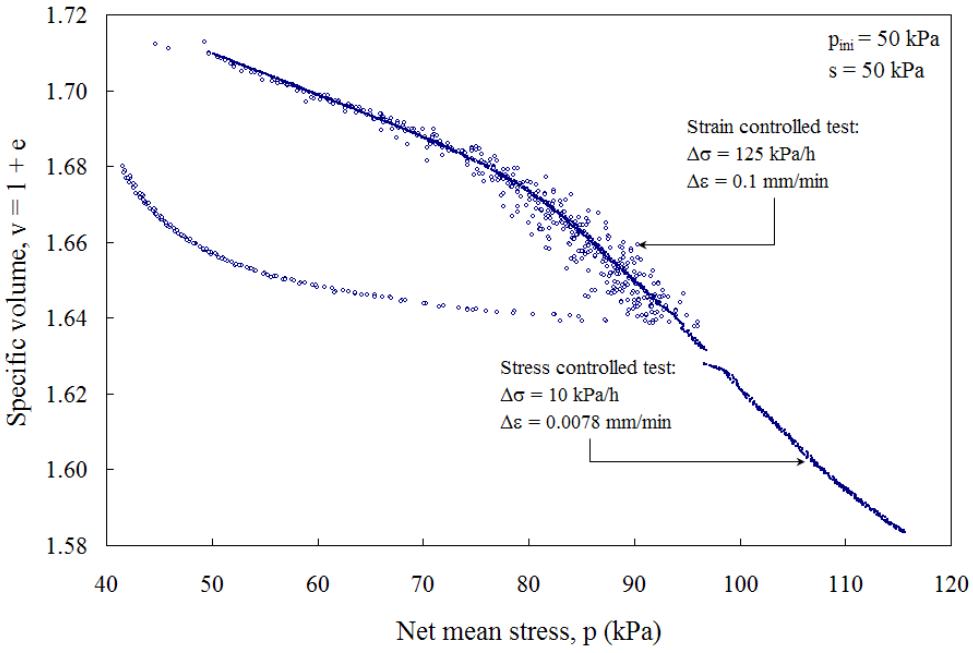

Figure 6.17 Variation of specific volume from strain-controlled and stress-controlled CTC tests at s = 50 kPa on compacted SP-SC soil.

On the other hand, a drained strain-controlled CTC tests was conducted at strain rate of 0.1 mm/min (i.e. 125 kPa approximately), constant matric suction, s = 100 kPa, and initial net mean stress p_{ini} = 50 kPa. Additionaly, a drained stress-controlled CTC test was conducted at stress rate of 5 kPa (i.e. 0.0078 mm/min approximately), maintaining the conditions of suction, s = 100 kPa, and net mean stress, p_{ini} = 50 kPa. The principal strain and total shear strain response of the soil samples tested, for both strain-controlled and stress-controlled tests are shown in Figure 6.18 and Figure 6.19, respectively. Figure 6.20 shows the variation of specific volume, v = 1 + e with the net mean stress, p.

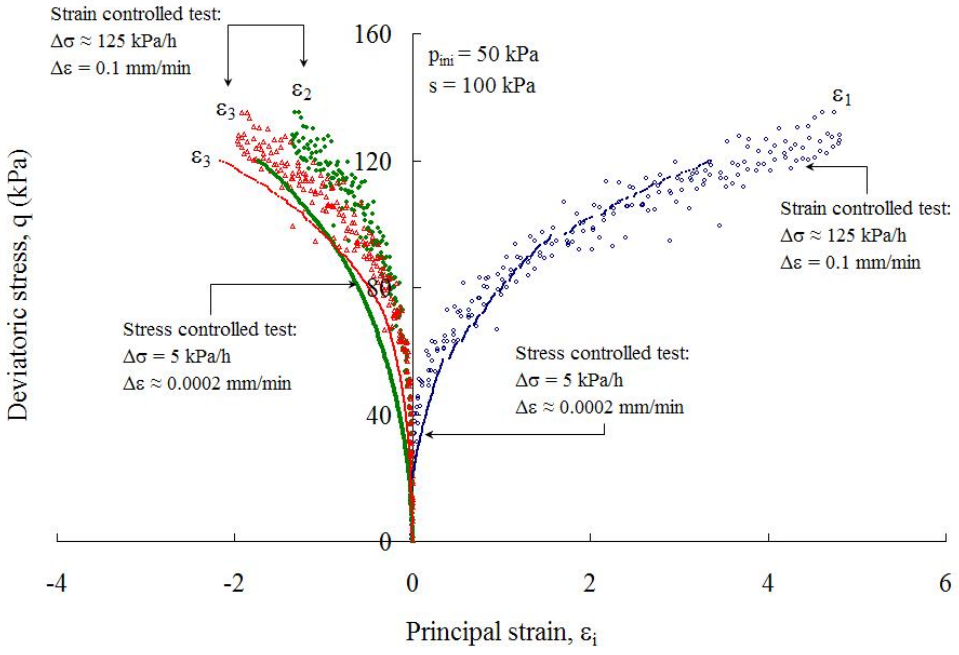

Figure 6.18 Response from strain-controlled and stress-controlled CTC tests at s = 100 kPa on compacted SP-SC soil.

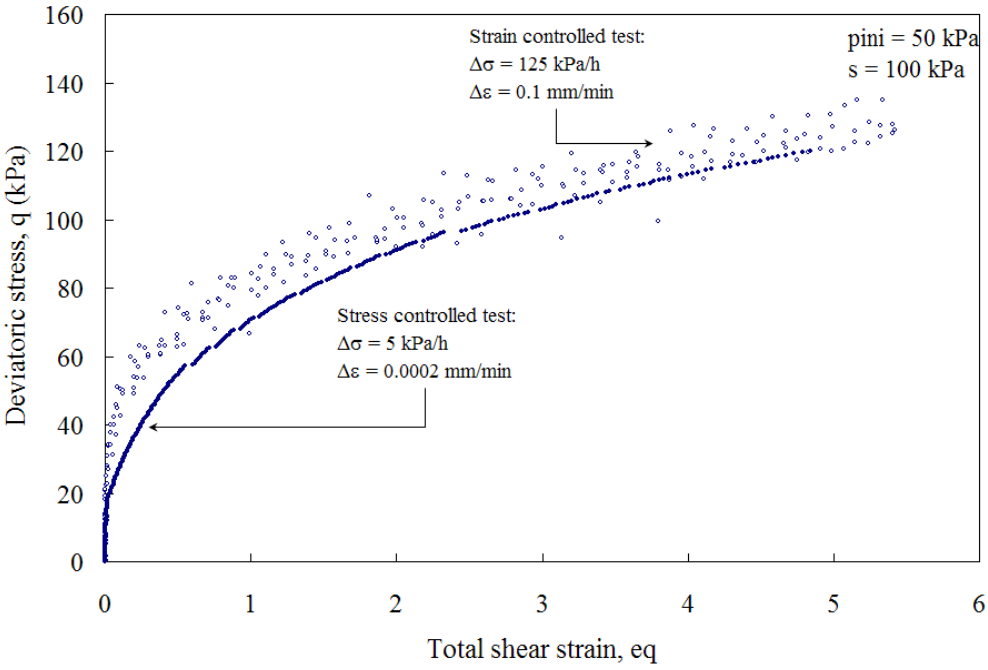

Figure 6.19 Total shear strain response from strain-controlled and stress-controlled CTC tests at s = 100 kPa on compacted SP-SC soil.

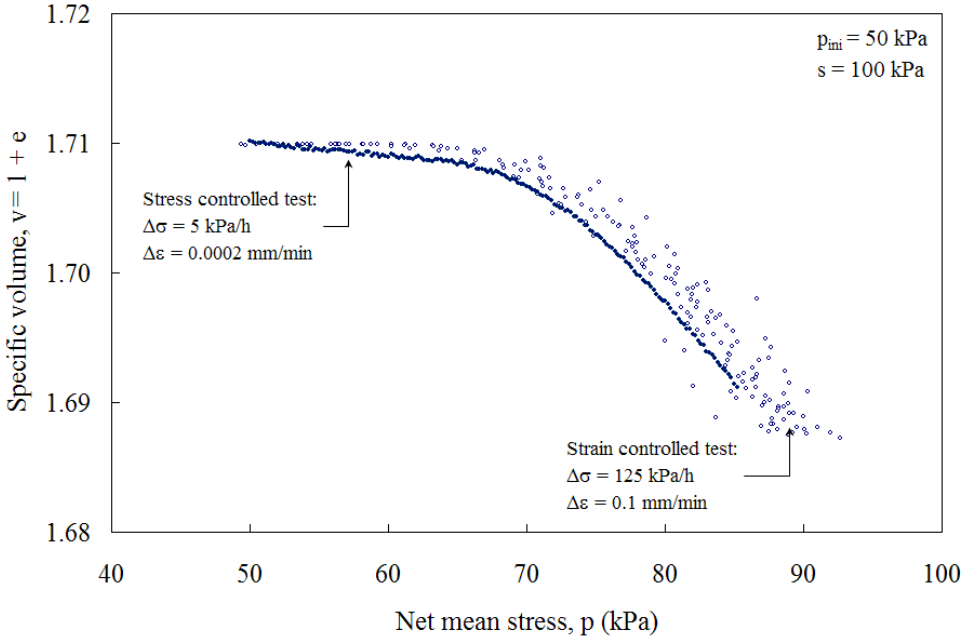

Figure 6.20 Variation of specific volume from strain-controlled and stress-controlled CTC tests at s = 100 kPa on compacted SP-SC soil.

The results presented in Figure 6.15 through Figure 6.20 show no effect of the stress rate on the response of the soil samples tested. That is, the permeability of the SP-SC soil allows the water drain from the sample easily. However, the scattered data results obtained in the strain-controlled CTC tests compared with the results obtained in the stress-controlled CTC test substantiate the conclusion that the true triaxial apparatus used in this research should be used to perform stress-controlled test rather than strain-controlled tests.

6.4 Selection of Appropriate Stress-Controlled Loading Rate

Four different samples were tested at different stress rate under isotropic consolidation compaction. Two drained stress-controlled HC tests where conducted on two identically prepared samples of SP-SC soils, at constant matric suction s = 50 and 100 kPa, initial net mean stress p_{ini}, = 50 kPa, and stress rate of 10 and 2 kPa, respectively. The variation of specific volume, v = 1 + e, with the net mean stress, p in arithmetic scale is presented in Figure 6.21 and Figure 6.23. In addition, Figure 6.22 and Figure 6.24 show the variation of specific volume, v = 1 + e, with the net mean stress, p in semi-logarithmic scale. Again the results confirm that the permeability of the sand allows water drain easily and no effect of the stress rate should be expected during the experimental program. Considering this a stress rate of 8 kPa/h has been selected for the execution of the suction-controlled experimental program designed for this research work and to be documented in the following sections. This loading rate was selected in order to accomplish the experimental program writhing a reasonable time frame of 12 months.

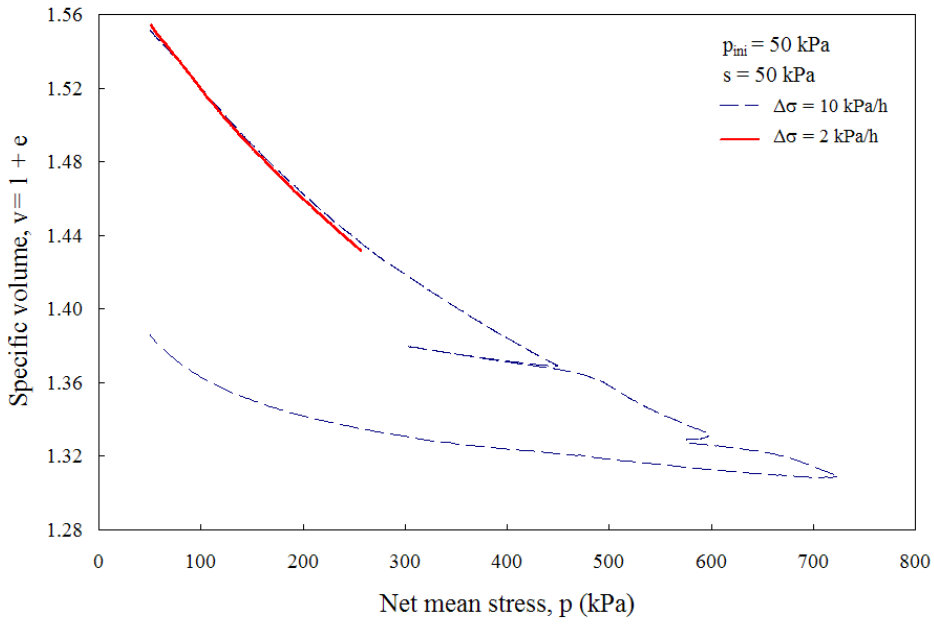

Figure 6.21 Variation of specific volume from HC tests at s = 50 kPa on compacted SP-SC soil – Arithmetic scale.

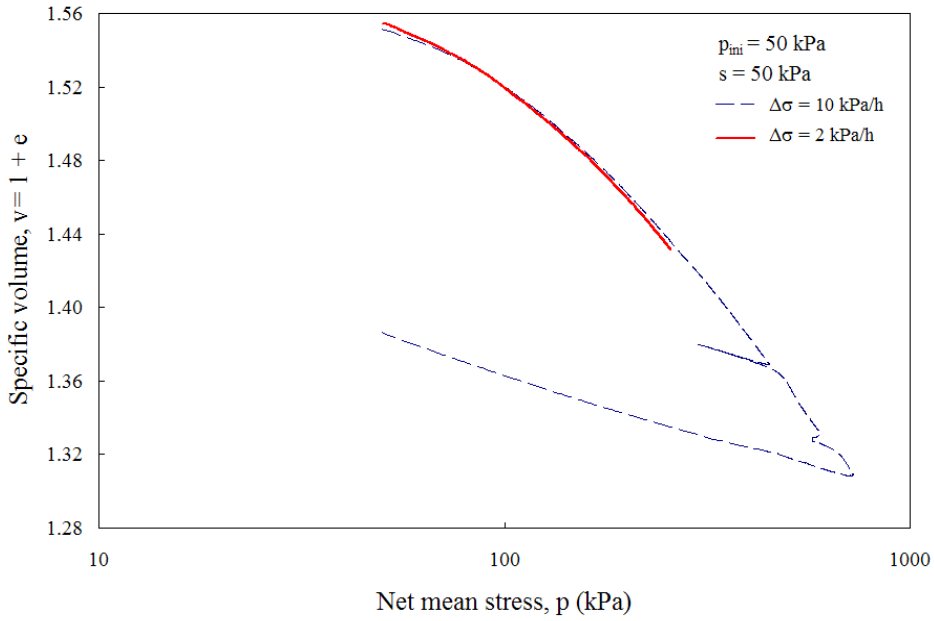

Figure 6.22 Variation of specific volume from HC tests at s = 50 kPa on compacted SP-SC soil – Semi-log scale.

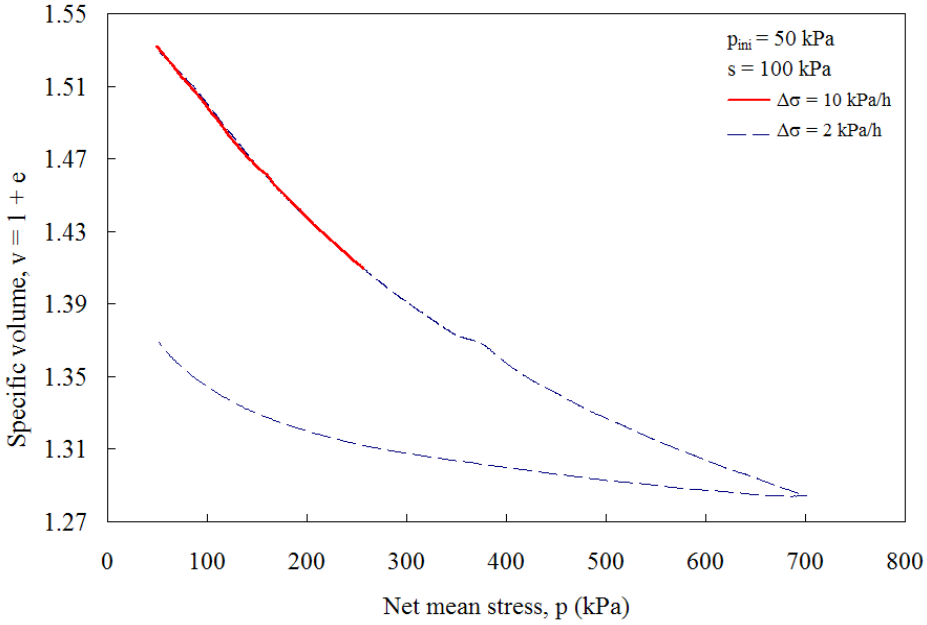

Figure 6.23 Variation of specific volume from HC tests at s = 100 kPa on compacted SP-SC soil – Arithmetic scale.

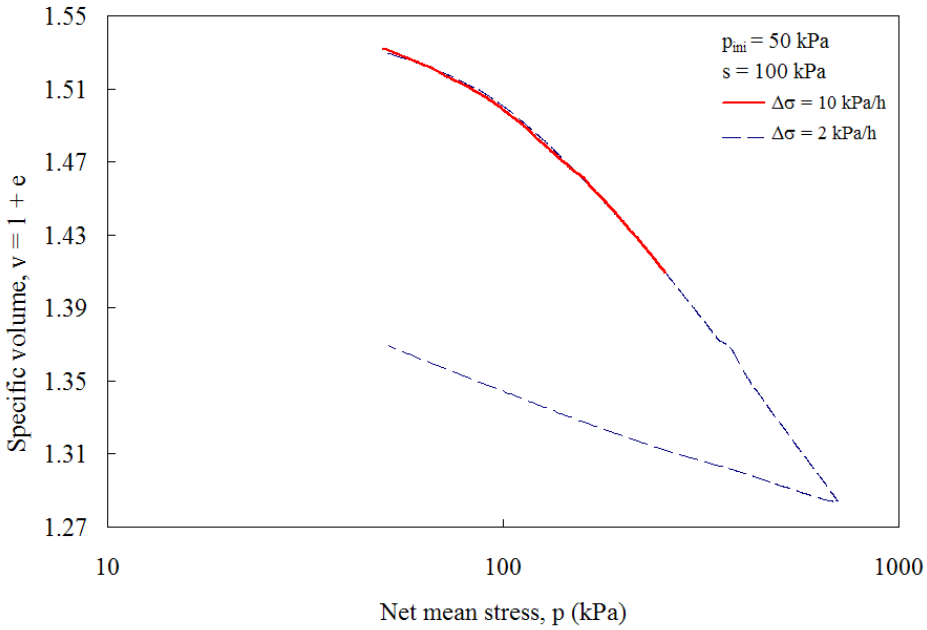

Figure 6.24 Variation of specific volume from HC tests at s = 100 kPa on compacted SP-SC soil – Semi-logarithmic scale.

6.5 Potential Sources of Experimental Error

Experimental results are subjected generally to one or more types of error: human error, systematic error, and random error (Montgomery, 2005). Human errors are frequent in the laboratory and its identification is important to guarantee the repeatability of the test. Although the suction-controlled true triaxial testing device used during the experimental phase of this research work is computer driven, the sample preparation, sample mounting, cubical device assemblage, as well as confinement are processes were human errors are highly probable.

On the other hand, systematic error is an error related with the experimental set up which causes the results to be skewed in the same direction every time (Montgomery, 2005). A sensor incorrectly calibrated could be a cause of systematic error in the cubical cell device. Additionally, all experiments have random error, which occurs because no measurement can be made with infinite precision (Montgomery, 2005). Noise may be added to a signal in a sensor. A frequent cause of this type of error is unexpected vibration affecting a specific sensor. In order to guaranty the repeatability of the experiments, especial attention must be given to the calibration of the sensors as well as the reduction of unexpected vibration. In addition, special care must be taken at the initial phase of the experimental process to reduce the possibility of human errors.

6.6 Repeatability of Stress-controlled Testing at Constant Matric Suction

Once selected the stress loading rate and considering the possible sources of experimental error, the dependability of the true triaxial cubical device and the computerized pressure control system has been experimentally validate through a series

of repeated tests conduced in different compacted SP-SC soil specimens. Four drained stress-controlled HC tests and two drained stress-controlled TC test were conducted on four different compacted SP-SC soil specimens. All six tests were completed at constant matric suction, s = 50 kPa. The results from the HC tests are presented in Figure 6.25 and Figure 6.26 in arithmetic and semi-logarithmic scale, respectively. In addition, two stress-controlled TC tests were conducted on equal number of SP-SC soil specimens at matric suction, s = 100 kPa, and initial net mean pressure, p_{ini} = 100 kPa. Figure 6.27 and Figure 6.28 shown the results of the TC test conducted at constant matric, s = 50 kPa and s = 100 kPa, respectively.

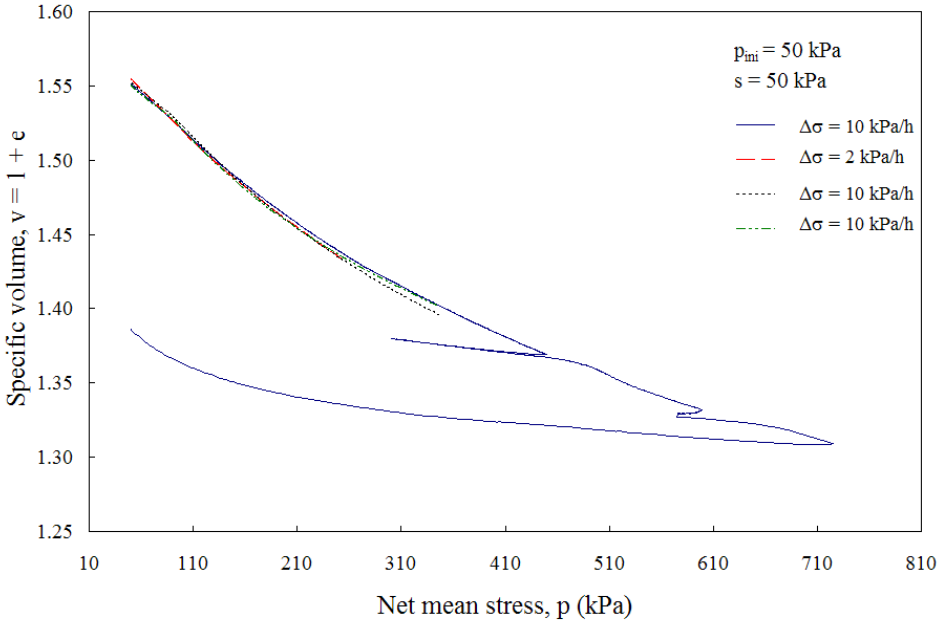

Figure 6.25 Repeatability of HC test results at s = 50 kPa on four identically prepared SP-SC specimens – Arithmetic scale.

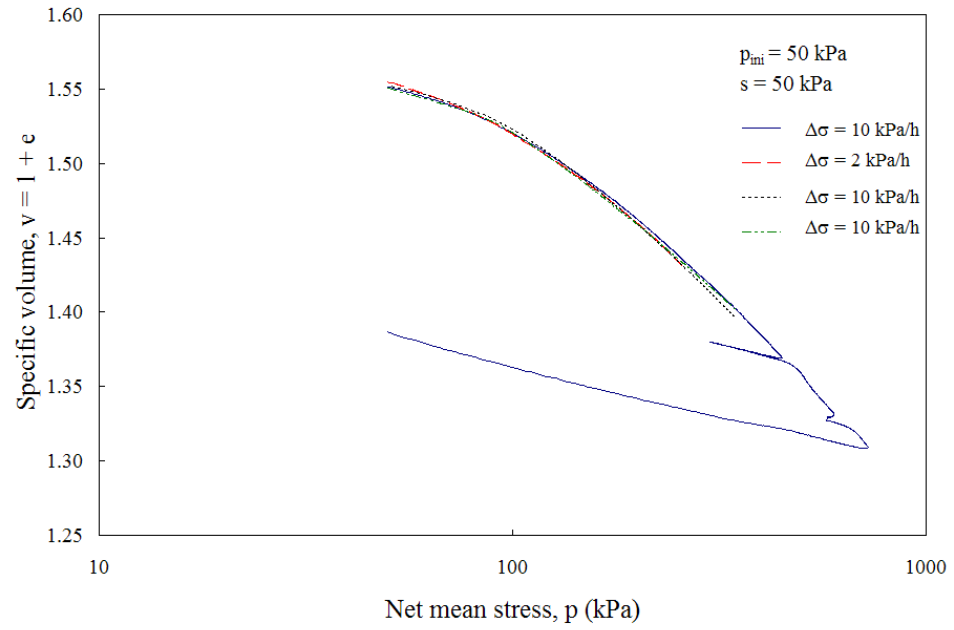

Figure 6.26 Repeatability of HC test results at s = 50 kPa on four identically prepared SP-SC specimens – Semi-log scale.

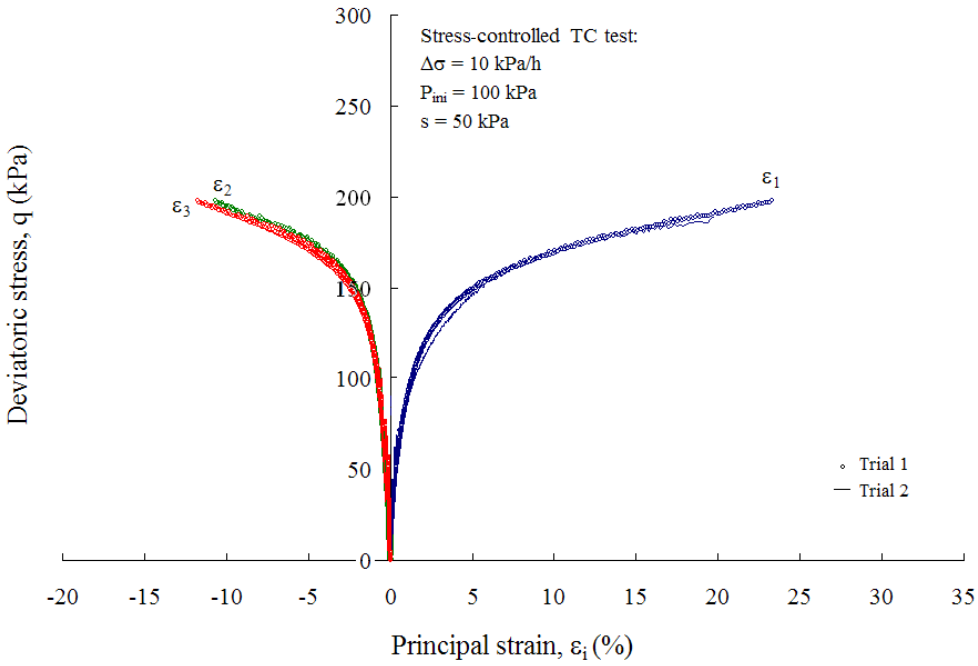

Figure 6.27 Repeatability of TC test results at s = 50 kPa on two identically prepared SP-SC specimens.

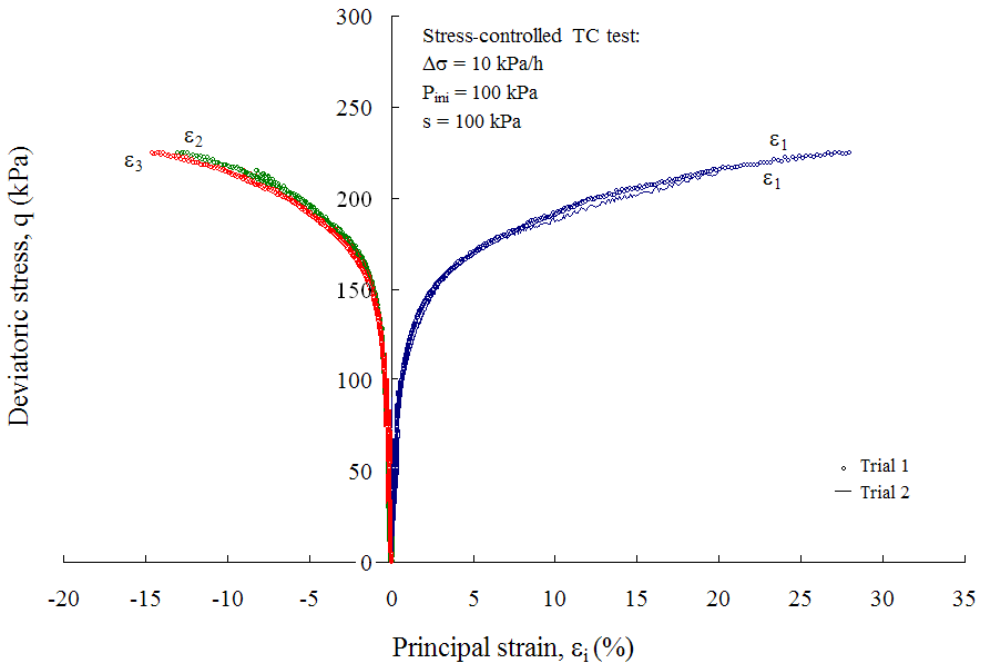

Figure 6.28 Repeatability of CTC test results at s = 100 kPa on two identically prepared SP-SC specimens.

In general, the results presented in Figure 6.25 to Figure 6.28 as well as those obtained from the tests conducted to determine the loading rate (i.e. Figure 6.15 to Figure 6.24), confirm the repeatability of the tests conducted on the true triaxial device.

6.7 Experimental Program Results

The tests discussed here were carried out using a true traiaxial apparatus, located in the Geomechanical Research Laboratory of the University of Texas at Arlington. As the equipment is computer driven, fully automated, and feedback-controlled, it is possible to a specimen under any stress path. Change in volume were measured on real time, taking in account the shape adopted by the flexible rubber membranes.

The testing program consisted of 8 fully drained hydrostatic compression (HC) tests, 6 fully drained triaxial conventional (CTC) tests, 6 fully drained triaxial

compression (TC) tests, 3 fully drained triaxial extension (TE) tests, and 3 fully drained simple shear (SS) tests.

6.7.1 Mechanical Response Under Isotropic Loading

To study the mechanical response of an unsaturated soil under isotropic loading conditions, a series of 8 cubical compacted SP-SC soil specimens was identically prepared using static compaction, to conduct equal number of drained suction-controlled hydrostatic compression (HC) tests at constant matric suction. Once completed the equalization stage for the pre-selected constant matric suction, s = 50 kPa, s = 100 kPa, s = 200 kPa, s = 350 kPa, an isotropic ramped loading was applied at a rate of 8 kPa/h. After reached the final principal stress (i.e. σ_i = 800 kPa for s = 50, 100, and 200 kPa; and σ_i = 950 kPa for s = 350 kPa) the specimen was unloaded to the initial stress state.

Figure 6.29 shows the variation of the specific volume, v = 1 +e, with the net mean stress, p, obtained during the isotropic loading tets conducted on SP-SC soil samples at initial net mean stress, p_{ini} = 50 kPa, and different values of matric suction, s = 50 kPa, s = 100 kPa, s = 200 kPa, and s = 350 kPa, respectively. The initial change in the slope of the continuous v–p plot allows identifying the yield stress value, $p_o(s)$, for each value of constant matric suction. This behaviour further substantiate the existence of an initial loading collapse (LC) yield curve induced by the equalization stage, as described later in Chapter 8.

On the other hand, the variation of principal strains, ε_1, ε_2, ε_3, with the net mean stress, p, for each value of matric suction, s = 50 kPa, s = 100 kPa, s = 200 kPa, and s =

350 kPa, is presented in Figure 6.30, Figure 6.31, Figure 6.32, and Figure 6.33, respectively. The difference is response among the intermediate principal strain, ε_2, and minor principal strain, ε_3, along the HC stress path, shows the degree of anisotropy induced by the static compaction method on the horizontal plane of each sample. No influence of the matric suction, s, on the degree of anisotropy is observed. For unloading paths, the specimens showed a similar response in terms of the unloading reloading line, regardless the value of matric suction. This result is in accordance with the assumption of a constant and independent of suction made for Alonso et al. (1990) for the elastic stiffness parameter, κ.

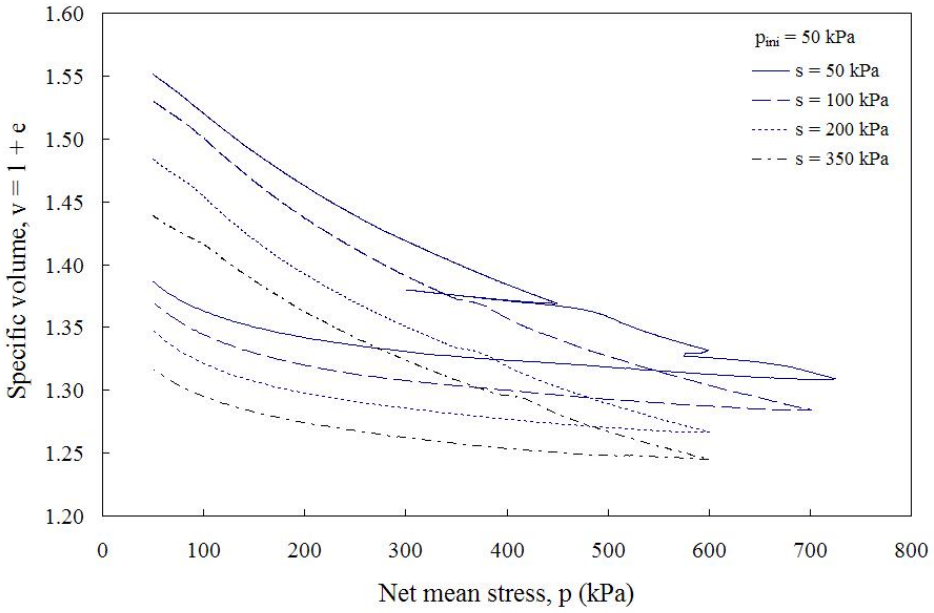

Figure 6.29 Variation of specific volume from HC tests at s = 50, 100, 200, and 350 kPa on a SP-SC soil.

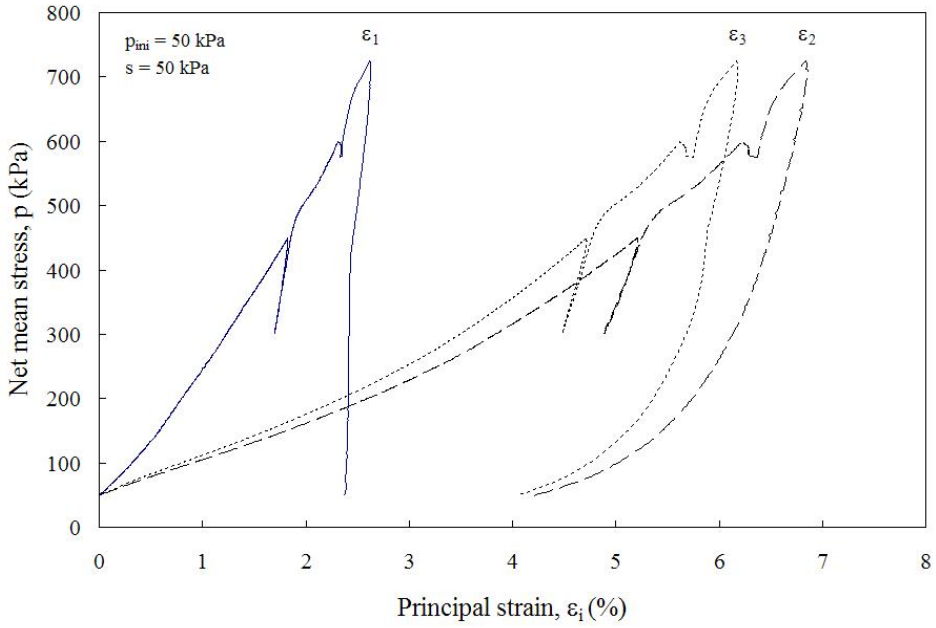

Figure 6.30 Principal strain response from HC test at s = 50 kPa on SP-SC soil.

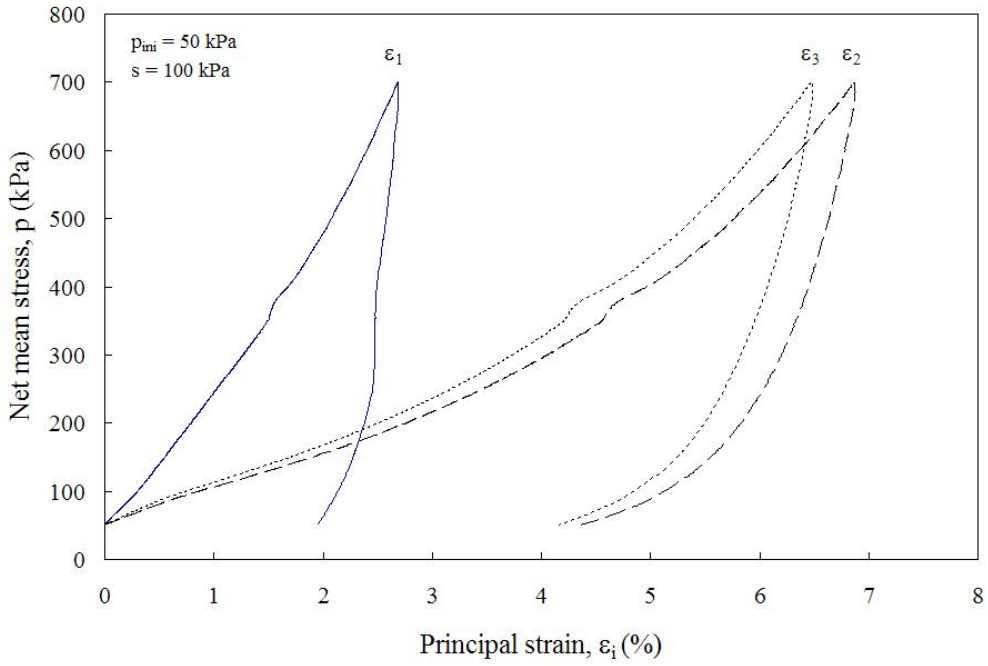

Figure 6.31 Principal strain response from HC test at s = 100 kPa on SP-SC soil.

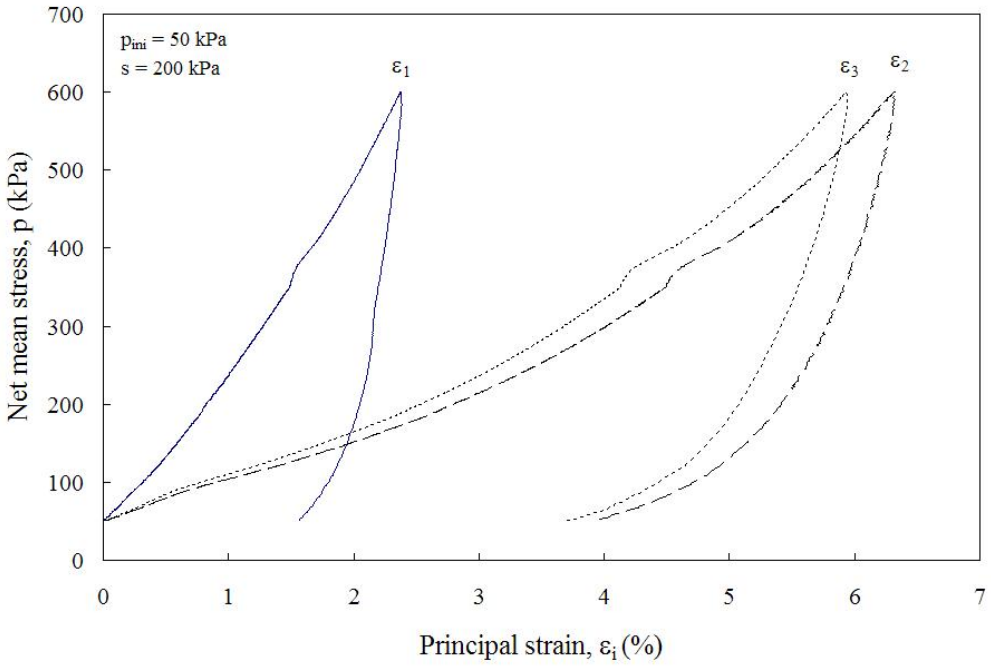

Figure 6.32 Principal strain response from HC test at s = 200 kPa on SP-SC soil.

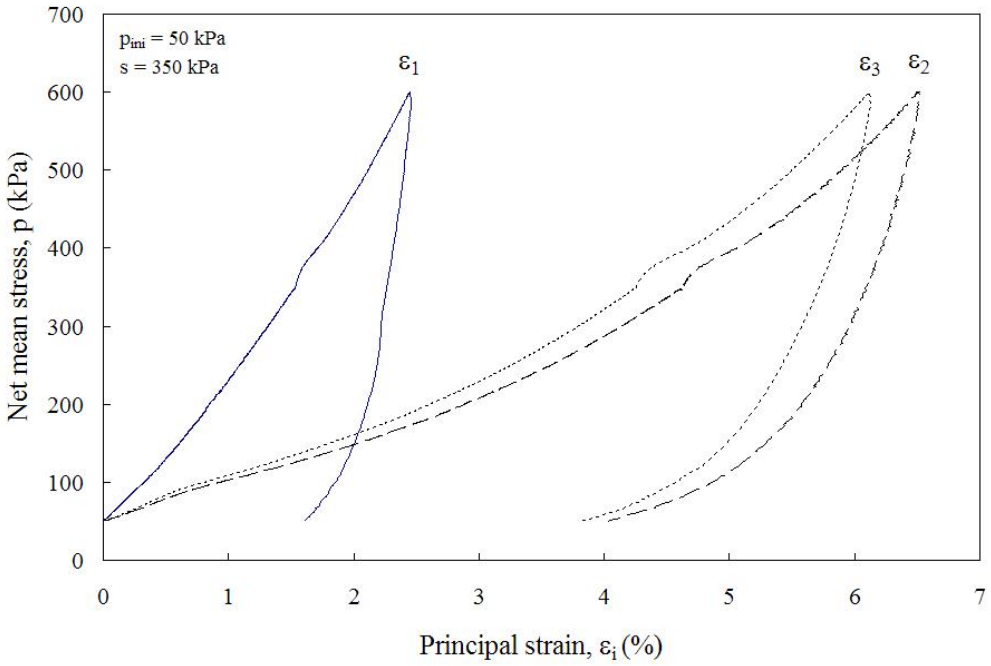

Figure 6.33 Principal strain response from HC test at s = 350 kPa on SP-SC soil.

6.7.2 Mechanical Response Under Shear Loading

A series of 6 drained suction-controlled CTC tests was conducted on equal number of cubical compacted SP-SC soil specimens, to experimentally study the mechanical behaviour of an unsaturated soil under axisymmetric shear loading ($\sigma_2 = \sigma_3$ = constant) and constant matric suction, s = 50 kPa, s = 100 kPa, and s = 200 kPa. Figure 6.34 and Figure 6.35 show the experimental variation of principal strains, ε_1, ε_2, ε_3, with the net mean stress, p, for initial net mean stress, p_{ini} = 50 kPa and 200 kPa, respectively. In addition, Figure 6.36 presents the results obtained during a CTC test conducted at constant matric suction, s = 50 kPa, and initial net mean stress, p_{ini} = 100 kPa.

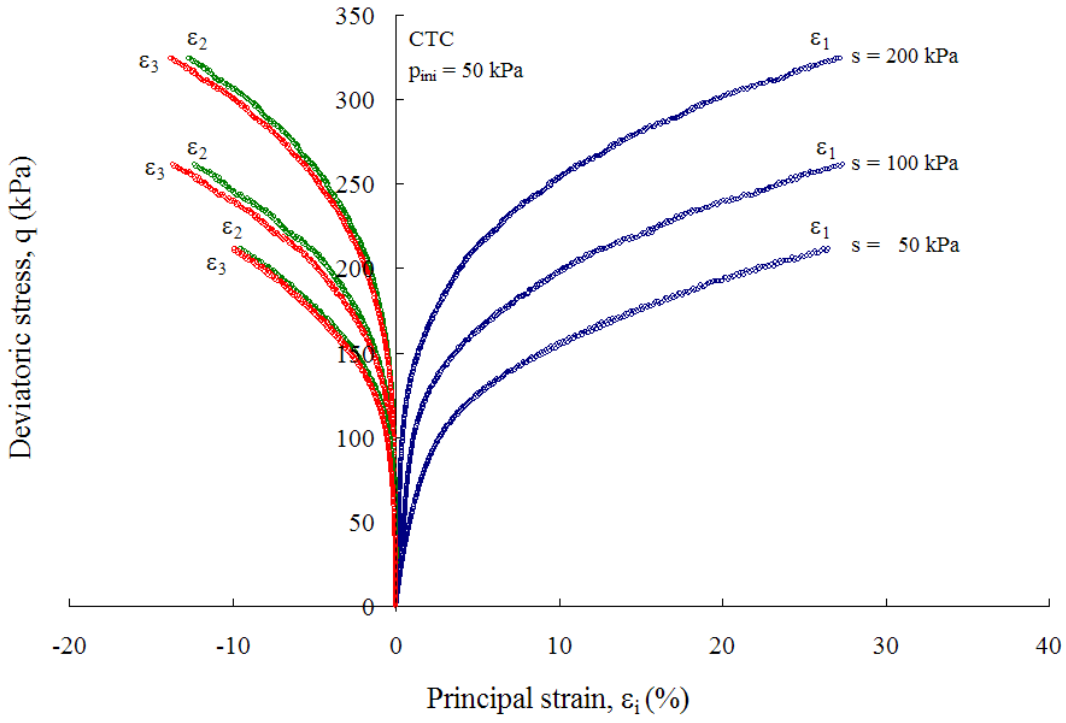

Figure 6.34 Experimental deviatoric stress – principal strain response CTC tests at s = 50, 100, and 200 kPa; and $_{pini}$ = 50 kPa on SP-SC soil.

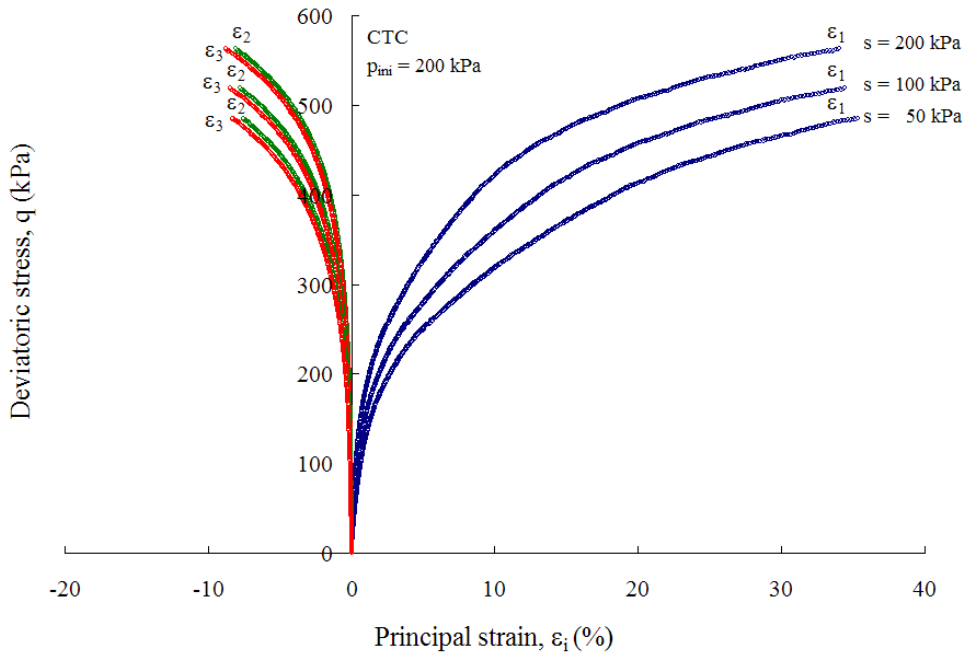

Figure 6.35 Experimental deviatoric stress – principal strain response CTC tests at s = 50, 100, and 200 kPa; and $_{pini}$ = 200 kPa on SP-SC soil.

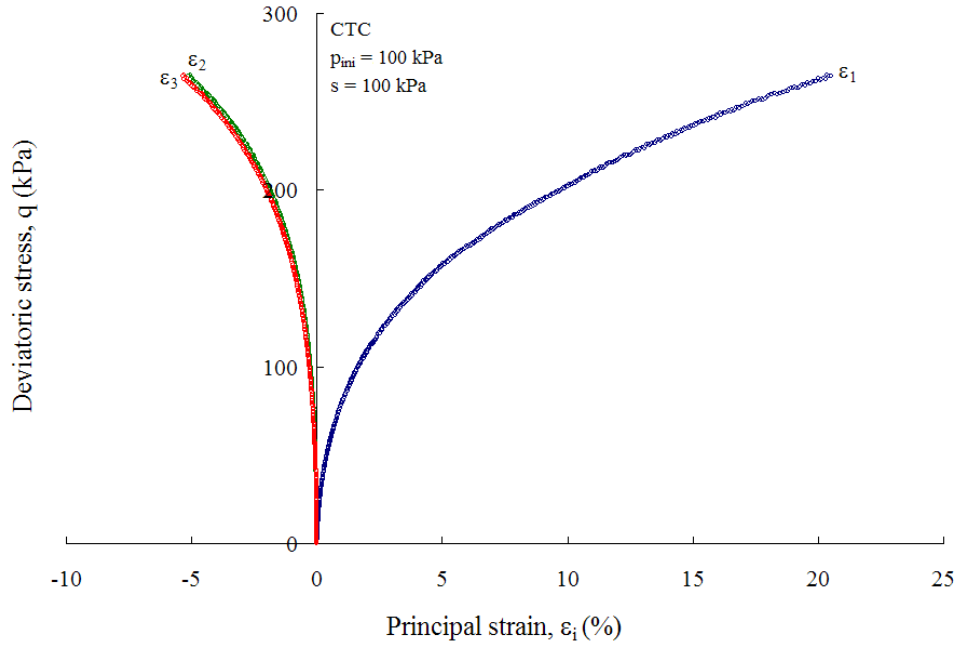

Figure 6.36 Experimental deviatoric stress – principal strain response CTC tests at s = 100 kPa and $_{pini}$ = 50 kPa on SP-SC soil.

Furthermore, A series of 6 drained suction-controlled triaxial compression (TC) tests, 3 triaxial extension (TE) tests, and 3 simple shear (SS) tests was conducted on compacted SP-SC soil specimens at constant matric suction, s = 50 kPa, s = 100 kPa, and s = 200 kPa, for initial net mean stress, pini = 100 kPa. The variation of principal strains, ε_1, ε_2, ε_3, with the net mean stress, p, for TC, TE, and SS stress paths is shown in Figure 6.37, Figure 6.38, and Figure 6.39, respectively. The effect of matric suction can be studied by observing the difference in response of the major principal strain, ε_1, intermediate principal strain, ε_2, and minor principal strain, ε_3. Results in Figure 6.34 to Figure 6.39 show a noticeable influence of matric suction on the shear resistance of the compacted SP-SC soil specimens.

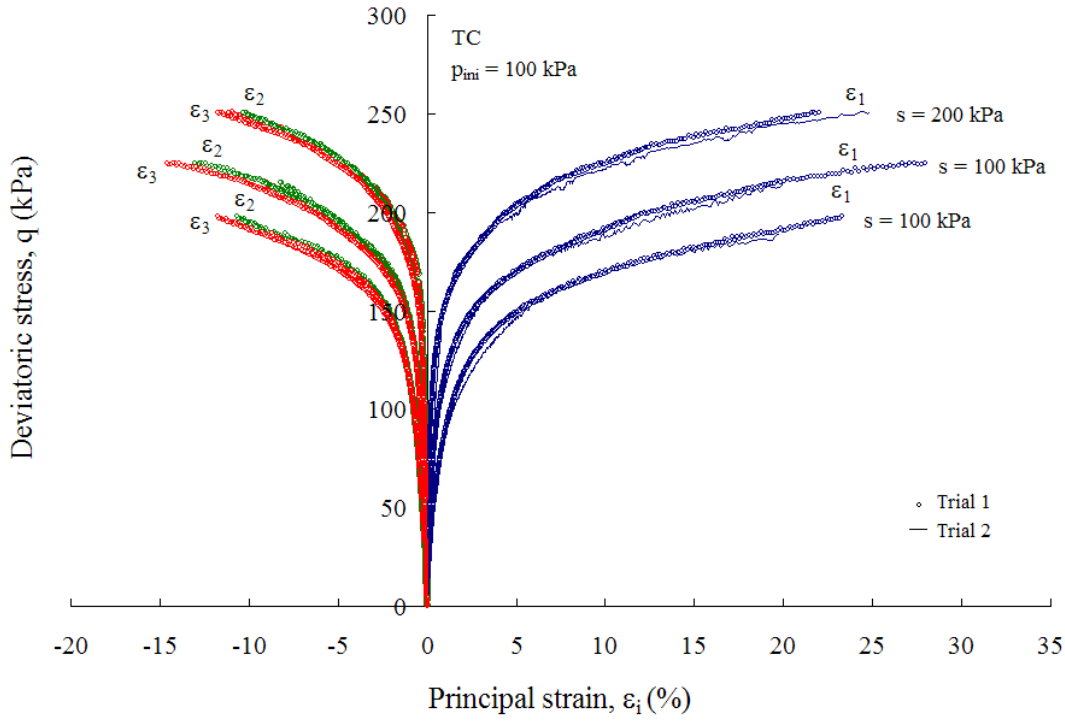

Figure 6.37 Experimental deviatoric stress – principal strain response TC tests at s = 50, 100, and 200 kPa; and $_{pini}$ = 100 kPa on SP-SC soil.

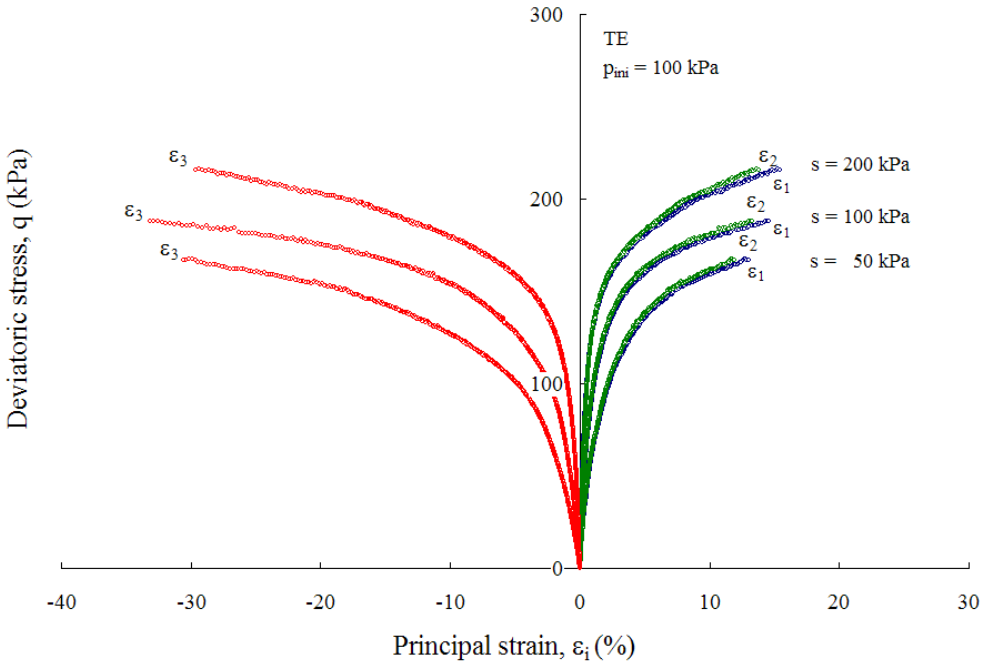

Figure 6.38 Experimental deviatoric stress – principal strain response TE tests at s = 50, 100, and 200 kPa; and $_{pini}$ = 100 kPa on SP-SC soil.

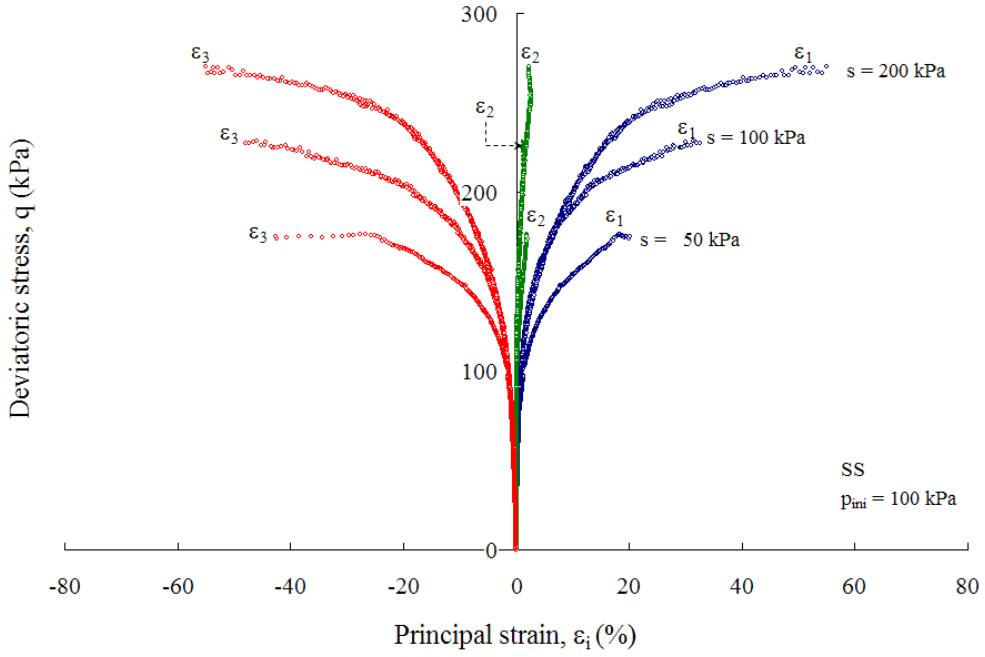

Figure 6.39 Experimental deviatoric stress – principal strain response SS tests at s = 50, 100, and 200 kPa; and $_{pini}$ = 100 kPa on SP-SC soil.

Next chapter describes the calibration process and numerical predictions obtained by using the Barcelona Basic Model (BBM), the Modified Barcelona Basic Model (MBBM), and the Oxford Model (OM), as well as the Refined Barcelona Basic Model (RBBM) proposed as result of the current research work.

CHAPTER 7

MODELS CALIBRATION AND NUMERICAL PREDICTIONS

7.1 Introduction

Critical state models have been used successfully in describing the features of the mechanical behaviour of fully saturated soils (Gens and Potts, 1988; Wood, 1990; Wood, 2004; Matsuoka and Sun, 2006; Yu, 2006). However, these models can not be used to describe partially saturated soil behaviour. To overcome this limitation, constitutive model developed for partially saturated soils introduce suction as an additional state variable (Alonso et al, 1990, Josa et al., 1992; Wheeler and Sivakumar, 1995; Wheeler et al, 2002; Georgiadis, 2003; Yu, 2006).

Several different constitutive models have been proposed to describe partially saturated soil behaviour. Among them, the earliest model and most widely used is the Barcelona Basic Model (BBM) proposed by Alonso et al. (1990). This model was later modified by Josa et al. (1992). Wheeler and Sivakumar (1995), proposed an elasto-plastic critical state constitutive framework for partially saturated soils similar to that proposed by Alonso et al. (1990). However, this framework assumes that all the model parameters are suction-dependent which is different from those assumed in Alonso et al. (1990).

All these constitutive models require information on model parameters, initial volumetric state and stress state conditions of the unsaturated soil. Suitable selection of

parameter values is important to ensure the adequate numerical prediction of the model. This chapter describes the procedure followed to determine the parameters on the three constitutive models mentioned above.

7.2 Calibration of Barcelona Basic Model

Although many constitutive models have been proposed for partially saturated soils, the earliest model and perhaps the most influential, and most widely used has been the critical state model proposed by Alonso et al. (1990). The application of the model requires the experimental determination of several parameters associated with the isotropic stress state, change in suction, and parameter associated with changes in shear stress and shear strength (Alonso et al., 1990).

7.2.1 Yield Functions

As proposed by Alonso et al. (1990), due to the effect of both pressure and suction in partially saturated soils, it is convenient to define two separate yield functions. The first yield function, which is an expansion of the elliptical yield surface in the p-q plane proposed by Roscoe and Burland (1968), is related to the plastic compression that can occur because of increase of stress or decrease of suction (see Figure 3.15)

$$f_1 = f(p,q,s) = q^2 - M^2(p + p_s)\left[p_o(s) - p\right] = 0 \qquad (7.1)$$

where

M = slope of the critical state line in the p-q plane

$p_s = ks$

k = constant

s = soil suction

The second yield function, known as the suction increase (SI) yield surface (see Figure 3.14), is related to the plastic compression that can occur with increase of suction, s

$$f_2 = f(s, s_o) = s - s_o = 0 \qquad (7.2)$$

where, s_o is the maximum value of suction experienced during the soil history.

7.2.2 Loading Collapse (LC) Yield Curve

The yield surface for a soil sample at a constant matric suction, s, may be described by an ellipse which will exhibit an isotropic consolidation stress, $p_o(s)$, which lies on the loading collapse (LC) yield curve. The LC yield curve in a p-s plane takes the following form (Alonso et al., 1990)

$$\frac{p_o(s)}{p^c} = \left[\frac{p_o(0)}{p^c}\right]^{\frac{\lambda(0)-\kappa}{\lambda(s)-\kappa}} \qquad (7.3)$$

where

$p_o(s)$ = generic yield stress which depend on matric suction, s

$p_o(0)$ = saturated preconsolidation stress

p^c = reference stress

$\lambda(0)$ = compressibility coefficient for the saturated state along virgin loading

$\lambda(s)$ = soil stiffness parameter which depend on matric suction, s

κ = compressibility coefficient along the elastic path.

Alonso et al. (1992) assumed that the elastic behavior inside the yield curve with variations in matric suction, s, is determined by the LC yield surface which is controlled

by the slope of the normal compression line, $\lambda(s)$. These assumptions led explicitly to the shape of the yield curve on expansion to higher values of $p_o(0)$. The soil stiffness parameter can be obtained from the following equation:

$$\lambda(s) = \lambda(0)[(1-r)e^{-\beta s} + r] \qquad (7.4)$$

where

r = constant related to the maximum stiffness of the soil, $r = \lambda(s \rightarrow \infty)/\lambda(0)$

β = parameter which control the rate of soil stiffness with matric suction.

7.2.3 Constitutive Behaviour Under Isotropic Loading

In order to determine the parameters in Equation (7.4) and Equation (7.3), eight SP-SC soil specimens were identically prepared to conduct equal number of hydrostatic compression tests. Figure 7.1 to Figure 7.4 show the variation of the specific volume, v = 1 + e, with the net mean pressure, p, during the ramped consolidation stage conducted on samples at constant matric suction, s = 50 kPa, s = 100 kPa, s = 200 kPa, and s = 350 kPa, respectively. A yield stress value, $p_o(s)$, has been identified in each figure. This values were determined based on the clear change in the slope of the curve showing the specific volume variation with net mean pressure, p. Hence, yield values of $p_o(50)$ = 75 kPa, $p_o(100)$ = 85 kPa, $p_o(200)$ = 100 kPa, $p_o(350)$ = 111 kPa, were identified for matric suction values, s = 50 kPa, s = 100 kPa, s = 200 kPa, s = 350 kPa, respectively. This behavior corroborate the existence of a initial loading collapse (LC) yield curve induced by the consolidation process experienced for each sample during the equalization stage. Figure 7.5 shows the initial LC yield curve obtained in this research work compared with previously reported LC yield curves.

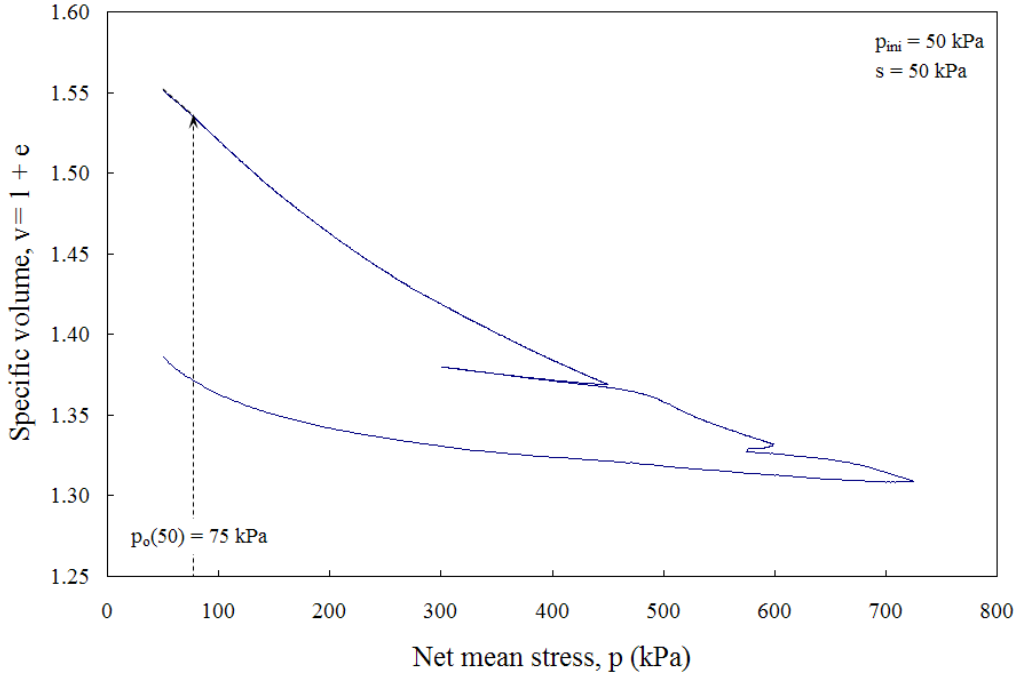

Figure 7.1 Variation of specific volume from HC test consucted on a SP-SC soil sample at matric suction, s = 50 kPa.

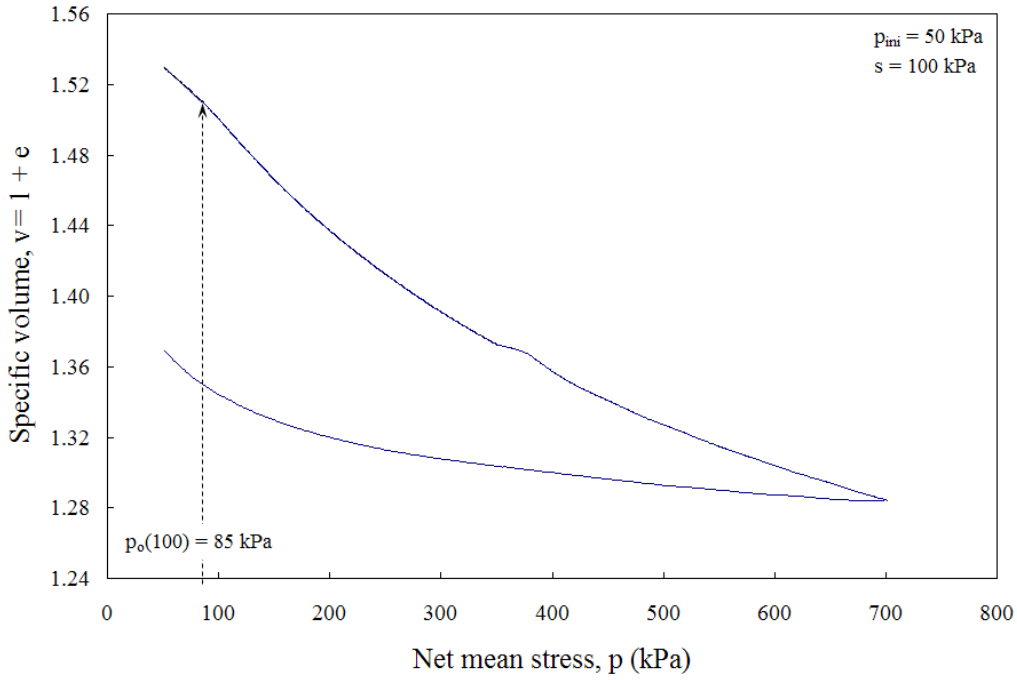

Figure 7.2 Variation of specific volume from HC tests conducted om a SP-SC soil sample at matric suction, s = 100 kPa.

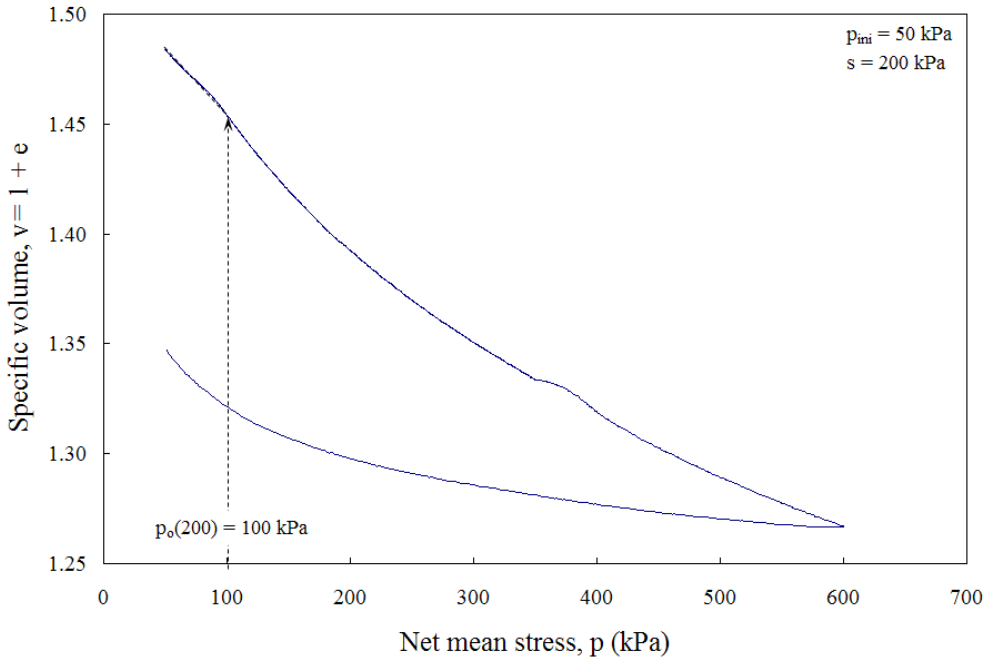

Figure 7.3 Variation of specific volume from HC test conducted on a SP-SC soil sample at matric suction, s = 200 kPa.

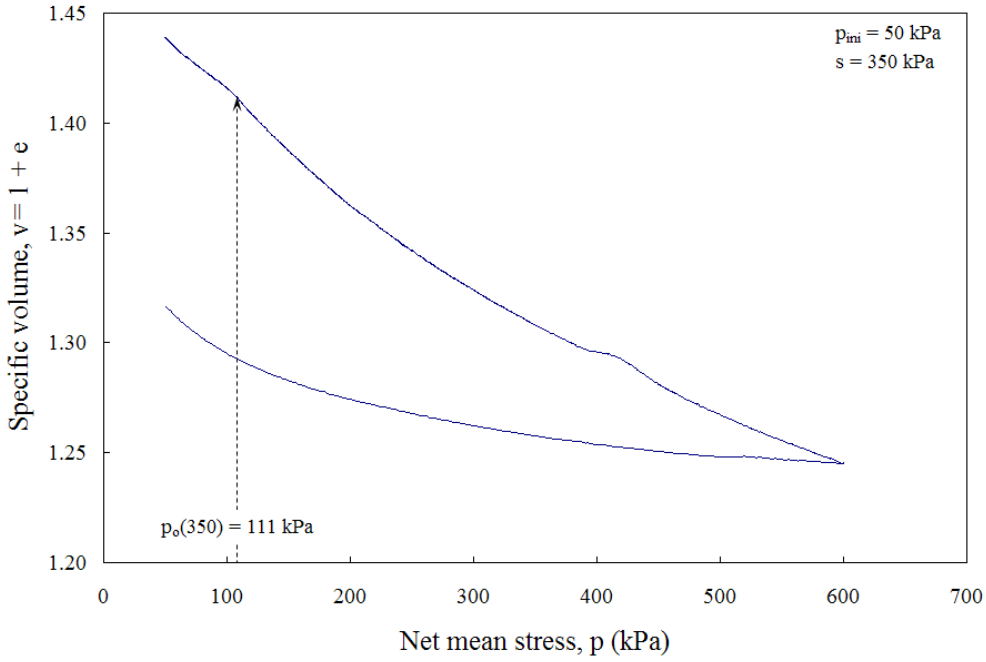

Figure 7.4 Variation of specific volume from HC test conducted on a SP-SC soil sample at matric suction, s = 350 kPa.

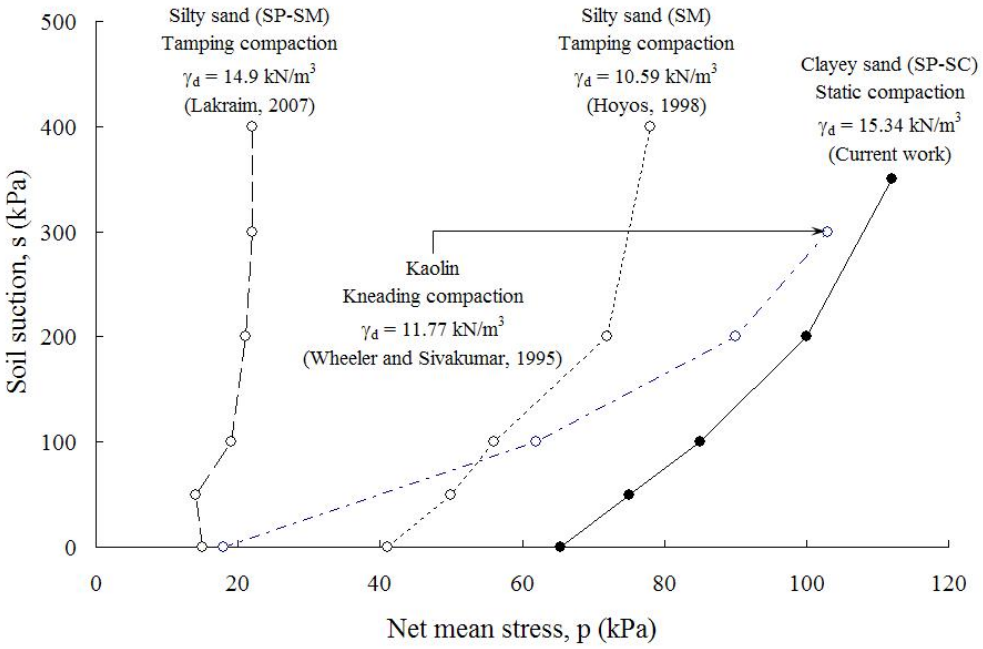

Figure 7.5 Initial experimental LC yield curve and previous experimental curves.

The experimental results presented in Figure 7.5 show that the static compaction method used in this study can be used to induce a compactive effort higher than that induced with tamping and kneading compaction. Special attention must be given to the volume of solid particles and water content used during compaction process, in order to obtain samples with approximately the same dry unit weight, γ_d.

On the other hand, Figure 7.6 shows the behavior of the soil under virgin state obtained for various values of matric suction, s. Inspection of this figure suggest a decrease in stiffness parameter, $\lambda(s)$, with increase in matric suction, which is consistent with the variation observed by Alonso et al. (1990). Best fit values of the stiffness parameter, $\lambda(s)$, are presented in Figure 7.7 through Figure 7.10.

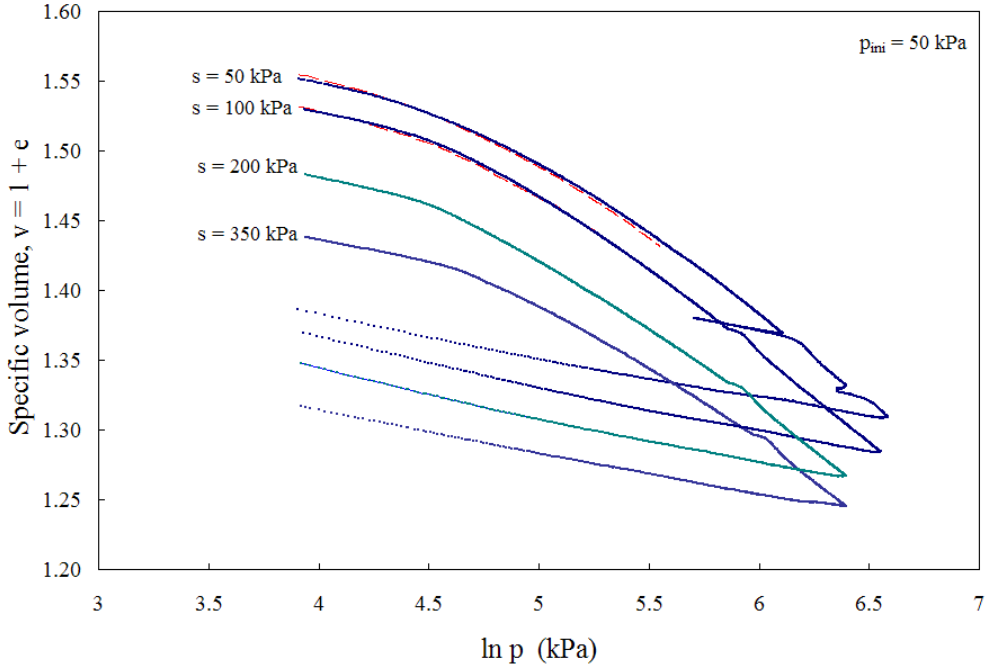

Figure 7.6 Variation of specific volume with ln(p) from HC tests conducted on SP-SC soil samples at various matric suctions, s.

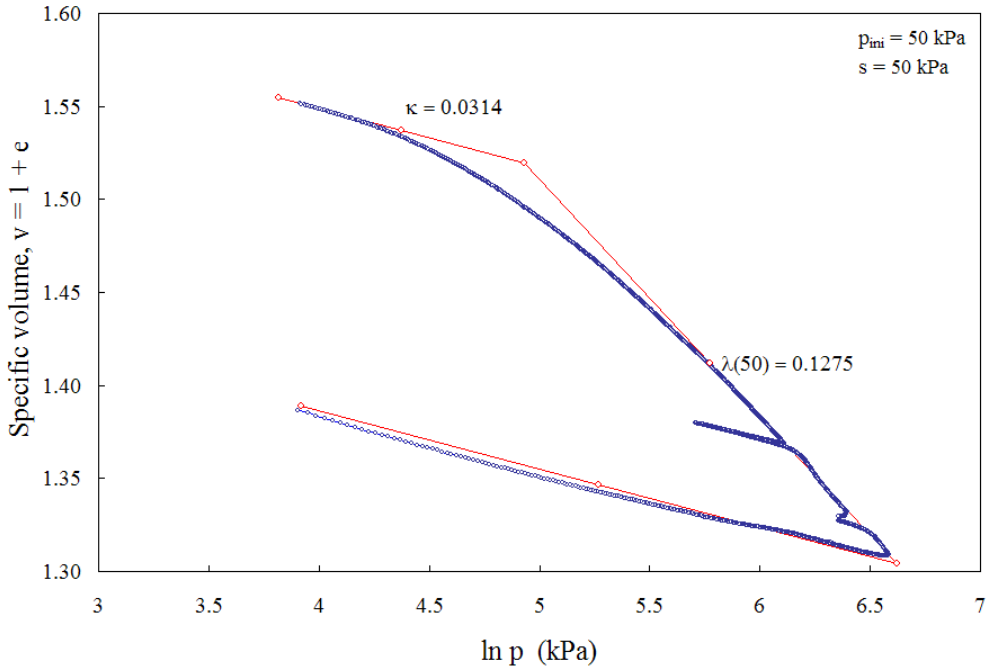

Figure 7.7 Variation of specific volume with ln(p) from HC test conducted on a SP-SC soil sample at matric suction, s = 50 kPa.

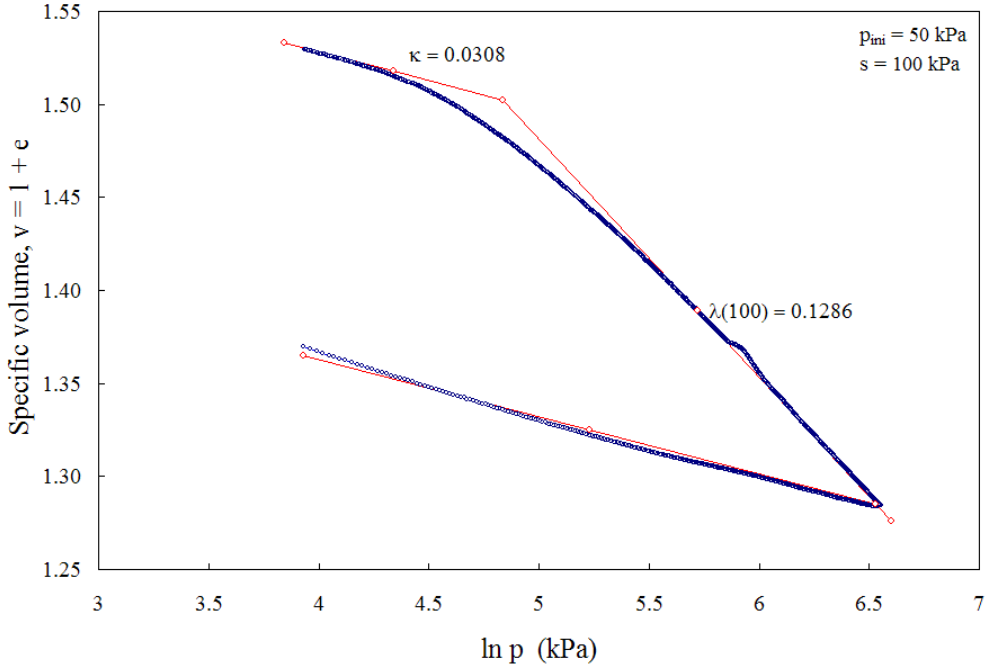

Figure 7.8 Variation of specific volume with ln(p) from HC test conducted on a SP-SC soil sample at matric suction, s = 100 kPa.

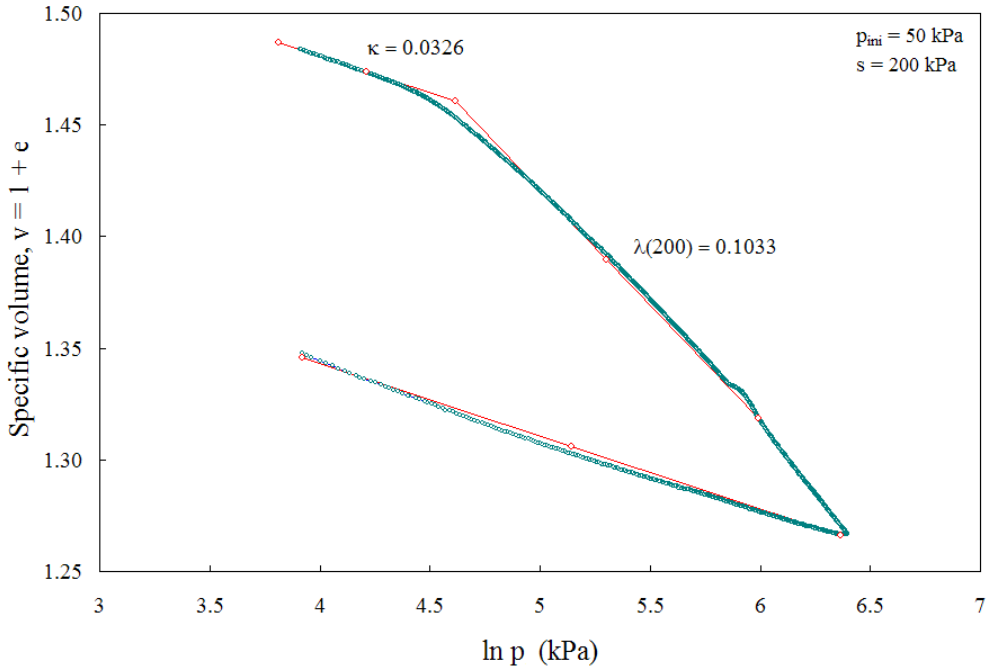

Figure 7.9 Variation of specific volume with ln(p) from HC test conducted on a SP-SC soil sample at matric suction, s = 200 kPa.

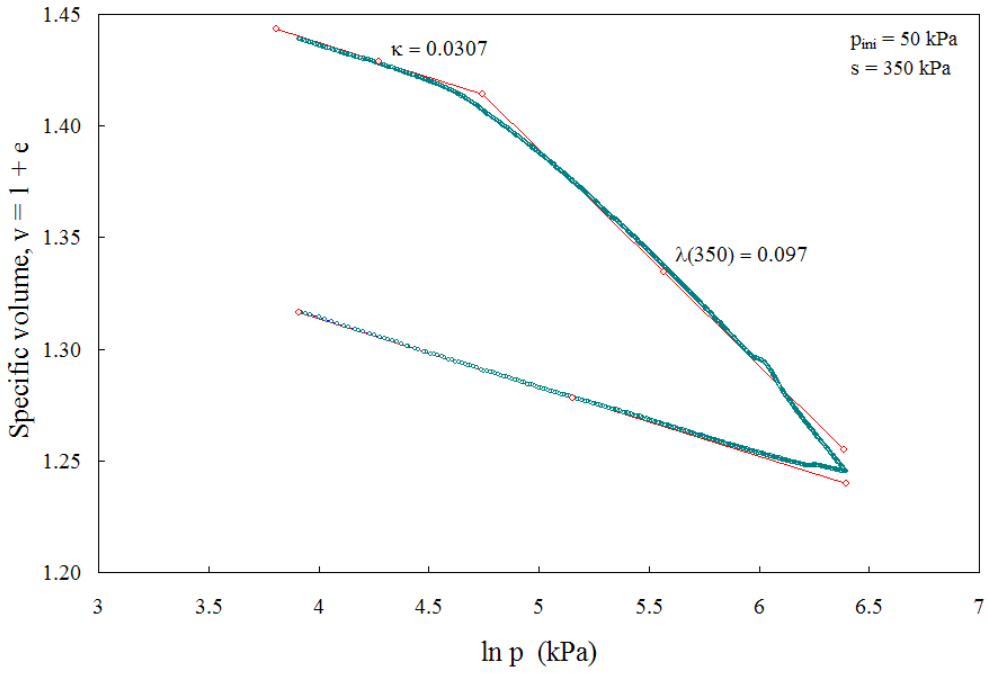

Figure 7.10 Variation of specific volume with ln(p) from HC test conducted on a SP-SC soil sample at matric suction, s = 350 kPa.

The slope of the normal consolidation line were found to be, $\lambda(50) = 0.1275$, $\lambda(100) = 0.1286$, $\lambda(200) = 0.1033$, and $\lambda(350) = 0.0970$, for matric suction values, s = 50 kPa, s = 100 kPa, s = 200 kPa, s = 350 kPa, respectively. In addition, best fit values of the compressibility coefficient, κ, were found to be $\kappa(50) = 0.0314$, $\kappa(100) = 0.0308$, $\kappa(200) = 0.0326$, and $\kappa(350) = 0.0307$, for matric suction values, s = 50 kPa, s = 100 kPa, s = 200 kPa, s = 350 kPa, respectively. Considering that no trend is observed in this parameter, an average value, $\kappa = 0.3138$ is assumed from the elastic portion of the specific volume, v = 1 + e, curve on the p – v plane.

7.2.4 Loading Collapse (LC) Yield Curve Parameters

The least squares method has been used to approximately solve the over-determined system proposed in Equation (7.4). Hence, using the experimental values

obtained for the slope of the isotropic normal consolidation line (ncl), $\lambda(50) = 0.1275$, $\lambda(100) = 0.1286$, $\lambda(200) = 0.1033$, and $\lambda(350) = 0.0970$, the best fit values of the parameters $\lambda(0)$, r, and β were found to be, $\lambda(0) = 0.146$, r = 0.649, and $\beta = 0.0089517$ kPa^{-1}. Figure 7.11 and Figure 7.12 show the experimental stiffness parameter data along with the predicted curves using Equation (7.3) for different values of r and β, respectively. Good agreement is observed between the experimental data and predicted values, which is confirmed by a correlation coefficient of 0.999.

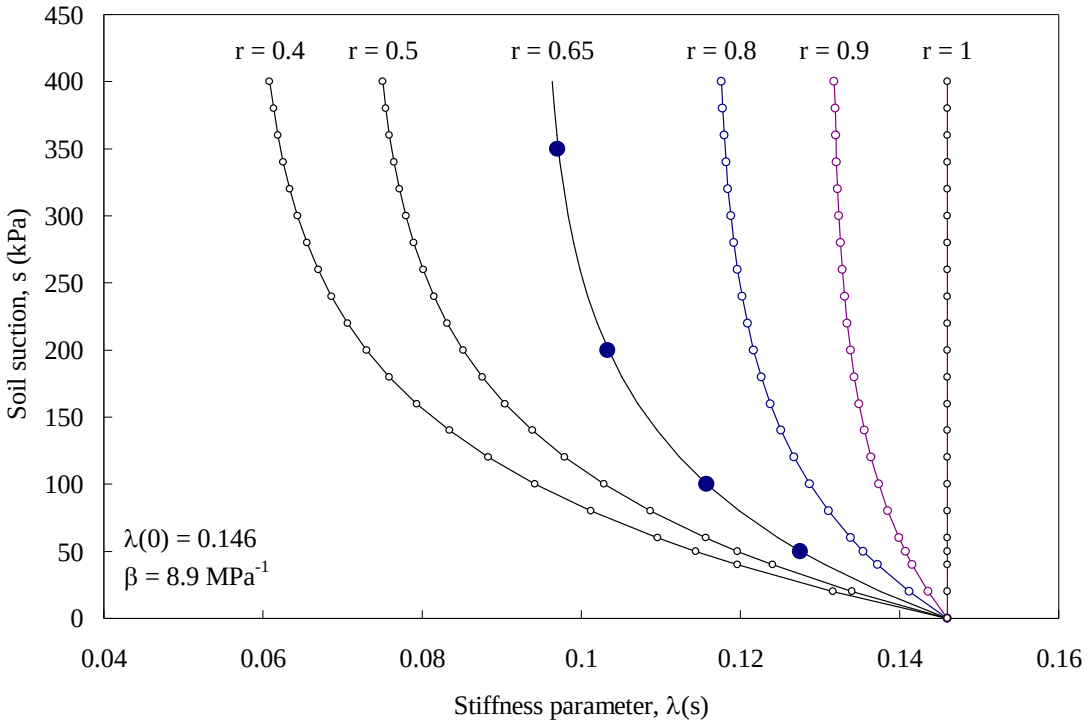

Figure 7.11 Experimental stiffness parameter, $\lambda(s)$, for a compacted SP-SC soil and predicted curves for various values of r using Equation (7.3).

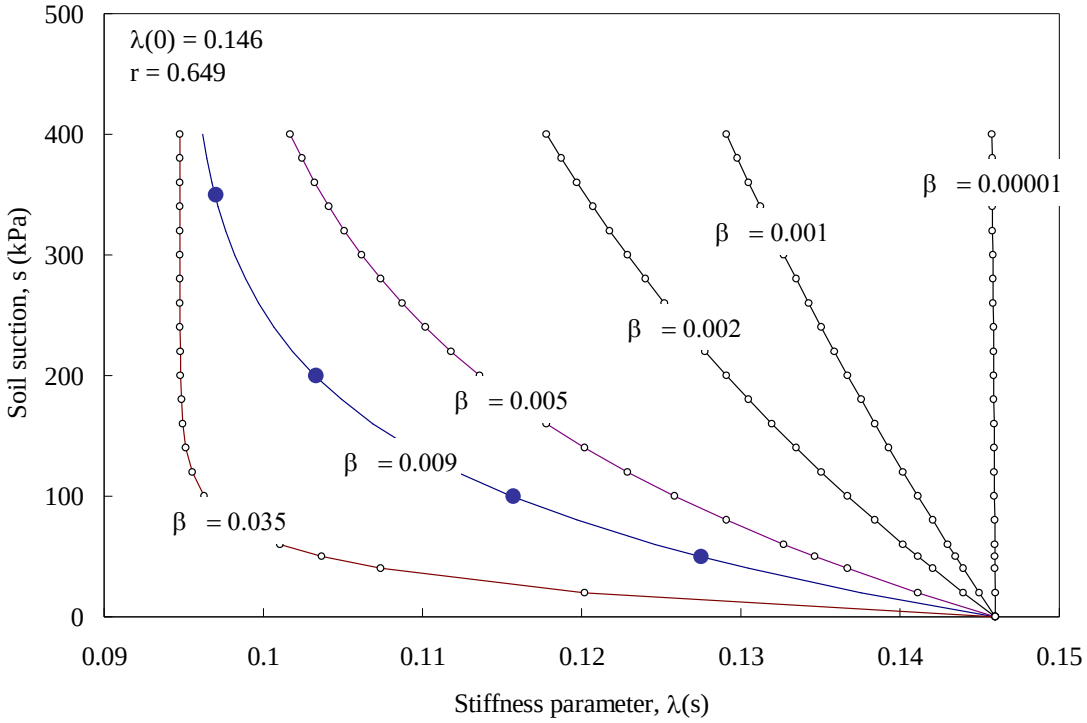

Figure 7.12 Experimental stiffness parameter, λ(s), for a compacted SP-SC soil and predicted curves for various values of β using Equation (7.3).

Similarly, experimental yield stress value, $p_o(50)$ = 75 kPa, $p_o(100)$ = 85 kPa, $p_o(200)$ = 100 kPa, $p_o(350)$ = 111 kPa, have been used to approximately solve the over-determined analytical expression proposed for the LC yield curve. The best fit equation obtained using least squares method to solve Equation (7.3) results in a reference stress, p^c = 31.91 kPa, and saturated preconsolidation stress, $p_o(0)$ = 65.44 kPa, for the SP-SC soil. Figure 7.13 shows the experimental yield stress value obtained for the compacted SP-SC soil specimens used in this study, along with the best fit curve and typical curves predicted by Equation (7.4) for different values of $p_o(0)$ with λ(0) = 0.146, r = 0.649, and β = 0.0089517 kPa^{-1}.

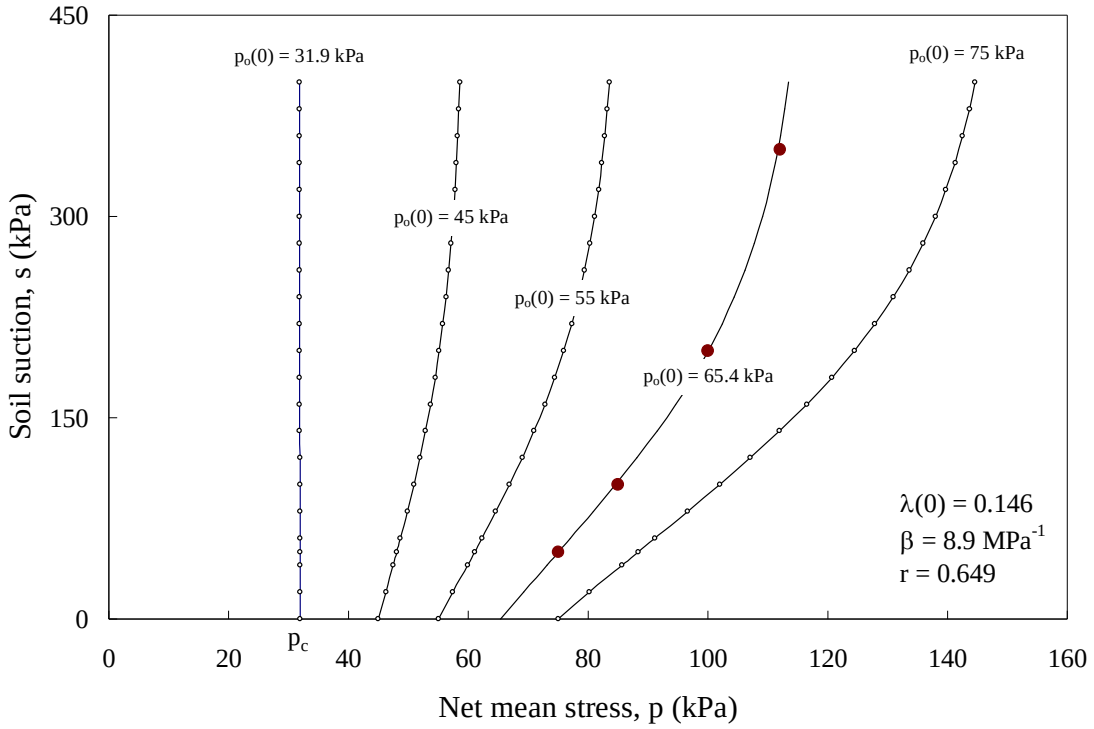

Figure 7.13 Experimental yield stress value along the best fit LC curve and typical curves predicted for different values of $p_o(0)$.

As proposed by Alonso et al. (1990), Figure 7.13 shows the existence of a net mean stress value, p^c, at which the soil may reach the saturated virgin state. In this case, changes in matric suction, s, has not resulting in plastic deformations.

The values of the parameters obtained for the calculation of the LC yield curve basis in the equations and calibration procedure proposed by Alonso et al (1990), are summarized in Table 7.1.

Table 7.1 Model parameters for calculation of LC yield curve proposed by Alonso et al. (1990)

Parameter	Description	Value
$\lambda(0)$	Compressibility coefficient for the saturated state	0.146
r	Constant related to the maximum stiffness of the soil	0.649
β	Parameter which control the rate of soil stiffness with s	895.17x 10^{-5} kPa^{-1}
p^c	Reference stress	31.922 kPa
$p_o(0)$	Saturated preconsolidation stress	65.44 kPa
κ	Compressibility coefficient along the elastic path	0.03138

7.2.5 Constitutive Behaviour Under Shear Loading

In order to study the behaviour of the partially saturated SP-SC soil under axisymmetric shear loading at various suction conditions, a series of 8 drained suction-controlled CTC tests and 6 drained suction-controlled TC tests were conducted on equal number of cubical SP-SC soil specimens. As described in section 7.2, the specimens were compacted using static compaction and the shear strength tests were conducted by applying an incremental load until the condition of failure was reached. Before starting the shear loading, the soil specimens were subjected to a specific net confining pressure (i.e. initial net mean normal stress, p_{ini}).

Under shear loading the specimens are failed by increasing the net axial pressure following a specific stress path. The difference between the major and minor normal stresses, commonly referred to as the deviatoric stress, q, is a measure of the shear stress developed in the soil. As the soil specimen is compressed, the deviatoric stress increases gradually until the maximum value is obtained. The applied deviatoric stress is usually plotted with respect to the axial strain, ε_1, or total shear strain, ε_q^{tot}. The experimental variation of the total shear strain, ε_q^{tot}, measured on SP-SC soil samples tested following

a drained CTC path is plotted against the deviatoric stress, q. The results from the fully drained CTC tests conducted at initial net mean stress, p_{ini} = 50 kPa, p_{ini} = 100 kPa, and p_{ini} = 200 kPa are presented in Figure 7.14, Figure 7.15, and Figure 7.16, respectively. Figure 7.17 shows the experimental variation of the total shear strain, ε_q^{tot}, with deviatoric stress, q, for the fully drained TC tests conducted at constant matric suction, s = 50 kPa, s = 100 kPa, and s = 200 kPa; and at initial net mean pressure, p_{ini} = 100 kPa. In addition, experimental variation of the total shear strain, ε_q^{tot}, plotted against the q/p ratio is presented in Figure 7.18 to Figure 7.21. Although it is not totally clear, inspection of the Figure 7.18 to Figure 7.21 suggest that critical state condition for all the samples has been achieved at ε_q^{tot} = 15%.

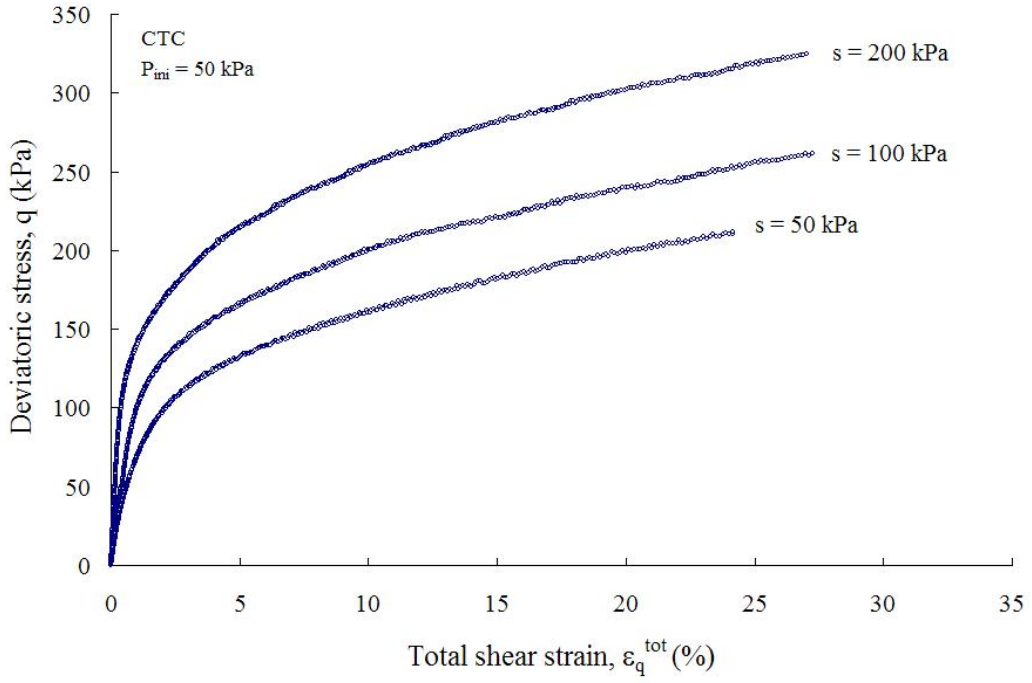

Figure 7.14 Experimental variation of the total shear strain, ε_q^{tot}, with deviatoric stress, q, from CTC tests at s = 50, 100, and 200 kPa, and p_{ini} = 50 kPa on SP-SC soil.

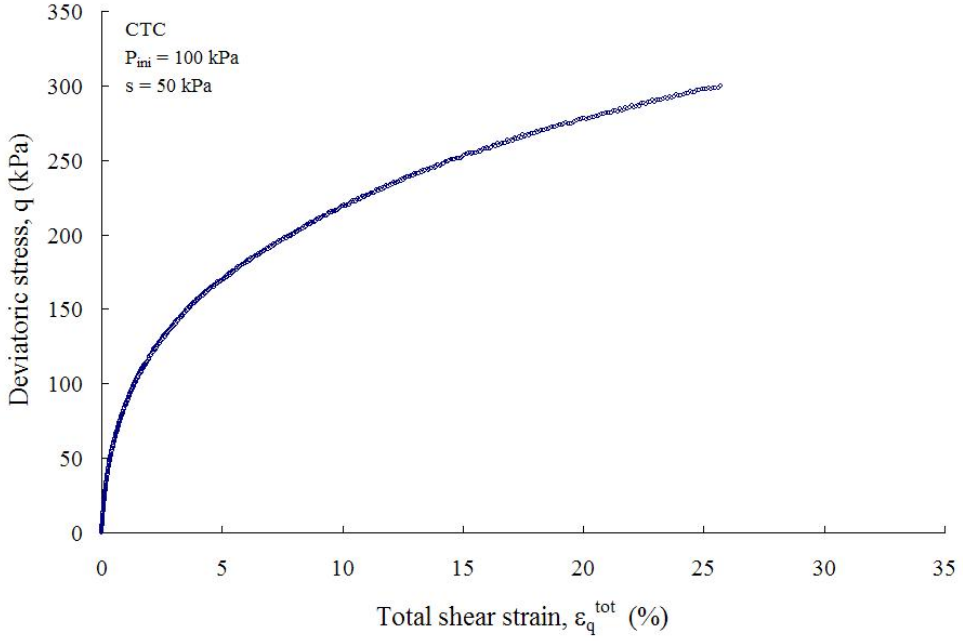

Figure 7.15 Experimental variation of the total shear strain, ε_q^{tot}, with deviatoric stress, q, from CTC test at s = 50 kPa and p_{ini} = 100 kPa on SP-SC soil..

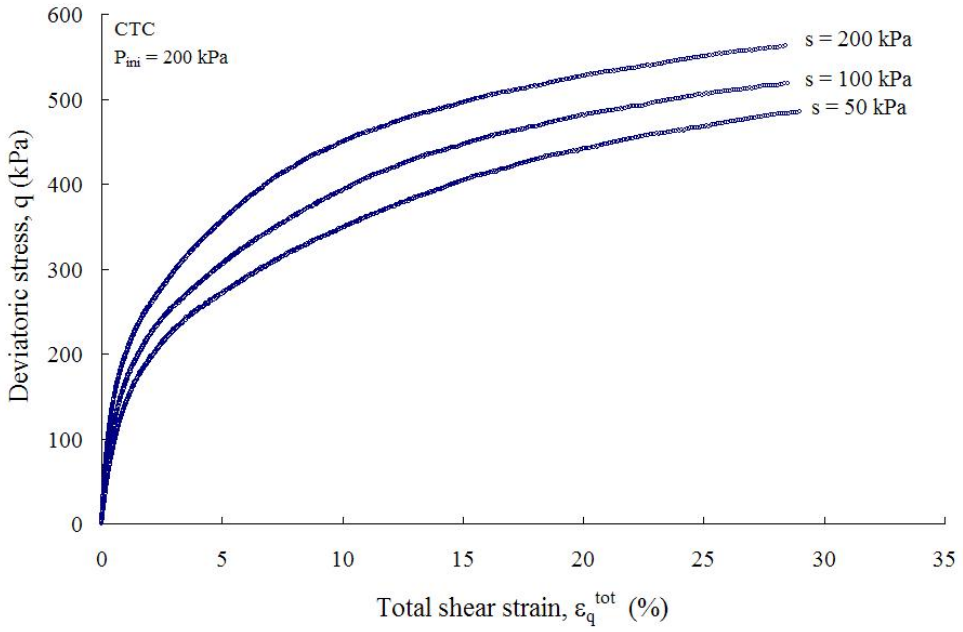

Figure 7.16 Experimental variation of the total shear strain, ε_q^{tot}, with deviatoric stress, q, from CTC tests at s = 50, 100, and 200 kPa, and p_{ini} = 200 kPa on SP-SC soil.

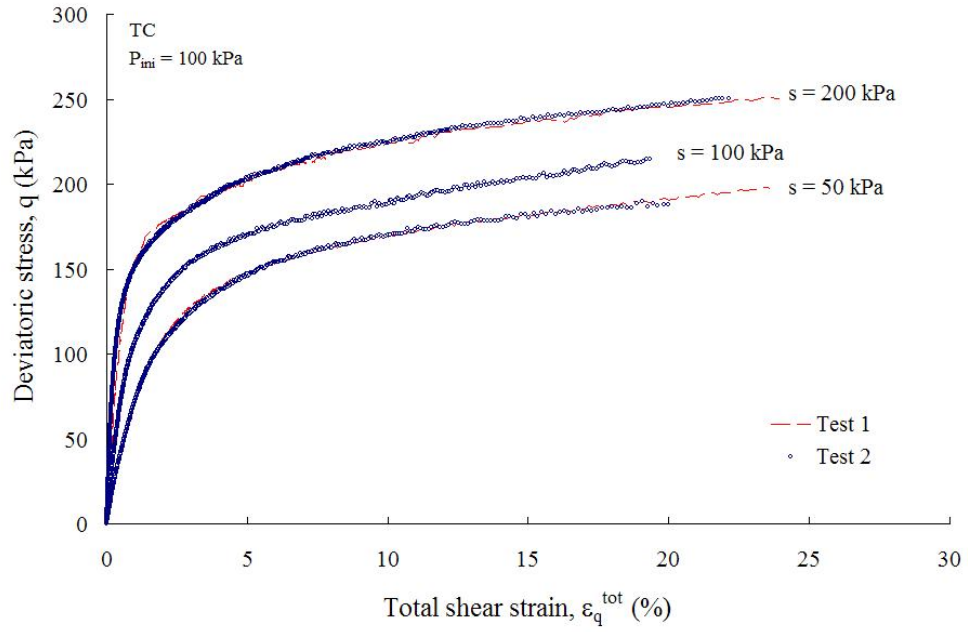

Figure 7.17 Experimental variation of the total shear strain, ε_q^{tot}, with deviatoric stress, q, from TC tests at s = 50, 100, and 200 kPa, and p_{ini} = 100 kPa on SP-SC soil.

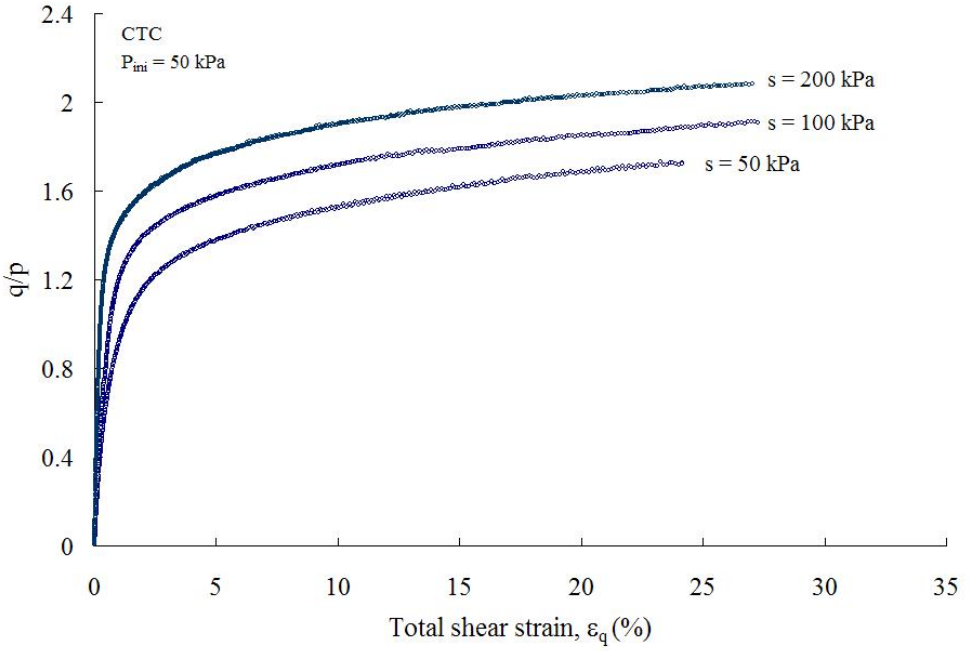

Figure 7.18 Experimental variation of the total shear strain, ε_q^{tot}, with q/p stress ratio, from CTC tests at at s = 50, 100, and 200 kPa, and p_{ini} = 50 kPa on SP-SC soil.

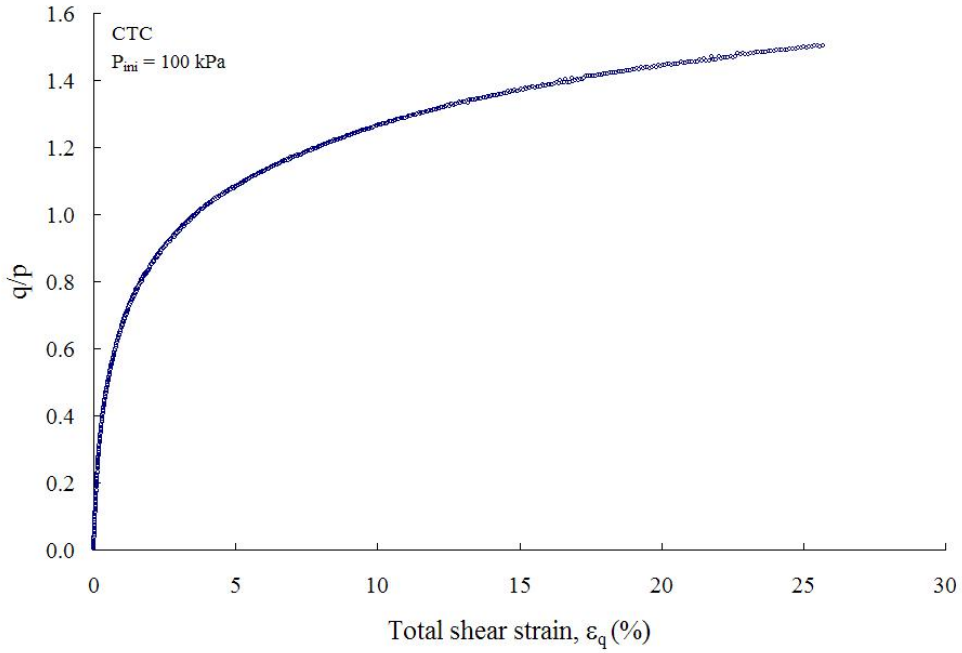

Figure 7.19 Experimental variation of the total shear strain, ε_q^{tot}, with q/p stress ratio, from CTC tests at s = 50 kPa, and p_{ini} = 100 kPa on SP-SC soil.

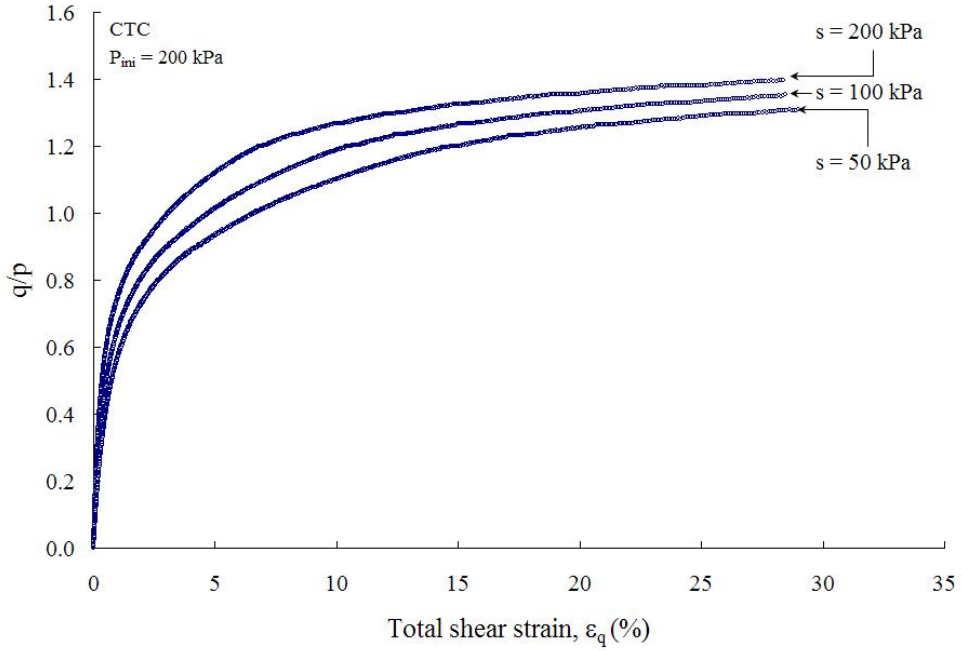

Figure 7.20 Experimental variation of the total shear strain, ε_q^{tot}, with q/p stress ratio, from CTC tests at s = 50, 100, and 200 kPa, and p_{ini} = 200 kPa on SP-SC soil.

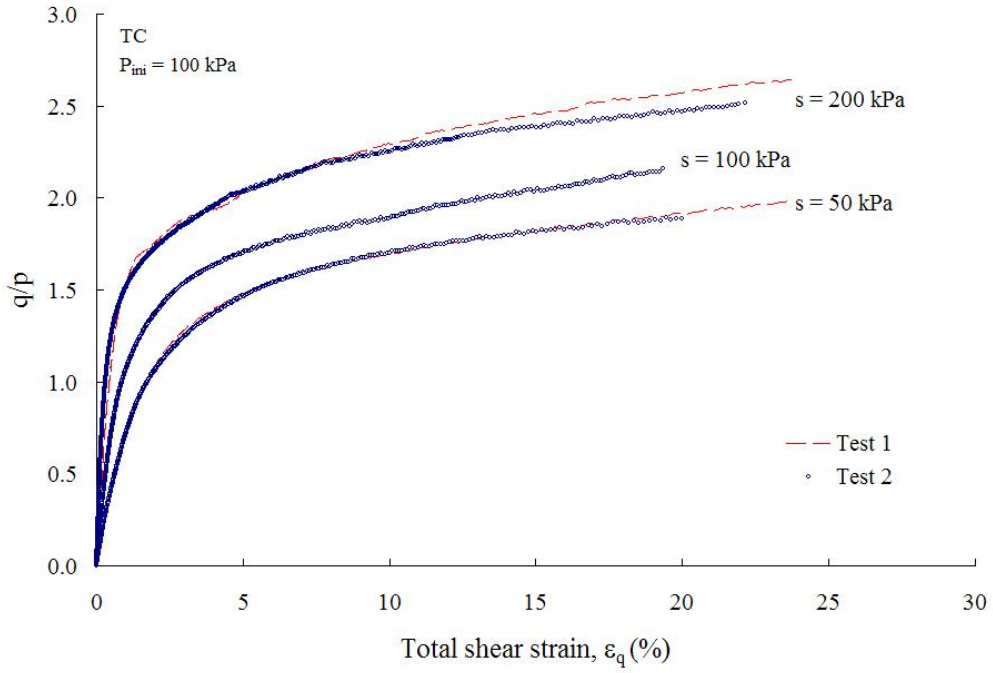

Figure 7.21 Experimental variation of the total shear strain, ε_q^{tot}, with q/p stress ratio, from TC tests at s = 50, 100, and 200 kPa, and p_{ini} = 100 kPa on SP-SC soil.

7.2.6 Critical State Condition

Under shearing, continued loading is associated with plastic hardening expansion of the yield surface and increase of stress ratio, until ultimately the effective stress state is at the top of the current yield surface plotted on the p-q stress plane (See Figure 3.15). There, the plastic strain increment vector is directed vertically parallel to the q axis, and a perfectly critical state is reached (Wood, 1990). Hence, when the stress state is at the top of the current yield locus, it is assumed that an indefinitely plastic shearing can occur without changes in volume or stress. In other words, plastic shearing could continue indefinitely without further expansion or contraction of the yield surface. This condition of perfect plasticity has become known as a critical state.

The locus of critical state in the p-q stress plane is the line joining the top of the yield surfaces (see Figure 3.8) and can be calculated by

$$q_{cs} = Mp_{cs} \tag{7.5}$$

The subscript cs denotes the critical state condition of the line described in Equation (7.5) which is called the critical state line (cls).

7.2.7 Model Parameters Associated With Shear Strength

Following the procedure recommended by Alonso et al. (1990), the results of the CTC and TC tests, presented in Figure 7.14 to Figure 7.17, are used to determine the slope of the critical state line, M, and the parameter that controls the increase in cohesion with suction, k. Hence, the plane described by Alonso et al. (1990) as:

$$q = Mp + Mks \tag{7.6}$$

has been adjusted to the p, q data obtained at critical state condition which was previously identified at approximately 15% of the total shear strain ε_q^{tot}.

The best fit values of the parameters M and k in the over-determined Equation (7.6) were found to be, M = 1.103 and k = 0.616. The experimental data along with the predicted values in the p-q plane are presented in Figure 7.22. Although a correlation coefficient of 0.904 has been obtained, no agreement is observed between the experimental and predicted values. This observation is corroborated by the results presented in Figure 7.23. Notice that the tests were conducted at different values of constant matric suction, s, and initial net mean pressure, p_{ini}. The range of stresses applied were, constantan matric suction, s = 50 kPa to 200 kPa, and initial net mean stress, p_{ini} = 50 kPa to 200 kPa.

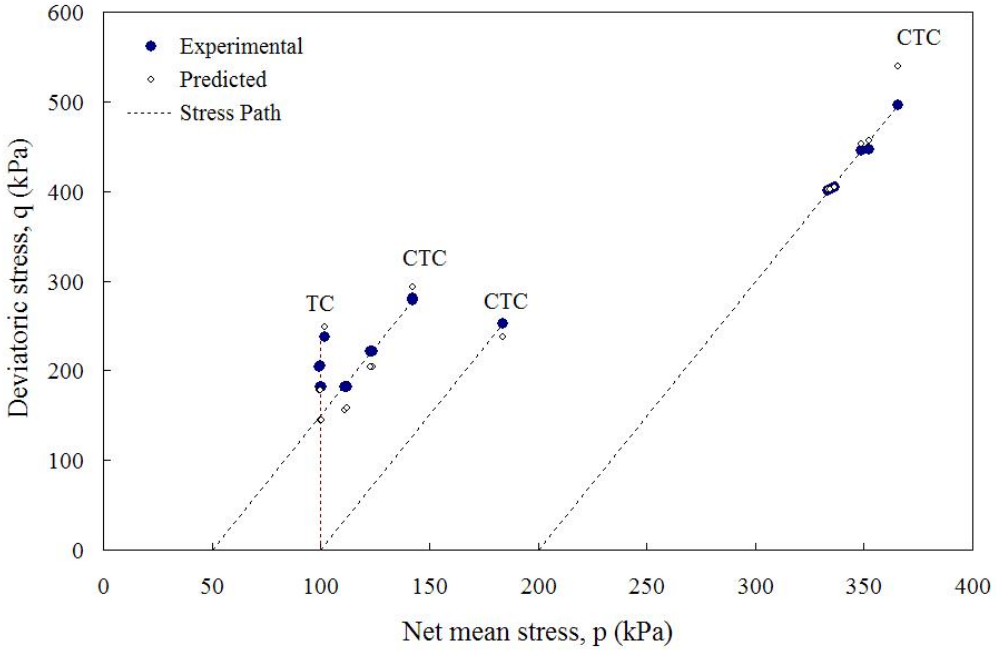

Figure 7.22 Experimental and predicted values of the deviatoric stress, q, at 15% of total shear strain, ε_q^{tot} plotted in the p-q plane.

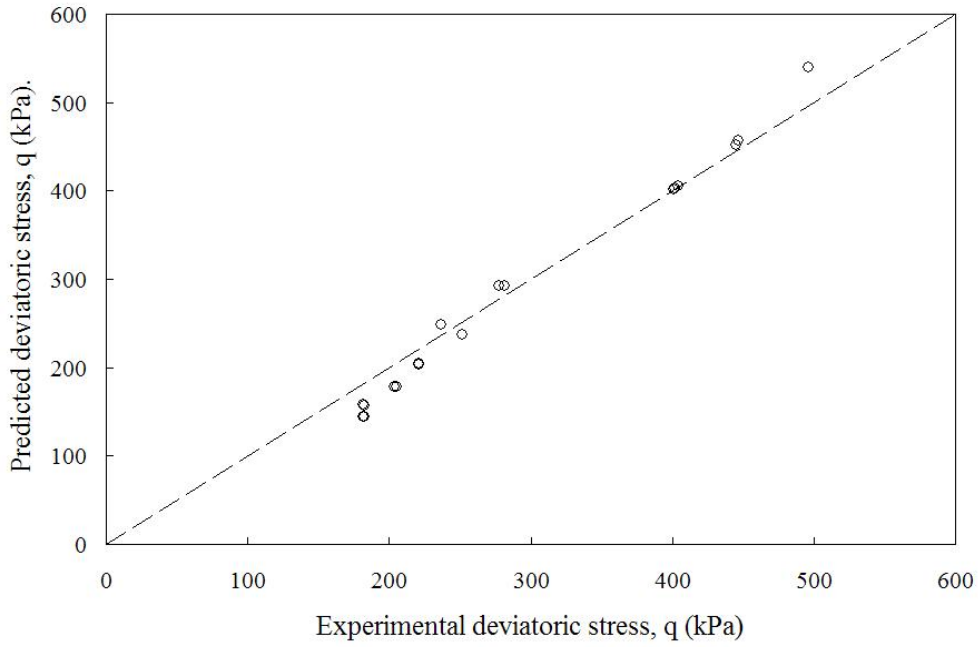

Figure 7.23 Comparison between experimental and predicted values of the deviatoric stress, q, at 15% of total shear strain, ε_q^{tot}.

7.2.8 Shear Modulus

As a consequence of the flow rule assumed in the Barcelona basic model, no shear strain occurs at the beginning of the shearing tests (Alonso et al., 1990). Hence, in a drained shear test where the axial stress is increased while the lateral is held constant, the initial linear section of the stress-strain curve might be interpreted as the elastic response of the soil to the imposed changes of the stress (Wood, 1990). Therefore, the shear modulus, G, was obtained using the initial linear section of the deviatoric stress-total shear strain curves. An average value of G = 5500 kPa has been obtained.

7.3 Implementation of Barcelona Basic Model

According to Alonso et al. (1990), the BBM is intended for partially saturated soils such as sand, silts, clayey sands, sandy clays and low plasticity clays which are slightly or moderately expansive. The representation of this model can be successfully followed and it will become relatively straightforward to make the changes that are required to incorporate more realistic features of soil response.

Following the Cam clay framework, the BBM assume that any change in net mean stress, p, produce recoverable changes in volume expressed by

$$d\varepsilon_{vp}^{e} = \frac{\kappa}{v}\frac{dp}{p} \qquad (7.7)$$

which Implies that there is a linear relation, in the compression plane, between specific volume, v, and logarithm of mean stress, p, for the elastic unloading reloading (url) of the soil. It is also assumed that any change in deviatoric stress, q, produces recoverable shear strain as per

$$d\varepsilon_d^e = \frac{\sqrt{2}}{3}\sqrt{(d\varepsilon_1^e - d\varepsilon_2^e)^2 + (d\varepsilon_2^e - d\varepsilon_3^e)^2 + (d\varepsilon_3^e - d\varepsilon_1^e)^2} = \frac{1}{3G}dq \qquad (7.8)$$

In addition, the model assumes that the yield locus in the p-q stress plane might be described by an elliptical shape according to Equation (7.1). Elliptical shape is simple and permits to use the ratio of major to minor axis as a shape parameter of the model. It is assumed that yield surface expand at constant shape, with the size been controlled by the yield stress, $p_o(s)$. The expansion of the yield surface and the hardening of the soil are linked with the normal compression of the soil. The relationship between specific volume, v = 1 + e, and logarithmic of net mean stress, p, during isotropic normal compression (iso-ncl) is assumed to be described by

$$v = N(s) - \lambda(s)\ln\frac{p}{p^c} \qquad (7.9)$$

The magnitude of the plastic volumetric strain is given by

$$d\varepsilon_{vp} = \frac{\lambda(s) - \kappa}{v}\frac{dp_o(s)}{p_o(s)} \qquad (7.10)$$

The BBM is completely general and is applicable for all stress paths that might be followed in the p-q stress plane. Hence, the use of the BBM model is most easily understood by deducing the strain increments of effective stress as shown in Figure 7.24 and Figure 7.25.

7.3.1 Conventional Triaxial Compression Test

In a drained suction-controlled conventional triaxial compression (CTC) test, the soil specimen is subjected to constant matric suction and initially surrounded by a constant confining net mean pressure, p_{ini}. Then, the specimen is failed by increasing

the net axial pressure, σ_1, while the lateral pressure is kept constant (i.e. $\Delta\sigma_3 = \Delta\sigma_2 =$ constant). The difference between major and minor normal stresses, commonly referred as deviatoric stress, q, can be calculated as

$$q = 3(p - p_{ini}) \tag{7.11}$$

Therefore, as shown in Figure 7.24, during a CTC test the deviatoric stress, q, is increased with a shear loading ratio, dq = 3dq, until the critical state line (CSL) is intercepted. At this point, unlimited plastic shear strain develop with no plastic volumetric strain and the loading can continue no further.

7.3.1.1 Numerical Predictions in p-q Stress Plane

In order to define the elliptical yield surface in the p-q stress plane, it is necessary to specify the failure state. Alonso et al. (1990) assumed that the critical state line (CSL) for non-zero suction can represent the increased strength induced by suction. Hence, maintaining the slope of the CSL for saturated conditions, M, the increase in suction will be represented by an increase in cohesion which is assumed to follow a linear relationship with suction given by

$$p = -ps = -ks \tag{7.12}$$

According to Equation (7.1), the major axis of the ellipse extents from –ps to $p_o(s)$ and the trajectory of the critical state line can be described by

$$q = M(p + p_s) \tag{7.13}$$

The preconsolidation or stress state history of the soil is a parameter that defines how the soil sample could respond under and additional applied load. As shown in Figure 7.24, soils samples whose initial net yield stress, $p_o(s) = p_o^A(s)$, exceed the initial

mean stress, p_{ini}, are said to be lightly overconsolidated. On the other hand, soil samples in which the initial mean stress, p_{ini}, applied during the equalization stage exceed the initial net yield stress, $p_o(s)$, as shown in Figure 7.25, are normally consolidated.

The size of the initial yield surface on lightly overconsolidated soils is controlled by the initial yield stress, $p_o^A(s)$, and p_s. In this case, the initial yield stress, which lies on the loading collapse (LC) yield curve, is calculated using Equation (7.3). The initial LC yield curve and increase in cohesion, p_s, is presented in Figure 7.26. Hence, for lightly overconsolidated soils, it is assumed that given an initial net stress state, p_{ini}, and the current yield surface defined by $p_o(s) = p_o^A(s)$, any loading increment lying on the initial yield surface do not generate plastic deformations and the yield surface does not change in size. On the other hand, if the increment of stress goes beyond of the initial yield surface, the yield surface expands to accommodate the new stress state, and plastic strain is expected to occurin the soil sample. As shown in Figure 7.24, the yield surface will expand to the next net yield stress, $p_o^B(s)$, which controls the size of the new yield surface in the p-q stress plane. The new LC yield curve can be calculated using Equation (7.3). Figure 7.27 show the expansion of the LC yield curve induced for the expansion of the yield surface. Explicit integration is used to compute the constitutive relations that simulate the incremental stress-strain behaviour of unsaturated soils under varying stress.

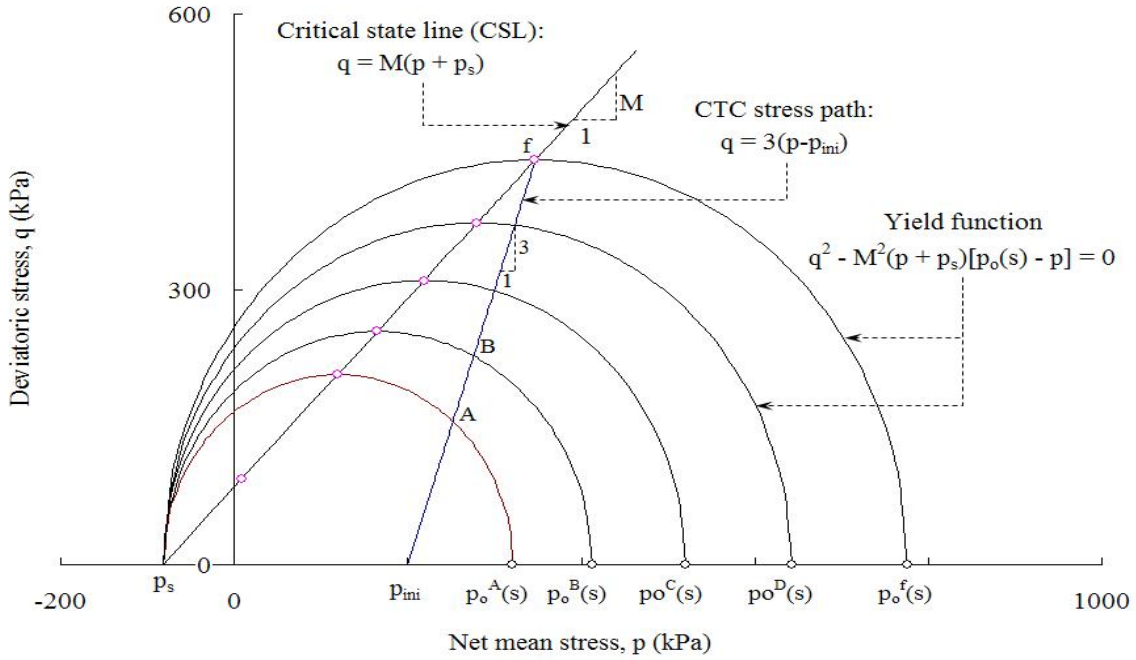

Figure 7.24 Stress increment expanding current yield surface for a drained CTC test conducted at constant matric suction, s, on a lightly overconsolidated soil.

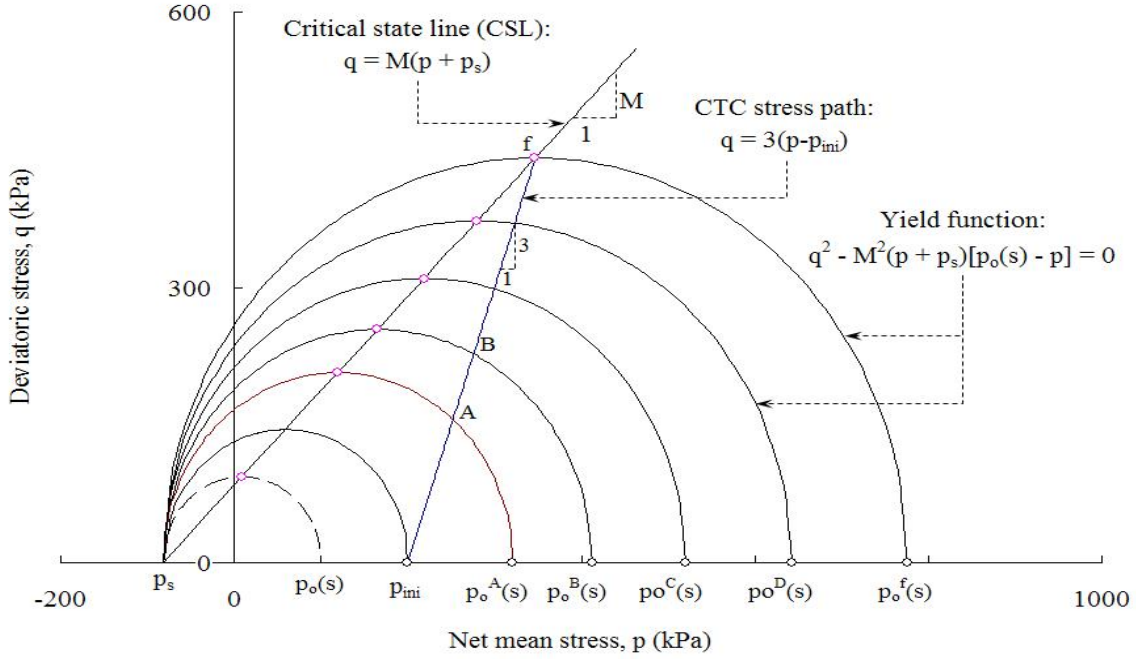

Figure 7.25 Stress increment expanding current yield surface for a drained CTC test performed at constant matric suction, s, on a normally consolidated soil.

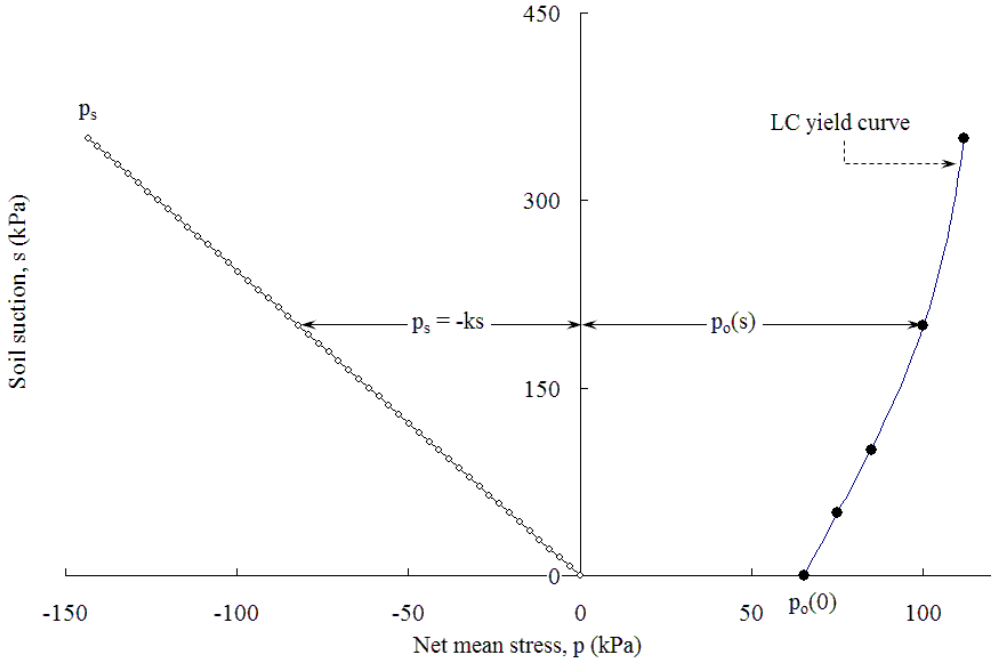

Figure 7.26 Experimental yield stress values and predicted LC yield curve in p-s stress plane, as proposed by Alonso et al. (1990).

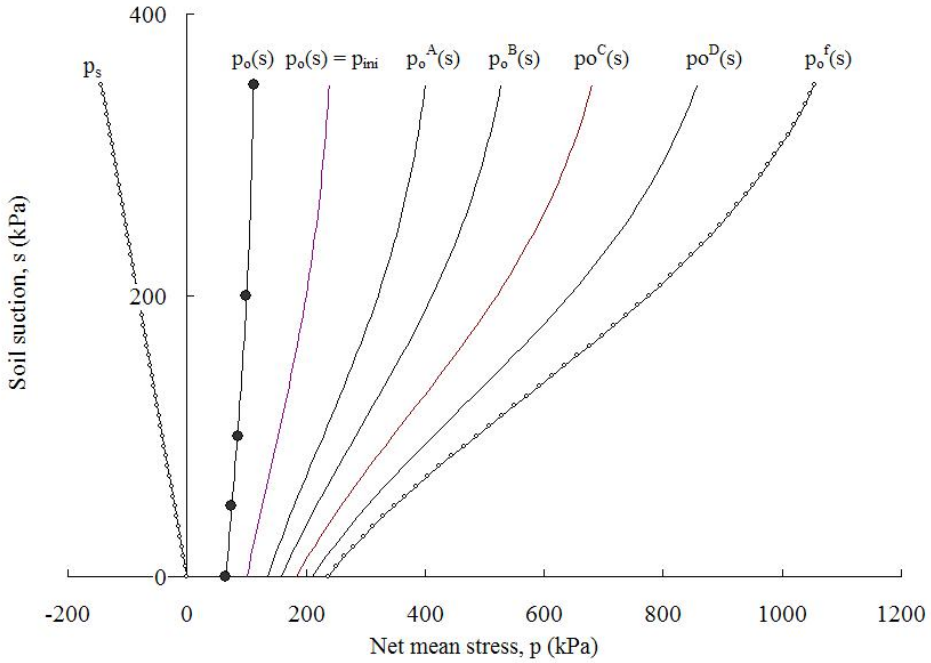

Figure 7.27 Stress increment expanding loading collapse (LC) yield surface in BBM.

The intersection of the CTC stress path and the initial yield surface can be calculated by replacing Equation (7.11) in Equation (7.1) and solving the following quadratic equation by p_A

$$ap_A^2 + bp_A + c = 0 \qquad (7.14)$$

where

$$a = 9 + M^2$$

$$b = [p_s - p_o(s)]M^2 - 18p_{ini}$$

$$c = 9p_{ini}^2 - p_s p_o(s)M^2$$

The deviatoric stress at point A, q_A, in Figure 7.24 can be calculated by replacing in Equation (7.11) the value of the net mean stress, p_A. This is the point used to start the loading increment when explicit integration is used to solve the model.

Different to lightly overconsolidated conditions, in normally consolidated samples the initial yield surface of the specimen has been exceeded during the equalization stage, and the yield surface at the beginning of the shearing stage is controlled by the initial yield stress, $p_o(s) = p_{ini}$, and p_s. As shown in Figure 7.25, the intersection of the CTC stress path and the initial yield surface coincide with the tip of the yield surface, at $q = 0$ and $p = p_{ini}$. This is exactly the point where the CTC stress path begins.

In both, lightly overconsolidated and normally consolidated cases, further loading increments result in expansion of yield surface. The size of the expanded yield surface will be determined by its intersection with the CTC stress path and the new

yield stress surface. The coordinates of the intersection point of the CTC stress path with the expanded yield surface are given by

$$q = q_A + dq \tag{7.15}$$

$$p = p_A + \frac{dq}{3} \tag{7.16}$$

From Equation (7.1), the yield stress generated by the new yield surface, $p_o^C(s)$, can be calculated by

$$p_o(s) = p + \frac{(q)^2}{M^2(p + p_s)} \tag{7.17}$$

Since there is a common point where the stress path intersects the yield function and the CSL, the stress state at failure, (p_f, q_f) can be obtained by combining Equation (7.12) and (8.13)

$$p_f = \frac{Mp_s + 3p_{ini}}{3 - M} \tag{7.18}$$

$$q_f = 3(p_f - p_{ini}) \tag{7.19}$$

From Equation (7.1), the yield stress at failure, $p_o^f(s)$, can be calculated by

$$p_o^f(s) = p_f + \frac{(q_f)^2}{M^2(p_f + p_s)} \tag{7.20}$$

Once the yield stress at failure, $p_o^f(s)$, has been determined it is possible to calculate the yield surface at failure by replacing, $p_o^f(s)$ and p_s in Equation (7.1) and solving either by deviatoric stress, q, or net mean stress, p.

It is clear that the size of the yield surface in not controlled by the yield stress, $p_o(s)$. Instead of that, the size of the ellipse is controlled by the increase in cohesion, p_s,

which has been assumed to follow a linear relationship with suction (Alonso et al., 1990). Thus, the LC yield curve which according to Alonso et al. (1990) “plays an important role in the development of the model” is used only to calculate the yield stress on the initial yield surface for lightly overconsolidated soils, but indeed has nothing to do with the calculation of the expanded yield surface and the stress state at failure.

Figure 7.28, Figure 7.29, and Figure 7.30 show the predicted yield surface and the experimental stress state at failure resulting from a drained conventional triaxial compression test conducted on different SP-SC soil specimens at constant matric suction, s = 50 kPa,100 kPa, and 200 kPa, respectively. The experimental values of the BBM parameters used to predict the soil response are summarized in Table 7.2.

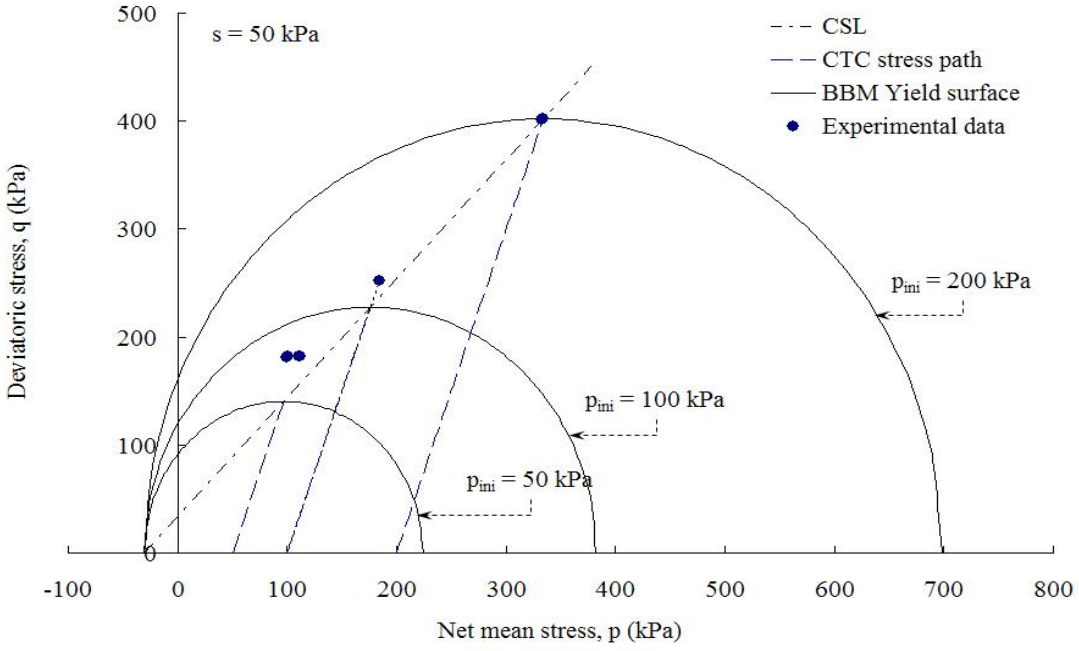

Figure 7.28 Predicted yield surface of BBM in drained CTC tests conducted at constant matric suction, s = 50 kPa and initial net mean stresses, p_{ini} = 50, 100, and 200 kPa.

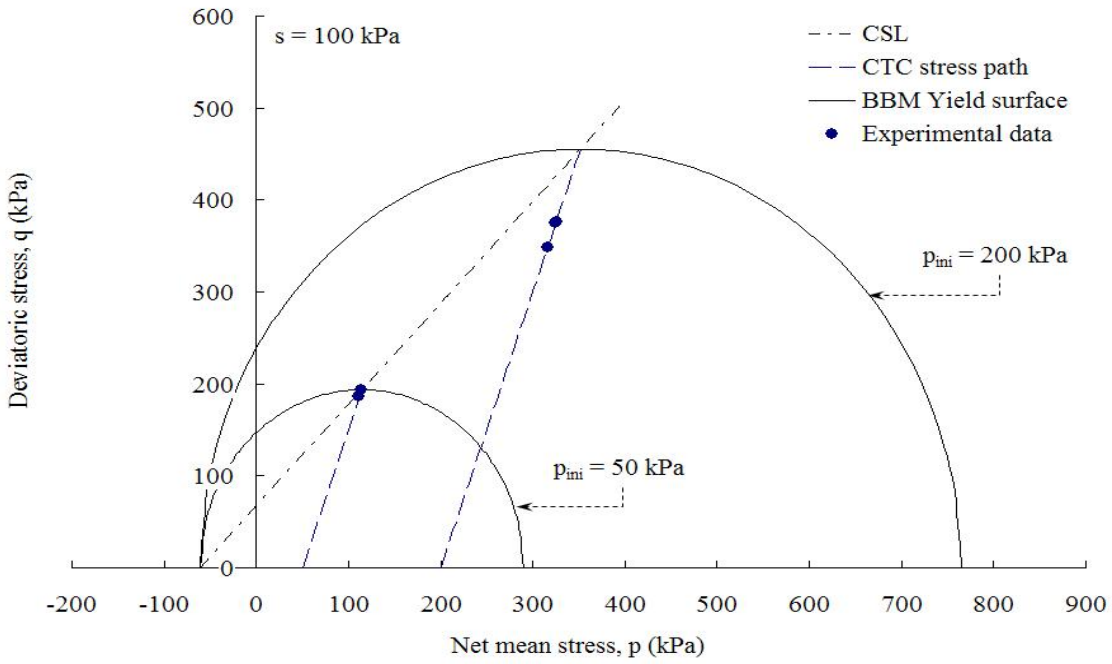

Figure 7.29 Predicted yield surface of BBM in drained CTC tests conducted at constant matric suction, s = 100 kPa and initial net mean stresses, p_{ini} = 50, 100, and 200 kPa.

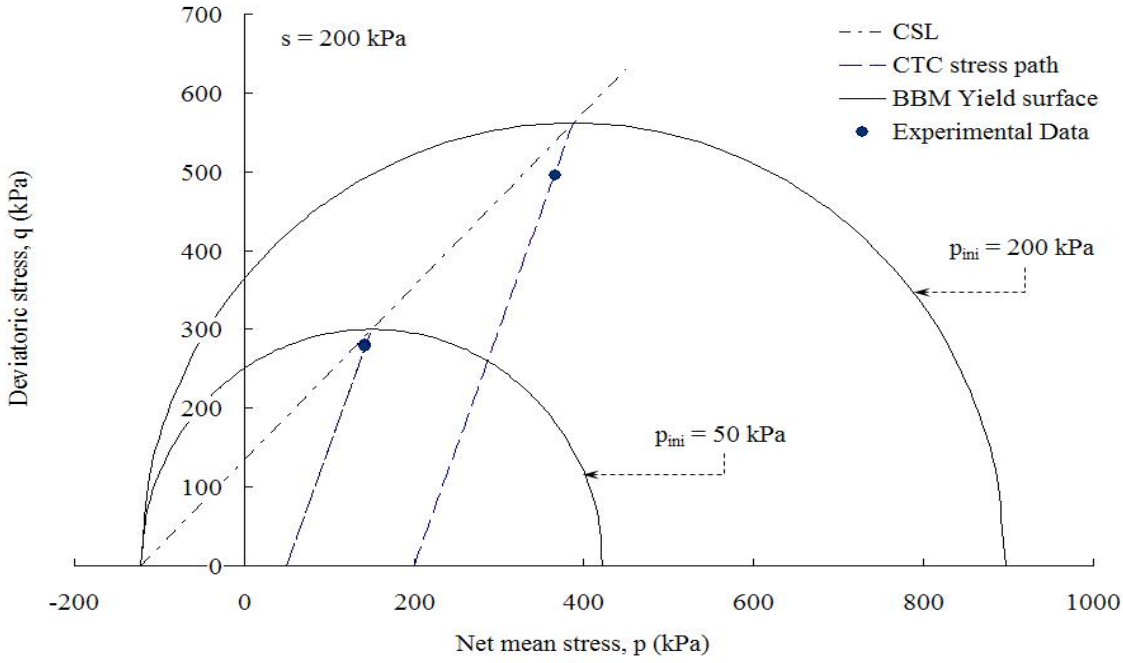

Figure 7.30 Predicted yield surface of BBM in drained CTC tests conducted at constant matric suction, s = 200 kPa and initial net mean stresses, p_{ini} = 50, 100, and 200 kPa.

Table 7.2 Experimental values of model parameters used to validate the BBM

Parameter	Description	Value
$\lambda(0)$	Compressibility coefficient for the saturated state	0.146
r	Constant related to the maximum stiffness of the soil	0.649
β	Parameter which control the rate of soil stiffness with s	895.17×10^{-5} kPa^{-1}
p^c	Reference stress	31.922 kPa
$p_o(0)$	Saturated preconsolidation stress	65.44 kPa
κ	Compressibility coefficient along the elastic path	0.03138
M	Slope of the critical state line (CSL)	1.103
k	Parameter describing the increase in cohesion with s	0.616
G	Elastic shear modulus	5500 kPa

Although the BBM is able to adequately predict the critical stress state at failure for some of the experimental conditions, in general, no agreement is observed between the experimental and predicted values in Figure 7.28, Figure 7.29, Figure 7.30

7.3.1.2 Numerical Predictions in the Normal Compression Plane

So far, the progress of the drained CTC test has been described with reference only to the p-q stress plane. As mentioned before, a yield surface describes the boundary of the region where any state stress combination may generate pure elastic or recoverable deformations. Hence, following the drained CTC stress path, at each point A, B, C, …, f, where a new yield surface has been identified is possible to calculate the specific volume, v = 1 + e, corresponding to the unloading-reloading line (url) in the p-v compression plane. As shown in Figure 7.31 and Figure 7.32, each new yield surface expands up to the corresponding net yield stress, $p_o^A(s)$, $p_o^B(s)$, $p_o^C(s)$, …, $p_o^f(s)$, that can be associated with the respective elastic unloading-reloading line, url_A, url_B, url_C,.., url_f, ending on its respective net mean stress, $p_o^A(s)$, $p_o^B(s)$, $p_o^C(s)$, …, $p_o^f(s)$, on the isotropic normal compression line (ncl).

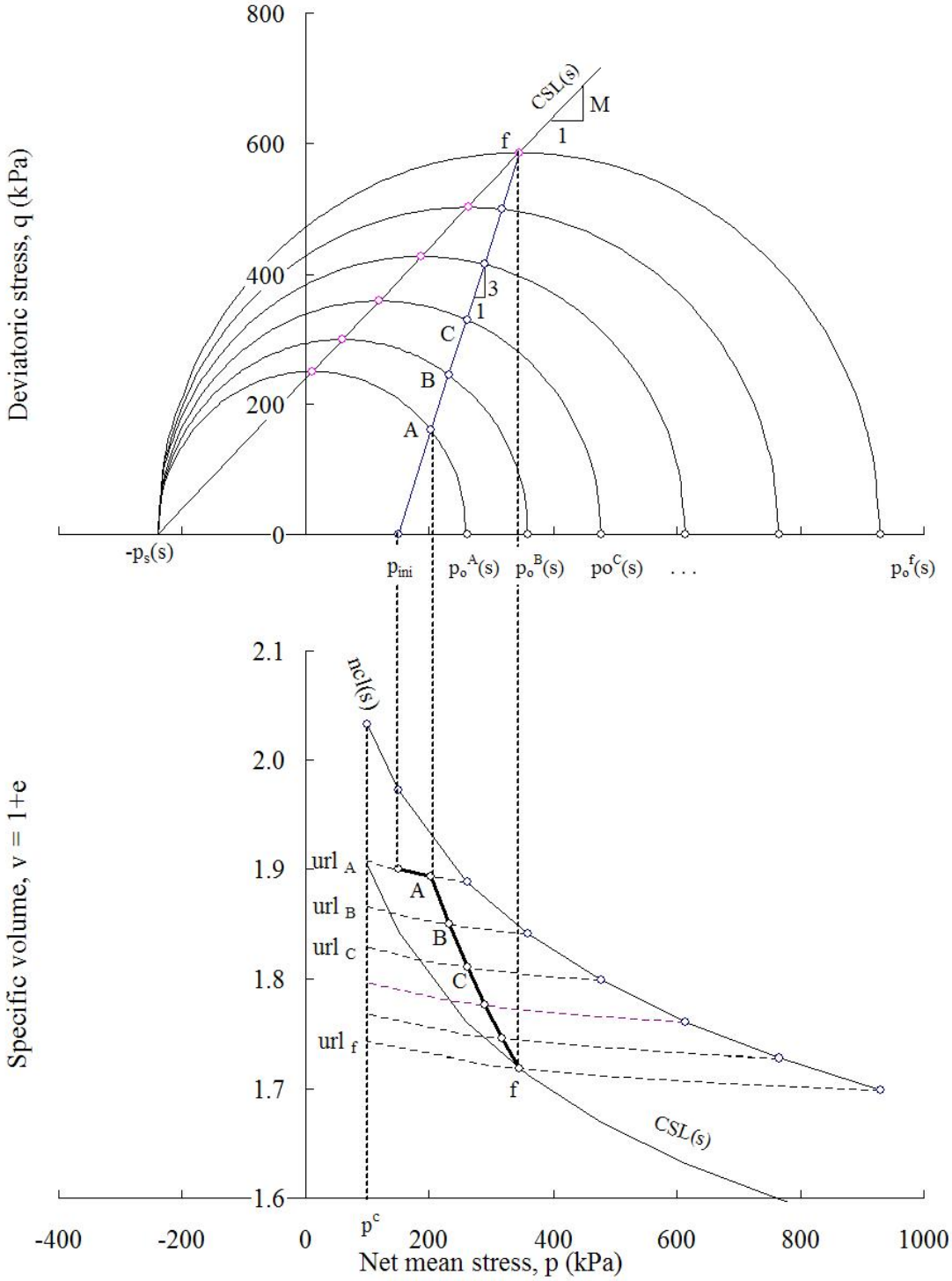

Figure 7.31 Successive yield surfaces and the associated unloading-reloading lines (url) resulting from a CTC test conducted on a lightly overconsolidated soil.

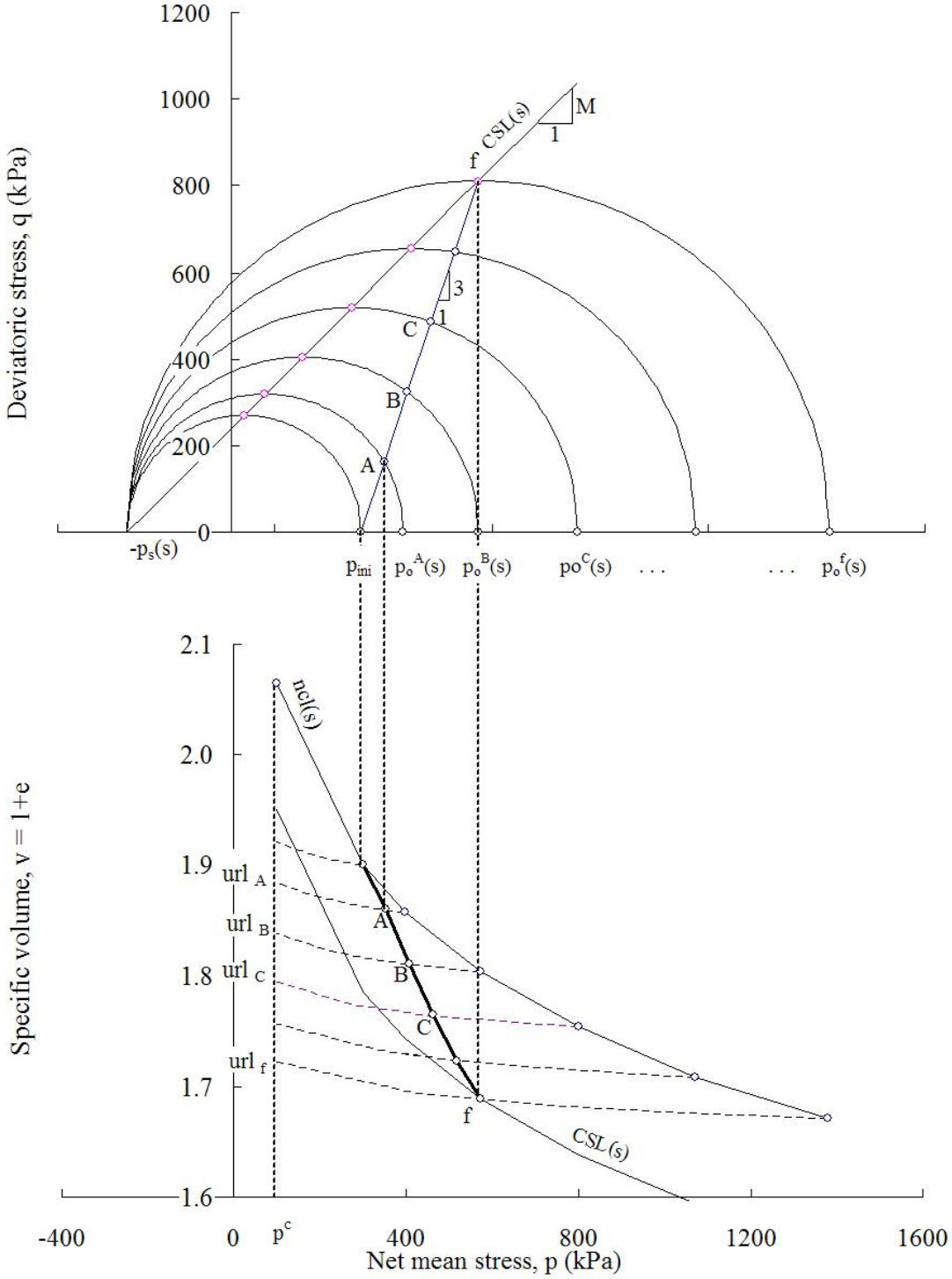

Figure 7.32 Successive yield surfaces and the associated unloading-reloading lines (url) resulting from a CTC test conducted on a normally consolidated soil.

As shown in Figure 7.31, for a drained CTC test performed on a lightly overconsolidated soil sample at initial mean pressure, p_{ini}, and constant matric suction, s, the initial specific volume, v_{ini}, lays on the url defined by the yield surface associated with the initial net yield stress, $p_o^A(s)$. Therefore, the drain compression experienced by the soil from point p_{ini} to point A represent changes in stress laying inside the initial yield surface and consequently generate pure elastic deformations. The projection of points, p_{ini} and point A lies on the unloading-reloading line url_A associated with the initial net yield stress $p_o^A(s)$. The specific volume v_A defined for the projection of point A on the unloading reloading line url_A, can be calculated by

$$v_A = v_{ini} - k \ln\left(\frac{p_A}{p_{ini}}\right) \tag{7.21}$$

Similarly, the projection of point $p_o^A(s)$ which lies on the intersection of the unloading reloading line, url_A, and the isotropic normal compression line (ncl) can be calculated by

$$v_o^A = v_{ini} - \kappa \ln\left(\frac{p_0^A(s)}{p_{ini}}\right) \tag{7.22}$$

Once the specific volume on the isotropic-ncl, v_o^A, corresponding to the initial net yield stress $p_o^A(s)$ has been calculated, it is possible to calculate the specific volume on the isotropic normal compression line (ncl) associated to any net yield stress, $p_o(s)$, (i.e. $p_o^B(s)$, $p_o^C(s)$, …, $p_o^f(s)$ in Figure 7.31).

$$v_o = v_o^B - \lambda(s) \ln\left(\frac{p_o(s)}{p_o^A}\right) \tag{7.23}$$

This specific volume, v_o, also corresponds to the ending of the respective elastic unloading-reloading line (i.e. url_B, url_C,.., url_f in Figure 7.31). Therefore, the specific volume associated with the point B on the stress path can be calculated by

$$v_B = v_o^B + \kappa \ln\left(\frac{p_0^B(s)}{p_B}\right) \tag{7.24}$$

Equation (7.21) can be used to calculate the specific volume associated to any point on the drained CTC stress path by replacing the corresponding net mean stress, p, net yield stress, $p_o(s)$, and the associated specific volume on the isotropic normal compression line (ncl), v_o.

The same procedure can be used to calculate the specific volume for a drained CTC test performed on a normally consolidated soil sample at initial mean pressure, p_{ini}, and constant matric suction, s. The isotropic normal compression (iso-ncl) has been calculated using Equation (7.10) and the parameters presented in Table 7.1. The predicted specific volume for four different values of matric suction, s = 50 kPa, s = 100 kPa, s = 200 kPa, and s = 350 kPa and initial net mean stress, p_{ini} = 50 kPa, have been plotted against net mean stress results in Figure 7.33 and Figure 7.34.

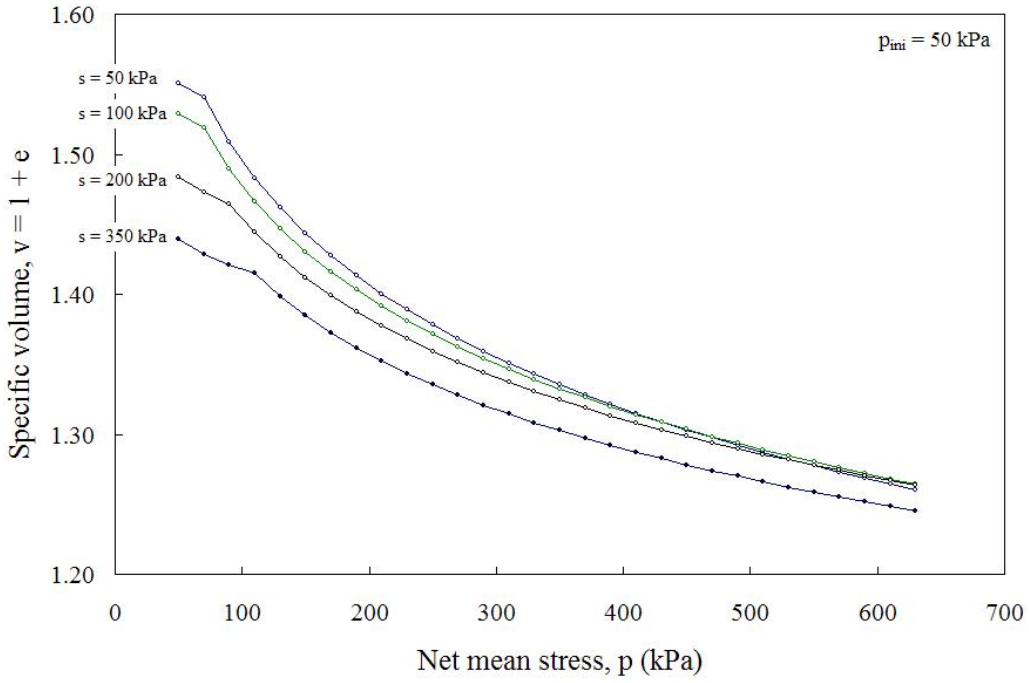

Figure 7.33 Specific volume predicted for compacted SP-SC soil using BBM.

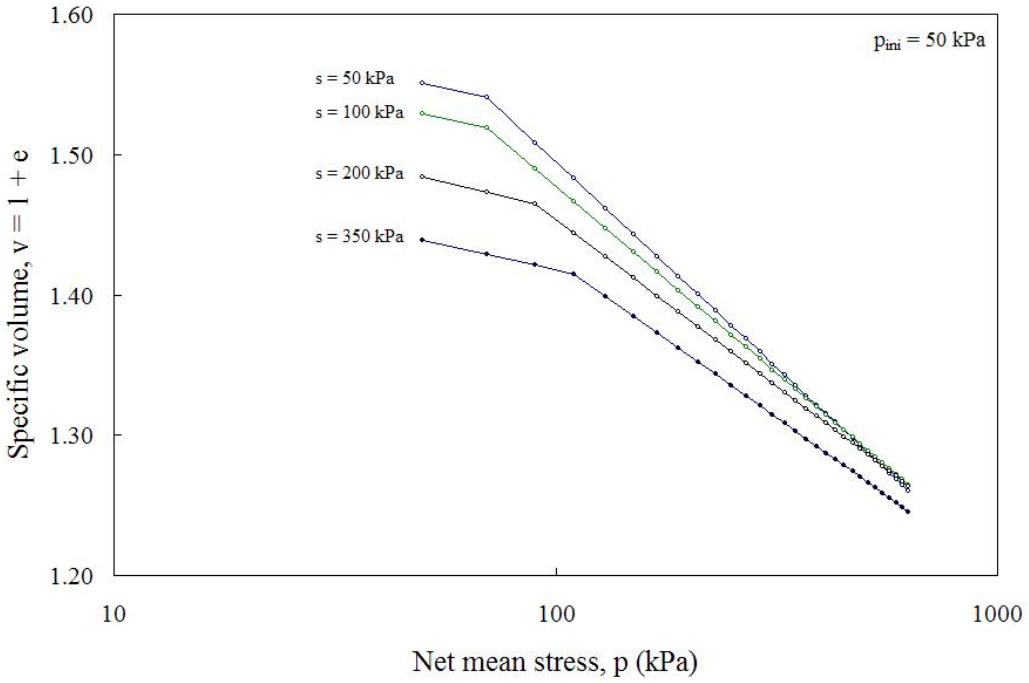

Figure 7.34 Specific volume predicted for compacted SP-SC soil using BBM- Net mean stress, p, in logarithmic scale

7.3.1.3 Numerical Predictions in the Shear-Strain Plane

Following the drained CTC stress path, the changes in volume between two consecutive yield surfaces (e.g. A and B in Figure 7.35 and Figure 7.36) will have recoverable elastic deformations resulting from the change in net mean stress, p, and irrecoverable plastic deformations resulting from the expansion of the yield surface. Plastic deformations are represented by the change in volume or vertical separation between the correspondent unloading-reloading lines (e.g. url_A and url_B) in the compression plane.

From Equation (7.8), the elastic deformation between points A and B, also known as elastic shear strain increments, can be calculated as

$$d\varepsilon_d^e = \frac{1}{3G} dq = \frac{1}{3G}\left(q_B - q_A\right) \tag{7.25}$$

On the other hand, from specific volume of the soil at points A and B (i.e. v_A and v_B), the irrecoverable change in volume between points A and B can be used to calculate the elastic volumetric strain increment by using Equation (7.7)

$$d\varepsilon_{vp}^e = \frac{\kappa}{v}\frac{dp}{p} = \frac{\kappa}{v_B}\left(\frac{p_B - p_A}{p_A}\right) \tag{7.26}$$

The total volumetric strain increments between points A and B can be calculated by

$$d\varepsilon_{vp}^{tot} = \frac{-dv_{AB}}{v_A} = \frac{v_A - v_B}{v_A} \tag{7.27}$$

Hence, from Equation (3.20) the plastic volumetric strain increment can be computed as

$$d\varepsilon_{vp}^{p} = d\varepsilon_{vp}^{tot} - d\varepsilon_{vp}^{e} \tag{7.28}$$

Finally, considering the assumption of a non-associative flow rule for the direction of plastic shear strain increments due to the deviatoric stress, $d\varepsilon_q^p$, the plastic shear strain increments between points A and B can be calculated from Equation (3.30) as (Alonso et al., 1990)

$$d\varepsilon_{d}^{p} = \frac{2q\alpha}{M^2[2p + p_s - p_0(s)]} d\varepsilon_{vp}^{p} = \frac{2q_B\alpha}{M^2[2p_B + p_s - p_0^B(s)]} d\varepsilon_{vp}^{p} \tag{7.29}$$

Explicit integration has been used in this research to simulate a drained CTC test conducted on a lightly overconsolidated soil and normally consolidated soil. A schematic of the results for both lightly overconsolidated and normally consolidated soils is presented in Figure 7.35 and Figure 7.36 respectively.

Figure 7.37, Figure 7.38, and Figure 7.39, show the comparison of experimental and predicted stress-shear strain relationship resulting from the fully drained CTC tests conducted on cubical SP-SC soil specimens at different values of constant matric suction, s = 50 kPa, s = 100 kPa, and s = 200 kPa, with initial values of net mean stress, p_{ini} = 50 kPa, p_{ini} = 100 kPa, and p_{ini} = 200 kPa, respectively. Numerical predictions were calculated using explicit integration technique. As expected, no good agreement is observed among the comparison between experimental and predicted values.

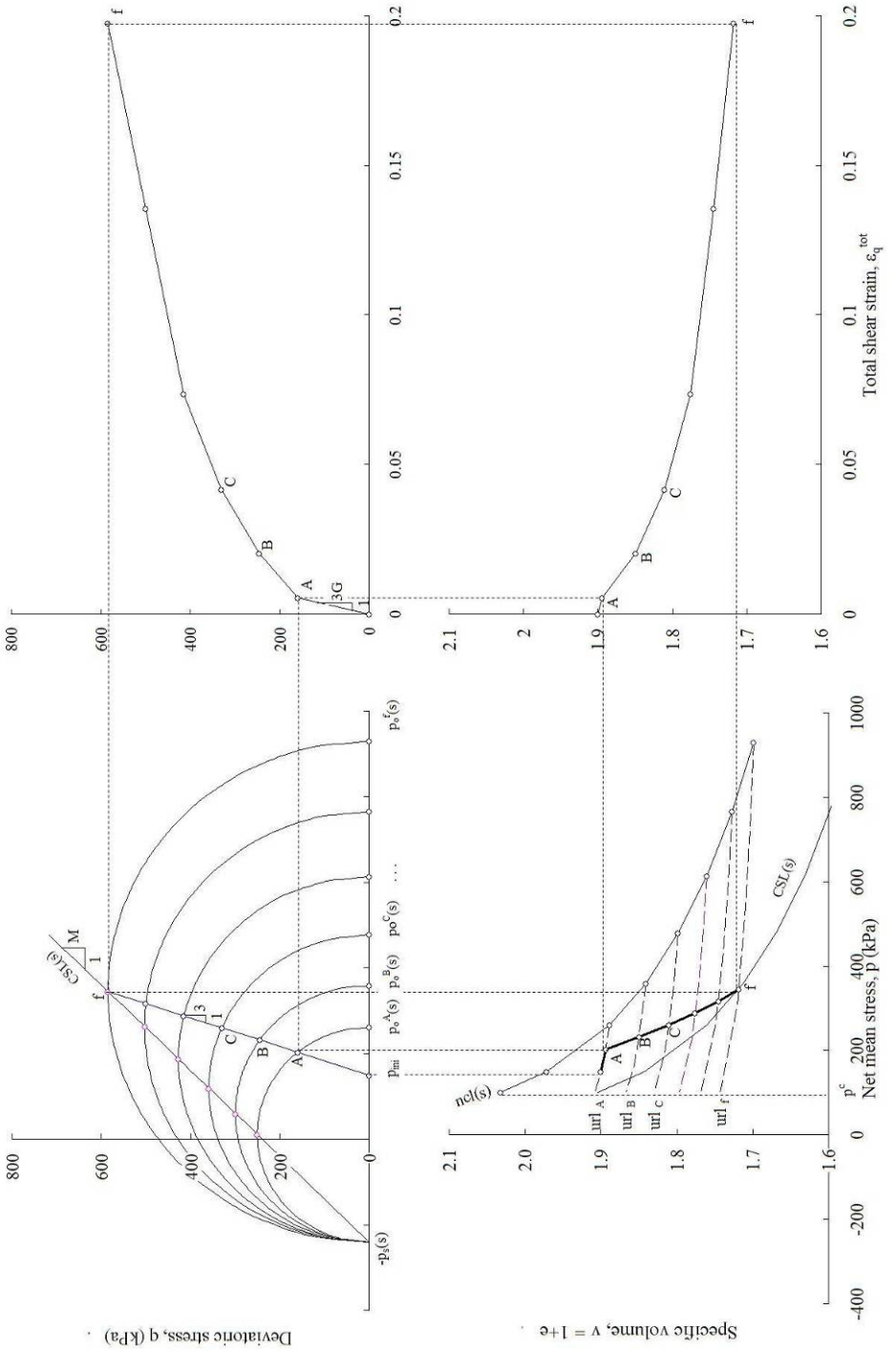

Figure 7.35 Sequence of stress increments resulting from BBM for a drained CTC conducted on a lightly overconsolidated soil at constant matric suction, s.

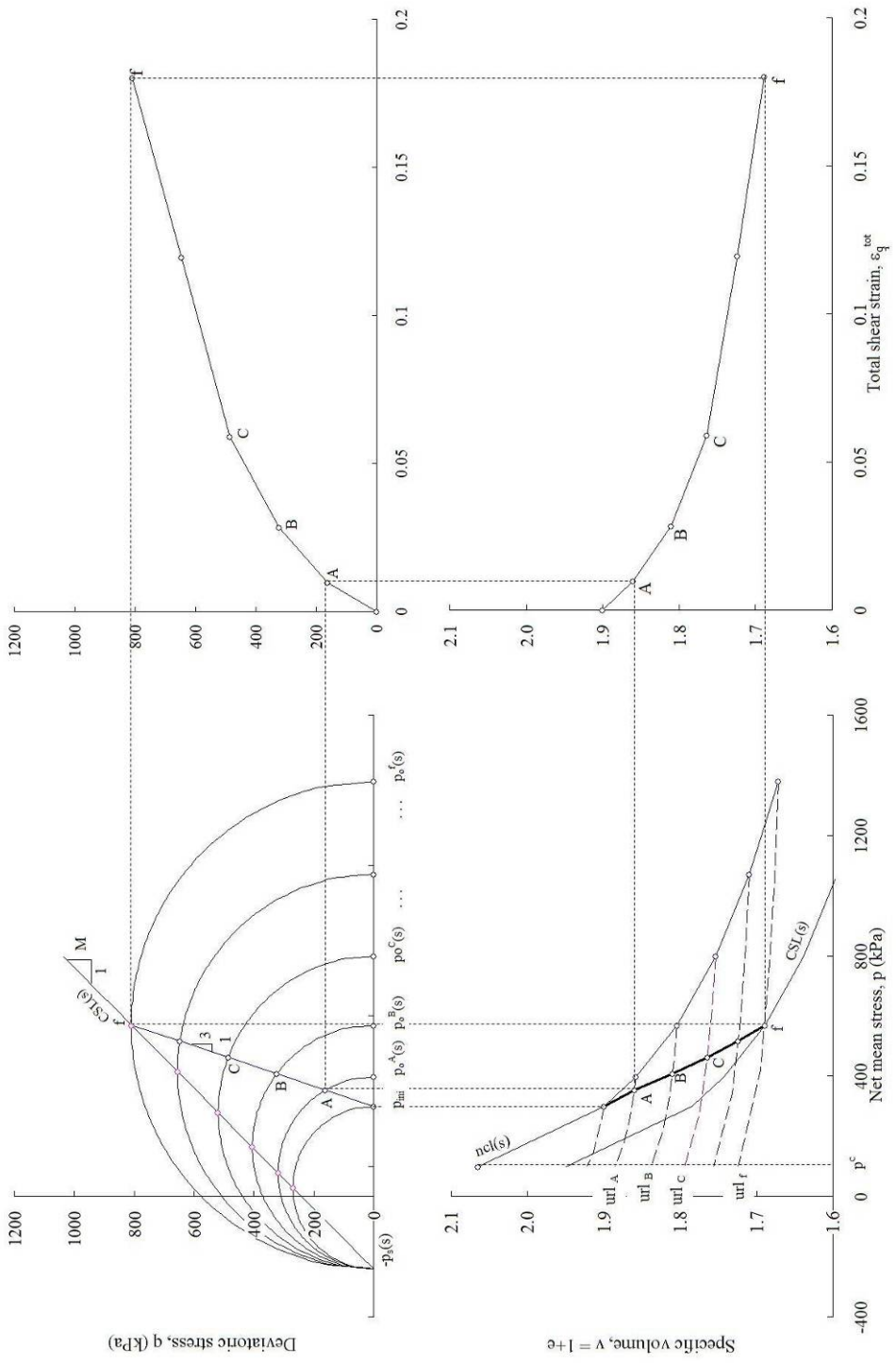

Figure 7.36 Sequence of stress increments resulting from BBM for a drained CTC conducted on a normally consolidated soil at constant matric suction, s.

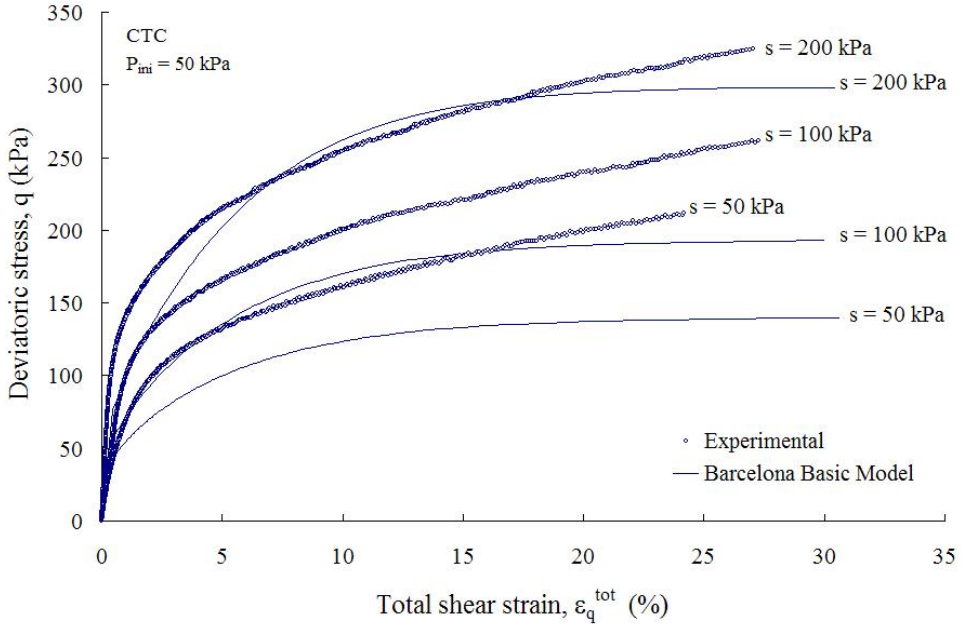

Figure 7.37 Measured and predicted stress-shear strain relationship from CTC tests conducted on compacted SP-SC soil at at s = 50, 100, and 200 kPa, and p_{ini} = 50 kPa.

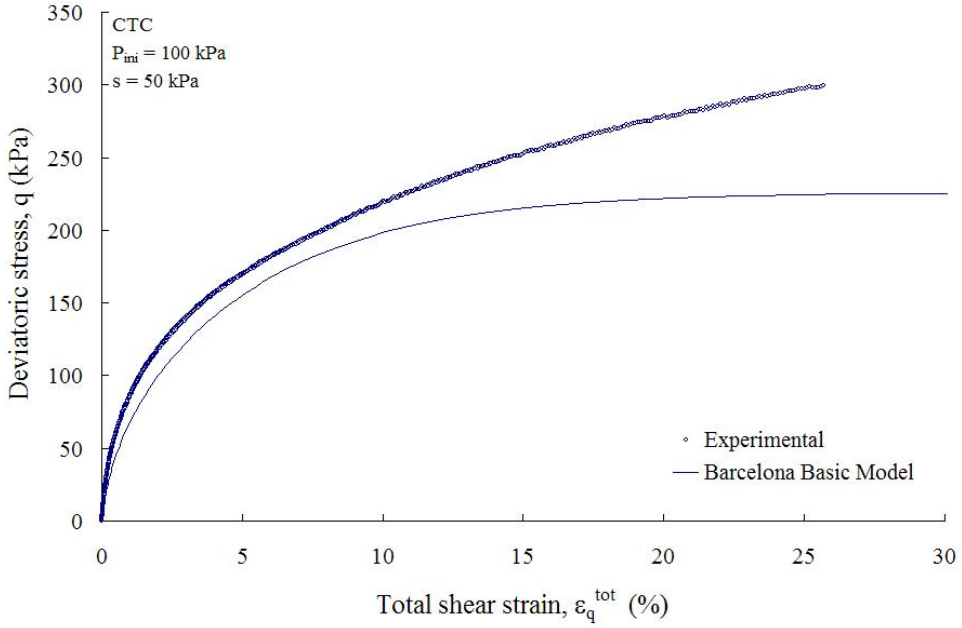

Figure 7.38 Measured and predicted stress-shear strain relationship from CTC tests conducted on compacted SP-SC soil at at s = 50 kPa, and p_{ini} = 100 kPa.

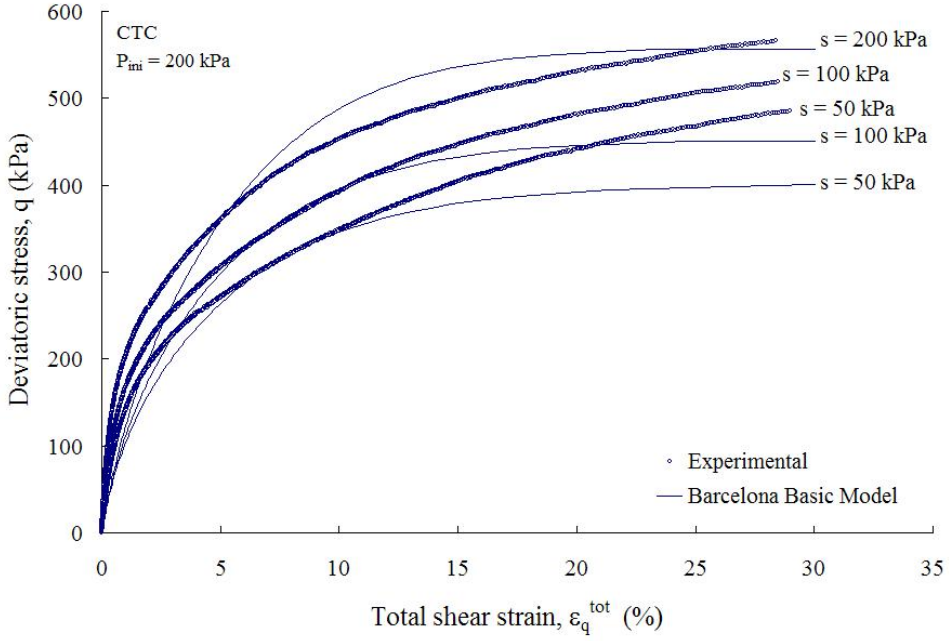

Figure 7.39 Measured and predicted stress-shear strain relationship from CTC tests conducted on compacted SP-SC soil at at s = 50, 100, and 200 kPa, and p_{ini} = 200 kPa.

7.3.2 Triaxial Compression Test

Similar to a CTC test, in a suction controlled drained triaxial compression (TC) test, the soil specimen is subjected to constant matric suction and initially surrounded by a constant confining net mean pressure, p_{ini}. Then, the soil specimen is failed by increasing the net axial pressure, σ_1. However, the lateral pressure is not kept constant, instead of that, lateral pressure is reduced in half of the amount increased in the axial direction (i.e. $\Delta\sigma_3 = \Delta\sigma_2 = -\frac{1}{2}\Delta\sigma_1$). Therefore, the mean total stress, p_{ini}, remains constant throughout the test (i.e. $p = p_{ini}$) and the deviatoric stress, q, is increased with a shear loading ratio, dq, until the critical state line (CSL) is intercepted (see Figure 7.40 and Figure 7.41).

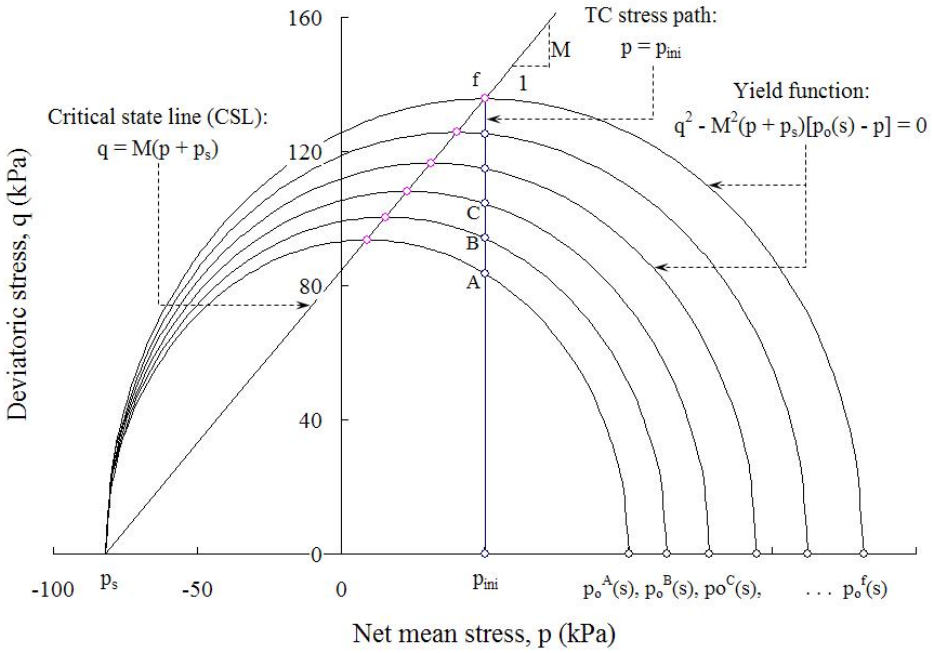

Figure 7.40 Stress increment expanding current yield surface for a drained TC test conducted at constant matric suction, s, on a lightly overconsolidated soil.

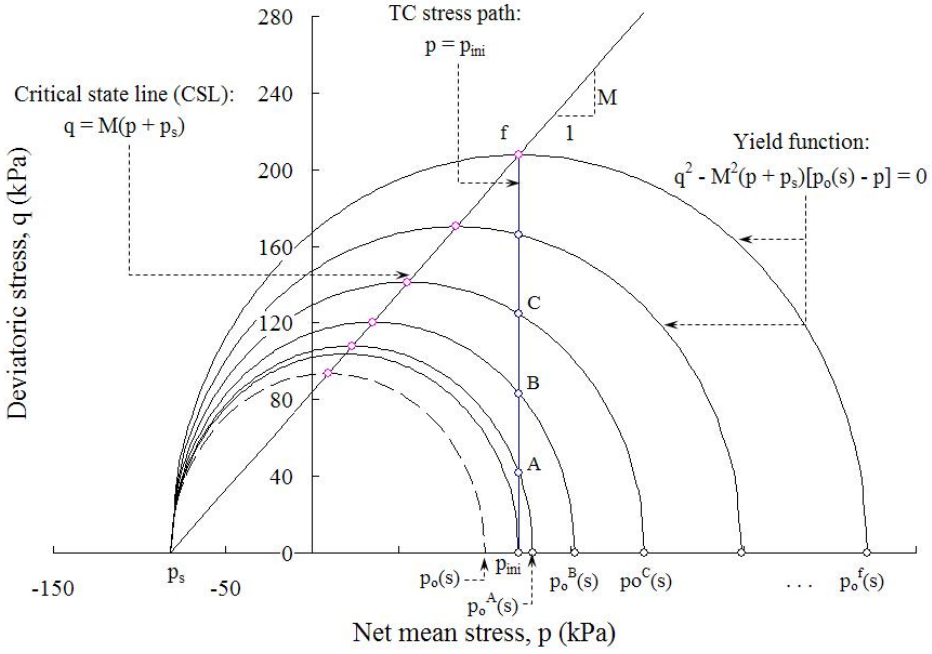

Figure 7.41 Stress increment expanding current yield surface for a drained TC test conducted at constant matric suction, s, on a normally consolidated soil.

7.3.2.1 Numerical Predictions in p-q Stress Plane

During a constant suction drained TC tests conducted on lightly overconsolidated soils, the initial yield stress, $p_o(s) = p_o^A(s)$, is calculated using Equation (7.3). As shown in Figure 7.40, using explicit integration to compute the constitutive relations that simulate the incremental stress-strain behaviour of unsaturated lightly overconsolidated soils, it is expected that given an initial net stress state, p_{ini}, and the current yield surface defined by $p_o(s) = p_o^A(s)$, any loading increment lying into the initial yield surface do not generate plastic deformations and the yield surface does not change in size. However, if the increment of stress goes beyond of the initial yield surface, the yield surface expands to accommodate the new stress state, and plastic strain will occur.

The intersection point between the TC loading path and the initial yield surface (i.e. point A in Figure 7.40) can be calculated by replacing $p = p_{ini}$ in Equation (7.1)

$$q_A = \left\{M^2 (p_{ini} + p_s)\left[p_o^A(s) - p_{ini}\right]\right\}^{\frac{1}{2}} \qquad (7.30)$$

This point is taken as the initial point to start the deviatoric stress increments and calculate de correspondent specific volume and deformations. Notice that, for normally consolidated soils where the initial net mean pressure, p_{ini}, exceeds the initial net yield stress of the soil sample, $p_o(s)$, a new yield surface has been created in the soil during the equalization stage and the confinement pressure become the new yield stress controlling the size of the initial yield surface (i.e. $p_o(s) = p_{ini}$). Therefore, by replacing $p = p_{ini}$ in Equation (7.27) the initial point to star the deviatoric stress increment correspond to the $p = p_{ini}$ and $q = 0$.

The yield stress generated by the new yield surface, $p_o^B(s)$, for both lightly overconsolidated and normally consolidated soils can be calculated using Equation (7.14). Since there is a common point where the drained TC stress path intersect the yield function and the CSL, the stress state at failure, (p_f, q_f) can be obtained by replacing $p = p_{ini}$ in Equation (7.13)

$$p_f = p_{ini} \tag{7.31}$$

$$q_f = M(p_{ini} - p_s) \tag{7.32}$$

The yield stress at failure, $p_o^f(s)$, can be calculated using Equation (7.17)

Once the yield stress at failure, $p_o^f(s)$, has been determined it is possible to calculate the yield surface at failure by replacing, $p_o^f(s)$ and p_s in Equation (7.1) and solving either by deviatoric stress, q, or net mean stress, p.

Figure 7.42 shows the predicted yield surface and the experimental results obtained from drained suction-controlled triaxial compression (TC) tests conducted on SP-SC soil specimens at constant matric suction, s = 50,100, and 200 kPa and initial net mean stresses, p_{ini} = 100 kPa. In general, no agreement is observed between the experimental and predicted values presented in Figure 7.42.

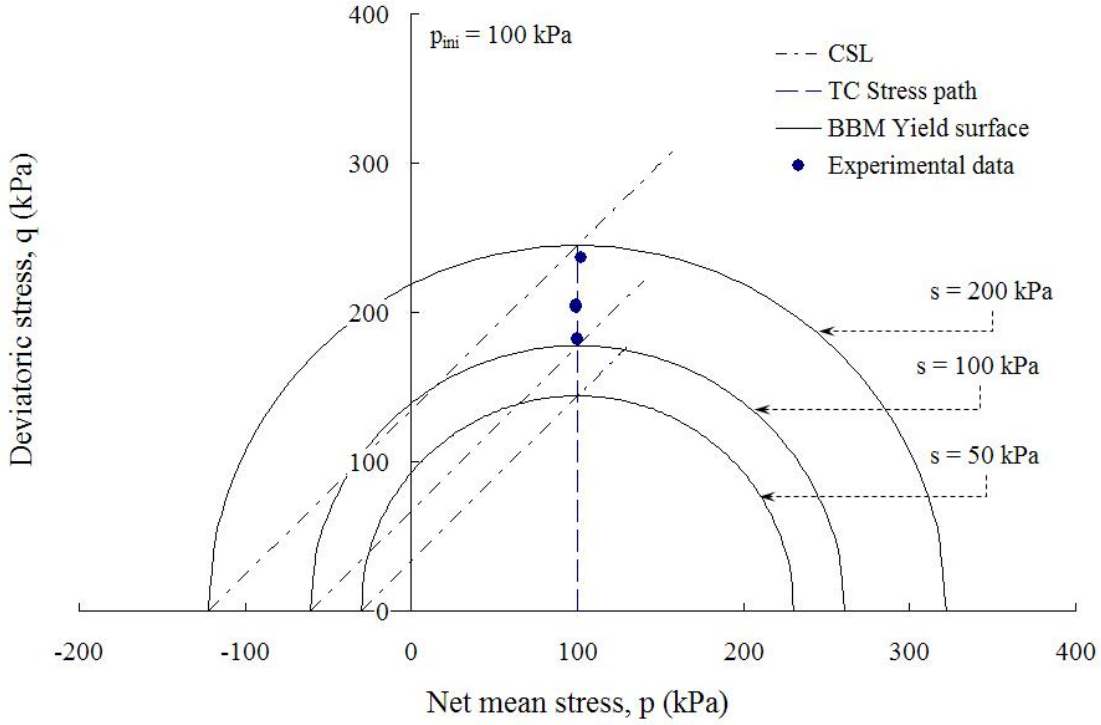

Figure 7.42 Predicted yield surface of BBM in drained TC tests conducted at initial net mean stresses, p_{ini} = 100 kPa and constant matric suction, s = 50, 100, and 200 kPa.

7.3.2.2 Numerical Predictions in Shear-strain Plane

As shown in Figure 7.43 and Figure 7.44, during a drained triaxial compression (TC) test, each new net yield stress, $p_o^A(s)$, $p_o^B(s)$, $p_o^C(s)$, …, $p_o^f(s)$, can be associated with its respective net mean stress, $p_o^A(s)$, $p_o^B(s)$, $p_o^C(s)$, …, $p_o^f(s)$, on the isotropic normal compression line (ncl). These point correspond to the intersection of the isotropic ncl with its respective elastic unloading-reloading line, url_A, url_B, url_C,.., url_f. Hence, the variation of the specific volume can be computed by using Equations (8.18) to (8.21). Furthermore, shear strain increments can be calculated using Equations (8.22) to (8.26).

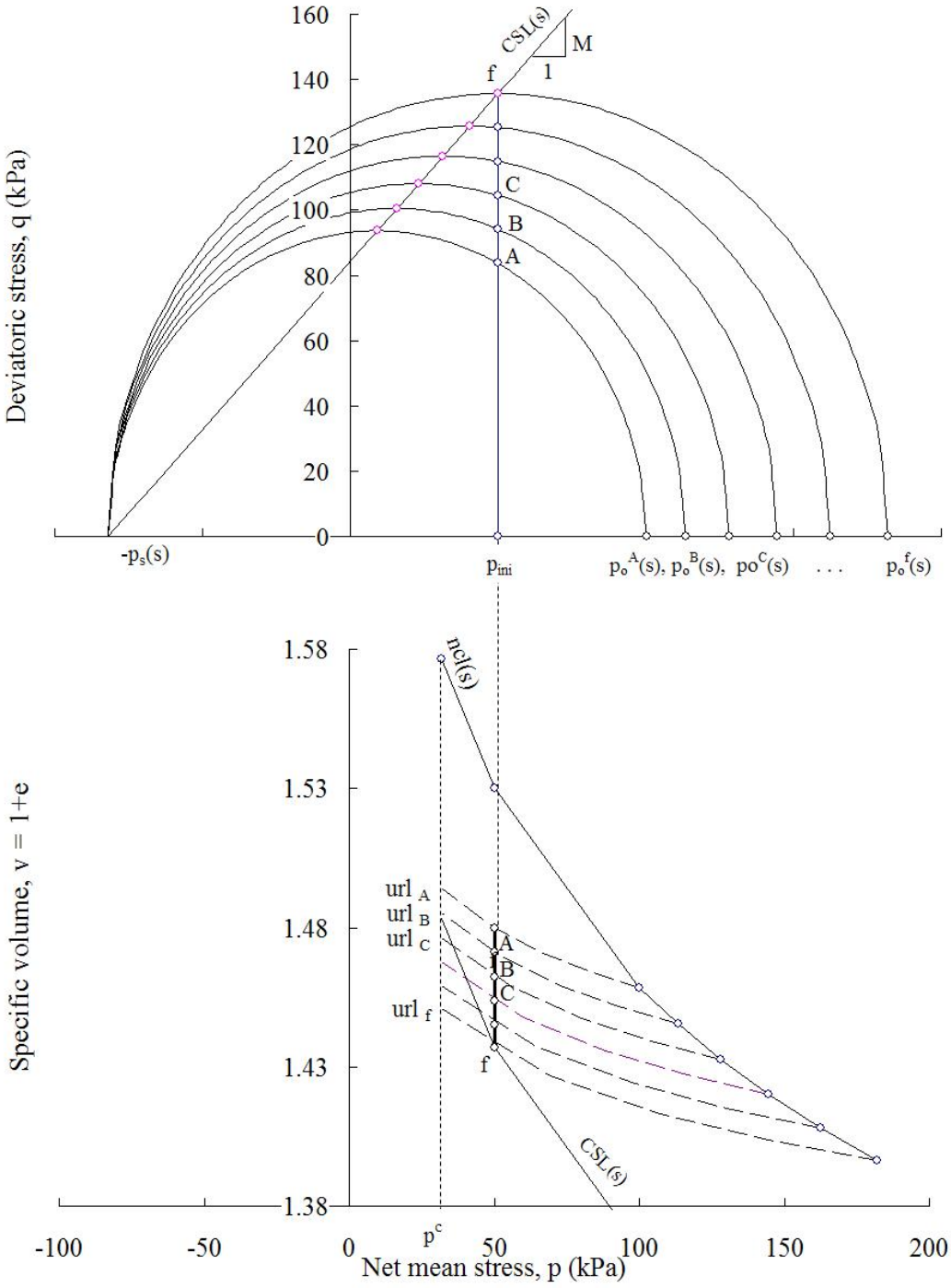

Figure 7.43 Successive yield surfaces and the associated unloading-reloading lines (url) resulting from a TC test conducted on a lightly overconsolidated soil.

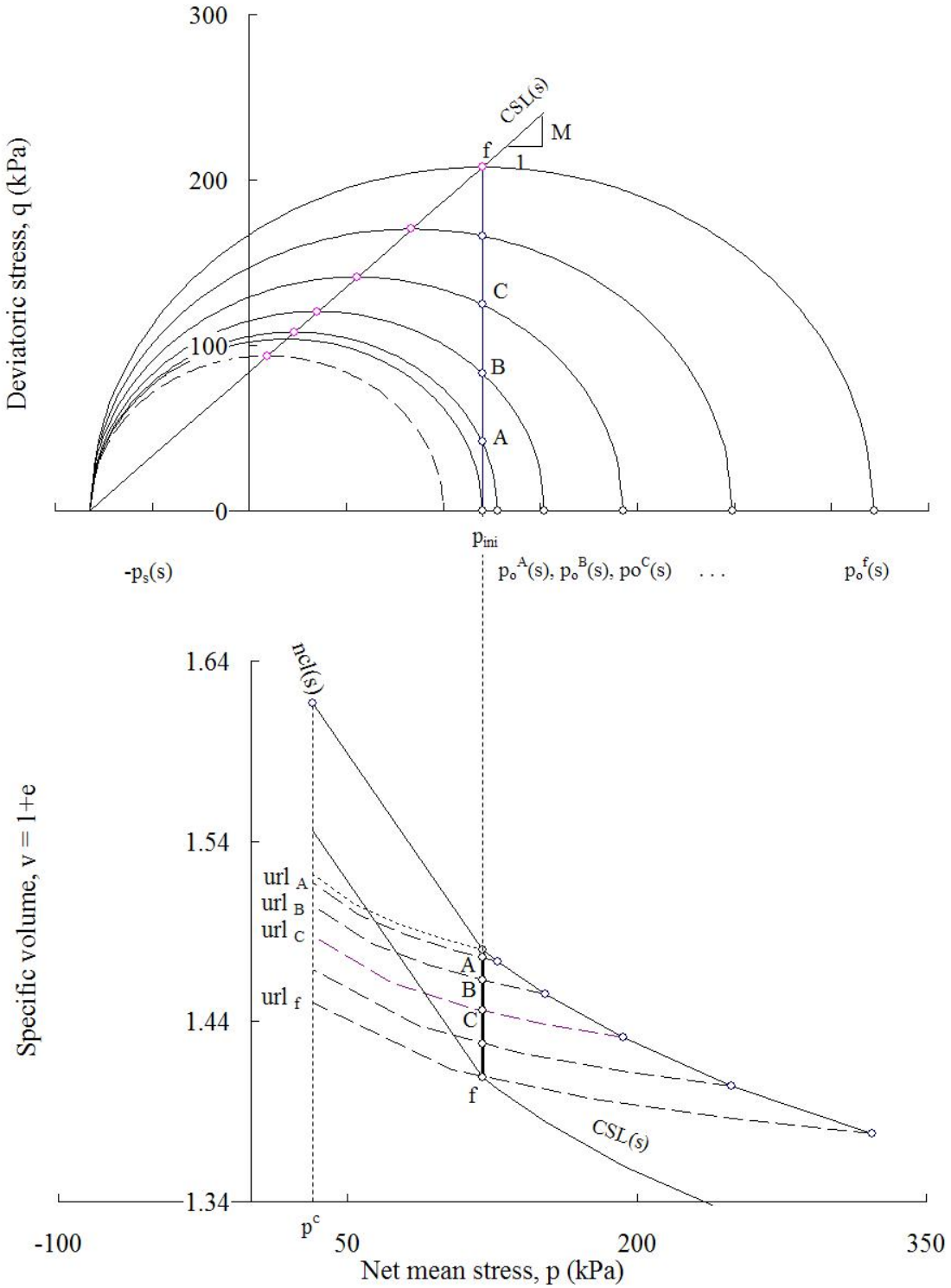

Figure 7.44 Successive yield surfaces and the associated unloading-reloading lines (url) resulting from a TC test conducted on a normally consolidated soil.

Figure 7.45 shows the comparison of experimental and predicted stress-shear strain relationship resulting from the drained suction-controlled TC tests conducted on 6 cubical compacted SP-SC soil specimens. The tests were conducted for different values of constant matric suction, s = 50 kPa, s = 100 kPa, and s = 200 kPa, with initial values of net mean stress, p_{ini} = 100 kPa. Numerical predictions were calculated using explicit integration technique to solve the BBM. As expected, no good agreement is observed between the experimental and predicted values.

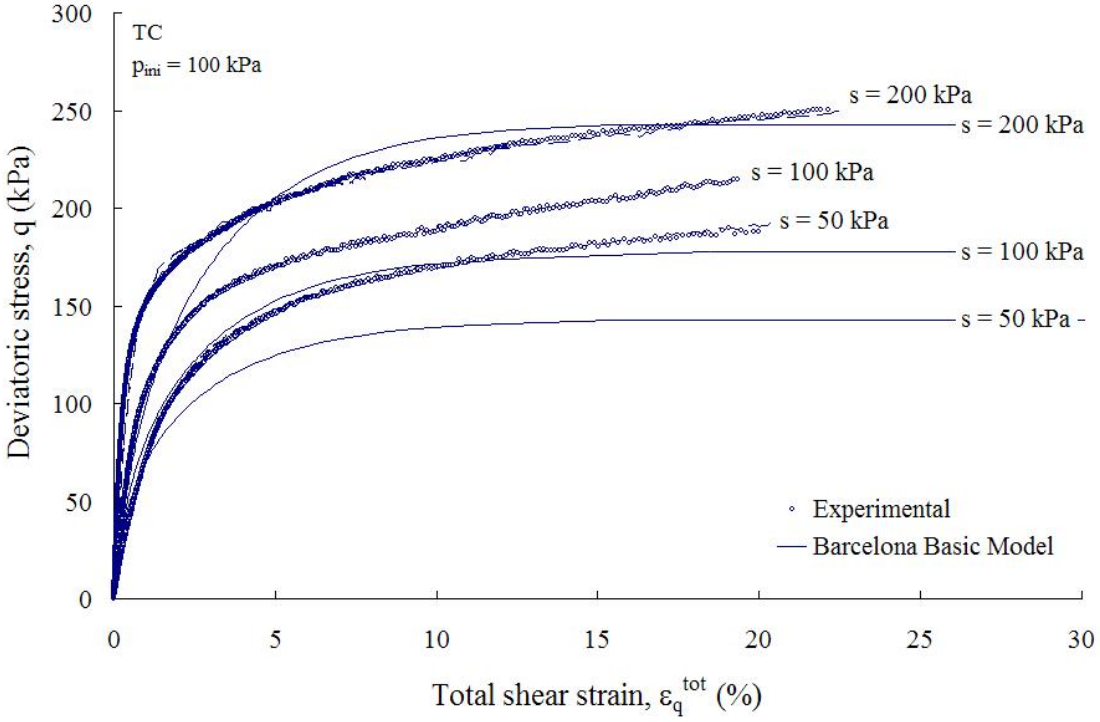

Figure 7.45 Measured and predicted stress-shear strain relationship from TC tests on SP-SC soil at s = 50, 100, and 200 kPa, and p_{ini} = 100 kPa.

7.4 Calibration of Modified Barcelona Basic Model

The model formulated by Josa et al., (1992) is similar to the Barcelonan Basic Model. However, the proposed modification allows the prediction of the maximum collapse at some value of confining stress through the introduction of a new expression to calculate the loading collapse (LC) yield surface in the p – s space. The new expression replaces Equation (7.3) of the Barcelona Basic model by

$$p_o(s) = \left(p_o(0) - p^c\right) + p^c[(1-m)e^{-\alpha s} + m] \tag{7.33}$$

where,

α = parameter controlling the shape of yield surface

m = parameter related to the difference between $p_o(s)$ for high suction values (i.e. s = ∞) and $p_o(0)$.

The parameter m, which is always higher that one, can be calculated by

$$m = 1 + \frac{\zeta_y - 1}{\zeta_x - p^c}\left(p_0(0) - p^c\right)e^{\frac{\zeta_x - p_o(0)}{\zeta_x - p^c}} \tag{7.34}$$

As suggested by Josa et al. (1992), ζ_x has been replaced by the value of $p_o(0)$ corresponding to maximum collapse and ζ_y by the maximum plastic volumetric strain, $e_v^{p}{}_{max}$. Hence, using the experimental yield stress value, $p_o(50)$ = 75 kPa, $p_o(100)$ = 85 kPa, $p_o(200)$ = 100 kPa, $p_o(350)$ = 111 kPa, the least squares method has been used to approximately solve the over-determined system proposed in Equations (8.33) and (8.31). The best fit values of the parameters ζ_x, ζ_y, pc, $p_o(0)$, m, and α, were found to be, ζ_x = 61.35, ζ_y = 3.494, p_c = 28.37 kPa, $p_o(0)$ = 61.35 kPa, m = 3.494, and α = 0.00382. Figure 7.46 and Figure 7.47 show the experimental yield stress value, $p_o(s)$,

along with the LC curves predicted using Equation (7.33) for different values of po(0) and α, respectively. Good agreement is observed between the experimental data and predicted values, which is confirmed by a correlation coefficient of 0.999.

Figure 7.48 shows the experimental yield stress value, $p_o(s)$, along with the LC curves predicted using the equation proposed by Josa et al. (1992) and the equation proposed by Alonso et al., (1990). Although good agreement is observed in both cases, the equation proposed by Josa et al. (1992) appear to over-predict the yield stress value, $p_o(s)$, for high values of matric suction, s.

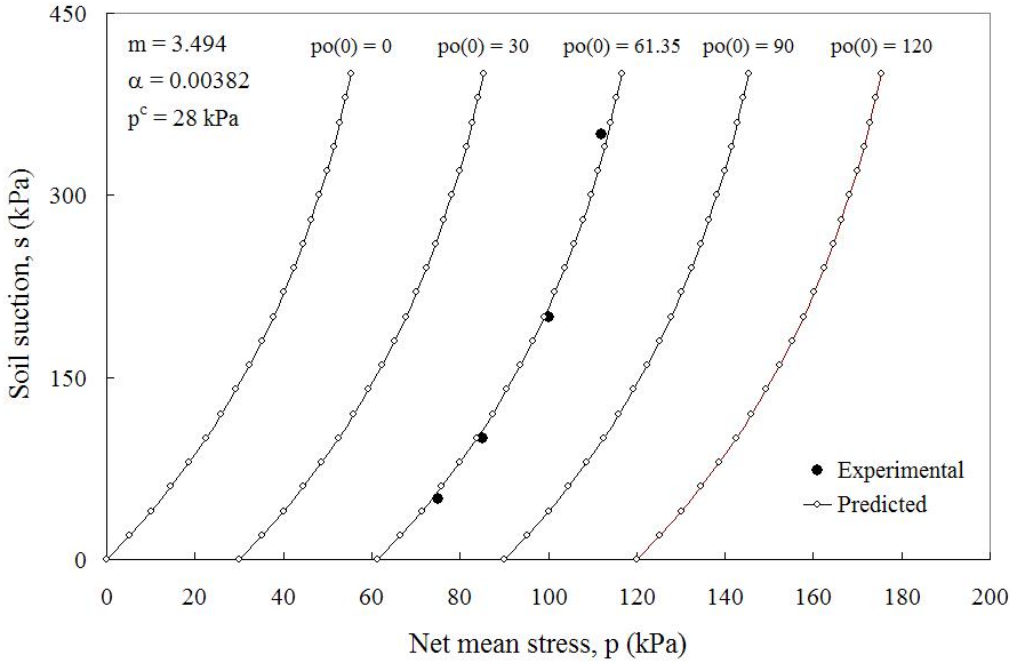

Figure 7.46 Experimental yield stress value, $p_o(s)$, along the best fit LC curve and typical LC curves predicted for different values of $p_o(0)$ - Equation (7.30).

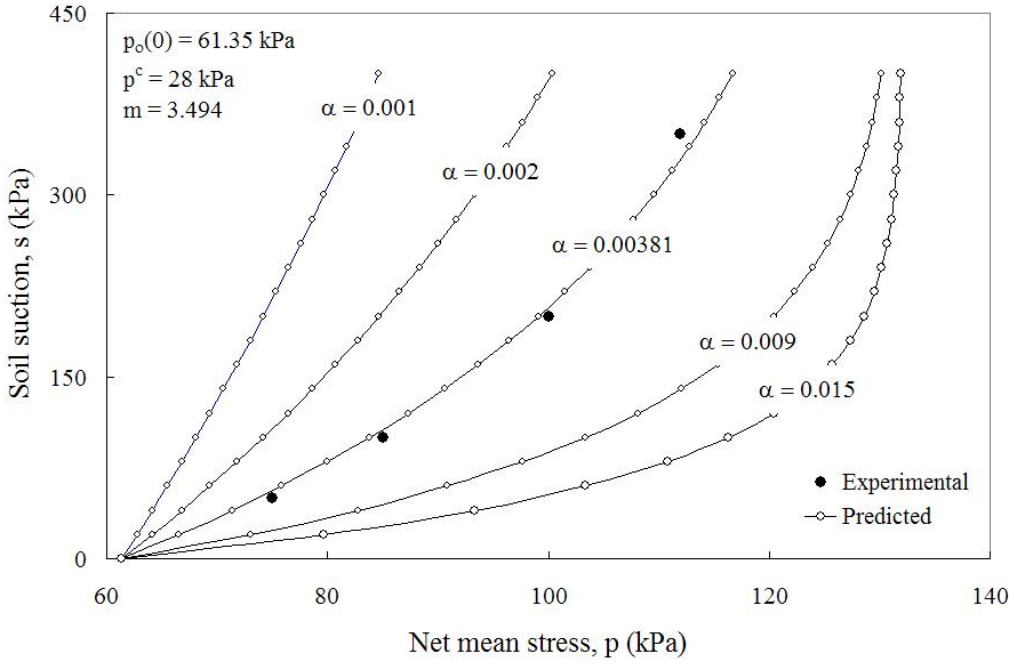

Figure 7.47 Experimental yield stress value, $p_o(s)$, along the best fit LC curve and typical LC curves predicted for different values of α using - Equation (7.30).

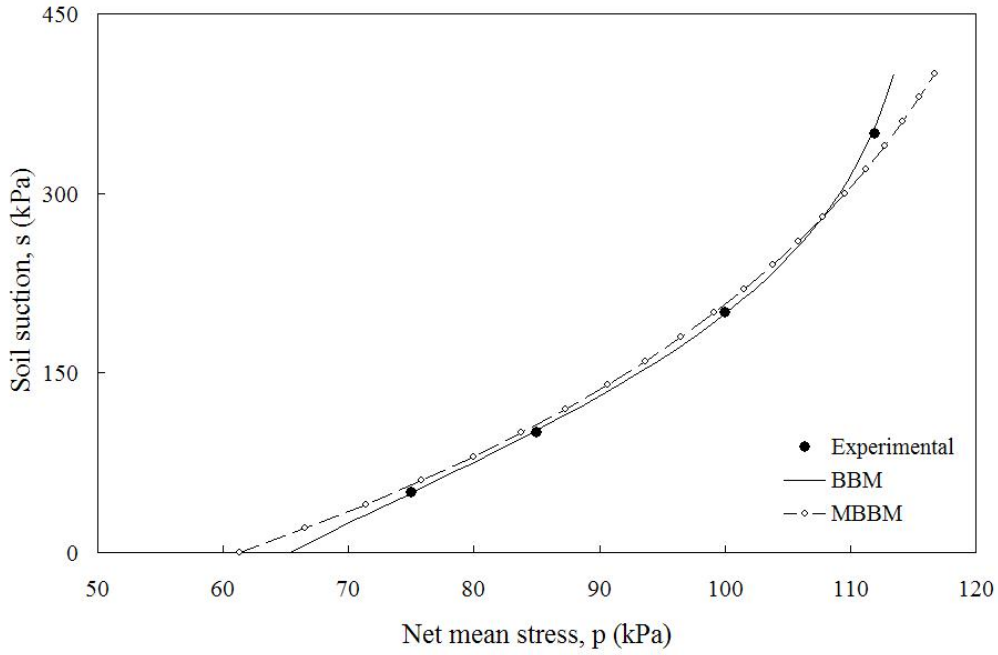

Figure 7.48 Experimental yield stress value, $p_o(s)$, along the best fit LC curves proposed by Alonso et al. (1990) and Josa et al. (1992).

The values of the parameters obtained for the calculation of the LC yield curve basis in the equations proposed by Josa et al (1992), are summarized in Table 7.3. The other parameters necessary to solve the model proposed by Josa et al. (1992) are the same parameters already calculated for the BBM, presented in Table 7.1.

Table 7.3 Model parameters for calculation of LC yield curve proposed by Josa et al. (1992)

Parameter	Description	Value
$p_o(0)$	Saturated preconsolidation stress	61.35 kPa
p^c	Reference stress	28.37 kPa
m	parameter related to the difference between $p_o(s)$ for high suction values	3.494
α	Constant related to the maximum stiffness of the soil	0.00382

7.5 Implementation of Modified Barcelona Basic Model

The procedure described in section 8.3.2 can be extended to solve the constitutive relations proposed by Josa et al. (1992). Hence, using the experimental values of the parameters summarized in Table 7.4, it is possible to predict the soil response under shear loading. Figure 7.49 shows the initial LC yield curve and p_s linear relationship on the p – s plane, along the experimental data. Although Figure 7.48 shows difference between the LC curve proposed by Alonso et al. (1990) and Josa et al. (1992), this difference does not have effect on the calculation of the yield surface on the p- q plane.

Table 7.4 Experimental values of model parameters used to validate the MBBM

Parameter	Description	Value
m	parameter related to the difference between $p_o(s)$ for high suction values	3.494
α	Constant related to the maximum stiffness of the soil	0.00382
p^c	Reference stress	18.37 kPa
$p_o(0)$	Saturated preconsolidation stress	61.35 kPa
$\lambda(0)$	Compressibility coefficient for the saturated state	0.146
r	Constant related to the maximum stiffness of the soil	0.649
β	Parameter which control the rate of soil stiffness with s	895.17×10^{-5} kPa^{-1}
κ	Compressibility coefficient along the elastic path	0.03138
M	Slope of the critical state line (CSL)	1.103
k	Parameter describing the increase in cohesion with s	0.616
G	Elastic shear modulus	5500 kPa

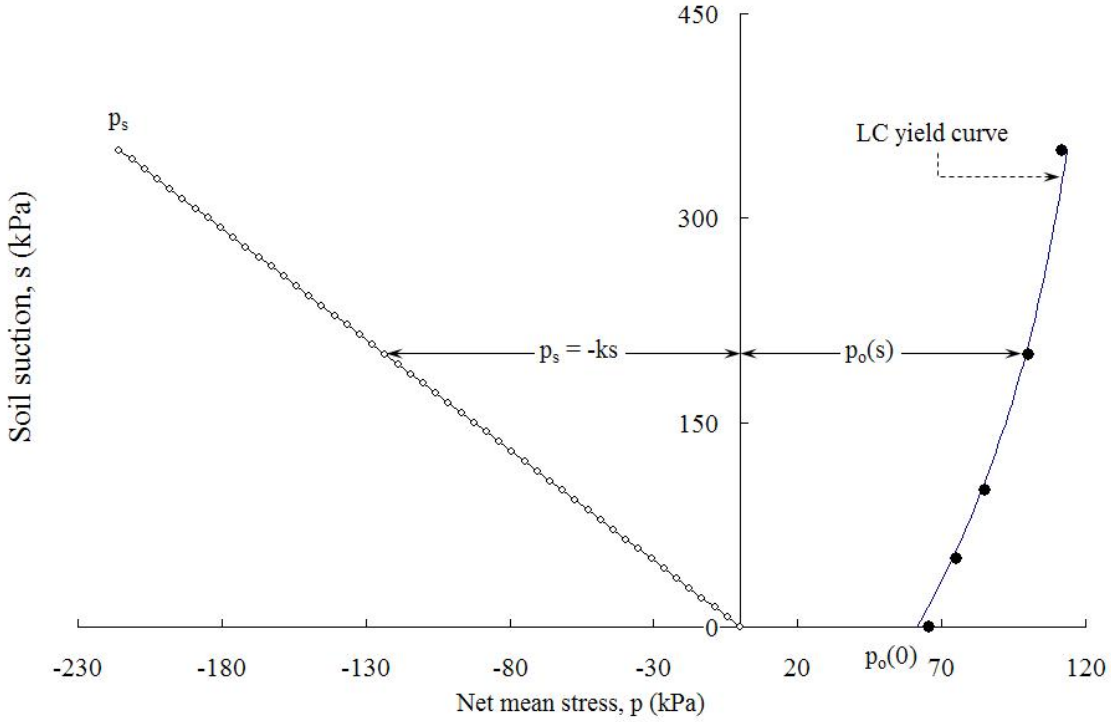

Figure 7.49 Experimental yield stress values and predicted initial LC yield curve in p-s stress plane, as proposed by Josa et al. (1990).

On the other hand, Figure 7.50 and Figure 7.51 show the predicted values for CTC tests conducted at constant soil matric suction, s = 50 kPa, s = 100 kPa, and s = 200 kPa, and initial net mean stress, p_{ini} = 50 kPa and p_{ini} = 200 kPa, respectively. No significant difference is observed between total shear strain values, ε_q^{tot}, obtained using BBM and the MBBM proposed by Josa et al. (1992).

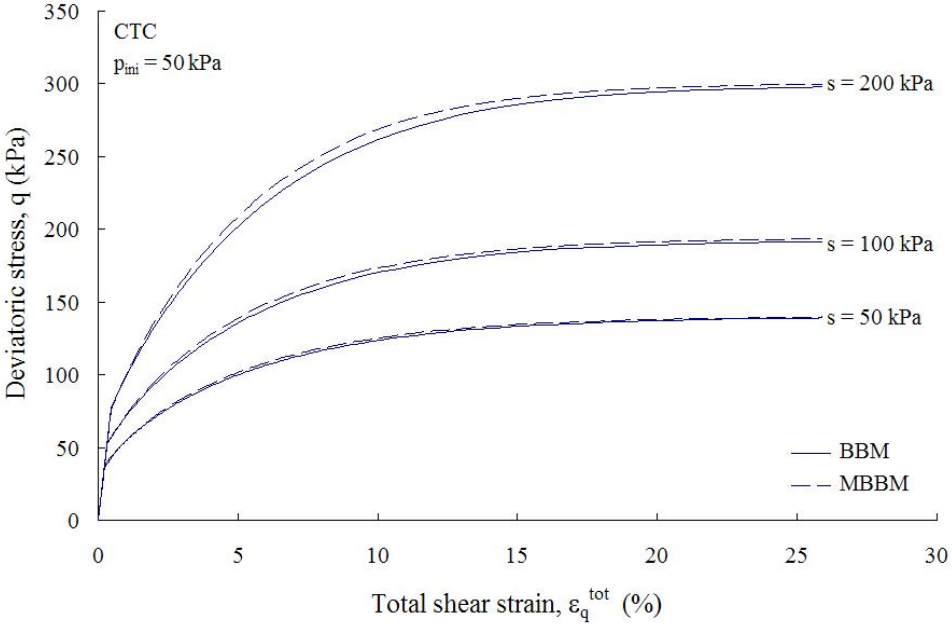

Figure 7.50 Predicted stress-shear strain relationship from CTC tests at s = 50, 100 kPa, and s = 200 kPa, and initial mean stress, p_{ini} = 50 kPa.

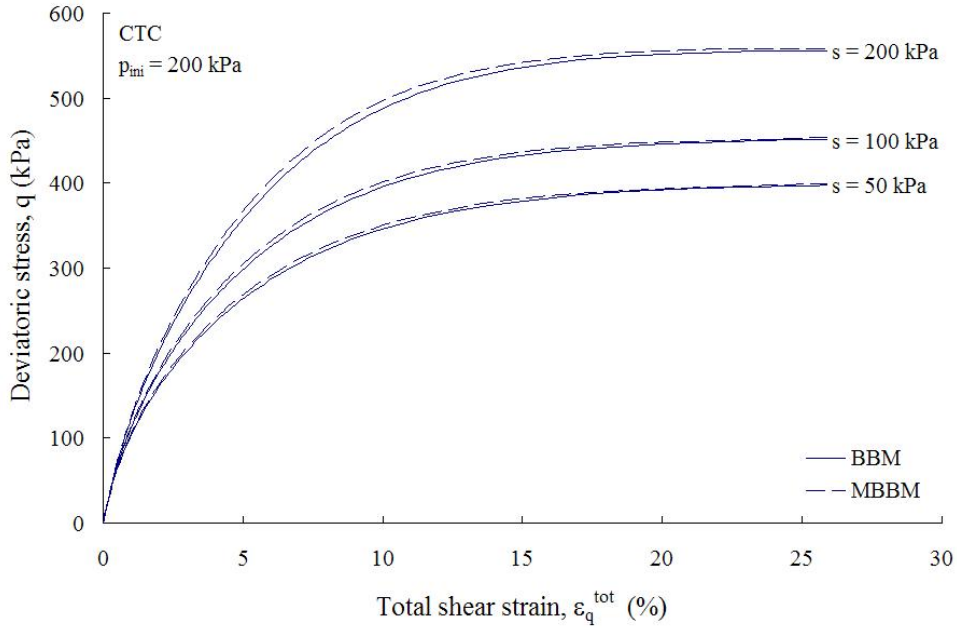

Figure 7.51 Predicted stress-shear strain relationship from CTC tests at s = 50, 100 kPa, and s = 200 kPa, and initial mean stress, p_{ini} = 200 kPa.

7.6 Calibration of Oxford Model

The framework proposed by Wheeler and Sivakumar (1995) is very similar to that proposed by Alonso et al. (1990). However, the new framework assumes that all the model parameters are suction-dependent. In addition, instead of use the reference stress, p_c, proposed by Alonso et al. (1990), the authors use the atmospheric pressure, p_{atm}, as reference stress.

7.6.1 Yield Function

The yield surface for a particular value of suction, with the apex located at the intersection of the yield curve with the critical state line and crossing the isotropic normal compression line at $p = p_o(s)$ can be computed by

$$q = M_*^2[p_o(s) - p][p + p_o(s) - 2p_x] \quad (7.35)$$

where

M_* = aspect ratio of the ellipse

$p_o(s)$ = Yield net stress at matric suction, s

p_x = net mean stress at the intersection of the yields surface with the CSL.

The aspect ration of the ellipse, M_*, is the minor axis (i.e. $b = M(s)p_x + \mu(s)$) to major axis (i.e. $a = p_o - p_x$) given by

$$M_* = \frac{M(s)p_x + \mu(s)}{Po - P_x} \tag{7.36}$$

$\mu(s)$ = intersection of the critical state line with the deviatoric stress axis.

Figure 7.52 shows the expansion of the yield surface for a drained conventional triaxial compression (CTC) test predicted by the Oxfor model (OM).

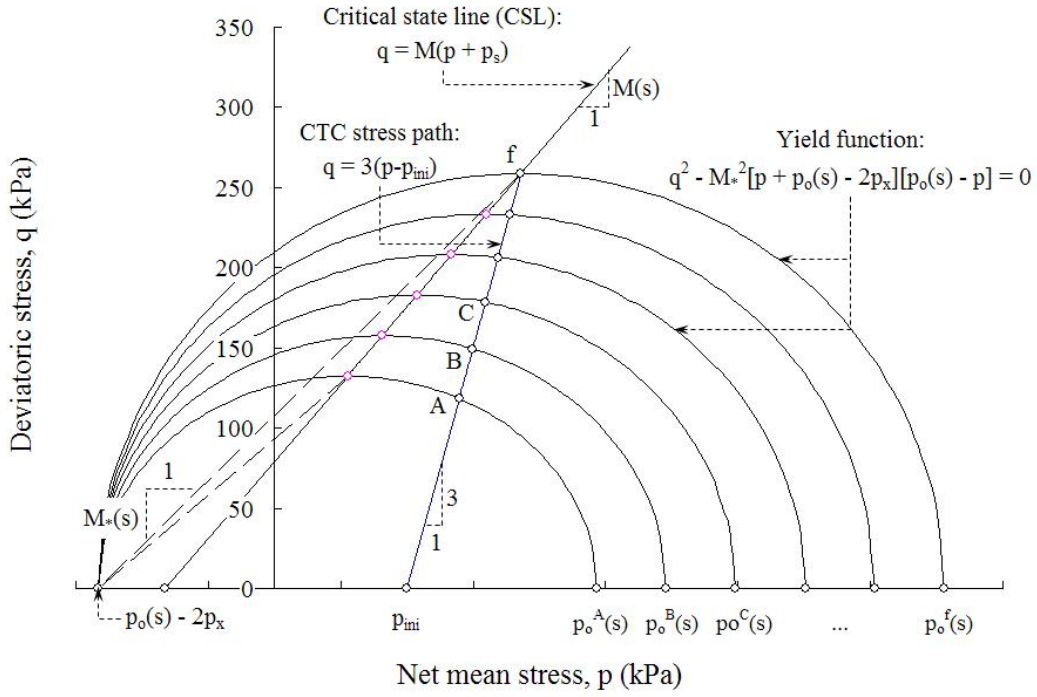

Figure 7.52 Expansion of the yield surface predicted by W&S model during drained CTC test performed at constant matric suction, s, on a lightly overconsolidated soil.

7.6.2 Constitutive Behaviour Under Isotropic Loading

The variation of the specific volume, v = 1 + e, with net mean stress, p, during drained isotropic consolidation tests conducted on SP-SC soil specimens is shown in Figure 7.53. For each test shown, there was a clear net yield stress, $p_o(s)$, identified by the marked change in slope of the continuous plot of specific volume against the net mean stress, p, as shown in Figure 7.1 to Figure 7.4. Once the net yield stress for a particular matric suction, s, is exceeded, the soil state fell on an isotropic normal compression line (iso-ncl). The iso-ncl can be described by a linear relationship as

$$v = N(s) - \lambda(s) \ln \frac{p}{p_{atm}} \qquad (7.37)$$

where

$\lambda(s)$ = soil stiffness parameter which depend on matric suction, s

p_{atm} = atmospheric pressure = 100 kPa

N(s) = specific volume at $p = p_{atm}$ which vary with matric suction, s

The best fit values of parameter N(s) for matric suction values, s = 50 kPa, s = 100 kPa, s = 200 kPa, s = 300 kPa were found to be, N(50) = 1.700, N(100) = 1.704, N(200) = 1.707, and N(350) = 1.703, respectively. In addition, The slope of the normal consolidation line were found to be, $\lambda(50) = 0.1275$, $\lambda(100) = 0.1286$, $\lambda(200) = 0.1033$, and $\lambda(350) = 0.0970$. Both, the slope $\lambda(s)$ and the intercept N(s) of the iso-ncl were found to be function of soil suction. Nevertheless, an average value, $\kappa = 0.03138$ is assumed from the elastic portion of the specific volume, v = 1 + e, curve on the p – v plane.

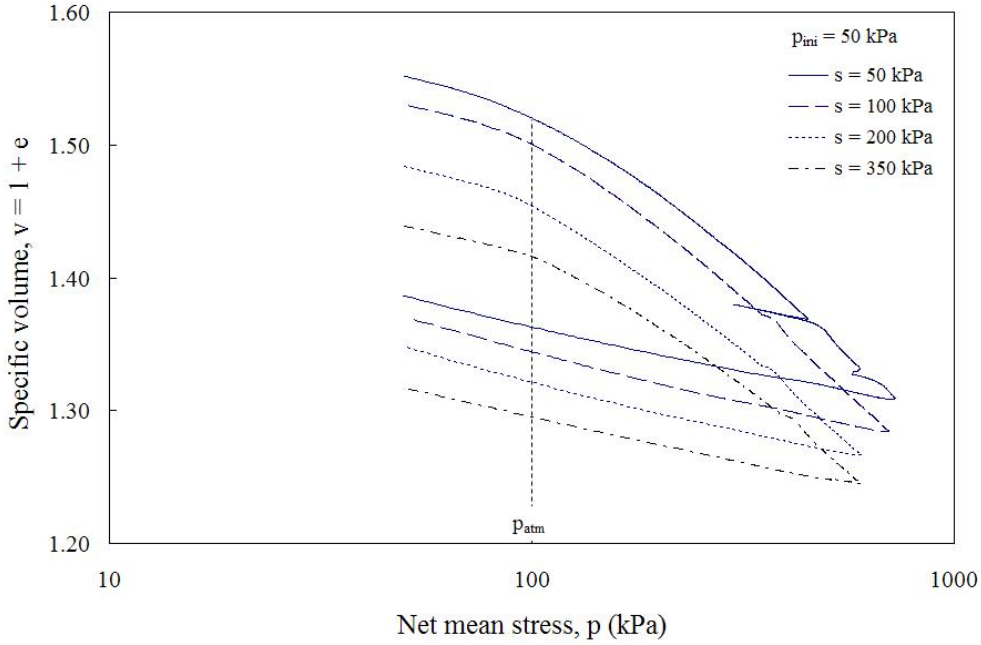

Figure 7.53 Variation of specific volume with net mean stress from HC tests at s = 50, 100, and 200 kPa, and p_{ini} = 50 kPa on SP-SC soil.

7.6.3 Loading Collapse (LC) Yield Curve Parameters

The expression to compute the LC yield curve is given by (Wheeler and Sivakumar, 1995)

$$[\lambda(s)-\kappa]\ln\frac{p_o(s)}{p_{atm}}=[\lambda(0)-\kappa]\ln\frac{p_o(0)}{p_{atm}}+N(s)-N(0)+\kappa_s\ln\frac{s+p_{atm}}{p_{atm}} \quad (7.38)$$

where

$\lambda(0)$ = soil stiffness parameter for saturated conditions (i.e. s = 0)

$p_o(0)$ = Isotropic yield stress for s = 0

N(0) = specific volume at $p = p_{atm}$ for s = 0

κ = elastic stiffness parameter for changes in net mean stress, p

κ_s = elastic stiffness parameter for changes in suction, s.

Using the experimental yield stress value, $p_o(50)$ = 75 kPa, $p_o(100)$ = 85 kPa, $p_o(200)$ = 100 kPa, $p_o(350)$ = 111 kPa, the elastic stiffness parameter for changes in suction, $\kappa_s = \kappa = 0.03138$, and P_{atm} = 101.3 kPa, the over-determined system proposed in Equations (8.38) has been approximately solved by using the least squares method. The best fit values of the parameters, $\lambda(0)$, $p_o(0)$, N(0), were found to be, $\lambda(0) = 0.146$, $p_o(0)$ = 63.86 kPa, and N(0) = 1.691. Figure 7.54 and Figure 7.55 show the experimental yield stress value, $p_o(s)$, along with the predicted LC curves predicted using Equation (7.38) for different values of $p_o(0)$ and N(0), respectively. Good agreement is observed between the experimental data and predicted values, which is confirmed by a correlation coefficient of 0.999.

In addition Figure 7.56 shows the experimental yield stress value, $p_o(s)$, along with the LC curves predicted using the equation proposed by Wheeler and Sivakumar (1995), the equation proposed by Alonso et al., (1990), and that proposed by Josa et al. (1992). Although all three models show a good agreement with the experimental data, The model proposed by Alonso et al. (1990) shows better agreement with the experimental data.

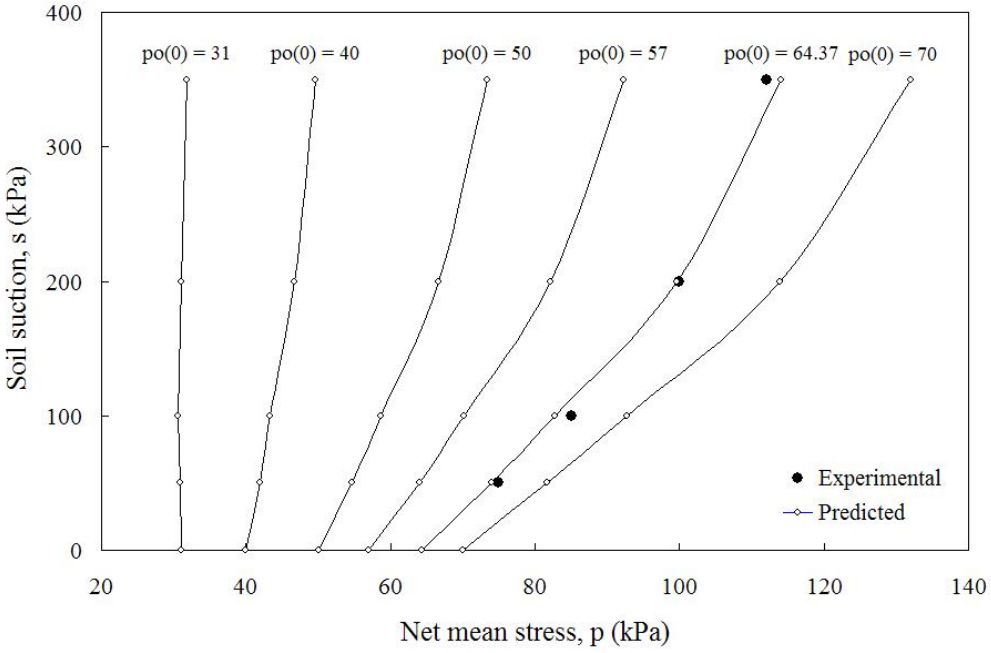

Figure 7.54 Experimental yield stress value, $p_o(s)$, along the best fit LC curve and typical LC curves predicted for different values of $p_o(0)$ - Equation (7.38).

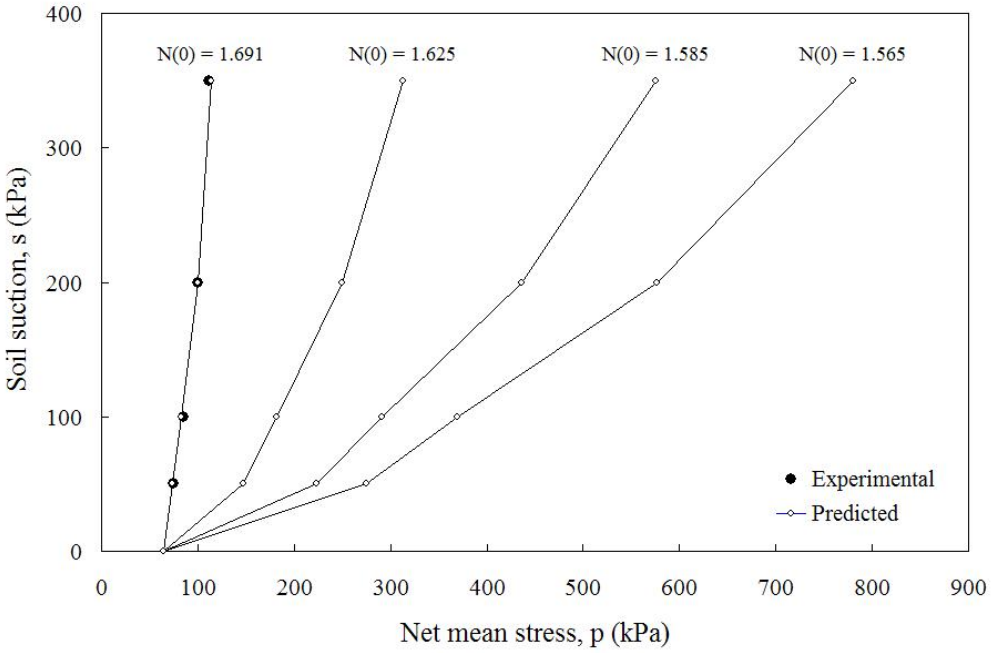

Figure 7.55 Experimental yield stress value, $p_o(s)$, along the best fit LC curve and typical LC curves predicted for different values of N(0) using - Equation (7.38).

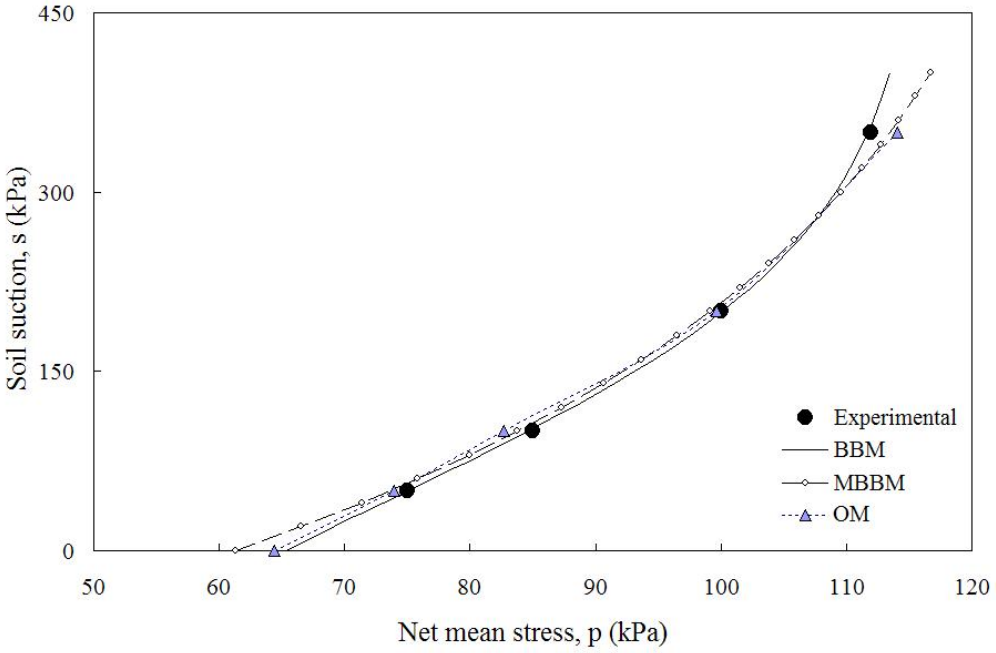

Figure 7.56 Experimental yield stress value, $p_o(s)$, along the best fit LC curves proposed by Wheeler and Sivakumar (1995), Alonso et al. (1990) and Josa et al. (1992).

7.6.4 Model Parameters Associated With Shear Strength

The results of the CTC and TC tests, presented in Figure 7.14 to Figure 7.17, were used to determine the slope of the critical state line in the p – q plane, M(s), and its intersection with the deviatoric stress axis, μ(s). Figure 7.57 shows the critical state value of deviatoric stress, q, plotted against the net mean pressure, p, for shear tests conducted at constant matric suction, s = 50 kPa, s = 100 kPa, and s = 200 kPa. The critical state condition has been previously determined to occur at approximately 15% of the total shear strain ε_q^{tot}.

The critical state line at constant matric suction, s, can be represented by a linear equation as

$$q = M(s)p + \mu(s) \tag{7.39}$$

The best fit values of parameters M(s) in Equation (7.33) for matric suction values, s = 50 kPa, s = 100 kPa, s = 200 kPa, were found to be, M(50) = 0.963, M(100) = 0.971, M(200) = 0.975, respectively. Furthermore, the parameters, μ(50) = 79.29 kPa, μ(100) = 105.16 kPa, μ(200) = 139.41 kPa, were identified for constant matric suction, s = 50 kPa, s = 100 kPa, s = 200 kPa, respectively. Both the slope M(s) and the intercept μ(s) of the critical state line were found to be function of soil suction. The experimental data along with the predicted values in the p-q plane are presented in Figure 7.58. Good agreement is observed between the experimental and predicted values. This observation is corroborated by the results presented in Figure 7.59 and a correlation coefficient of 0.998.

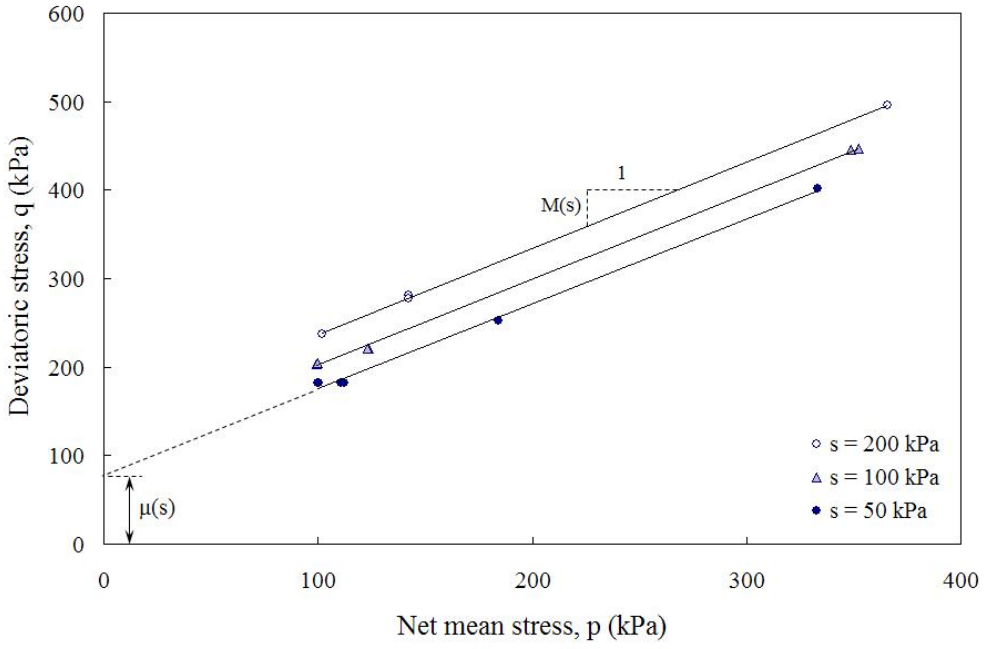

Figure 7.57 Experimental deviatoric stress, q, plotted against net mean stress, p, at critical state.

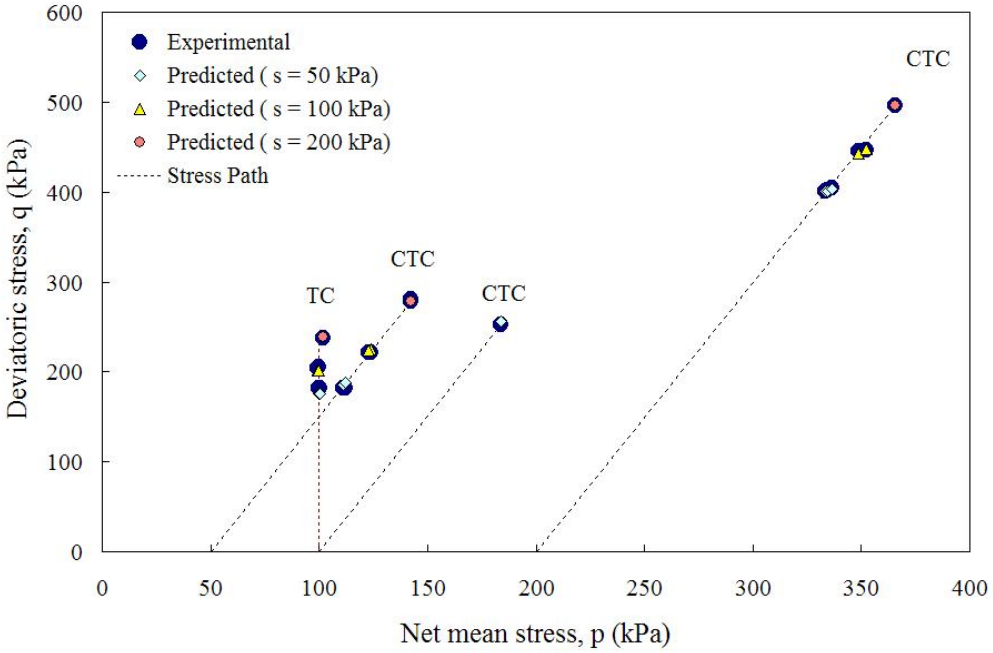

Figure 7.58 Experimental and predicted values of the deviatoric stress, q, using the model proposed by Wheeler and Sivakumar.

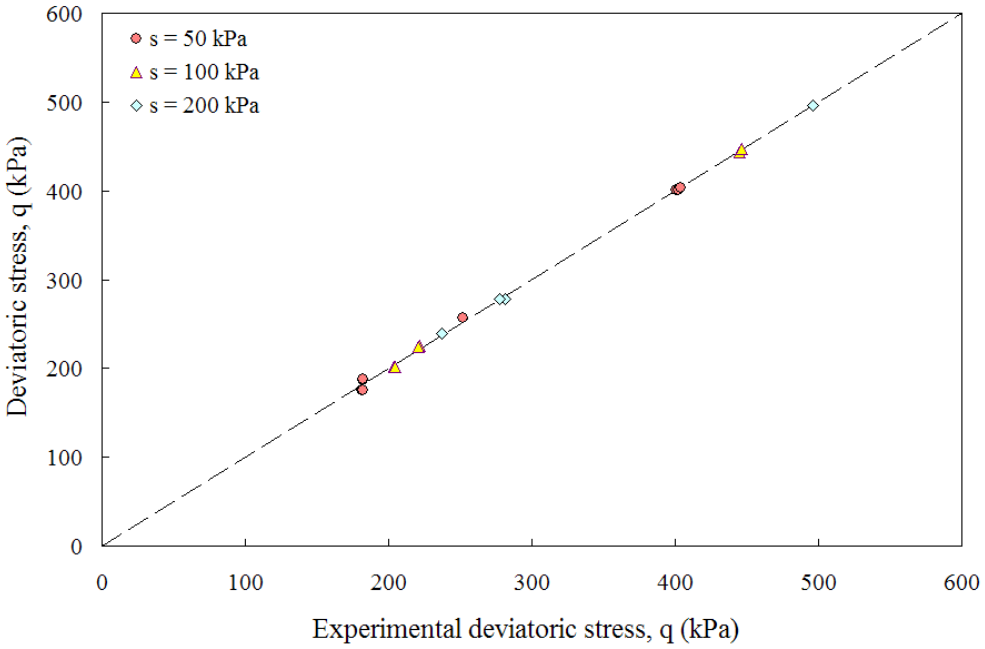

Figure 7.59 Comparison between experimental and predicted values of the deviatoric stress, q, using the model proposed by Wheeler and Sivakumar.

As established by Wheeler and Sivakumar (1995), the slope of the critical state line (CSL) varies with the matric suction, s. The assumption of constant M, proposed in the critical state model developed by Alonso et al. (1990) could be a reasonable approach to reduce the complexity of the model. Therefore, the linear equation in Equation (7.39) with constant parameters, M = 0.956 and μ = 103.8 kPa, can be fitted to the experimental data as shown in Figure 7.60. However, no good agreement is observed between the experimental data and the predicted values as shown in Figure 7.61 and Figure 7.62.

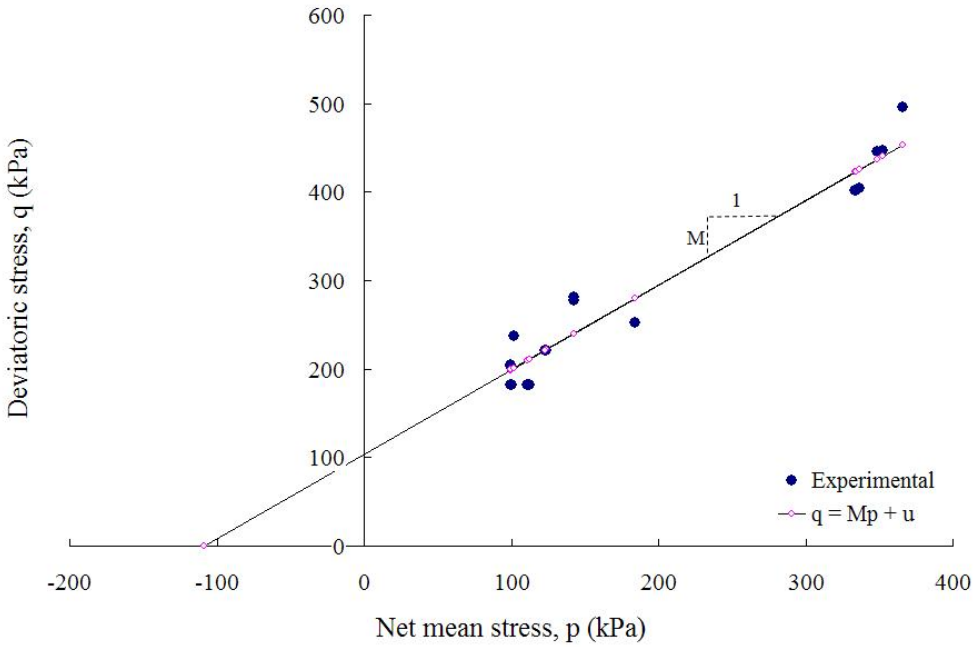

Figure 7.60 Experimental and predicted values of the deviatoric stress, q, using linear regression, q = Mp + μ.

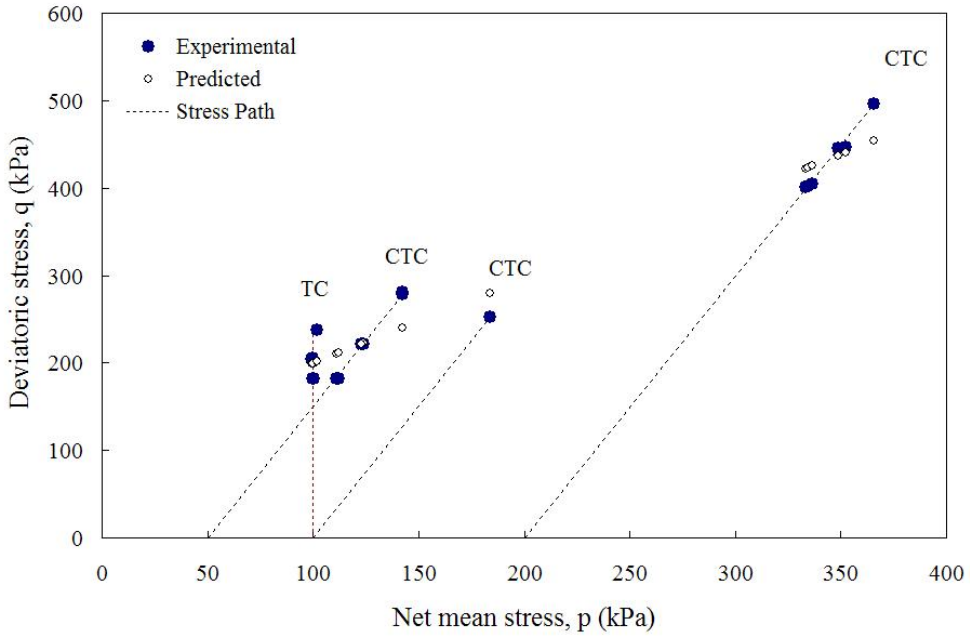

Figure 7.61 Experimental and predicted values of the deviatoric stress, q, using the model proposed by Wheeler and Sivakumar.

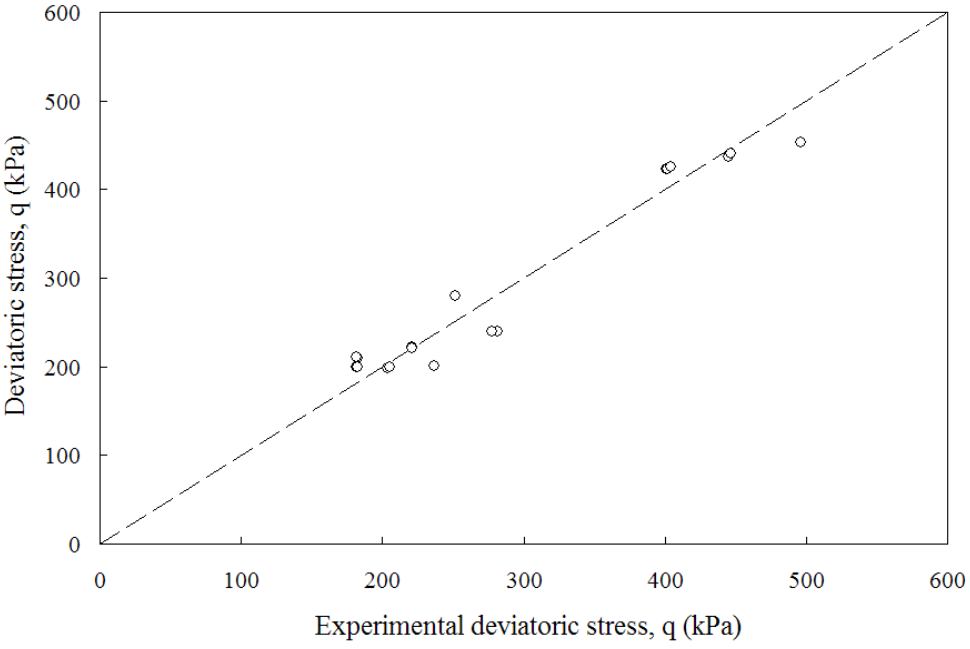

Figure 7.62 Comparison between experimental and predicted values of the deviatoric stress, q, using the model proposed by Wheeler and Sivakumar.

On the other hand, it can be observed in Figure 7.63 that the intercept of the critical state line, $\mu(s)$, varied in a non linear fashion with the matric suction, s. This observation is consistent with the experimental data presented by Wheeler and Sivakumar (1995), Escario and Saez (1996) and Laikram (2007). Variation on $\mu(s)$ would be equivalent to variation of ϕ^b with suction in the shear strength expression (Equation 3.42) reported by Fredlund et al. (1978). Figure 7.64 shows the curvature of the lines joining the deviatoric stress, q, obtained at different values of initial net mean stress, p_{ini}, for shearing tests conducted on cubical SP-SC soil specimens at constant matric suction, s = 50 kPa, s = 100 kPa, and s = 200 kPa. Although, the results presented in Figure 7.64 are not conclusive due to the low number of matric suctions selected for tests purposes, the results agree with that presented by Escario and Saez (1996) and support their affirmation of the existence of a non constant ϕ^b parameter.

Similarly, the results of the CTC and TC tests, presented in Figure 7.14 to Figure 7.17, were used to determine the slope of the critical state line in the p – v plane, $\psi(s)$, and its intersection with the specific volume, v = 1 + e, axis, $\Gamma(s)$. Figure 7.57 shows the critical state value of specific volume, v = 1 + e, plotted with the net mean pressure, p, for shear tests conducted at constant matric suction, s = 50 kPa, s = 100 kPa, and s = 200 kPa. The critical state line at constant matric suction, s, can be represented by a linear equation as

$$v = \Gamma(s) - \psi(s) \ln \frac{p}{p_{atm}} \qquad (7.40)$$

The best fit values of parameters $\psi(s)$ in Equation (7.40) for matric suction values, s = 50 kPa, s = 100 kPa, s = 200 kPa, were found to be, $\psi(50) = 0.2268$, $\psi(100) = 0.2380$, $\psi(200) = 0.2804$, respectively. In addition, the parameters, $\Gamma(50) = 1.416$ kPa, $\Gamma(100) = 1.459$ kPa, $\Gamma(200) = 1.530$ kPa, were identified for constant matric suction, s = 50 kPa, s = 100 kPa, s = 200 kPa, respectively. The experimental data along with the predicted values in the p – v plane are presented in Figure 7.65.

Table 7.5 summarizes the experimental values of the parameters required to solve the model proposed by Wheeler and Sivakumar (1995).

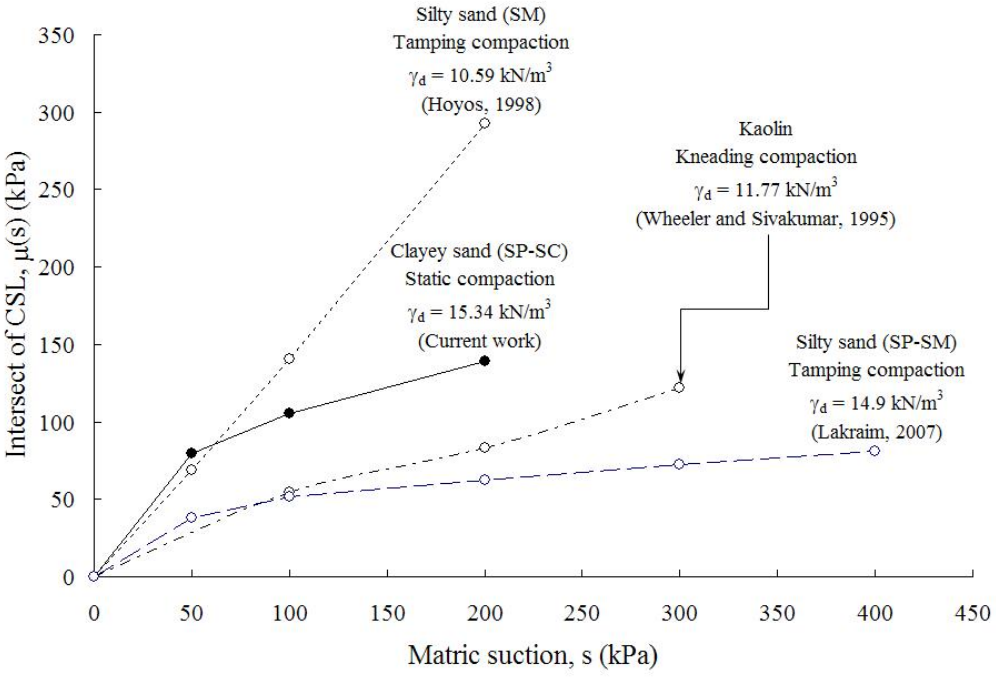

Figure 7.63 Experimental variation of CSL intercept, $\mu(s)$, with matric suction, s.

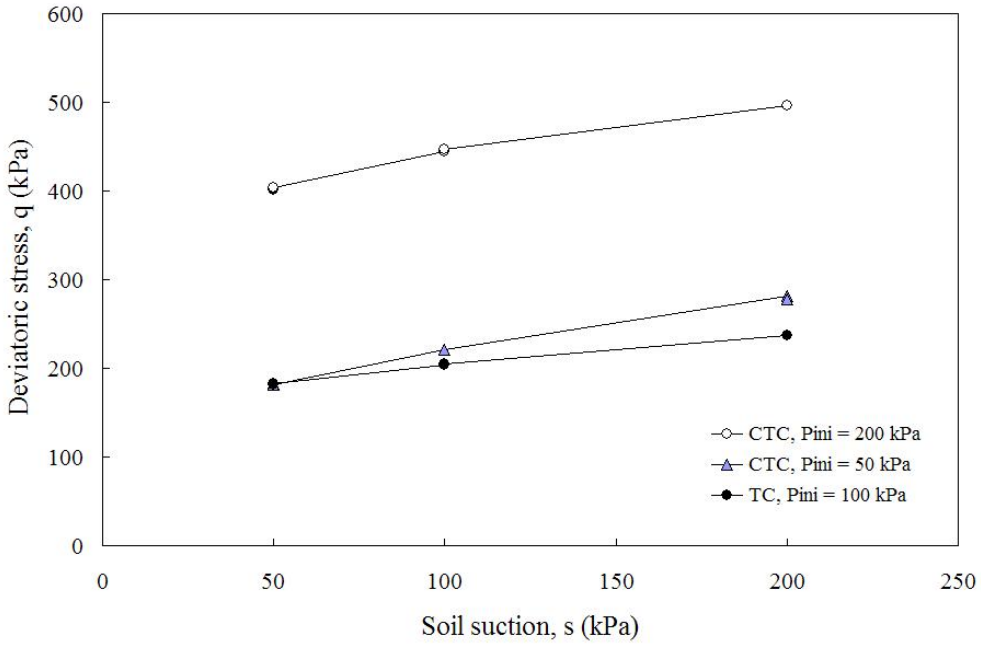

Figure 7.64 Deviatoric stress, q, versus soil suction, s, for different values of initial net mean stress, p_{ini}.

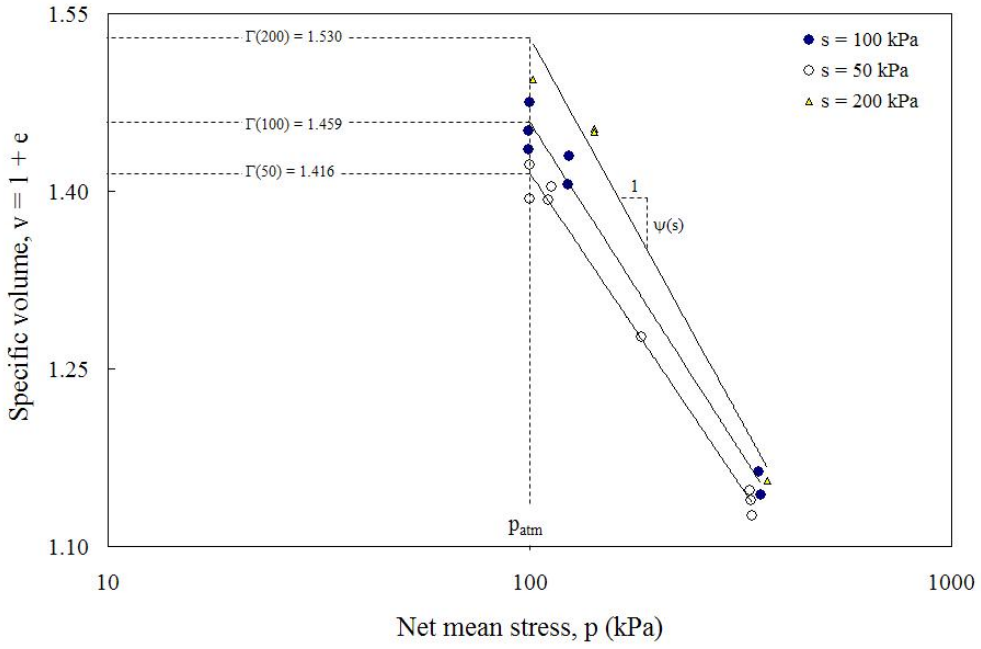

Figure 7.65 Experimental specific volume plotted against net mean stress, p, at critical state – p in logarithmic scale.

Table 7.5 Experimental values of model parameters used to validate the Oxford Model

S (kPa)	λ(s)	N(s)	M(s)	μ(s) (kPa)	ψ(s) (kPa)	Γ(s)
0	0.1460	1.691				
50	0.1275	1.700	0.963	79.29	0.2268	1.416
100	0.1157	1.704	0.971	105.16	0.2380	1.459
200	0.1033	1.707	0.975	139.41	0.2804	1.530
350	0.097	1.703				

7.6.5 Shear Modulus

Wheeler and Sivakumar (1995) adopted an associative flow rule to predict the development of plastic shear strain during constant suction shear loading. Although the shear modulus, G, likely varies with both, matric suction, s, and net mean stress, p, Wheeler and Sivakumar (1995) also assume a constant value for shear modulus, G. Hence, based on the initial linear section of the stress-strain curve the elastic components of shear strain can be predicted by considering a shear modulus, G, equal to the average value of the slope of the initial linear section of the experimental stress-strain curve. An average value of G = 5500 kPa has been obtained from the constant-suction tests for which the shearing path has been followed.

7.7 Implementation of Oxford Model

Similar to Alonso et al. (1990) the authors propose the use of an elliptical yield surface equivalent to the modified Cam clay model for saturated soils proposed by Roscoe and Burland (1968). However, the aspect ratio of the ellipse in not controlled by the slope of the critical state line, M, as proposed in the modified Cam clay model. Instead, Wheeler and Sivakumar (1995) proposed the aspect ratio, M_*, of the ellipse,

which is a function of soil matric suction and the size of the yield surface (Equation (7.36)). As shown in Figure 7.66, the explicit integration procedure described in section 8.3 can be extended to solve the constitutive relations proposed by Wheeler and Sivakumar (1995).

The constitutive framework defined by Equations (8.35) to (8.40) together with the initial state of the soil specimen and test conditions, has been used to predict the shear strain variation with the increment of the deviatoric stress.

7.7.1 Conventional Triaxial Compression Test

Figure 7.67, Figure 7.68, and Figure 7.69, show the comparison of experimental and predicted stress-shear strain relationship resulting from drained CTC tests conducted on cubical SP-SC soil specimens at different values of constant matric suction, s = 50 kPa, s = 100 kPa, and s = 200 kPa, with initial values of net mean stress, p_{ini} = 50 kPa, p_{ini} = 100 kPa, and p_{ini} = 200 kPa. The predicted values of shear strain obtained by using the Oxford Model show better agreement with the experimental data than the predictions obtained with both, the BBM and the MBBM.

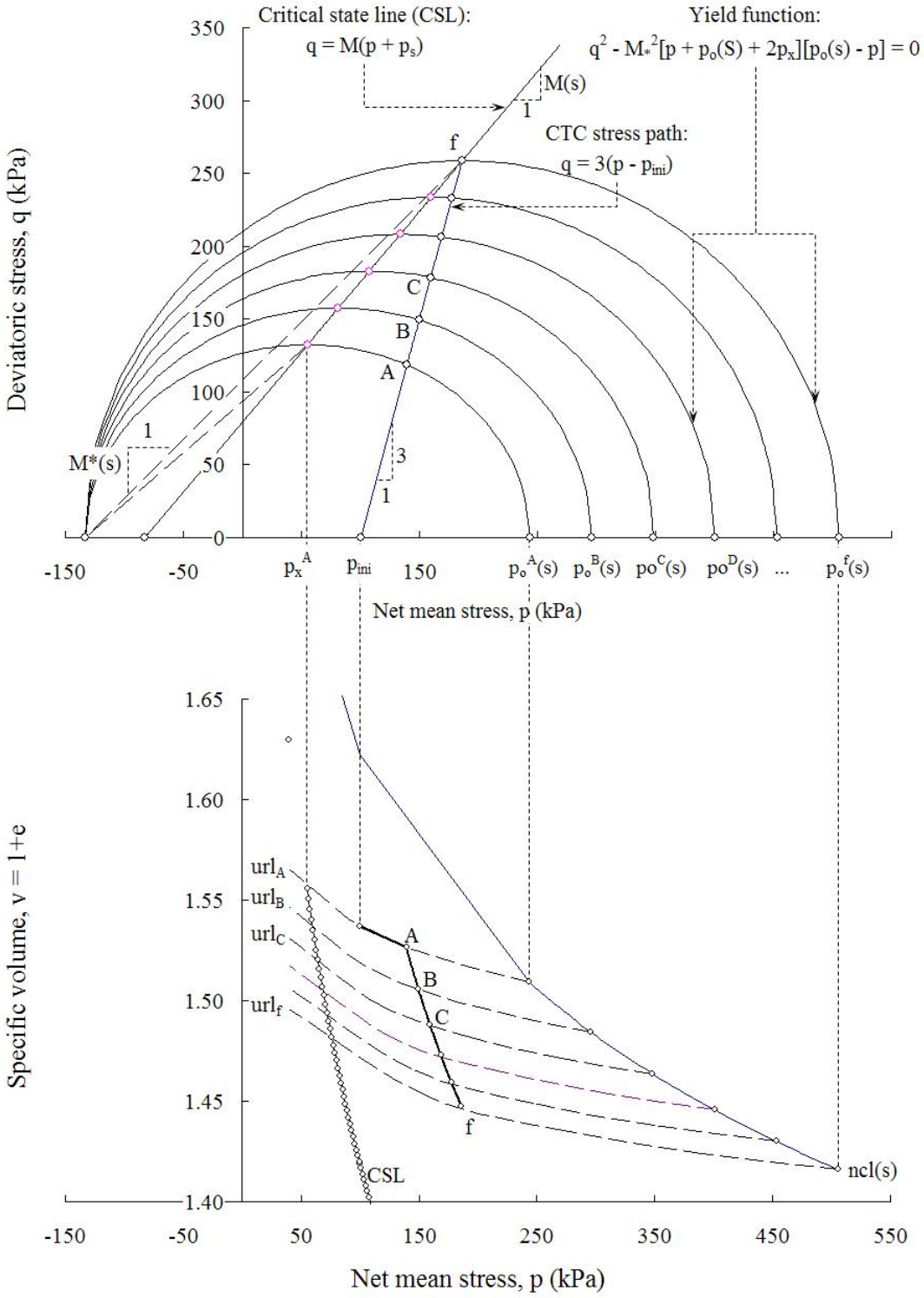

Figure 7.66 Successive yield surfaces and associated url using Oxford Model to predict results from a CTC test conducted on a lightly overconsolidated soil.

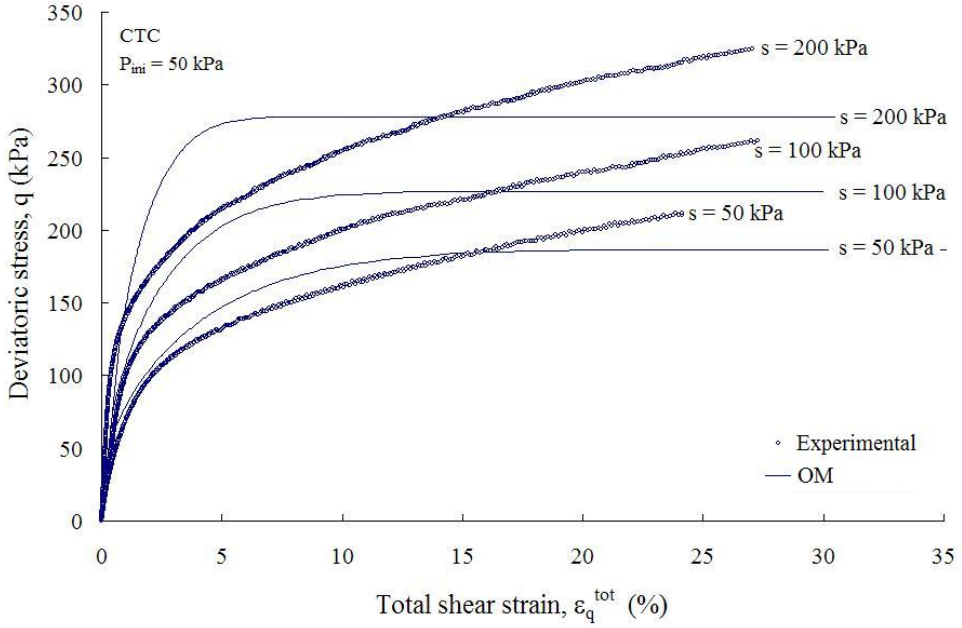

Figure 7.67 Measured and predicted stress-shear strain relationship from drained CTC tests conducted on compacted SP-SC soil specimens at constant matric suction and initial mean stress, p_{ini} = 50 kPa – Oxford Model.

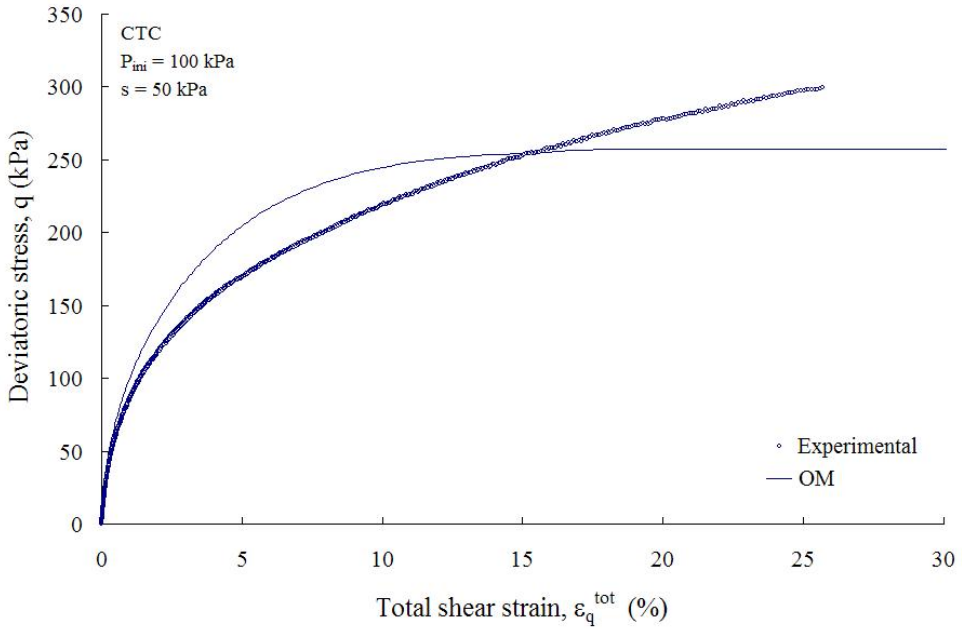

Figure 7.68 Measured and predicted stress-shear strain relationship from drained CTC tests conducted on compacted SP-SC soil specimens at constant matric suction and initial mean stress, p_{ini} = 100 kPa – Oxford Model.

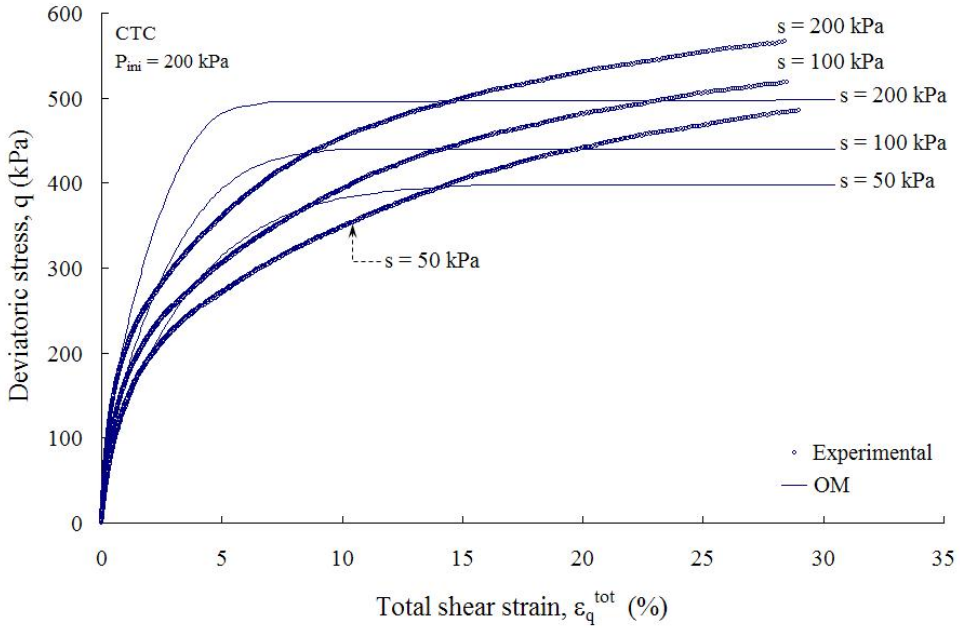

Figure 7.69 Measured and predicted stress-shear strain relationship from drained CTC tests conducted on compacted SP-SC soil specimens at constant matric suction and initial net mean stress, p_{ini} = 200 kPa – Oxford Model.

7.7.2 Triaxial Compression Test

Figure 7.45 shows the comparison of experimental and predicted stress-shear strain relationship resulting from drained TC tests conducted on cubical compacted SP-SC soil specimens. The tests were conducted for different values of constant matric suction, s = 50 kPa, s = 100 kPa, and s = 200 kPa, with initial values of net mean stress, p_{ini} = 100 kPa. Numerical predictions were calculated using explicit integration technique to solve the Oxford Model.

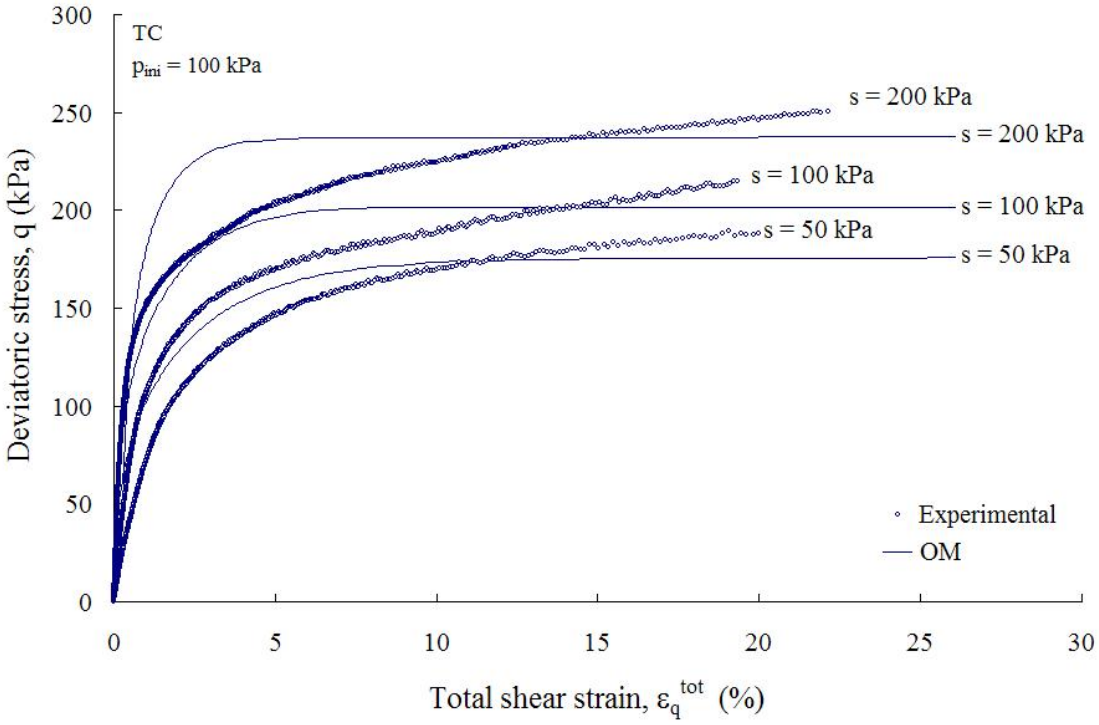

Figure 7.70 Measured and predicted stress-shear strain relationship from drained TC tests conducted on compacted SP-SC soil specimens at constant matric suction and initial net mean stress, p_{ini} = 100 kPa – Oxford Model.

7.8 Refined Barcelona Basic Model

Alonso et al. (1990) assumed that the slope of the normal compression line, λ(s), decreases with the increase in soil suction, s. Although the experimental results presented in this research works support this assumption, Wheeler and Sivakumar, (1995) shown experimental evidence of normal compression lines where the stiffness parameter, λ(s), increased with increase in suction. To overcome this limitation, Josa et al. (1992) proposed a modified elasto-plastic model for partially saturated soils which incorporates curved compression lines. However, this type of refinement can be avoided considering a value greater than 1 for the constant related to the maximum stiffness of

the soil, r, in Equation (7.4). Therefore, values of r parameter greater than 1 will extend the applicability of the BBM to consider the possibility of result stiffness parameter, $\lambda(s)$, increasing with increase in soil suction, s (Wheeler et al. 2002).

On the other hand, the model proposed by Wheeler and Sivakumar (1995) although produce better results; no good agreement is observed between the experimental and predicted values. In addition, the Oxford Model does not allow prediction of soil response for matric suction different to those evaluated experimentally in the laboratory. Moreover, a more complicated expression for the LC yield curve which requires the determination of additional parameters is proposed to replace the expression proposed by Alonso et al. (1990). On the other hand, the inclusion of the aspect ratio, M*, different to the slope of the critical state line, M, add to the model a degree of freedom which could result in illogical predictions of the yield surface in the p – q plane. These limitations together with the large number the parameters required become a disincentive in the use of this model.

Therefore, considering the limited improvement achieved with the modifications proposed by Josa et al. (1992) and the complexity and large number of parameters required by the model proposed by Wheeler and Sivakumar (1995), special attention has been focused in the Barcelona Basic Model originally proposed by Alonso et al. (1990) in order to preserve a simple model. Some modifications to the Barcelona Basic Model as well as the calibration process proposed by Alonso et al. (1990) are recommended in this section to improve the ability of the model to predict the soil response of a soil specimen under shearing loading.

7.8.1 Loading Collapse (LC) Yield Curve

Although the LC yield curve plays an important role in the development of the Barcelona basic model proposed by Alonso et al. (1990), its importance become diminished when the model is solved for separated values of soil suction, s. As shown in Figure 7.71, for lightly overconsolidated specimens subjected to a shear loading path (i.e. $p_o(s) > p_{ini}$), the initial yield surface and consequently the region were only plastic deformation are experienced by the soil will be defined by the LC yield curve. However, Figure 7.72 shows that for normally consolidated specimens (i.e. $p_o(s) \leq p_{ini}$) the LC yield curve does not play any role in the evolution of the yield surface. In this case, the initial yield surface will be defined by the initial net mean stress, p_{ini}.

On the other hand, for identically prepared soil specimens with the same initial conditions of confinement (i.e. p_{ini}) the initial net mean yield stress, $p_o(s)$ could be lower than p_{ini} for low values of constant matric suction, s, and higher than p_{ini} for high values of matric suction, s. As shown in Figure 7.73, the initial net mean stress, p_{ini}, will define the initial yield surface for low values of matric suction, s, were the soil behaves as normally consolidated (i.e. $p_o(s) \leq p_{ini}$). Once the increase in suction generates a net yield stress, $p_o(s)$, which become larger that the p_{ini}, the specimen will behave as a lightly overconsolidated (i.e. $p_o(s) > p_{ini}$) and the initial yield surface will be defined by the LC yield curve.

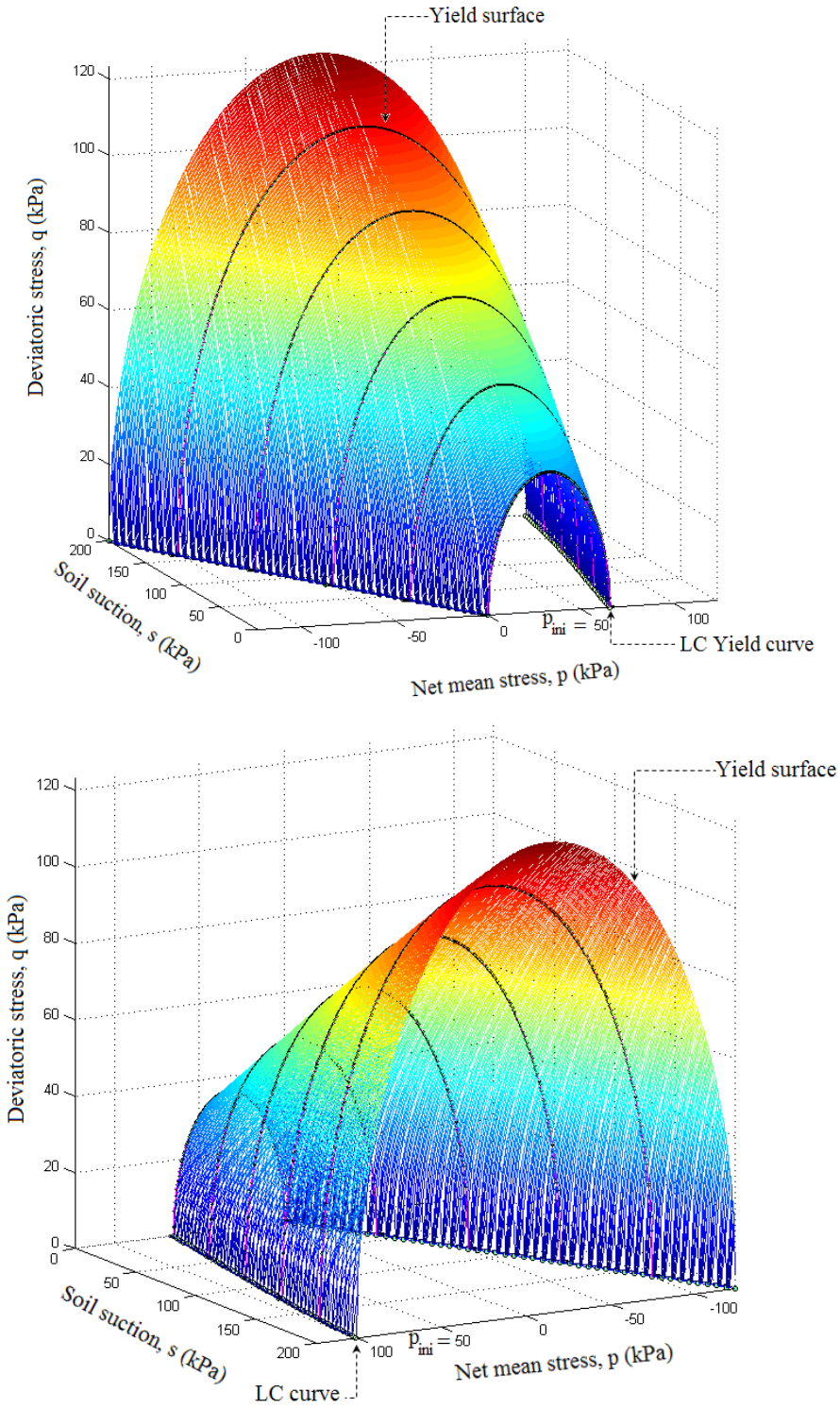

Figure 7.71 Three-dimensional yield surface for a lightly overconsolidated SP-SC soil specimen subjected to CTC stress path (BBM).

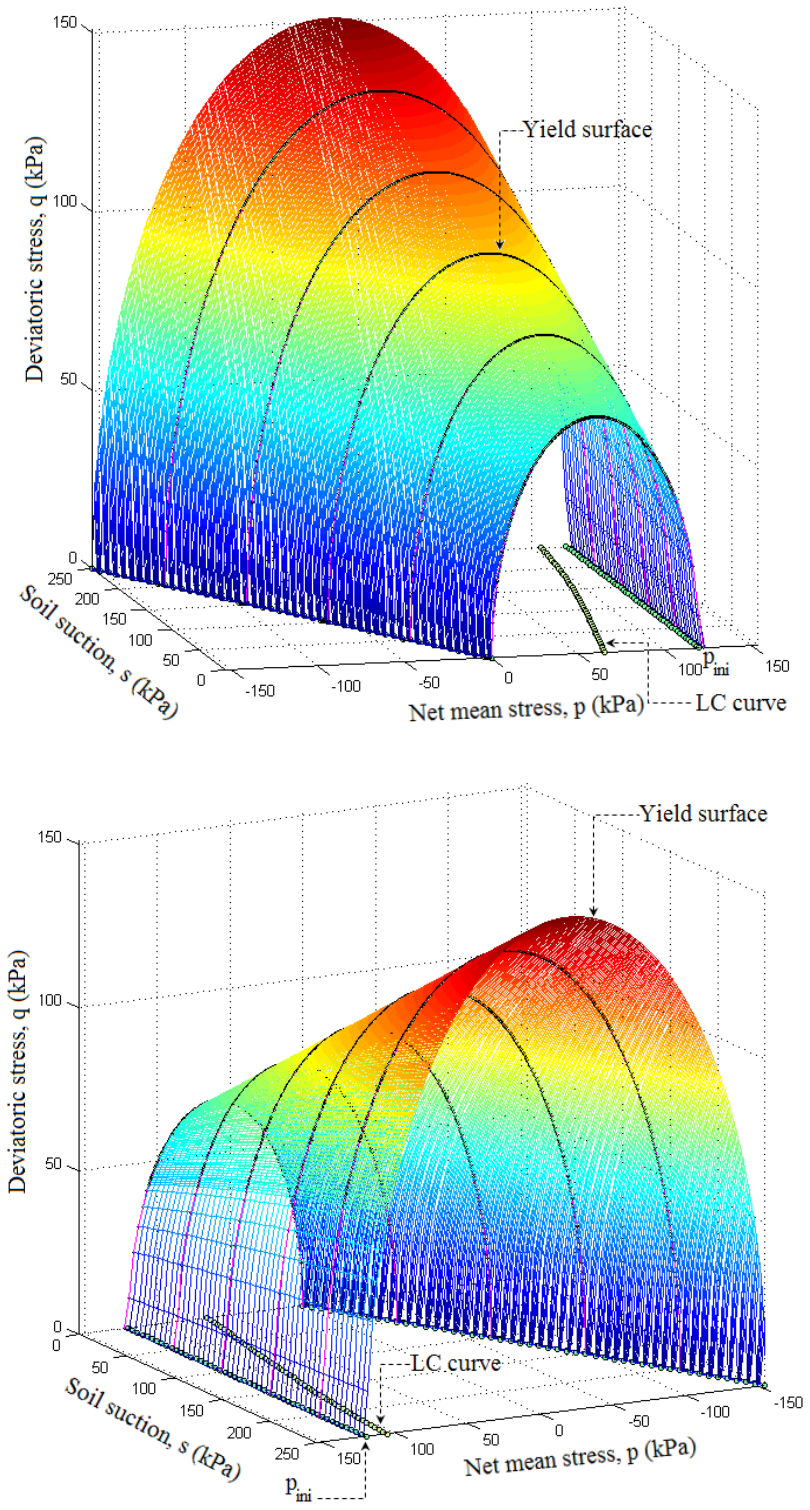

Figure 7.72 Three-dimensional yield surface for a normally consolidated SP-SC soil specimen subjected to CTC stress path (BBM).

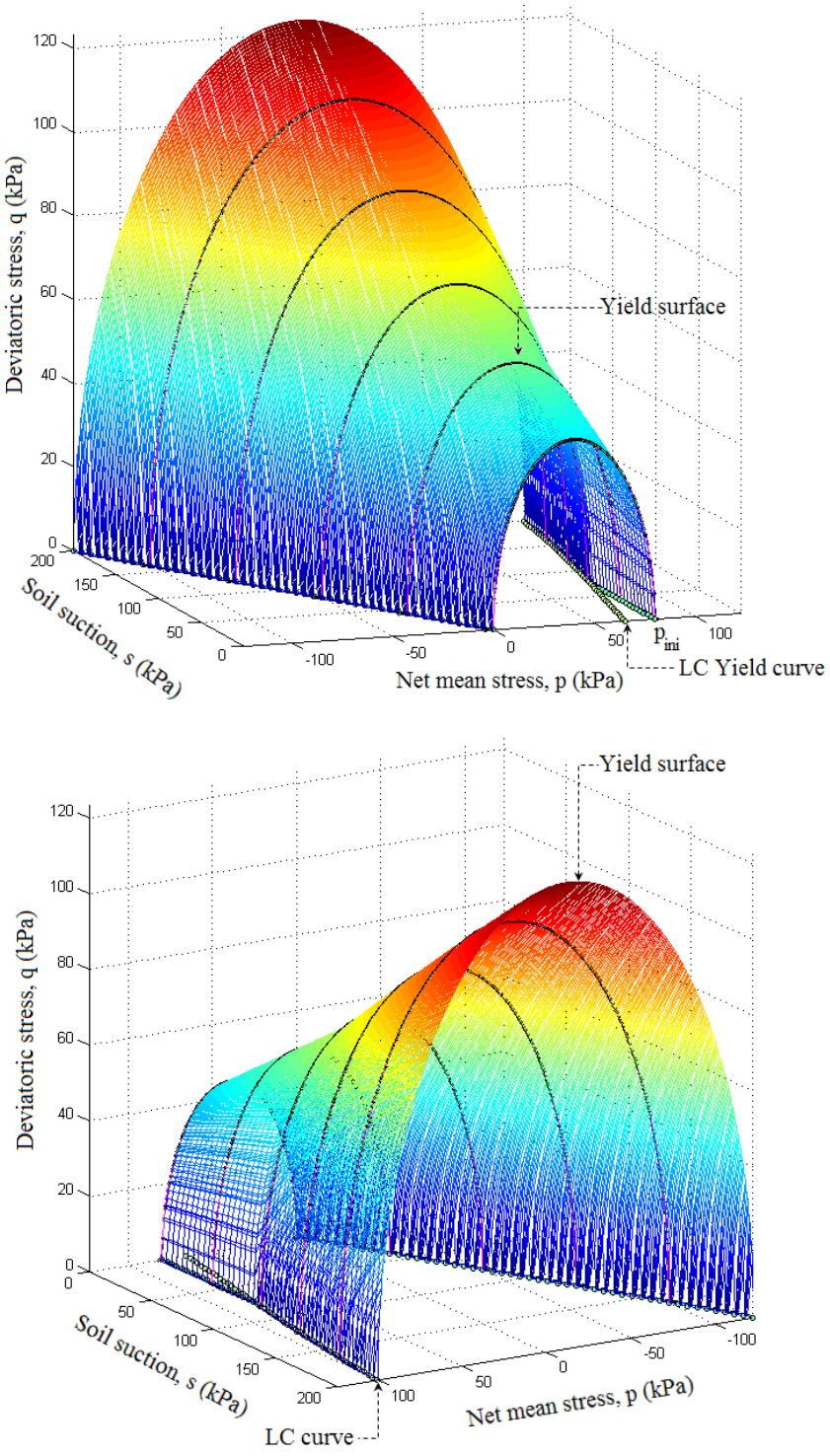

Figure 7.73 Effect of matric suction, s, in the behaviour of an unsaturated SP-SC soil specimen (BBM).

Therefore, due to the low impact of the LC yield curve on the development of the yield surface and considering the results presented in Figure 7.56, it is not convenient to introduce an additional degree of complexity in the determination of the initial net yield stress, $p_o(s)$, to the model originally proposed by Alonso et al. (1990).

7.8.2 Model Parameters Associated With Shear Strength

The major assumption of Alonso et al. (1990) is that the yield surface for a specimen at constant matric suction, s, will be described by an ellipse which will exhibit an isotropic preconsolidation stress, p_o. This assumption aggresses with the assumption established for the modified Cam clay model (Roscoe and Burland, 1968). In addition, the increase of strength induced by the increase in soil suction, s, is assumed to be adequately represented by an increase in cohesion, maintaining the slope of the critical state line (CSL) for saturated conditions. Two hypotheses have been established by Alonso et al. (1990) in order to guaranty the achievement of these assumptions. As a first hypothesis, the slope of the CSL, M, is considered constant and equal to the slope of the saturated condition. The second hypothesis states that the increase in apparent cohesion, p_s, due to the increase in matric suction, s, follows a linear relationship with suction (i.e. $p_s = ks$).

Experimental results presented in Figure 7.57 and Table 7.5 shown that the slope of the critical state line, M(s), in a SP-SC soil varies with suction, s. As shown in Figure 7.74, similar results have been reported by other researchers. However, considering the small variation of the slope M, it could be acceptable to assume a constant value of M, independent of soil suction, for the slope of the critical state line.

On the other hand, experimental results show clear evidence of a non-linear variation in the increase in cohesion, p_s, due to the increase in suction, s, in a SP-SC soil. Similar results in different type of soils have been reported for other authors. These results along with the experimental values obtained in this research work are presented in Figure 7.75. Therefore, considering that the increase in cohesion, p_s, is fundamental for the prediction of the yield surface in the p – q space, the prediction of the total shear strain, ε_q^{tot}, and the determination of the loading path; and consequently, the change in the specific volume, v = 1 + e, the hypothesis of linear relationship of the increase of cohesion, p_s, with suction, s, becomes a limitation in the BBM.

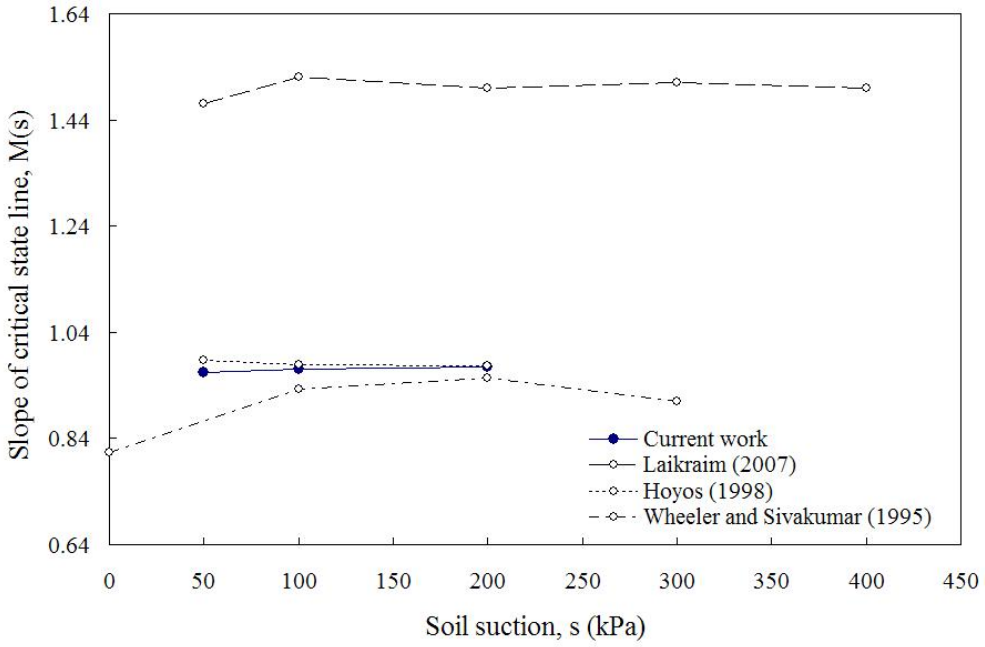

Figure 7.74 Variation of the slope of critical state line, M(s) with soil suction, s.

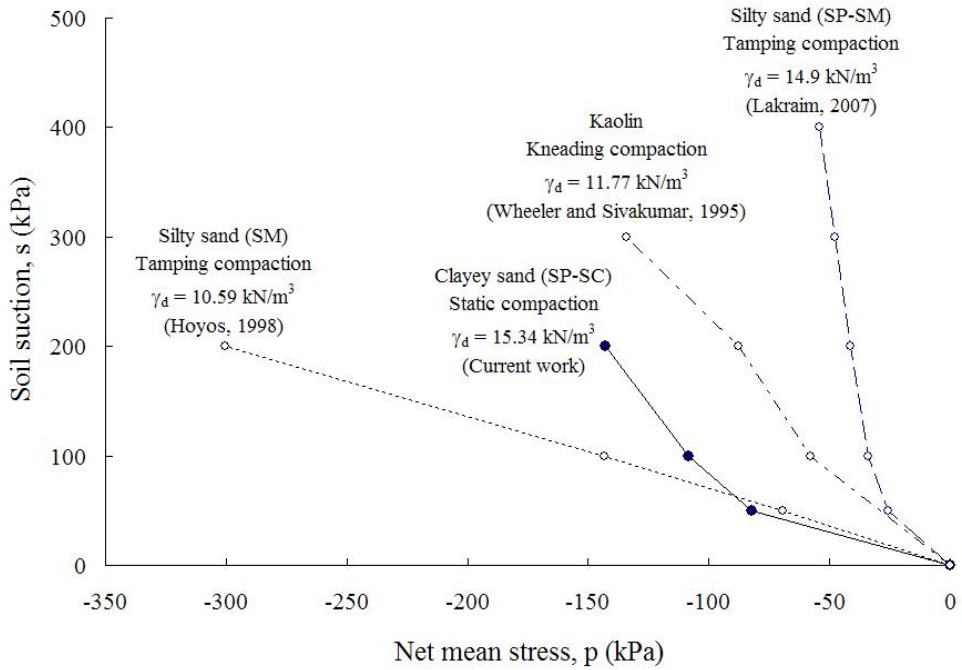

Figure 7.75 Variation in the increase in cohesion, p_s, due to the increase in suction, s

To overcome this limitation and consequently improve the prediction capability of the Barcelona Basic Model, a more general equation to calculate the increase in cohesion, p_s, is proposed in this research work. This new equation must consider the linear behavior in the increase in cohesion, p_s, initially assumed by Alonso et al. (1990). The simplest model that can be fitted to the experimental trend observed in this research work as well as these previously reported by Wheeler and Sivakumar (1995) and Laikram (2007), is the potential equation. Hence, continuing with the notation proposed by Alonso et al. (1990), the increase in cohesion, p_s, can be described by

$$p_s = ks^m \tag{7.41}$$

where

k = parameter controlling the magnitude of increase in cohesion, p_s, with suction

m = parameter controlling the curvature of the curve describing p_s.

7.8.3 Shear Modulus

The elastic strains induced by changes in deviatoric stress, q, in Barcelona Basic model are computed through the shear modulus, G, as described in Equation (7.8). Although the shear modulus, G, probably varies with both, matric suction, s, and net mean stress, p, the experimental data obtained in this research work is considered insufficient to validate the assumption of variable shear modulus, G. Hence, based on the initial linear section of the stress-strain curve the elastic components of shear strain can be predicted by considering a shear modulus, G, equal to the average value of the slope of the initial linear section of the experimental stress-strain curve. Therefore, no modifications are suggested in this matter.

7.8.4 Model Parameters Associated With Increase in Cohesion

The increase in cohesion, p_s, can be calculated using the p, q data obtained at critical state condition, which has been identified at approximately 15% of the total shear strain ε_q^{tot}. As shown Figure 7.76, experimental values of the slope of the critical state line, M(s), and its intersection with the deviatoric stress axis, B(s), can be used to calculate the increase in cohesion, p_s, as

$$p_s = -\frac{B(s)}{M(s)} \tag{7.42}$$

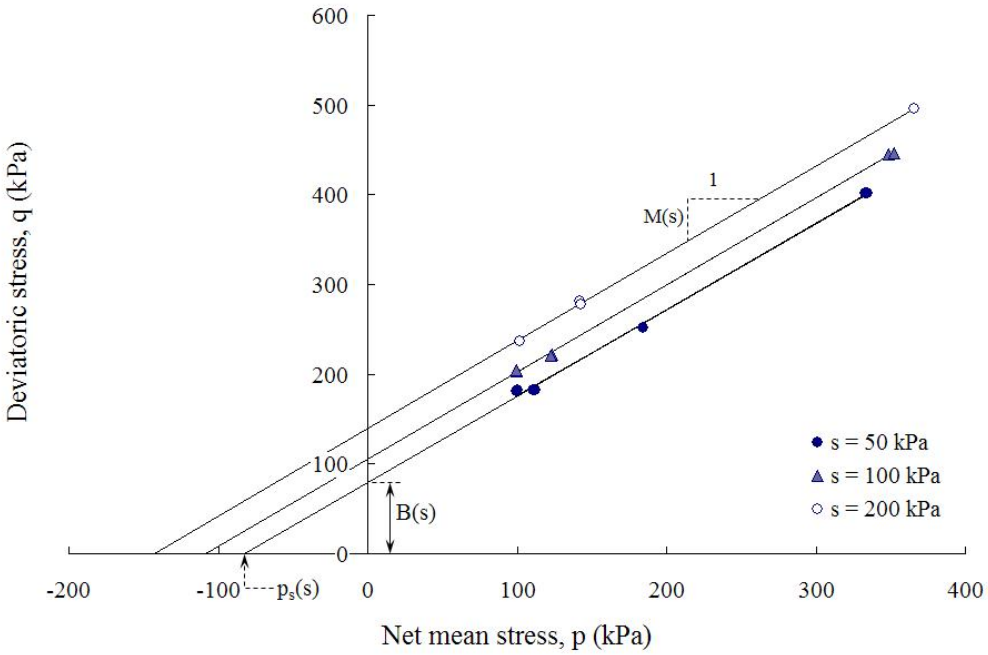

Figure 7.76 Variation of the increase in cohesion, p_s, with soil suction, s.

The least squares method has been used to approximately fit the Equation (7.41) to the experimental values obtained for change in cohesion, $p_s(0) = 0$ kPa, $p_s(50) = -82.3$ kPa, $p_s(100) = -108.36$ kPa, and $p_s(200) = -142.94$ kPa. The best fit values of the parameters k and m were found to be $k = 17.326$ and $m = 0.398$.

Figure 7.77 and Figure 7.78 show the experimental increase in cohesion with the predicted curves using Equation (7.41) for different values of k and m, respectively. Good agreement is observed between the experimental data and predicted values, which is confirmed by a correlation coefficient of 1.0. In addition, Figure 7.79 shows the experimental values of increase in cohesion, p_s, along the linear relationship proposed by Alonso et al. (1990) and the best fit curve as per Equation (7.41). No agreement is observed between the experimental data and the values predicted by using a linear relationship.

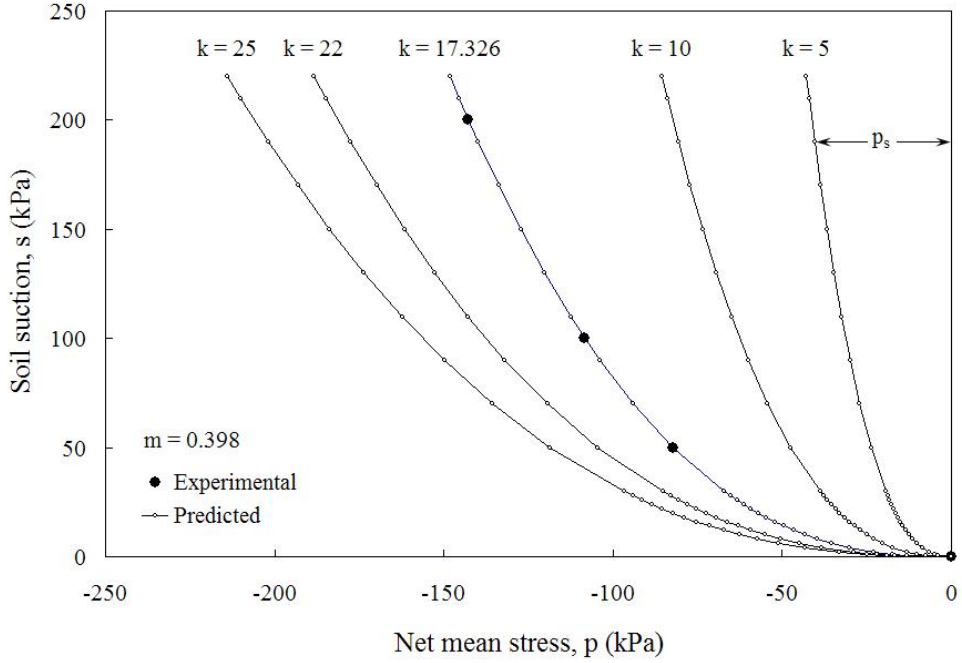

Figure 7.77 Experimental increase in cohesion, p_s, along the best fit curve and typical curves predicted for different values of k.

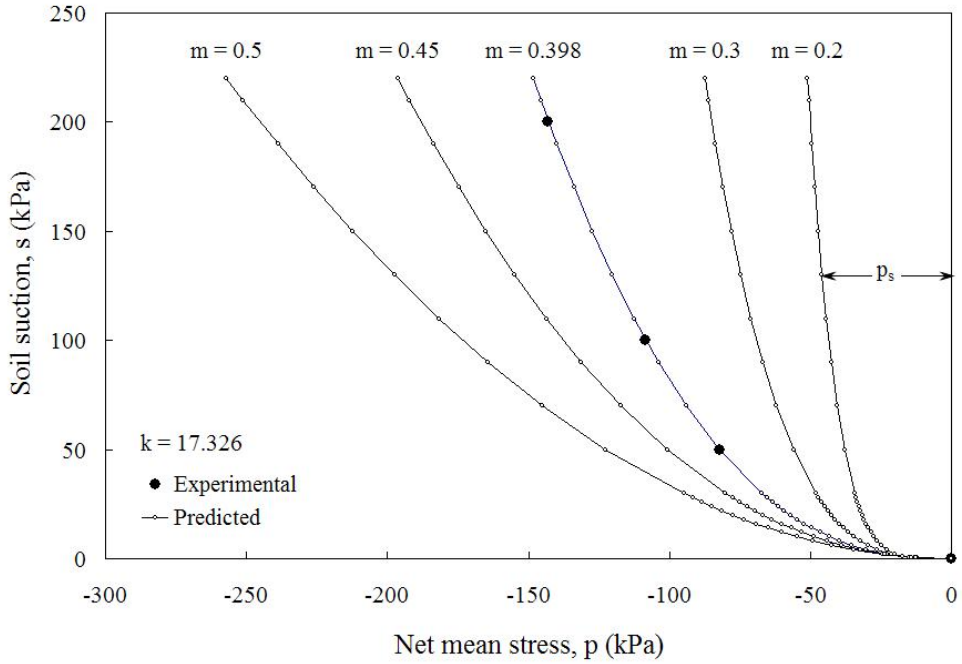

Figure 7.78 Experimental increase in cohesion, p_s, along the best fit curve and typical curves predicted for different values of k.

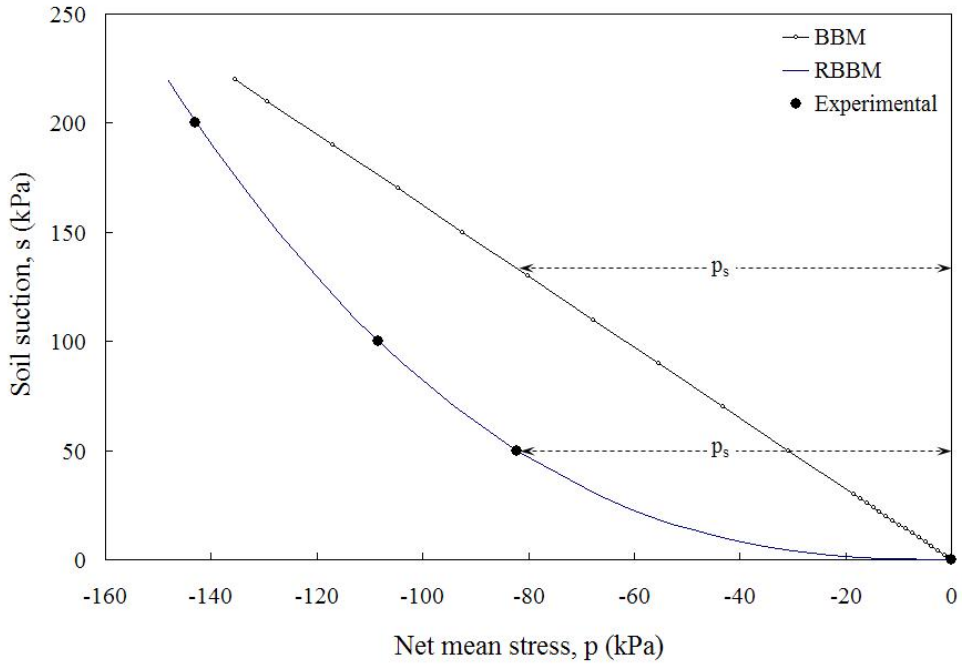

Figure 7.79 Experimental increase in cohesion, p_s, along the linear relationship proposed by Alonso et al. (1990) and the best fit curve as per Equation (7.41).

On the other hand, considering the small variation observed among the slope of the critical state line, M(s), with matric suction, s, it is necessary to evaluate the influence of the selection of the slope o the critical state line, M, in the final results of the Refined Barcelona Basic Model (RBBM). Two different calibration procedures are considered in this research work. The first alternative, is considering the slope of the critical state line, M(s), independent of matric suction, s. As described in section 8.6.4, a linear equation with constant parameters, M = 0.956 and u = 103.8 kPa, can be fitted to the experimental data. Although no good agreement is observed between the experimental data and the predicted values shown in Figure 7.61 and Figure 7.62, the effect of this assumption in the final results of the model will be evaluate latter in this section.

The second alternative, is considering the slope of the critical state line, M(s), varying with matric suction, s. In this case, no additional calibration will be required and the model must be evaluated by using the correspondent value of M(s) accordingly with the soil suction, s. The experimental values of the parameters required to predict the soil response using the Refined Barcelona basic model (RBBM) are summarized in Table 7.6.

Table 7.6 Experimental values of model parameters used to validate the RBBM

Parameter	Description	Value
$\lambda(0)$	Compressibility coefficient for the saturated state	0.146
r	Constant related to the maximum stiffness of the soil	0.649
β	Parameter which control the rate of soil stiffness with s	895.17×10^{-5} kPa^{-1}
p^c	Reference stress	31.922 kPa
$p_o(0)$	Saturated preconsolidation stress	65.44 kPa
κ	Compressibility coefficient along the elastic path	0.03138
M	Slope of the critical state line (CSL)	0.956
k	Parameter controlling the increase in cohesion with s	17.326
m	Parameter controlling the curvature of p_s	0.398
G	Elastic shear modulus	5500 kPa

7.9 Implementation of Refined Barcelona Basic Model

The procedure described in section 8.5 has been used to predict the soil response of soil samples subjected to drained suction-controlled shear loading path. The predicted values have been compared with the experimental results obtained from a series of suction-controlled shear loading (CTC, TC, TE, and SS) tests conducted on identically prepared specimens 3 in (7.62 cm) each side SP-SC soil. The RBBM has been evaluated assuming both a value of slope of the critical state line, M = 0.96, independent of soil suction, and values of M(s) varying as function of the soil suction.

7.9.1 Conventional Triaxial Compression Test

Figure 7.80, Figure 7.81, and Figure 7.82 show the predicted yield surface and the experimental stress state at failure resulting from a drained conventional triaxial compression (CTC) test conducted on different SP-SC soil specimens at constant matric suction, s = 50 kPa,100 kPa, and 200 kPa respectively. As expected, better results are obtained when the slope of the critical state line, M(s), depends on soil suction, s. However, considering the small difference between the predicted values of stress state at failure and its proximity to the experimental values, the assumption of constant M independent of soil suction, initially made by Alonso et al. (1990) could be a satisfactory approximation to reduce the complexity of the model.

In addition, Figure 7.83, Figure 7.84, and Figure 7.85 show the comparison between experimental and predicted stress-shear strain relationship resulting from the fully drained CTC tests conducted on cubical compacted SP-SC soil specimens at different values of constant matric suction, s = 50 kPa, s = 100 kPa, and s = 200 kPa, with initial values of net mean stress, p_{ini} = 50 kPa, p_{ini} = 100 kPa, and p_{ini} = 200 kPa. Although the RBBM does not perfectly fit the experimental data, better predictions are obtained. Additional adjustments to the model could be proposed in order to account for the variation of the variation of the shear modulus, G, with change in net mean stress, p, and matric suction, s. The expected yield surface at failure for untrained, suction-controlled CTC tests conducted on SP-SC specimens at initial net mean stress, p_{ini} = 200 kPa in the (p, q, s) space is presented in

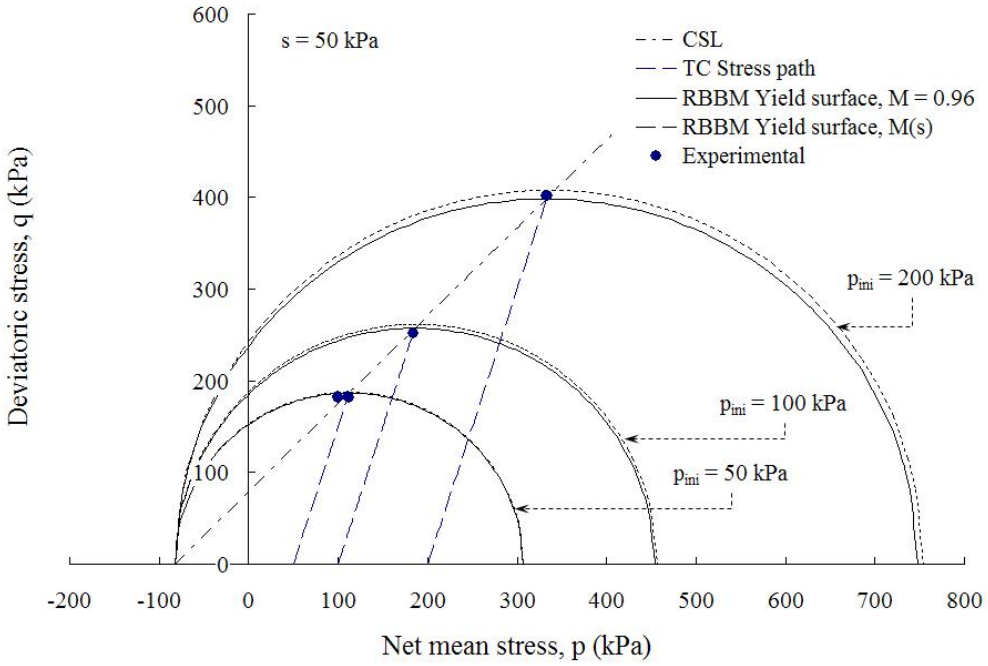

Figure 7.80 Predicted yield surface of RBBM in drained CTC tests at constant matric suction, s = 50 kPa and initial net mean stresses, p_{ini} = 50, 100, and 200 kPa.

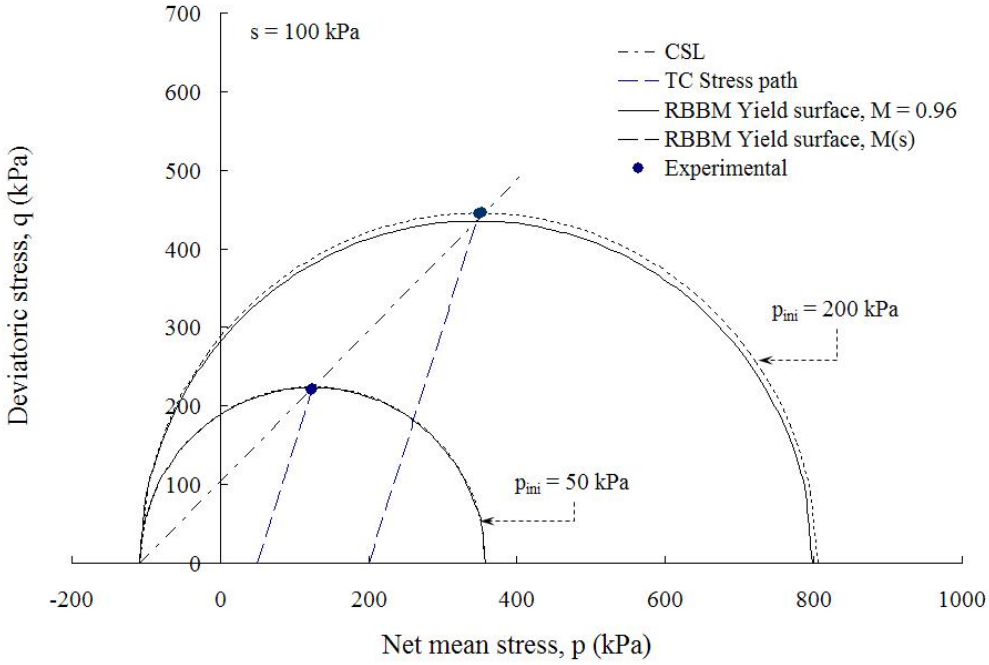

Figure 7.81 Predicted yield surface of RBBM in drained CTC tests at constant matric suction, s = 100 kPa and initial net mean stresses, p_{ini} = 50, 100, and 200 kPa.

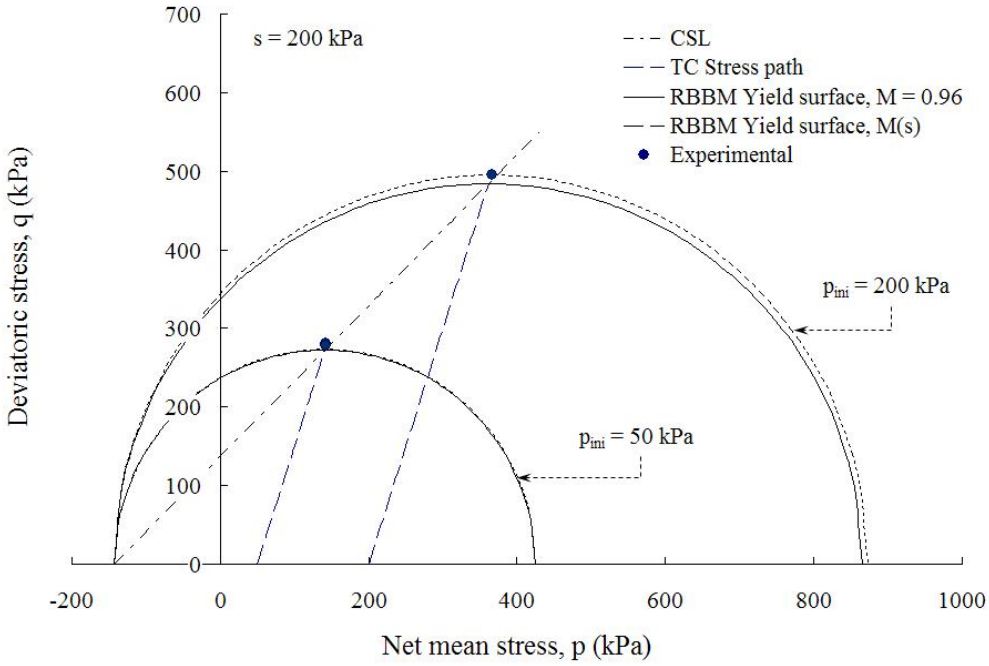

Figure 7.82 Predicted yield surface of RBBM in drained CTC tests at constant matric suction, s = 200 kPa and initial net mean stresses, p_{ini} = 50, 100, and 200 kPa.

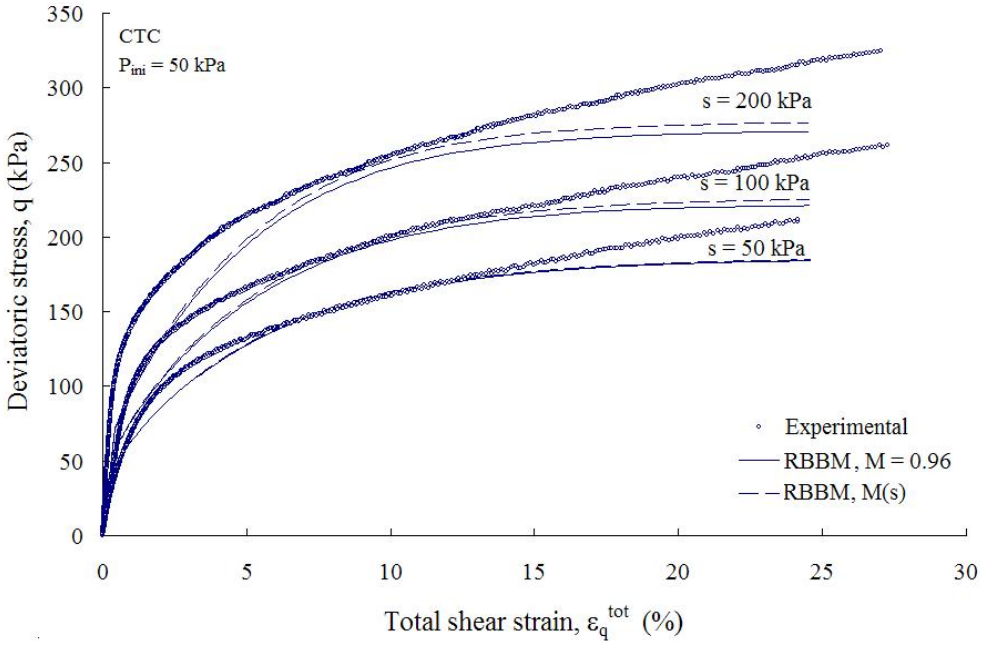

Figure 7.83 Measured and predicted stress-shear strain relationship from CTC tests on SP-SC soil at s = 50, 100, and 200 kPa and p_{ini} = 50 kPa (RBBM).

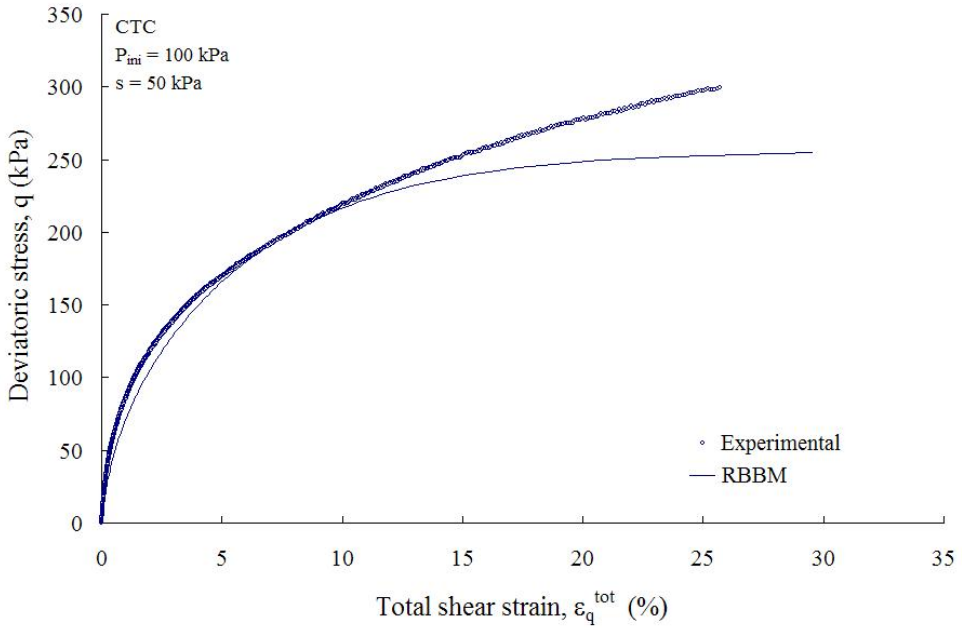

Figure 7.84 Measured and predicted stress-shear strain relationship from CTC tests on SP-SC soil at s = 50 kPa, and p_{ini} = 100 kPa (RBBM).

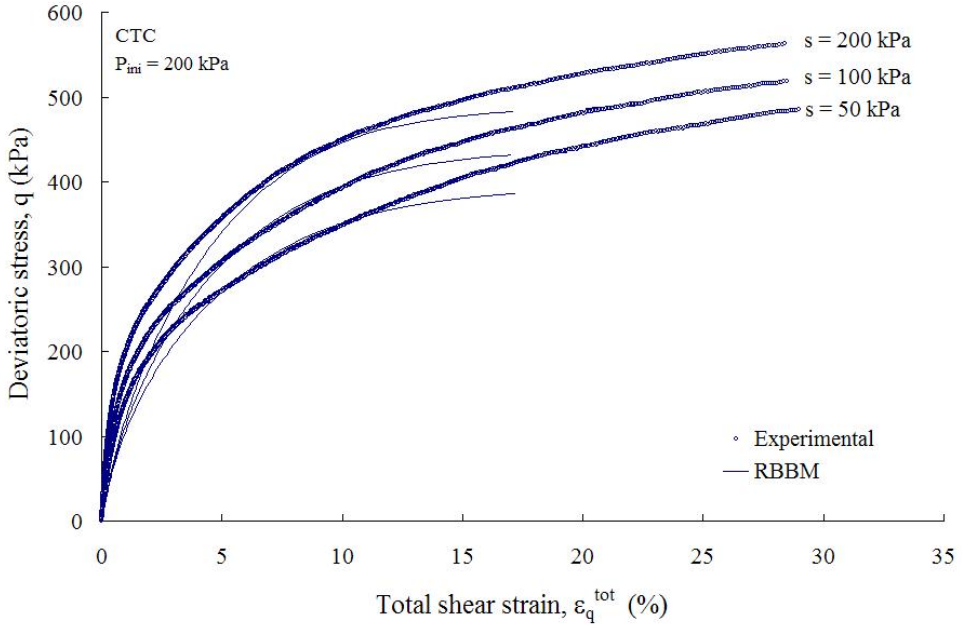

Figure 7.85 Measured and predicted stress-shear strain relationship from CTC tests on SP-SC soil at s = 50, 100, and 200 kPa, and p_{ini} = 200 kPa (RBBM).

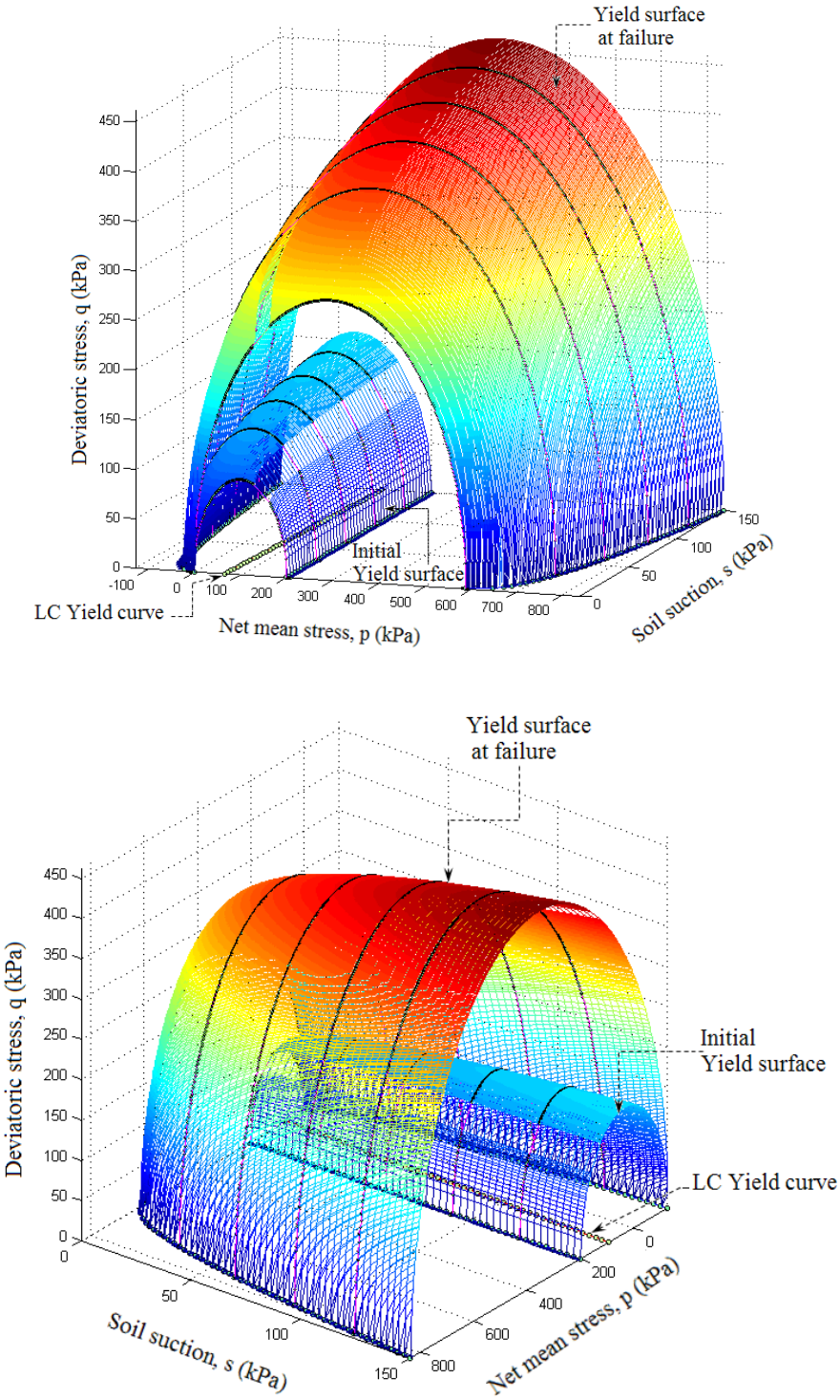

Figure 7.86 Expected yield surface at failure for untrained, suction-controlled CTC tests conducted on SP-SC specimens at p_{ini} = 200 kPa (RBBM).

7.9.2 Triaxial Compression Test

Similarly, Figure 7.87 shows the predicted yield surface and the experimental results drained triaxial compression (TC) test conducted on different SP-SC soil specimens at constant matric suction, s = 50,100, and 200 kPa and initial net mean stresses, p_{ini} = 100 kPa. In addition, Figure 7.45 shows the experimental and predicted stress-shear strain relationship resulting from the drained TC tests conducted on SP-SC soil specimens. The tests were conducted at initial net mean stress, p_{ini} = 100 kPa and different values of constant matric suction, s = 50 kPa, s = 100 kPa, and s = 200 kPa. In general, better agreement than that observed in BBM results is observed between the experimental and predicted values obtained with the RBBM.

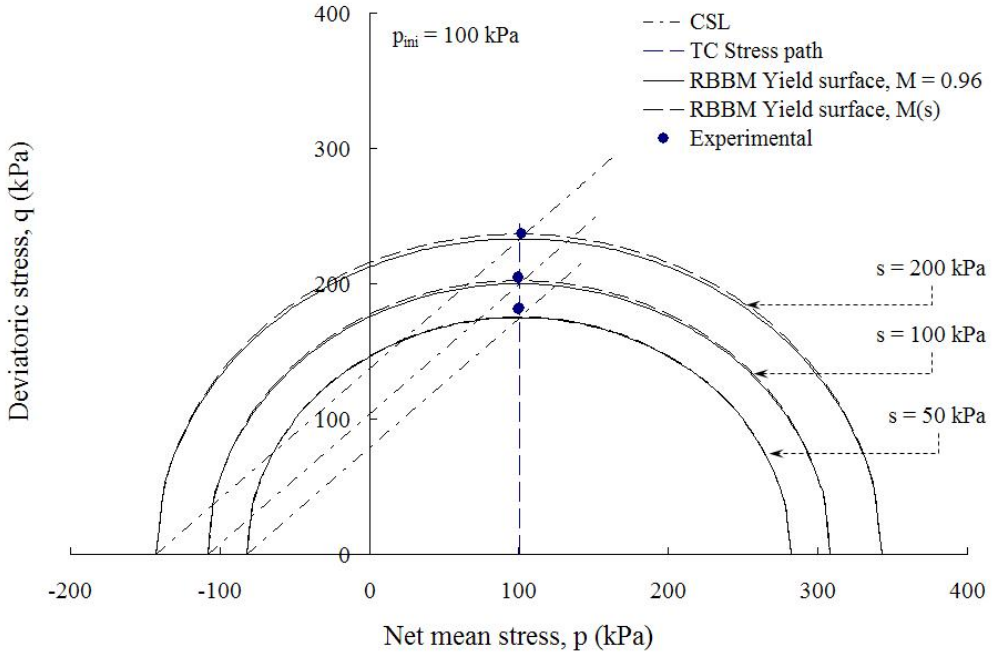

Figure 7.87 Predicted yield surface of RBBM in drained TC tests conducted at initial net mean stresses, p_{ini} = 100 kPa and constant matric suction, s = 50, 100, and 200 kPa.

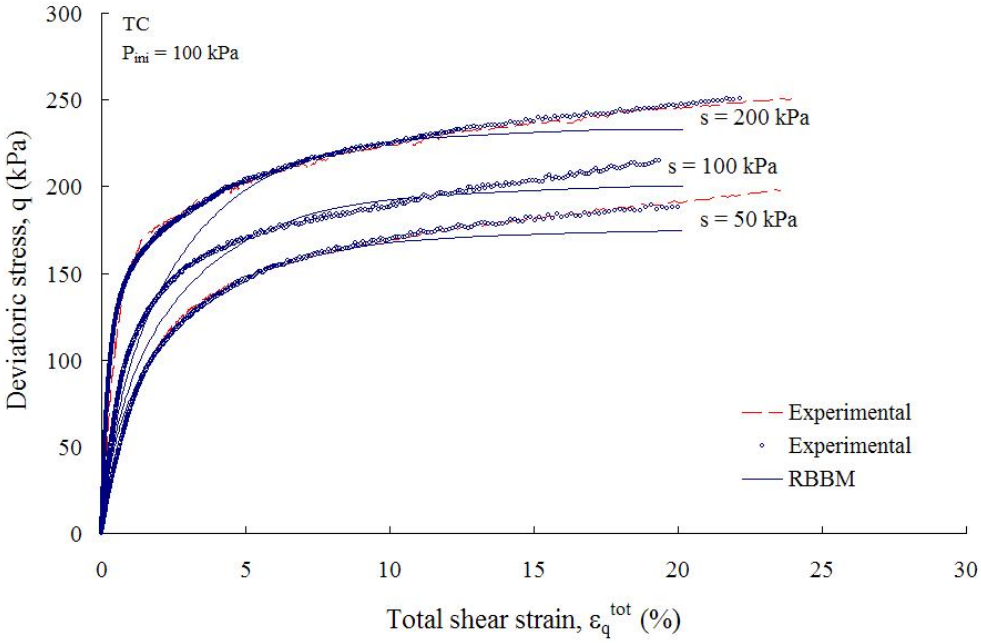

Figure 7.88 Measured and predicted stress-shear strain relationship from TE tests on SP-SC soil at s = 50, 100, and 200 kPa, and p_{ini} = 100 kPa (RBBM).

7.10 Failure Envelope in Deviatoric Plane

Figure 7.89 shows the predicted failure envelopes on the deviatoric plane (i.e. π plane) obtained by using the first yield criterion for metal proposed by Tresca in 1864, along with those predicted by using the yield criteria proposed for soils by Mohr-Coulomb in 1773, Matsuoka and Nakai in 1974, and Lade and Duncan in 1975 (Davis and Selvadurai, 2002). In addition, Figure 7.89 shows the projection of the experimental stresses obtained when the maximum shear stress reached a critical value identified during TC ($\theta = 0^o$), SS ($\theta = 30^o$), and TE ($\theta = 60^o$) tests, as a function of the initial net mean principal stress, p_{ini} and different values of matric suction, s = 50 kPa, s = 100 kPa, and s = 200 kPa. It is clear that the experimental failure stress state obtained from drained suction controlled TC, TE, and SS tests conducted on SP-SC soil specimens are

closest to the Lade and Duncan failure criterion and are further from the Tresca, Mohr-Coulomb, and Matsuoka and Nakai criterion. A significant influence of matric suction is observed on the size and shape of the yield loci, with a considerable expansion of the surface for s = 200 kPa.

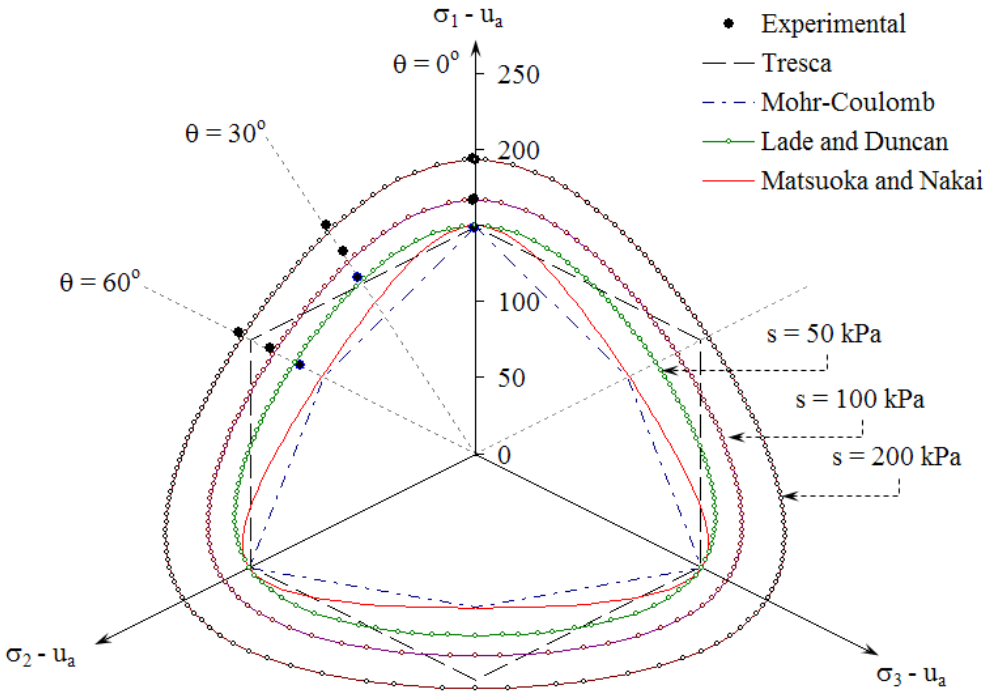

Figure 7.89 Experimental data and predicted yield loci in the deviatoric plane.

CHAPTER 8

CONCLUSIONS AND RECOMMENDATIONS

8.1 Summary

A computer-driven, fully servo-controlled, mixed-boundary type of true triaxial device has been implemented to test unsaturated soil specimens under general stress states and controlled matric suction states. A comprehensive series of drained (constant suction) hydrostatic compression (HC), conventional triaxial compression (CTC), triaxial compression (TC), triaxial extension (TE), and simple shear (SS) tests were conducted on compacted, 3 in (7.62 cm) per side, cubical specimens of clayey sand (SP-SC) under controlled suction states. Suction-controlled shearing was considered to have induced a critical state in all test samples when the applied deviator stress reached a peak value corresponding to a shear strain of approximately 15 %.

Results from suction-controlled tests under axisymmetric conditions ($\sigma_2 = \sigma_3$) were used for calibration of the elasto-plastic, critical state-based frameworks postulated by the Barcelona Basic Model (Alonso et al., 1990), the Modified Barcelona Basic Model (Josa et al., 1992) and the Oxford Model (Wheeler and Sivakumar, 1995). Results from suction-controlled CTC and TC tests were used for validation of the models in predicting stress-strain response of compacted clayey sand under 50, 100, 200 kPa suction states. Results were also used to validate the modifications proposed under the Refined Barcelona Basic Model framework developed in the present work.

Test data were also presented in the octahedral plane to study the influence of matric suction on the size and position of the failure envelopes of compacted clayey sand under suction-controlled general stress states.

8.2 Main Conclusions

1. The servo-controlled system adapted to the cubical cell has proven to be feasible for testing soils under controlled suction states and for real time measurements of matric suction, net principal stresses, and soil deformations along a wide range of simple-to-complex stress paths.

2. The pore-water pressure and pore-air pressure application systems housed at the bottom wall assembly were found to be suitable for testing cubical soil specimens under suction states up to 350 kPa using a 5-bar HAE ceramic disk via the axis-translation technique (Hilf, 1956). Testing at suction states above 350 kPa was not possible due to excessive diffused air through the ceramic.

3. Comparison with previously reported results suggests that the static compaction method adopted in this study to prepare the cubical test specimens delivers a compactive effort considerably higher than that induced by in-place tamping or kneading compaction. Moreover, the static compaction process yields considerably more homogeneous and compact samples that those produced via in-place tamping. A more consistent stress-strain response (repeatability of soil behavior under same stress paths) is observed in samples prepared by static compaction when compared to the layered samples prepared by tamping. Special attention must be given to the volume of

solid particles and water content to be applied during the static compaction process in order to ensure a reasonably identical dry unit weight, γ_d, in all compacted samples.

4. A suitable loading rate of 8 kPa/hr was empirically assessed for all suction-controlled testing performed in this study via axis-translation technique. This loading rate was proved to allow for sufficient equalization time (equilibrium of pore fluids) during suction-controlled isotropic loading or shearing.

5. Reasonably good agreement was observed between the experimental loading-collapse (LC) yield curve induced by static compaction on clayey sand specimens and those predicted by the modeling frameworks postulated by Alonso et al. (1990), Josa et al. (1992) and Wheeler and Sivakumar (1995).

6. In general, during suction-controlled shearing, the intercept of the critical state line, $\mu(s)$, with the deviator stress axis varied in a non linear fashion with the matric suction, s. This observation is consistent with the experimental findings reported by Wheeler and Sivakumar (1995), Escario and Saez (1996), and Laikram (2007). The variation with suction of parameter $\mu(s)$ would be equivalent to the variation of the angle ϕ^b in the unsaturated shear strength equation proposed by Fredlund et al. (1978).

7. Predictions of deviator stress vs. shear strain response of SP-SC soil under suction-controlled CTC and TC tests, from all previously proposed models, offer plenty of room for improvement and further refinement. The experimental results substantiate the assumption of a non-linear increase in cohesion, ps, due to an increase in suction, s. Similar results have been reported in different types of soil by previous authors. Therefore, considering that the increase in cohesion, p_s, with suction is critical in

predicting the yield surface in p–q space, total shear strain, ε_q^{tot}, sequence of loading path and, consequently, change in specific volume, v = 1+e, the postulated hypothesis of a linear relationship between cohesion, p_s, and matric suction, s, can be further evaluated and refined.

8. In light of experimental observations, a few modifications to the original BBM model, as well as its calibration process, have been devised in this work in order to improve the model's capabilities in predicting soil response under suction-controlled shearing. The modifications to the BBM resulted in a Refined BBM model which allows for reasonably better predictions of stress-strain response of SP-SC soil under constant suction states.

9. Matric suction was observed to exert a significant influence on the size and shape of the failure loci of compacted SP-SC soil in the octahedral plane (p-plane), with a considerable expansion of the failure locus for s = 200 kPa.

10. Failure loci of compacted SP-SC soil in the octahedral plane are closest to those predicted by Lade and Duncan (1975) failure criterion, while farthest from those predicted by Tresca (1864), Mohr-Coulomb (1776), and Matsuoka and Nakai (1974) failure criteria.

8.3Recommendations for Future Work

Further improvements to the developed cell can be accomplished by installing wet/wet gage or differential pressure transducers to measure real-time changes in pore-water volume during drained (constant suction) tests. This capability would allow for the calibration of constitutive models that have been proposed to predict the variation of

specific water volume in unsaturated soil specimens. In addition, a miniature pore-water pressure sensor could be installed.

Further drained and untrained suction-controlled tests could be performed for a wider range of stress paths and matric suction states in order to fully describe the failure surface on both the deviatoric plane and the principal stress plane, and to study the true nature of the variation of the intercept of the critical state line, $\mu(s)$ with matric suction, s. Additional experimental evidence of this kind will play a fundamental role in further substantiating the refinements proposed in the present work for the increase in cohesion, p_s, with matric suction, s.

REFERENCES

Adams, B. A. (1996). “Critical state behaviour of an agricultural soil.” PhD dissertation, University of Saskatchewan, Saskatoon, Saskatchewan, Canada, 358 p.

Agus, S. S. and Schanz, T. (2007). “Errors in Total Suction Measurements.” *Experimental Unsaturated Soil Mechanics, T. Schanz, Ed., Springer Proceedings in Physics No. 122*, 59 – 70.

Airey, D. W., and Wood, D. M. (1988). "The Cambridge True Triaxial Apparatus." *ASTM STP 977*, Philadelphia, 796 – 805.

Albrecht, B. A., Benson, C. H. and Beuermann, S. (2003). “Polymer Capacitance Sensors for Measuring Gas Humidity In Drier Soils.” *Geotechnical Testing Journal*, 26(1), 3 – 11.

Alonso E. E., Gens A. and Hight D. W. (1987). “Special problems soils.” *Proceeding of the 9th European Conference on Soil Mechanics*, Dublin, 1087 – 1146.

Alonso E. E., Gens A. and Gehling W. Y. Y. (1994). “Elastoplastic model for unsaturated expansive soils.” *Proceedings of the 3rd European Conference on Numerical Methods in Geotechnical Engineering*, Manchester, 11 – 18.

Alonso E. E., Gens A. and Josa A. (1990). “A constitutive model for partially saturated soils.” *Geotechnique*, 40(3), 405 – 430.

Alonso E. E., Vaunat J. and Gens A. (1999). “Modelling the mechanical behaviour of expansive clays.” *Engineering Geology*, 54(1), 173 – 183.

Angulo-Jaramillo, R., Elrick, D., Parlange, J., Gerard-Marchant, P. and Haverkamp, R. (2003). “Analysis of short-time single-ringe infiltration under fallinghead conditions with gravitational effects.” *Hydrology Days Proceedings*, 16 – 23.

Arthur, J. R. F. (1988). "Cubical Devices: Versatility and Constraints," *Advanced Triaxial Testing of Soil and Rock, ASTM STP 977*, Philadelphia, pp. 743-765.

ASTM Standard D2487-00. (2003). “Standard Classification of Soils for Engineering Purposes (Unified Soil Classification System).” *Annual Book of ASTM Standards*, Soil and Rock (I), 4(8), ASTM International,West Conshohocken, PA.

ASTM Standard D4318-05. (2003). “Standard Test Methods for Liquid Limit, Plastic Limit, and Plasticity Index of Soils.” *Annual Book of ASTM Standards,* Soil and Rock (I), 4(8), ASTM International,West Conshohocken, PA.

ASTM Standard D5298-03, (2003), “Standard Test Method for Measurement of Soil Potential (Suction) Using Filter Paper,” *Annual Book of ASTM Standards,* 4(8), ASTM International, West Conshohocken, PA.

ASTM D6836–02. (2003) “Test methods for determination of the soil water characteristic curve for desorption using a hanging column, pressure extractor, chilled mirror hygrometer, and/or centrifuge.” *Annual Book of ASTM Standards,* 4(8), ASTM International, West Conshohocken, PA.

ASTM Standard D698-00a, (2003) “Standard Test Methods for Laboratory Compaction Characteristics of Soil Using Standard Effort (12 400 ft-lbf/ft3 (600 kN-m/m3)).” *Annual Book of ASTM Standards,* 4(8), ASTM International, West Conshohocken, PA.

ASTM Standard D 854-06. (2003).”Standard Test Methods for Specific Gravity of Soil Solids by Water Pycnometer.” *Annual Book of ASTM Standards,* 4(8), ASTM International, West Conshohocken, PA.

Aung, K. K. Rahardjo, H. Leong, E. C. and Toll, D. G. (2001). “Relationship between porosimetry measurement and soil^water characteristic curve for an unsaturated residual soil.” *Geotechnical and Geological Engineering*, 19, 401 – 416.

Assouline, S. and tartakovsky D. M. (2001). “Unsaturated hydraulic conductivity function based on a soil fragmentation process.” *Water Resources Research*, 37(5), 1309 – 1312.

Bear, J. (1979). *Hydraulic of groundwater,* McGraw-Hill, New York.

Beer, G., and Watson, J. O. (1992). *Introduction to finite and boundary elements methods for engineers.* Wiley-Interscience, New York.

Bell, J. M. (1965). “Stress-strain characteristics of cohesionless granular materials subjected to statically applied homogeneous loads in an open system.” Ph.D. dissertation, California Institute of Technology.

Bishop, A. W. and Wesley, L. D. (1975). “A hydraulic triaxial apparatus fro controlled stress path testing.” *Geotechnique,* 25(4), 657 – 670.

Bishop, A. W. (1959). "The principle of effective stress," *Teknisk Ukeblad I Samarbeide Med Tknikk*, Oslo, Norway, 106(39), 859 – 863.

Bolzon, G. and Schrefler, B. A. (1995). "State surfaces of partially saturated soils: an effective pressure approach." *Applied Mechanics Reviews*, 48, 643 – 649.

Bolzon G., Screfler B. A. & Zienkiewicz O. C. (1996). "Elastoplastic soil constitutive laws generalized to partially saturated states." *Geotechnique*, 46(2), 279 – 289.

Brooks, R. H., and Corey A. T. (1964). "Hydraulic properties of porous media," *Hydrology Paper No. 3*, Colorado State University, Fort Collins.

Brutsaert, W. (1967). "Some methods of calculating unsaturated permeability." *Transactions of the American Society of Agricultural Engineers*, 10, 400 – 404.

Bulut, R., Lytton, R. L. and Wray, W. K. (2001). Soil suction measurements by filter paper. ASCE Conference Proceding, DOI:10.1061/40592(270)14, 243 – 261.

Burland J.B. and Ridley A.M. (1996). "The importance of suction in soil mechanics." Proceedings of the 12th South-East Asian Conference on Soil Mechanics and Foundation Engineering. Kuala Lumpur. Malaysia, 2, 27 – 49.

Callisto, L. and Calabresi, G. (1998). "Mechanical behaviour of a natural soft clay." *Geotechnique*, 48(4), 495 – 513.

Chandler, R. J., and Gutierrez, G. I. (1986). "The filter paper method of suction measurements," *Geotechnique*, 36(4), 265 – 268.

Chandler, R. J., Crilly, M. S., and Montgomery-Smith, G. (1992a). "A low cost method of assessing clay desiccation for low- rise buildings." *Proceedings of the Institution of Civil Engineers*, 92(2), 82 – 89.

Chandler, R. J., Hardwood, A. H., and Skinner, P. J. (1992b). "Sample disturbance in london clay." *Geotechnique*, 42(4), 577 – 585.

Cresser, M., Killhan, K., and Edwards, T. (1993). *Soil Chemistry and its Applications.* Cambridge Environmental Chemistry Series.

Cui Y. J., Delage P. and Sultan N. (1995). "An elastoplastic model for compacted soils." *1st International Conference on Unsaturated Soils*, Paris, 2,703 – 709.

Cui Y. J. and Delage P. (1996). "Yielding and plastic behaviour of an unsaturated compacted silt." *Geotechnique*, 46(2), 291 – 311.

Davis R. O. and Selvadurai A. P. S. (2002). *Plasticity and geomechanics.* Cambridge University Press, Cambridge, UK.

Department of the Army USA. (1983). *Foundations in expansive soils*. (Technical manual No. 5-818-7). Washington, DC: Engineering and Design for Real Property Facilities.

Deka, R. N.,Wairiu, M., Mtakwa, P.W., Mullins, C. E., Veenendal, E. M., and Townend, J. (1995). "Use and accuracy of the filter paper technique for measurement of soil matric potential." European Journal of Soil Science, 46, 233 – 238.

Drucker D. C., Gibson R. E. and Henkel D. J. (1957). "Soil mechanics and work hardening theories of plasticity." *Trans. ASCE*, 122, 338 – 346.

Durner, W. (1994). "Hydraulic conductivity estimation for soils with heterogeneous pore structure". *Water Resources Research*, 50, 211 – 223.

Escario, V., Juca, J. and Coppe, M.S. (1989). "Strength and deformation on partly saturated soils," *Proceeding of the 12th International Conference on Soil Mechanics and Foundation Engineering*, Rio de Janeiro, Vol. 3, 43 – 36.

Escario V. and Saez J. (1973). "Measurement of the properties of swelling and collapsing soils under controlled suction." *3rd International Conference on Expansive Soils*, Haifa, 195 – 200.

Escario V. and Saez J. (1986). "The shear strength of partly saturated soils." *Geotechnique*, 36, 453 – 456.

Everett, D. H. (1955). "A general approach to hysteresis – Part 4: An alternative formulation of the domain model." *Faraday Society Transaction*, 50, 187 – 197.

Fawcett, R. G., and Collis-George, N. (1967). "A filter paper method for determining the moisture characteristics of soil," *Australian Journal of Experimental Agriculture and Animal Husbandry*, CSIRO Publishing, Collingwood, Australia, 7(25), 162 – 167.

Fredlund, D.G. (1989). "Soil suction monitoring for roads and airfields." *Symposium on the State of the Art of Pavement Response Monitoring Systems for Roads and Airfields, Sponsored by the US Army Corps of Engineers*, Hanover, NH.

Fredlund, D.G. (2000). "The 1999 R.M. Hardy lecture: The implementation of unsaturated soil mechanics into geotechnical engineering." *Canadian Geotechnical Journal*, 37, 963 – 986.

Fredlund, D. G. (2006). “Unsaturated soil mechanics in Engineering practice.” *Journal of Geotechnical and Environmental Engineering*, 132(3), 286 – 321.

Fredlund, D.G., and Morgenstern, N.R. (1977). “Stress state variables for unsaturated soils.” *Journal of Geotechnical Engineering Division*, Proceedings, American Society of Civil Engineers, GT5, 103, 447 – 466.

Fredlund, D. G.; Morgenstern, N. R.; and Widger, R. A. (1978). “The Shear Strength of Unsaturated Soils,” *Canadian Geotechnical journal*, 15(3), 313 – 321.

Fredlund, D. G. and Rahardjo, H. (1993). *Soil mechanics for unsaturated soils*. Wiley-Interscience, New York.

Fredlund, D. G., Vanapalli, S. K., Xing, A., and Pufahl, D. E. (1995). “Predicting the shear strength function for unsaturated soils using the soil-water characteristic curve.” *Proceedings of the First International Conference on Unsaturated Soils, Paris, France*, 1, 63 – 70.

Fredlund, D. G. and Xing, A. (1994). “Equations for the soil water characteristic curve.” *Canadian Geotechnical journal*, 31(3), 521 – 532.

Fredlund, D. G., Xing, A. and Huang, S. (1994). “Predicting the permeability function for unsaturated soils using the soil water characteristic curve.” *Canadian Geotechnical journal*, 31, 533 – 546.

Fredlund, D. G., Xing, A., Fredlund, M. D., and Barbour, S. L. (1996). “The relationship of the unsaturated soil shear strength to the soil-water characteristic curve.” *Canadian Geotechnical journal*, 32, 440 – 448.

Gan, J. K., Fredlund, D. G. and Rahardjo, H. (1988). “Determination of the shear strength parameters of an unsaturated soil using direct shear test.” *Canadian Geotechnical journal*, 25(3), 500 – 510.

Gandola, F., Debionne, S., Varado, N., Haverkamp, R., Ross, P.J., Sander, G. and Parlange, J.Y. (2004). “Simple soil water hysteresis prediction model based on theory and geometric scaling.” Proceding of Europian Geosciences Union conference, Vol. 6, 07289

Gardner, W.R. (1961). “Soil suction and water movement.” *Pore pressure and suction in soil’, London*, Butterworths, 137 – 140.

GCTS. (2004a). “Digital servo controller user’s guide.” Geotechnical Consulting & Testing Systems, Tempe, Arizona, 61 p.

GCTS. (2004b). “Universal program user’s guide.” Geotechnical Consulting & Testing Systems, Tempe, Arizona, 51 p.

Gens A. and Alonso E. E (1992). “A framework for the behaviour of unsaturated expansive clays.” *Canadian Geotechnical Journal*, 29, 1013 – 1032.

Gens, A. and Potts, D. M. (1988). “Critical state models in computational geomechanics.” *Engineering Computations,* 5(3), 178 – 197.

Gens, A. and Potts, D. M. (1982). “A theoretical model for describing the behaviour of soils not obeying Rendulic’s principle.” *Proceeding 1st International Symposium on Numerical Modelling in Geomechanics,* Zurich, 24 – 32.

Georgiadis, K. (2003). “Development, implementation and application of partially saturated soil models in finite element analysis.” PhD dissertation, imperoial College, University of London, London, UK, 251 p.

Georgiadis, K., Potts, D. M. and Zdravkovic, L. (2005). “Three-dimensional constitutive model for partially and fully saturated soils.” *International Journal of Geomechanics*, 5(3), 244 – 255.

Gibbs, J. W. (1928). The Collected Works of J. Willard Gibbs, I: Thermodynamics. Edited by W. R. Logley and R. G. Van Name. New York: Longmans, Green, and Company.

Greca, I. M. and Moreira, M. A. (2001). “Mental, physical, and mathematical models in the teaching and learning of physics.” *Science Education,* 86(1), 106 – 121.

Gourley, C. S. and Schreiner, H. D. (1995). “Field Measurements of Soil Suction,” *Proceedings of the 1st International Conference on Unsaturated Soils*, Paris, France, Vol. 2, 601–607.

Haines, W. B. (1930). “Studies in the physical proprieties of soil : V. The hysteresis effect in capillary proprieties, and the modes of moisture distribution associated therewith.” *Journal of Agricultural Science,* 20, 97 – 116.

Hamblin, A. P. (1981). “Filter paper method for routine measurement of field water potential,” *Journal of Hydrology,* 53, 355 – 360.

Hambley, E. C. (1969). "A New Triaxial Apparatus." *Geotechnique,* (19)2, 307 – 309.

Haverkamp, R. Vauclin, M. Touma, J., Wierenga, P. J. and Vachaud, G. (1977). "A comparison of numerical simulation models for one dimensional infiltration." *Soil Science Society of America Journal*, 41, 285 – 294.

Haverkamp, R. and Parlange, J-Y. (1986). "Predicting the water-retention curve from particle size distribution: 1. Sandy soils without organic matter." *Soil Science*, 142, 325 – 339.

Hillel, D. (1982). *Introduction to Soil Physics*, Academic Press, Inc., San Diego, California.

Hilf, J. W. (1956) "An investigation of pore-water pressure in compacted cohesive soils," Tech. Memo. No. 654, U.S. Dept. of the Interior, Bureau of Land Reclamation, Design and Construction Div., Denver, CO.

Hogarth, W., Hopmans, J. and Parlange, J-Y. (1988). "Application of a simple soil water hysteresis model." *Journal of hydrology*, 98, 21 – 29.

Hoyos, L.R., (1998). "Experimental and computational modeling of unsaturated soil behavior under true triaxial stress states," PhD dissertation, Georgia Institute of Technology, Atlanta, Georgia, 358 p.

Hoyos, L. R., and Macari, E. J. (2001). "Development of a stress/suctioncontrolled true triaxial testing device for unsaturated soils." Geotechnical Testing Journal, 24(1), 5 – 13.

Hoyos, L. R. and Arduino, P. (2008). "Implicit algorithm for modeling unsaturated soil response in three-invariant stress space." *International Journal of Geomechanics ASCE*, 8(4) 266 – 273.

Hoyos, L. R., Laloui, L. and Vassallo, R. (2008). "Mechanical testing in unsaturated soils." *Geotechnical and Geological Engineering*, 26(6), 675 – 689.

Iwata, S., Tabuchi, T., and Warkentin, B. P. (1995). *Soil-water interactions*, Marcel Dekker, New York.

Jaynes, D. (1984). "Comparison of soil-water hysteresis models." *Journal of Hydrology*, 75, 287 – 299.

Jaynes, D. (1992). "Estimating hysteresis in the soil water retention function." Proceedings of the International Workshop on Indirect Methods for Estimating the

Hydraulic Proprieties of Unsaturated Soils, University of California, Riverside, California, 219 – 232.

Josa A., Alonso E. E., Gens A. and Lloret A. (1987). "Stress-strain behaviour of partially saturated soils." Proceeding *9th International Conference on Soil Mechanics and Foundation Engineering,* Dublin, 2, 561 – 564.

Josa A., Balmaceda A., Gens A. and Alonso E. E. (1992). "An elastoplastic model for partially saturated soils exhibiting a maximum of collapse." *Proceedings, 3rd International Conference on Computational Plasticity,* Barcelona, 1, 815 – 826.

Kastanek, F. J. and Nielsen, D. R. (2001). "Description of soil water characteristics using cubic spline interpolation." *Soils Science Society of America Journal,* 65(2), 279 – 283.

Kayadelen, C., Tekinsoy, M. A. and Taskıran T. (2007). "Influence of matric suction on shear strength behavior of a residual clayey soil." *Environmental Geology*, 53(4), 891 – 901.

Kato S., Matsuoka H. and Sun D. A. (1995). "A constitutive model for unsaturated soil based on extended SMP." *1st International Conference on Unsaturated Soils,* Paris, 2, 739 – 744.

Khanzode R. M. (1999). "An alternative centrifuge method to obtain the soil-water characteristic curves for fine grained soils. M.Sc. thesis, University of Saskatchewan.

Khanzode, R, M., Fredlund, D. G. and Vanapalli, S. K. (1999). "An alternative method to for the measurement of soil-water characteristic curves for fine-grained soils." *Proceeding of the 52nd Canadian Geotechnical Conference*, Regina,S askatchewan, 623 – 630.

Kim M. K. and Lade P. V. (1988a). "Single hardening constitutive model for frictional materials I: Plastic potential function." *Computers and Geotechnics* 5, 307 – 324.

Kim M. K. and Lade P. V. (1988b). "Single hardening constitutive model for frictional materials II: Yield criterion and plastic work contours." *Computers and Geotechnics*, 6, 13 – 29.

Ko, H. Y. and Scott, R. F. (1967). "A new soil testing apparatus" *Geotechnique*, 17 40 – 57.

Kohgo Y., Nakano M. and Miyazaki T. (1993a). "Theoretical aspects of constitutive modelling for unsaturated soils." *Soils and Foundations*, 33(4), 49 – 63.

Kohgo Y., Nakano M. and Miyazaki T. (1993b). “Verification of the generalised elastoplastic model for unsaturated soils.” *Soils and Foundations,* 33(4), 64 – 73.

Kurtay, T. and Reece, A. R. (1970). “Plasticity theory and critical state soil mechanics.” *Journal of Terramechanics,* 7(30), 23 – 56.

Kuz, V. A., Vila, M. A., Garazo, A. N., and Zarragoicoechea, G. J. (1987). “Theory of surface tension and its application to Simple Fluids.” *Journal of Statistical Physics,* 49(5/6), 1209 – 1219.

Lade, P. V. (1988). "Effects of voids and volume changes on the behaviour of frictional materials." *International Journal for Numerical and Analytical Methods in Geomechanics,* 12(4), 351—370.

Lade, P. V., and Duncan, J. M.. (1973). "Cubical Triaxial Tests on Cohesionless Soil," *Journal of the Soil Mechanic Foundation Division, ASCE,* (99), 793 – 812.

Lade, P. V. and Nelson, R. B. (1987). “Modelling the elastic behaviour of granular materials.” *International Journal for Numerical and Analytical Methods in Geomechanics,* 11(5), 521 – 542.

Laikram, A. (2007). “Modeling unsaturated soil response under suction-controlled multi-axial stress states” PhD thesis, University of Texas at Arlington, Arlington, Texas, 235 p.

Lanier, J. (1988). "Special stress paths along the limit surface of a sands specimen with the use of a true triaxial apparatus." *Advanced Triaxial Testing of Soil and Rock, ASTM STP 977,* Philadelphia, 859 – 869.

Lappala E.G., Healy R.W. and Weeks E.P., (1987). Documentation of the Computer Program to Solve the Equations of Fluid Flow in Variably Saturated Porous Media, Water-Resources Investigation Reports, 83-4099, US Geological Survey, Denver, Colorado.

Leong, E. C. and Rajardjo, H. (1997). “Review of soil-water characteristic curve equations.” *Journal of Geotechnical and Geoenvironmental Engineering,* 123(12), 1106 – 1117.

Leong, E. C., He, L., and Rahardjo, H.. (2002). “Factors Affecting the Filter Paper Method for Total and Matric Suction Measurements,” Geotechnical Testing Journal, 25(3), 322 – 332.

Li, X. S. (2003). “Tensorial nature of suction in unsaturated granular soil.” 16th ASCE Engineering Mechanics Conference, 1 – 4.

Lu, N., and Likos, W. J. (2004). *Unsaturated Soil Mechanics*. John Wiley and Sons, Inc. New Jersey.

Lu, N., and Likos, W. J. (2006). "Suction stress characteristic curve for unsaturated soil." *Journal of Geotechnical and Geoenvironmental Engineering,* 132(2), 131 – 142.

Lloret A., Gens A., Battle F. and Alonso E. E. (1987). "Flow and deformation analysis of partially saturated soils." Proceeding *9th International Conference on Soil Mechanics and Foundation Engineering,* Dublin, Vol. 2, 565 – 568.

Navacués G. (1979). "Liquid surfaces: theory of surface tension". *Rep. Prog. Phys.*, 42, 1131 – 1186.

Maqsoud, A., Bussière, B., Mbonimpa, M. and Aubertin, M. (2004). "Hysteresis effects on the water retention curve: a comparison between laboratory results and predictive models." *57th Canadian Geotechnical Conference*, 3A, 8 – 15, Québec, Canada

Marinho, F. A. M. (1994). "Shrinkage behavior of some plastic clays," Ph.D. Thesis, University of London.

Marinho, F. A. M., Oliveira, O. M. (2006). "The filter paper method revisited." *Geotechnical Testing Journal*, 29(3), 1 – 9.

McKeen, R. G. (1980). "Field studies of airport pavements on expansive soils," *4th International Conference on Expansive Soils,* 242 – 261.

Matsuoka, H., Sun, D. A., Kogane, A., Fukuzawa, N. and Ichihara, W. (2002). "Stress-strain behaviour of unsaturated soil in true triaxial tests." *Canadian Geotechnical Journal*, 39, 608 – 619.

Matsuoka, H. and Sun, D. A. (2006). *The SMP Concept-based 3D Constitutive Models for Geomaterilas.* Taylor and Francis Group. London, UK.

Minshull, R. (1975). "An introduction to models in geography." *The Times Higher Educational Supplement*, Longman, London.

Montgomery, D. C. (2005). *Design and Analysis of Experiments.* John Wiley and Sons, Inc. New Jersey.

Mualem, Y. (1984). "A modified dependent-domain theory of hysteresis", *Journal of Soil Science*, 137(5), 283 – 291.

Muller, R. K. (1978). “Mathematical and physical models.” *Experimental Mechanics,* 18(7), 241 – 245.

Öberg, A-L. (1997). “Matrix suction in silt and sand slopes.” PhD thesis. Chalmers University of Technology, Sweden.

O’Kane, J.P., Pokrovskii, A. and Flynn, D. (2004). “The fest model for testing the importance of hysteresis in hydrology.” *Proceding of EGU conference,* Vol 6, 07303.

Ohmaki, S. (1982). “Stress-strain behaviour of anisotropic ally, normally consolidated cohesive soils. *Proceeding 1st International Symposium on Numerical Modelling in Geomechanics,* Zurich, 250-269.

Pakarinen, O. H., Foster, A. S., Paajanen, M., Kalinainen, T., Katainen, J., Makkonen, I., Lahtinen, J., and Nieminen, R. M. (20050. “Towards an accurate description of the capillary force in nanoparticle-surface interactions.” *Modelling Simul. Mater. Sci. Eng.*, 13, 1175 – 1186.

Parlange J.-Y., Water transport in soils, Annu. Rev. Fluid Mech., 12 (1980), 77 – 102.

Parlange, J., Steenhuis, T., Haverkamp, R., Barry, D., Culligan, P., Hogarth, W., Parlange, M.B., Ross, P. and Stagnitti, F. (1999) Soil Properties and Water Movement, Vadose Zone Hydrology - Cutting Across Disciplines, 99 – 129, Oxford University Press, New York.

Park J.H. (2005). “Performance and check-out verification testing of a new true triaxial apparatus using partially saturated silty sand,” M.Sc. thesis, University of Texas at Arlington, Arlington, Texas, 107 p.

Poulovassilis, A. (1962). “Hysteresis of pore water, an application of concept of independent domains.” *Soil Science Society of America Journal Soil Science,* 93, 405 – 412.

Poulovassilis, A. and Tzimas, E. (1974). “The hysteresis in the relationship between hydraulic conductivity and suction.” *Soil Science Society of America Journal,* 117, 250 – 256.

Poulovassilis, A. and Kargas, G. (2000). “A note on calculating hysteric behavior.” *Soil Science Society of America Journal,* 64, 1947 – 1950

Power, K. C., Vanapalli, S. K. and Garga, V. K. (2008). “A Revised Contact Filter Paper Method.” *Geotechnical Testing Journal*, 31(6), 1 – 9.

Pyo, S.C. (2006). “General response of partially saturated silty sand under drained and undrained true triaxial testing,” M.Sc. thesis, University of Texas at Arlington, Arlington, Texas, 127 p.

Rahardjo, H., Lim, T. T., Chang, M. F., and Fredlund, D. G. (1995). "Shear strength characteristics of a residual soil with suction." *Canadian Geotechnical Journal*, 32, 60 – 77.

Reddy, K. R. Saxena, S. K. and Budiman, J. S. (1992). “Developemant of a True Triaxial Testing Apparatus” *Geotechnical Testing Journal*, 15(2), 89 – 105.

Richards, L. A. (1941). “Uptake and retention of water by soil as determined by distance to a water table.” *Journal of the American Society of Agronomy,* 33, 778 – 786.

Ridley, A., McGinnity, B. and Vaughan, P. (2004). “Role of pore water pressures in embankment stability.” *Geotechnical Engineering*, 157(4), 193 – 198.

Ridley, A. M. and Wray, W. K. (1996) “Suction Measurements: A Review of Current Theory and Practices.” *Proceedings of the 1st International Conference on Unsaturated Soils*, Paris, France, Vol. 3, 1293 – 1322.

Ridley, A. M., Dineen, K., Burland, J. B. and Vaughan, P. R. (2003). “Soil Matrix Suction: Some Examples of its Measurements and Application in Geotechnical Engineering,” *Geotechnique,* 52(2), 1293 – 1322.

Roscoe, K. H., Schofield, A. N. and Wroth, C. P. (1958). “On the yielding of soils.” *Geotechnique,* 8, 22 – 53.

Roscoe K. H. & Burland J. B. (1968). “On the generalised stress-strain behaviour of ‘wet’ clay”. *Engineering Plasticity*, Cambridge University Press, 535-609.

Roscoe K. H. & Schofield A. N. (1963). “Mechanical behaviour of an idealised ‘wet’ clay”. *Proceeding 2nd European Conference on Soil Mechanics and Foundation Engineering*, Wiesbaden, 1, 47 – 54.

Schmelzer, J. W. P., Gutzow, I., and Schmelzer, J. (1996). “Curvature-dependent surface tension and nucleation theory.” *Journal of Colloid and Interface Science*, 178, 657 – 665.

Shuai, F. and Fredlun, D. G. (1998). “Model for the simulation of swelling-pressure measurements on expansive soils.” Canadian Geotechnical Journal, 35(1), 96 – 114.

Sillers, W. S. and Fredlund, D. G. (2001). “Statistical assessment of soil-water characteristic curve models for geotechnical engineering.” *Canadian Geotechnical Journal,* 38, 1297 – 1313.

Šimůnek, J. and M. Th. van Genuchten (2005). The HYDRUS-1D Software Package for Simulating the One-Dimensional Movement of Water, Heat, and Multiple Solutes in Variably-Saturated Media. Department of Environmental Sciences, University of California Riverside, Riverside, California.

Smith, I. M. and Griffiths, D. V. (2004). *Programming the finite element methods*. John Wiley & Sons, Ltd., West Sussex, England.

Spangler, M. G. and Handy, R. L. (1982). *Soil Engineering.* Harper & Row, Publishers, New York.

Sreedeep, S. and Singh, d. N. (2006). “Nonlinear curve-fitting procedures for developing soil-water characteristic curves.” *Geotechnical Testing Journal,* 29(5), 1 – 10.

Snoeyink, V. L. and Jenkins, D. (1980). *Water Chemistry*. John Wiley & Sons, Inc., New Jersey.

Sture, S., and Desai, C. S. (1979). "Fluid Cushion Truly Triaxial or Multiaxial Testing Device," *Geotechnical Testing Journal,* 2(1), 20 – 33.

Sun, D., Yao, Y. P. and Matsuoka, H. (2006). “ Modification of critical state models by Mohr-Coulomb criterion.” *Mechanics Research Communications,* 33, 217 – 232.

Suzuki, H. (2000). “Reconsideration of suction controlled techniques by thermodynamic theory of water in soil.” *Proc., Asian Conference on Unsaturated Soils. UNSAT ASIA 2000,* Singapore, 159 – 162.

Tami, D., Rahardjo, H., and Leong, E. C. (2004a). “Effects of hysteresis on steady-state infiltration in unsaturated slopes.” *Journal of Geotechnical and Geoenvirontal Engineering,* 130(9), 956 – 967.

Tarantino, A. and Mongiovi, L. (2005). “Development of a apparatus to investigate the stress variables governing unsaturated soil behavior.” *Geotechnical Testing Journal,* 28(2), 1 – 10.

Tartakovsky, D. M. (2001). “Unsaturated hydraulic conductivity function based on a soil fragmentation process.” *Water Resources Research,* 35(5), 1309 – 1312.

Terzaghi, K. (1936). “The Shear Resistance of Saturated Soils,” *Proceeding, 1st International Conference on Soil Mechanics and Foundation Engineering,* Harvard University, Cambridge, MA, 1, 54-56.

Terzaghi, K. (1943). *Theoretical soil mechanics*. Wiley, New York.

Tindall J.A. and Kundel J.R., (1999). *Unsaturated Zone Hydrology for Scientists and Engineers*. Prentice Hall, Inc., New Jersey.

Tolman, R. C. (1948). “Consideration of the Gibbs theory of surface tension.” *Journal of Chemical Physic*s, 16(8), 758 – 774.

Topp, G.C. and Miller, E. E. (1966). “Hysteresis moisture characteristics and hydraulic conductivities for glassbead media.” *Soil Science Society of America Journal*, 30, 156 – 162.

Topp, G. C. (1971). “Soil-water hysteresis: the domain theory extended to pore interaction conditions.” *Soil Science Society of America Journal*, 35, 219 – 225.

Tzimopoulos, C. D. and. Sakellariou-Makrantonak, M. (1996). “A new analytical model to predict the hydraulic conductivity of unsaturated soils.” *Water Resources Management,* 10, 397 – 414.

van Genuchten, M.T. (1980). “A closed form equation for predicting the hydraulic conductivity of unsaturated soils”. Soil Science Society of America Journal 44, 892 – 898.

Vanapalli, S. K. (1994). “Simple test procedures and their interpretation in evaluating the shear strength of an unsaturated soil.” PhD thesis, University of Saskatchewan, Canada.

Vanapalli, S.K., Fredlund, D.G., Pufahl, D.E. (1999). “The influence of soil structure and stress history on the soil-water characteristics of a compacted till.” *Geotechnique*, 49(2), 143 – 159.

Vanapalli, S.K., Fredlund, D.G., Pufahl, D.E., and Clifton, A.W (1996). “Model for the prediction of shear strength with respect to soil suction.” *Canadian Geotechnical Journal*, 33, 379 – 392.

Wang, Y. H., and Fredlund, D. G. (2003). “Towards a better understanding of the role of the contractile skin.” Proceedings of the 2nd Asian Conference on Unsaturated Soils, Osaka, Japan. pp. 419-424. April 15-17.

Wheeler S. J (1991). “An alternative framework for unsaturated soil behaviour.” *Geotechnique,* 41(2), 257 – 261.

Wheeler, S. J. (1996). “Inclusion of specific water volume within and elasto-plastic model for unsaturated soil.” *Canadian Geotechnical Journal,* 33, 42 – 57.

Wheeler, S. J., Gallipoli, D. and Karstunen, M. (2002). “Comments on use of the Barcelona Basic Model for unsaturated soils.” *International Journal for Numerical and Analytical Methods in Geomechanics*, 26, 1561 – 1571.

Wheeler S. J. and Karube D. (1996). “Constitutive modelling: state of the art report.” *Unsaturated Soils,* Balkema, Rotterdam, 1179 – 1200.

Wheeler, S. J., and Sivakumar, V. (1995). “An elato-plastic critical state framework for unsaturated soils.” *Géotechnique*, 45(1), 35 – 53.

Wood, D. M. (1990). *Soil Behaviour and Critical State Soil Mechanics.* Cambridge University Press, New York.

Wood, D. M. (2004). *Geotechnical Modelling.* Spon Press, New York.

Yao, Y. P., Sun, D. A. and Matsuoka, H. (2008). “A unified constitutive model for both clay and sand with hardening parameters independent on stress path.” *Computer and Geotechnics*, 35, 210 – 222.

Yaldo, K. (1999). “Impact of soil type and compaction conditions on soil water characteristic curves,” Ph.D. Thesis, Wayne State University.

Yu, H. S. (2006). *Plasticity and geotechnics*. Springer, New York.

Zhang, X. and Lytton, R. L. (2006). “Stress state variables for unsaturated soils.” Proceedings *of the Fourth International Conference on Unsaturated Soils, ASCE Conf. Proc,* 189(202), 2380 – 2391.

Zhou, J. and Yu., J. L. (2005). “Influences affecting the soil-water characteristic curve.” *Journal of Zhejiang University Science,* 6A(8), 797 – 804.

BIOGRAPHICAL INFORMATION

Diego D. Pérez-Ruiz was born in Bolivar, Cauca, Colombia on Febrary 10, 1965. He received his B.S degree in Civil Engineering from the “Universidad del Cauca”, Popayán, Colombia in December, 1987.

In 1988, he was admitted to the graduate program of advanced studies in Highway Engineering at the “Universidad del Cauca” in Popayán, Colombia, where he received a M.Sc. degree in Transportation Engineering. In 1990, he was admitted to the graduate program at the University of Puerto Rico at Mayaguez, in the Environmental and Water Resources Area, where he received a M.Sc. degree in Civil Engineering in June, 1993.

From August 1993 to June, 1994, he worked as adjunct professor in the General Engineering Department at the University of Puerto Rico at Mayaguez, where he was given the opportunity to teach Computer Programming and Fluid Mechanics Laboratory courses. Then, he went back to Colombia to join the “Intituto Colombiano de Geología y Minería (INGEOMINAS)”.

From February 1995 to July 2000, he worked as assistant professor in the Civil Engineering Department at the “Universidad del Cauca” in Popayan, Colombia, Then, in August 2000 he joined to the Civil Engineering Department at the “Pontificia Universidad Javeriana de Cali” in Cali, Colombia.

In addition, from 1995 to 2005 he worked as consultant and design engineer for several consulting companies in Colombia, mainly in hydraulic, hydrologic and scour studies for bridge and road design projects; environmental impact studies; highway capacity analysis; traffic simulation; geometric design of intersections; and signals design.

In January, 2006, he was admitted to the graduate program in Department of Civil Engineering at the University of Texas at Arlington, as a doctoral student. Mr. Pérez has successfully completed all requirements for the Degree of Doctor of Philosophy in Civil Engineering on July 17, 2009 and he will receive the degree in Summer, 2009 Commencement ceremony.